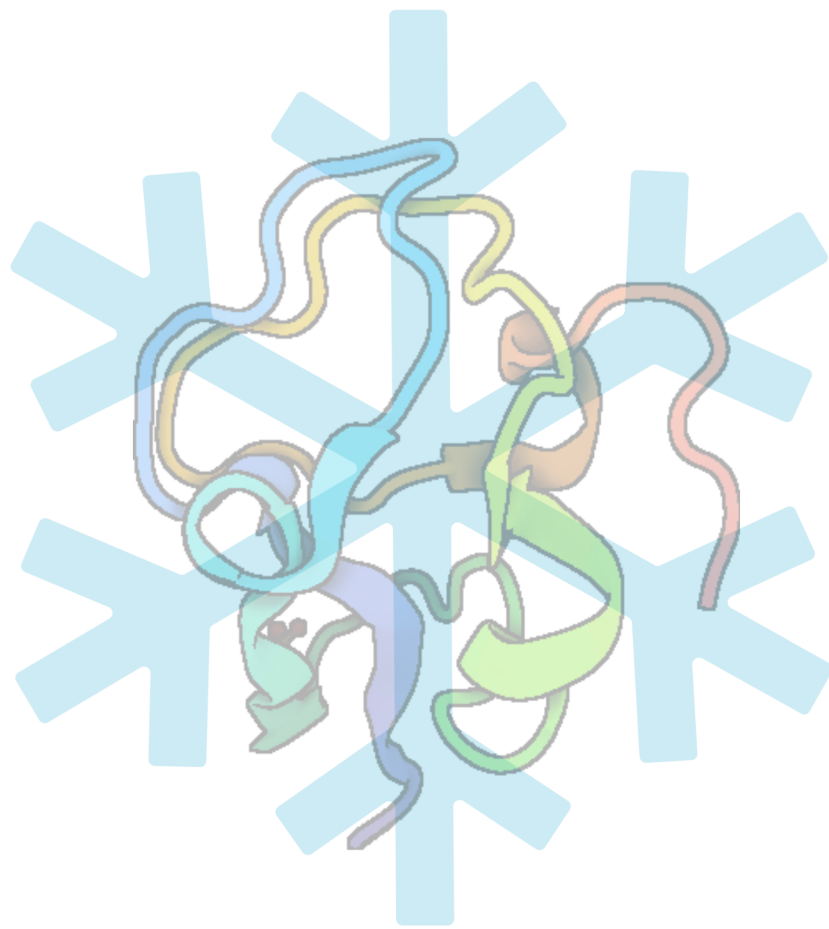# To Freeze or Not to Freeze

Investigating Ice-binding Proteins and their Role in Biological Ice Nucleation

Ralph Schwidetzky

Max-Planck-Institute for Polymer Research

To Freeze or Not to Freeze

Investigating Ice-binding Proteins and their Role in Biological Ice Nucleation

Dissertation
zur Erlangung des Grades
'Doctor rerum naturalium (Dr. rer. nat)'
im Promotionsfach Chemie
am Fachbereich Chemie, Pharmazie und Geowissenschaften der
Johannes Gutenberg-Universität
in Mainz

vorgelegt von

Ralph Schwidetzky
geb. 03.06.1990 in Speyer
Matrikel-Nummer 2691388
Betreuer: █████████████

Mainz, 2022

1. Berichterstatter:
2. Berichterstatter:

Tag der mündlichen Prüfung:

Publications

This thesis is based on the following publications:

Articles:

R. Schwidetzky, A. T. Kunert, M. Bonn, U. Pöschl, H. Ramløv, A. L. DeVries, J. Fröhlich-Nowoisky, and K. Meister. Inhibition of Bacterial Ice Nucleators Is Not an Intrinsic Property of Antifreeze Proteins. *J. Phys. Chem. B.*, 124(24), 4889-4895 (2020).

M. Lukas, R. Schwidetzky, A. T. Kunert, U. Pöschl, J. Fröhlich-Nowoisky, M. Bonn, and K. Meister. Electrostatic Interactions control the functionality of bacterial ice nucleators. *J. Am. Chem. Soc.*, 1142(15), 6842-6846 (2020).

M. Lukas*, R. Schwidetzky*, A. T. Kunert, E. H. G. Backus, U. Pöschl, J. Fröhlich-Nowoisky, M. Bonn, and K. Meister. Interfacial Water Ordering Is Insufficient to Explain Ice-Nucleating Protein Activity. *J. Phys. Chem. Lett.*, 12(1), 218-223 (2020).

R. Schwidetzky*, M. Lukas*, A. YazdanYar*, A. T. Kunert, U. Pöschl, K. F. Domke, J. Fröhlich-Nowoisky, M. Bonn, T. Koop, Y. Nagata, and K. Meister. Specific Ion–Protein Interactions Influence Bacterial Ice Nucleation. *Chem. Eur. J.*, 27(26), 7402-7407 (2021).

R. Schwidetzky, P. Sudera, A. T. Backes, U. Pöschl, M. Bonn, J. Fröhlich-Nowoisky, and K. Meister. Membranes Are Decisive for Maximum Freezing Efficiency of Bacterial Ice Nucleators. *J. Phys. Chem. Lett.*, 12(44), 10783-10787 (2021).

R. Schwidetzky, Y. Sun, J. Fröhlich-Nowoisky, A. T. Backes, M. Bonn, and K. Meister. Ice Nucleation Activity of Perfluorinated Organic Acids. *J. Phys. Chem. Lett.*, 12(13), 3431-3435 (2021).

M. Lukas, R. Schwidetzky, R. J. Eufemio, M. Bonn, and K. Meister. Toward Understanding Bacterial Ice Nucleation. *J. Phys. Chem. B.*, 126(9), 1861-1867 (2022).

Book chapters:

R. J. Eufemio, R. Schwidetzky, and K. Meister. Measurement of Ice Nucleation Activity of Biological Samples. In: R. Drori (eds) *Experimentation with ice-nucleation proteins. Methods Mol. Biol.* Springer Nature. *accepted*

In preparation:

Articles:

R. Schwidetzky, Y. Sun, A. T. Backes, A. L. DeVries, M. Bonn, J. Fröhlich-Nowoisky, and K. Meister. Protein Aggregates Enable Fungal Ice Nucleation.

R. Schwidetzky, J. Lui, U. Pöschl, J. Fröhlich-Nowoisky, M. Bonn, and K. Meister. Drastic Enhancement of Bacterial Ice Nucleation Efficiency By Polyols.

* These authors contributed equally.

Declaration

I hereby declare that I wrote the dissertation submitted without any unauthorized external assistance and used only sources acknowledged in the work. All textual passages which are appropriated verbatim or para-phrased from published and unpublished texts as well as all information obtained from oral sources are duly indicated and listed in accordance with bibliographical rules. In carrying out this research, I complied with the rules of standard scientific practice as formulated in the statutes of Johannes Gutenberg-University Mainz to insure standard scientific practice.

Ort, Datum   Unterschrift

Contents

List of Figures

Abbreviations

AFP   antifreeze protein
AFGP   antifreeze glycoprotein
atm   standard atmosphere (unit), 101325 Pa
CD   chircular dicroism
f_{ice} fraction of ice
IAP   ice affinity purification
IBP   ice-binding protein
IBS   ice-binding site
IN   ice nucleator
INA   ice nucleation activity
INP   ice nucleating protein
IRI   ice recrystallization inhibition
N_m cumulative number of active IN
PBS   phosphate-buffered saline
PFA   perfluorinated acids
SFG   sum frequency generation
TH   thermal hysteresis
T_{het} heterogeneous nucleation temperature
T_{hom} homogeneous nucleation temperature
TINA   twin-plate ice nucleation assay
T_m melting temperature
T_{50} temperature at $f_{ice} = 0.5$

Acknowledgement
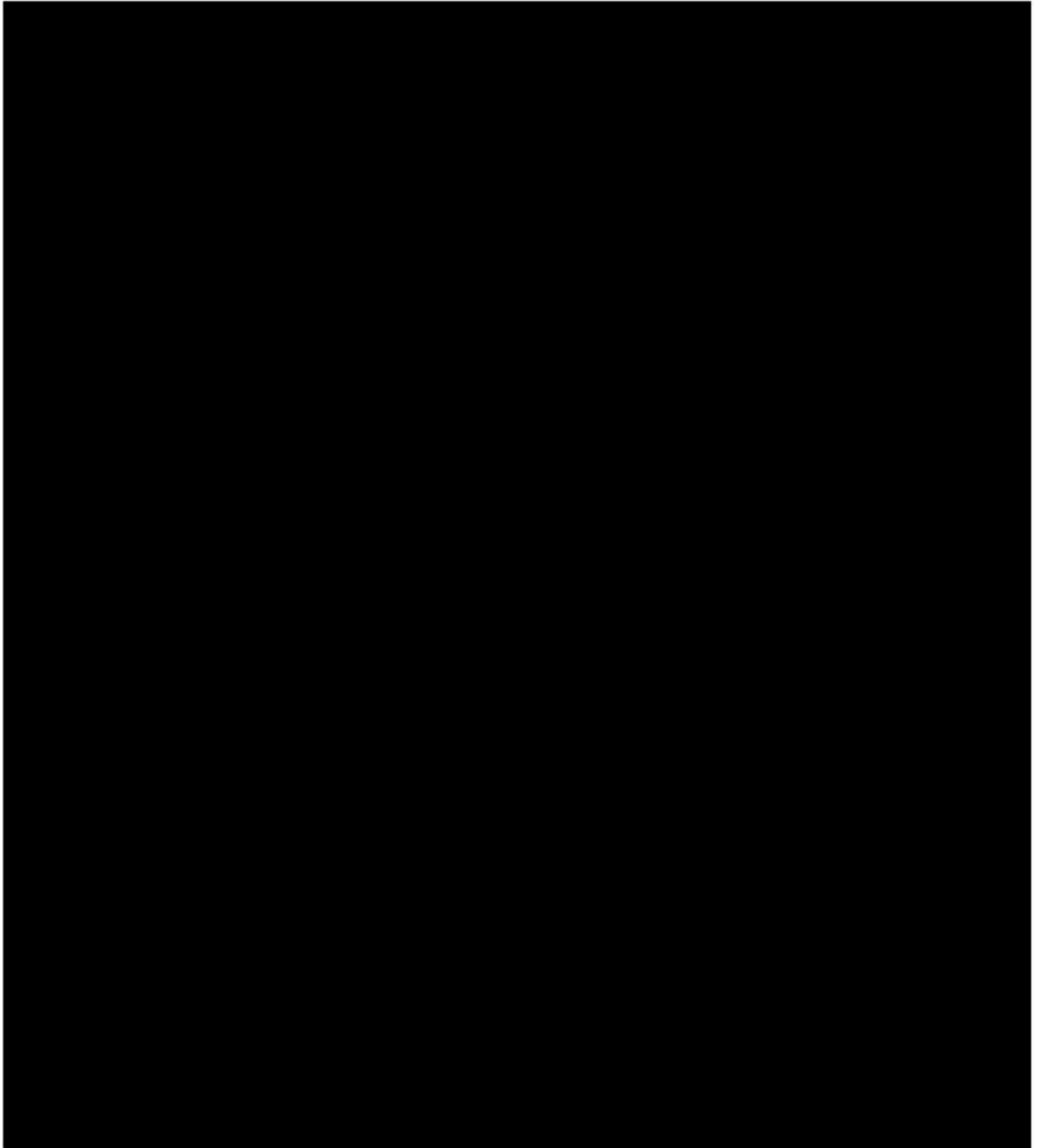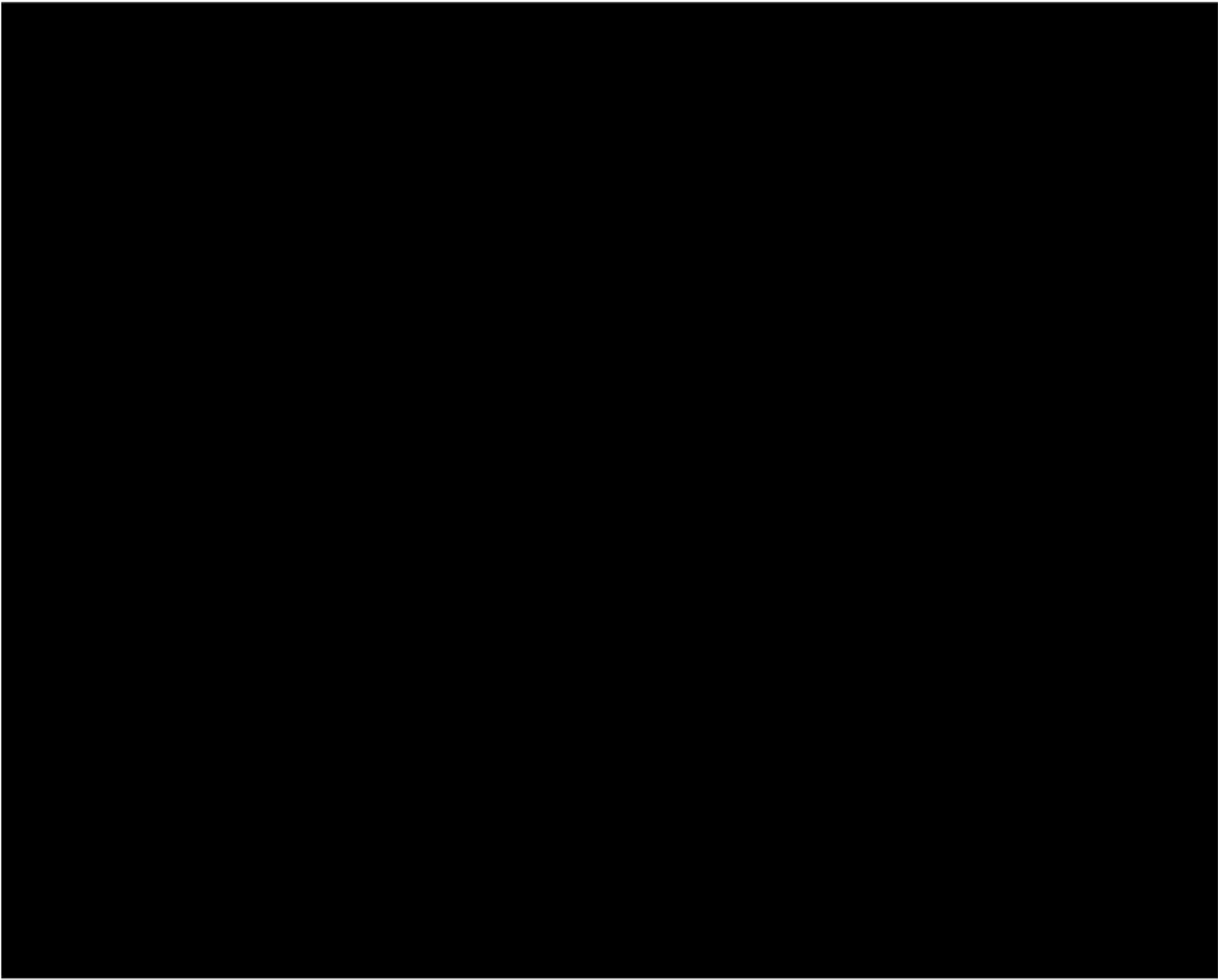
Abstract

Small droplets of pure water freeze at approximately –38 °C. The exact temperature depends on the random arrangement of the water molecules and cannot be predicted precisely. Control over the phase transition from water to ice is therefore a major goal of science, as it would enable countless technical applications. In nature, organisms can survive in polar environments by influencing ice crystallization. So-called ice-binding proteins interact with water molecules and either freeze water at low supercooling or block ice crystal growth.

So-called antifreeze and ice nucleating proteins have structural similarities despite opposite macroscopic effects. This work provides insights into the mechanisms of ice-binding proteins by focusing on ice nucleating proteins of the bacterium *Pseudomonas syringae*, the most effective ice nucleator known. Furthermore, the components of bacteria that influence ice nucleation activity were investigated. Environmentally-relevant effects on the ice nucleating proteins as well as the possible inhibition of ice nucleating proteins by antifreeze proteins were investigated.

As a side project, it was investigated whether perfluorinated compounds exhibit ice nucleation activity. These persistent compounds are present in countless products, but have also been detected in remote regions. Ice nucleation activity of the compounds explains possible pathways of the compounds through the atmosphere.

Zusammenfassung

Kleinste Wassertropfen gefrieren bei ungefähr –38 °C. Die genaue Temperatur hängt dabei von der zufälligen Anordnung der Wassermoleküle ab und ist nicht genau vorhersagbar. Die Kontrolle über den Phasenübergang von Wasser zu Eis ist daher ein großes Ziel der Wissenschaft, das unzählige technische Anwendungen ermöglichen würde. In der Natur findet man Organismen, die ein Überleben im Polarraum ermöglichen, indem die Eiskristallisation beeinflusst wird.

Sogenannte eisbindende Proteine interagieren mit Wassermolekülen und lassen entweder Wasser bei geringer Unterkühlung gefrieren oder blocken das Wachstum des Eiskristalls. Die sogenannten Antifrost und Eisnukleationsproteine weisen trotz gegensätzlicher makroskopischer Effekte strukturelle Gemeinsamkeiten auf. Diese Arbeit gibt Einblicke in die Mechanismen der sogenannten eisbindenden Proteine mit Fokus auf Eisnukleationsproteinen des Bakteriums *Pseudomonas syringae*, dem effektivsten bekannten Eisnukleator. Desweiteren wurde untersucht, welche Komponenten des Bakteriums für die Eisnukleationsaktivität eine Rolle spielen. Es werden dabei Umwelteffekte auf die Eisnukleationsproteine sowie die mögliche Inhibierung dieser durch Antifrost Proteine untersucht.

Als Nebenprojekt der Arbeit wurde zudem untersucht, ob perfluorierte Verbindungen eine Eisnukleationsaktivität aufweisen. Diese persistenten Verbindungen sind in unzähligen Produkten enthalten, wurden aber auch in fernabgelegenen Regionen nachgewiesen. Eisnukleationsaktivität der Verbindungen erklärt mögliche Wege der Verbindungen über die Atmosphere.

1 Introduction

1.1 Ice in Nature

Around two thirds of the earth are covered with water which is essential for life and numerous geophysical processes.[1, 2, 3] Due to Earth's climate, ice formation as well as ice growth are among the most fundamental phenomena and play major roles for organisms.[4] Large parts of the earth have year-round or seasonal temperatures below 0 °C, and, as a result, in polar regions even the temperature of the oceans is below the melting point of pure water. Since the formation and growth of ice is potentially lethal for cells, life at subzero temperatures is challenging for organisms.

Nature evolved organisms which can affect the transition of water into ice and have thus adapted to the environment and the respective climatic conditions. [5, 6, 7] Organisms are classified based on their working mechanism as either freeze-avoiding or freeze-tolerant. Freeze-avoiding species are able to prevent freezing, while freeze-tolerant organisms survive it. Hence, freeze-tolerant organisms control body-freezing by ice nucleating proteins (INP) initiated extracellular ice nucleation at relatively low supercooling.[8] Plants and bacteria often use antifreeze proteins (AFPs) to inhibit the recrystallization of ice and hence limit the damage caused by ice growth at temperatures close to the melting point. [9, 10, 11, 12] Freeze-avoiding species of fish and insects depress the freezing point in their body fluids by colligative effects caused by higher glycerol levels. [13, 14] In other freeze-avoiding fishes and insects, AFPs or AFGPs have been discovered that specifically adsorb to the ice surface and prevent further ice growth. The freezing point of body fluids in the organisms is thereby reduced as a non-colligative effect. [6, 15, 16] Interestingly, certain bacterias were reported to contain both, AFPs and INPs.[17, 18]

Figure 1.1 summarizes the functional diversity of IBPs based on their specific adsorption to ice, which enables cold adapted organisms to survive in subzero regions. A process known as thermal hysteresis (TH) occurs, when adsorption to the surface of embryonic ice crystals blocks further crystal growth in a certain supercooling range. Adsorption to specific ice

planes leads to structural changes in the crystal. Bacterial IBPs are able to access oxygen by binding to floating ice. Ice recrystallization inhibition (IRI) stops crystal growth at temperatures close to the melting point and prevents further cell damages. Ice nucleation initiated by IBPs does not involve supercooling and instead enables crystallization at temperatures just below the melting point.
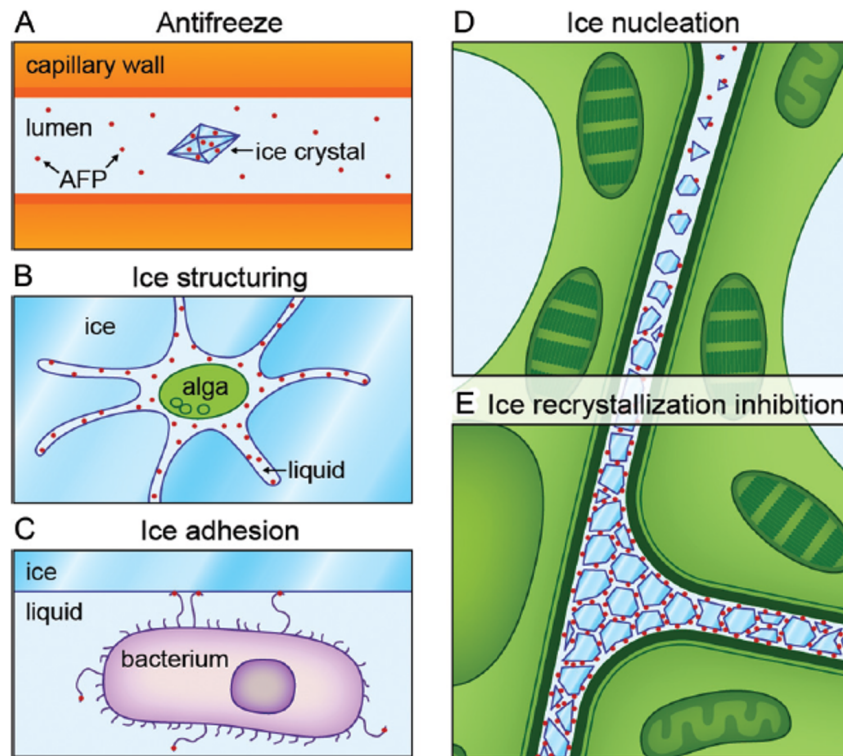
Figure 1.1: Biological functions of ice-binding proteins. Figure taken from Vrielink *et al.*[8] A: AF(G)Ps inhibit the growth of embryonic ice crystals. B: IBPs in microorganisms structure ice crystals to maintain a liquid environment. C: Antarctic bacteria bind to floating ice to access oxygen. D: INPs enable IN at temperatures close to the melting point and hence prevent supercooling. E: Ice recrystallization inhibition properties of IBP stop the crystal growth and prevent freeze damages.

Investigating the interactions of ice and water with biological INs allows comprehensive insights into their mechanism of action, provides a deeper understanding of natural systems, and enables the development of tuneable freezing with technological possibilities in cryobiology, food science and medical applications.

1.2 Ice Nucleation

1.2.1 Homogeneous Ice Nucleation

In 1721, Fahrenheit discovered that liquid water can exist in a supercooled state, in which it is cooled to lower temperature than the equilibrium melting point of ice, T_m. T_m is the temperature at which solid and liquid phase can coexist and is defined by thermodynamics. For pure water at 1 atm the equilibrium melting point is 0 °C. At temperatures above 0 °C liquid water is stable and at temperatures below T_m, the solid phase is favored. In the supercooled state at temperatures below T_m, water can still exist as liquid, however the crystalline phase, ice, is thermodynamically stable and therefore favored. [19] Consequently, supercooled water is a metastable state in which crystallization can start at any time by random nucleation of the water molecules. Ice nucleation occurs when thermal motion leads to randomly formed clusters of water molecules that resemble the structure of ice. For ice formation, a critical cluster size is required, although the clusters also fluctuate in size due to the motion of the water molecules. At lower temperatures, the critical size of the clusters decreases. When a water cluster reaches the critical size, ice formation begins and the liquid water crystallizes. The driving force for this phase transition is the reduction of the free enthalpy based on the thermodynamically favored state. All in all, so called *homogeneous ice nucleation* is a stochastic process in ultrapure water in the absence of any contamination.

1.2.2 Heterogeneous Ice Nucleation

Ice nucleation that occurs through interaction with other molecules is called *heterogeneous ice nucleation*. Molecules or substances which enable nucleation at higher temperatures than homogeneous nucleation are called ice nucleators (INs). INs stabilize the formation of water clusters at the IN–water interface which initiates nucleation at comparatively high subzero temperatures. Although many ice nucleators, such as minerals or dust, are inorganic, the most active INs are biological substances from bacteria, fungi or pollen.[20, 21, 22] Particles that promote the nucleation of ice at temperatures above –15 °C mainly originate from biological samples. [23] The most efficient IN known is from the bacteria *Pseudomonas syringae*, which facilitates nucleation at temperatures up to –2 °C. [20]
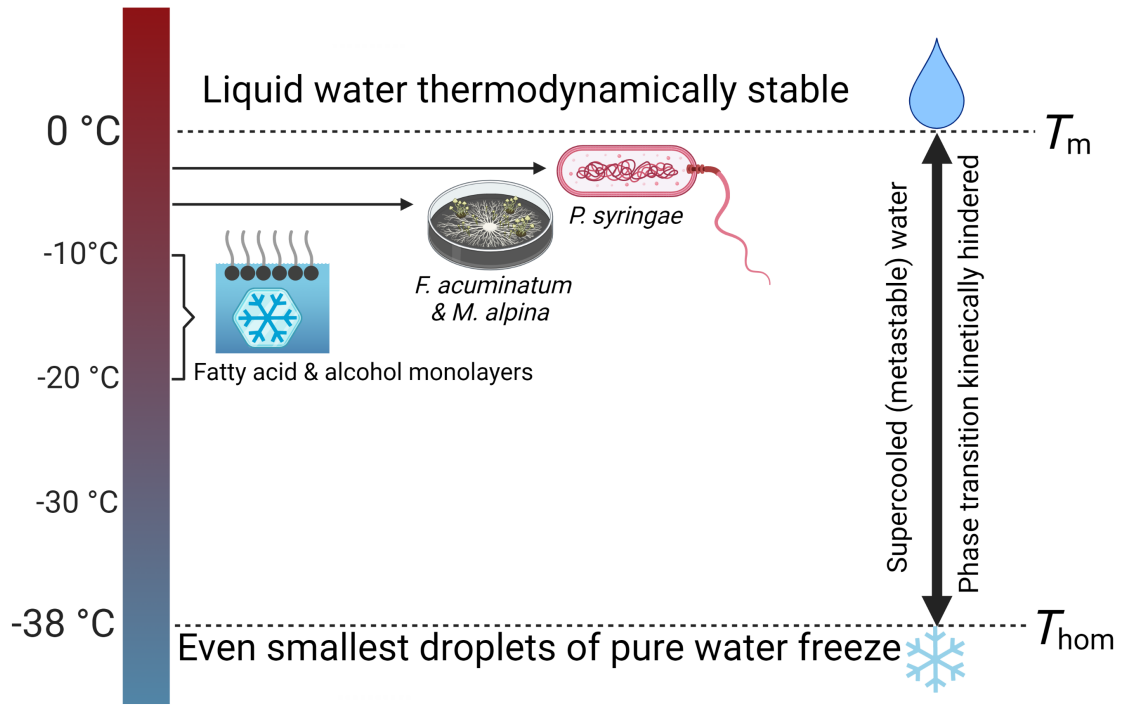
Figure 1.2: Basics of Ice Nucleation: At temperatures below 0 °C ice is thermodynamically favored but kinetically hindered. At temperatures below –38 °C even smallest droplets of pure water freeze. Heterogeneous ice nucleators enable ice nucleation at higher temperatures. Highly-efficient ice nucleators are from bacteria and fungi. Fatty acid monolayers also initiate ice nucleation in metastable, supercooled aqueous solutions.

1.2.3 Classical Nucleation Theory

A theoretical description of homogeneous ice nucleation is given by the *classical nucleation theory*. This theory was established by Turnbull and Fisher in 1949 and is still in the focus of research today as a precise description of thermodynamic parameters remains challenging.[24, 25, 26]

A decrease in entropy and subsequent kinetic hindrance enables water to exist in a supercooled, metastable state. Crystallization requires an embryonic ice crystal, which is randomly formed by the accumulation of water molecules. Due to the very small size and curvature of the assumed-spherical ice crystal, surface effects play an essential role. The energy barrier for crystallization, which depends on a volume term (red) and a surface term (blue), must be overcome.

$$\Delta G_k(T) = n_k \cdot [\mu_i(T) - \mu_w(T)] + 4\pi r_i^2 \cdot \sigma_{iw}(T) \tag{1.1}$$

n_k is the number of water molecules in the embryonic ice crystal, $\mu_{w,i}$ the chemical potential of the water/ice phase, r_i the radius of the embryonic ice crystal and σ_{iw} the interfacial tension between water and ice at a certain temperature T.

The surface term in equation 1.1 always has a positive value whereas the volume term indicates the decrease in the chemical potential due to the formation of the embryonic ice crystal in supersaturated water.

The decrease in chemical potential can be described as a function of temperature T and supersaturation S, where k_B is the Boltzmann constant. S is defined by the ratio of the saturation vapor pressures over water and ice phase p_{sw} and p_{si}.

$$\mu_i(T) - \mu_w(T) = -k_B T \cdot ln(\frac{p_{sw}(T)}{p_{si}(T)}) = -k_B T \cdot ln(S_i) \tag{1.2}$$

In supercooled water, the value of p_{sw} is higher than the value of p_{si}, which results in supersaturation and a negative volume term.[27]

When n_k is replaced by the ratio of the assumed-spherical embryonic ice crystal and the volume of molecular water in ice v_{ice}, the change in Gibbs energy can be expressed as:

$$\Delta G_k(T) = -\frac{k_B T \cdot ln(S_i(T))}{v_{ice}(T)} \cdot \frac{4\pi}{3} r_i^3 + 4\pi r_i^2 \cdot \sigma_{iw}(T) \tag{1.3}$$

The maximum of the energy barrier $\Delta G_k(T)$ (which is the equilibrium of volume and surface term) defines the critical radius r_{crit} of the embryonic ice crystal (see Fig. 1.3).

$$r_{crit} = \frac{2 \cdot v_{ice} \cdot \sigma_{iw}}{k_B T \cdot ln(S_i)} \tag{1.4}$$

An ice embryo smaller than the critical size thus decays immediately because the surface term predominates. Larger ice crystals result in a decreased surface-to-volume ratio and hence thermodynamically favor crystal growth.

To establish the heterogeneous ice nucleation in the classical nucleation theory in addition to the homogeneous ice nucleation, the surface of the IN needs to be considered. The critical energy barrier ΔG_{crit} decreases when the interfacial tension between ice and IN σ_{ii} is lower than between ice and water σ_{iw}. Nucleation is then initiated at the surface of the ice nucleator, which also stabilizes the newly formed ice nucleus by providing an increased volume to surface area ratio.
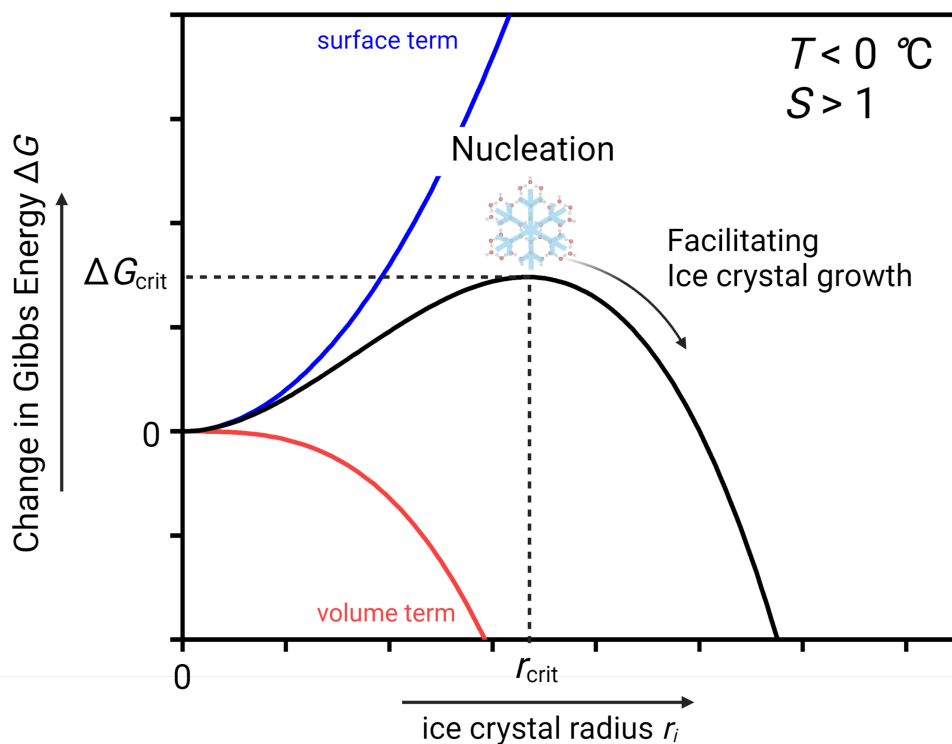
Figure 1.3: Classical Nucleation Theory: The transition of water to ice passes through a local energy maximum due to surface effects. Above a certain critical size, the ice nucleus is thermodynamically stable and further ice growth is favored.

1.3 Ice-binding Proteins

Ice-binding proteins (IBPs) are unique biomolecules which interact with water molecules and affect the transition between water and ice. The presence of IBPs assists organism survival in the presence of ice.[28] The classes of IBPs include antifreeze proteins (AFPs), which depress freezing by thermal hysteresis, and ice nucleating proteins (INPs), which initiate freezing at low supercooling temperatures. Both forms of IBP have a structural commonality: The so-called ice-binding site (IBS), which matches the structure of ice due to a specific amino acid sequence.

1.3.1 Antifreeze Proteins

AFPs are typically small proteins, which are soluble in aqueous solutions and inhibit the crystal growth of embryonic ice crystals by irreversible adsorption to the ice surface.[15] AFPs have been discovered in numerous organisms like fish, bacteria, plants, fungi and insects.[29, 30, 31] The effect of different AFPs on ice growth is as diverse as their structure

Figure 1.4: Antifreeze and ice nucleating proteins: Small antifreeze proteins show a structural variety. Crystal structures of large ice-nucleating proteins have not been determined experimentally, but molecular models indicate similarities to *Tm*AFPs from *Tenebrior molitor*.
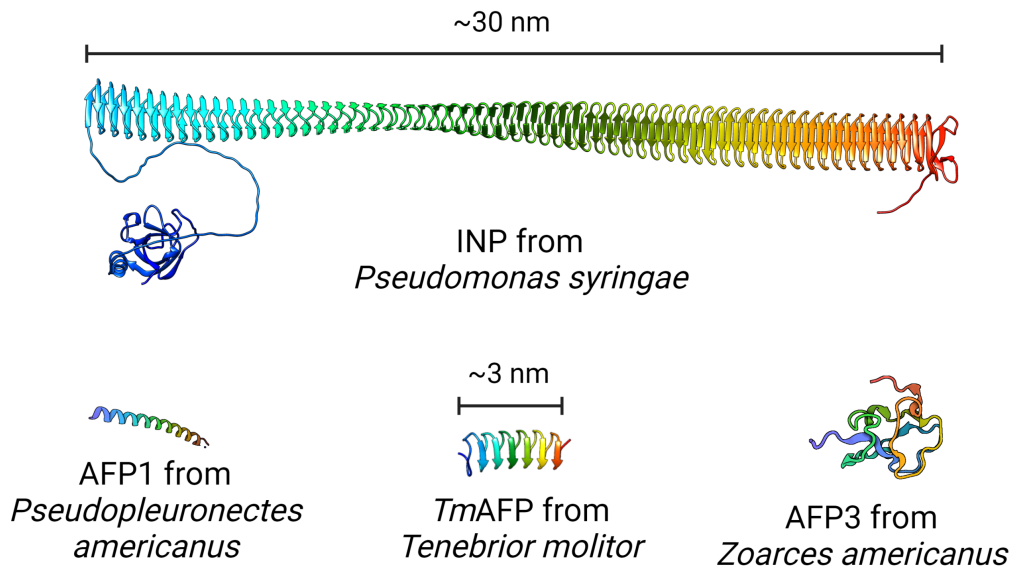
and commonly described by three properties: Thermal hysteresis (TH), ice recrystallization inhibition (IRI) and ice shaping. Physiological concentrations of AFP results in TH of $\sim$ –1 °C in polar fish to $\sim$ –5 °C in insects. Plants contain AFPs which show even lower TH but high IRI activity, which may reduce freeze damages even more. The primary structures of several AFPs are known. [32] Although AFPs share the ability to bind ice, the structures are diverse, ranging from *alpha*-helical structures to β-strands and coils. AFPs interact with relatively few water molecules. As a result, the nucleation temperature is only slightly above the homogeneous nucleation temperature.[33]

1.3.2 Ice Nucleating Proteins

INPs initiate the freezing of supercooled water at temperatures close to the melting point. Biologically catalyzed ice formation initiated by bacterial INPs is the most efficient heterogeneous ice nucleation known, promoting the freezing at temperatures as high as $\sim$ –2 °C. The effect was first discovered in strains of the bacteria *Pseudomonas syringae*, but other gram-negative bacteria such as *Pseudomonas fluorescens*, *Erwinia herbicola*, *Xanthomonas camperstris* and *Pseudomonas borealis* are known to show ice nucleation activity as well.[7, 34, 35, 36, 37]

Most important for this thesis are INPs, that originate from the gram-negative bacteria *Pseudomonas syringae*. The INPs have been described as large proteins anchored in the outer cell membrane. They initiate ice nucleation by ordering water and stabilizing water clusters.[38] The large size (>120 kDa) of the INPs is likely due to functional aggregates or large repetitive multimers, results in unique ice nucletion activity. [33, 39, 40] The primary structure of INPs remains unknown, however it has been determiend that the structure consists of precisely aligned loops of TxT motifs, where T is threonine and x a nonconserved amino acid. Thus, the amino acid sequence bears a very close resemblance to the known structure of *Tm*AFP. [33, 41]

The macroscopic antithetical function of both types of proteins originates from the different sizes of the corresponding IBS. These findings align with the classical nucleation theory, which predicts that for nucleation at higher temperatures a larger ice nucleus is needed.[24] Recently published studies suggest that AFP aggregates may act as INPs.[33]

Aggregation seems to play a major role for the functionality of bacterial ice nucleation.[42] Freezing experiments using the novel high-throughput ice nucleation assay TINA, which is described in Section 2.2, indicate that two IN are present in the bacteria *P. syringae*.
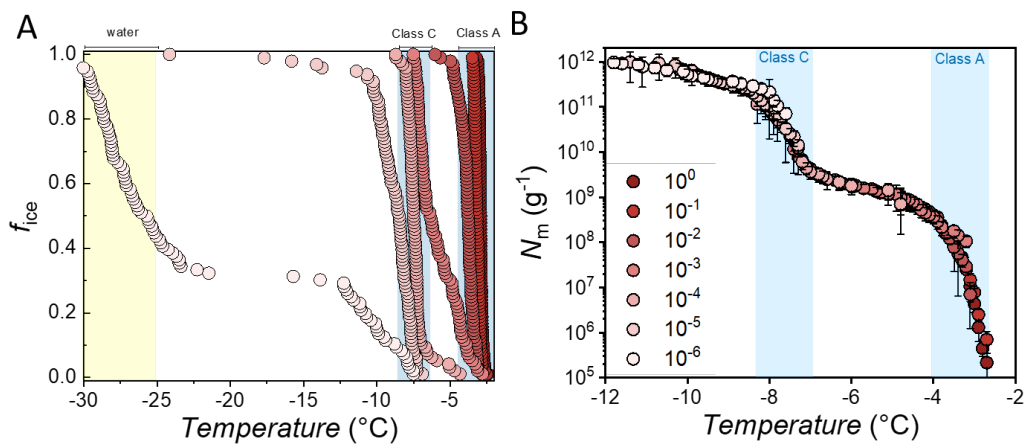
Figure 1.5: Freezing spectra of INPs contained in *P. syringae*. A: Fractions of ice of a wide concentration range from 0.1 mg/mL to 0.1 ng/mL. B: Corresponding cumulative number of active IN per gram present in the sample. The temperature ranges for classes A and C INs are shaded in light blue. The yellow-shaded region presents the temperature range in which pure water freezes in our setup.

The freezing experiments show two temperature ranges, in which the nucleation occurs. The freezing process causes steep increases in the cumulative number of IN N_m at $\sim -3\,°C$ and $\sim -7\,°C$. Previous studies have concluded that the highly-active IN, which nucleates at $\sim -3\,°C$, consists of large aggregates of smaller subunits. Alone, the subunits nucleate at

~ –7 °C. Both INs have been defined by Turner1990 et al. as Class A and Class C, which are indicated in Figure 1.5 plot B. [42]

2 Experimental Challenges

The investigation of biological samples is challenging because of the myriad of molecules present in the sample in addition to the molecules that exhibit the properties of interest. Unravelling the functionality on the molecular level requires a wide range of physicochemical methods to combine macroscopic observations such as ice nucleation activity and molecular insights into the system. Therefore, surface-sensitive sum frequency generation (SFG) and circular dichroism (CD) spectroscopy were used to obtain information about INP-water interphase and the secondary structure of the protein. Because experiments strongly depend on the sample, so-called ice affinity purifcation (IAP) was used to ensure a high quality of ice-binding molecules extracted from the samples.

2.1 Experiments in supercooled water

Performing experiments in the supercooled, metastable state is challenging since ice nucleation might occur due to impurities or large sample volume. Ultrapure water is needed to prevent heterogeneous nucleation initiated by impurities. Only one single ice nucleator is needed to trigger nucleation and freeze the entire sample. Since even the purest water may contain impurities, ice nucleation measurements are performed using microliter droplets. Dividing the sample into hundreds of tiny droplets leads to both homogeneous and heterogeneous nucleation (see Figure 2.1). [19] Another great advantage to small droplet size is the separation of different IN. Highly concentrated samples contain numerous IN, however, a freezing test only allows the determination of a single nucleation temperature. Thus, if different IN are present in the sample, only the heterogeneous nucleation temperature of the most active ice nucleator can be determined. Dividing the sample into droplets in combination with dilution of the sample enables the observation of homogeneous as well as heterogeneous ice nucleation. It is further possible to determine the ice nucleation activity of different IN in the origin sample.
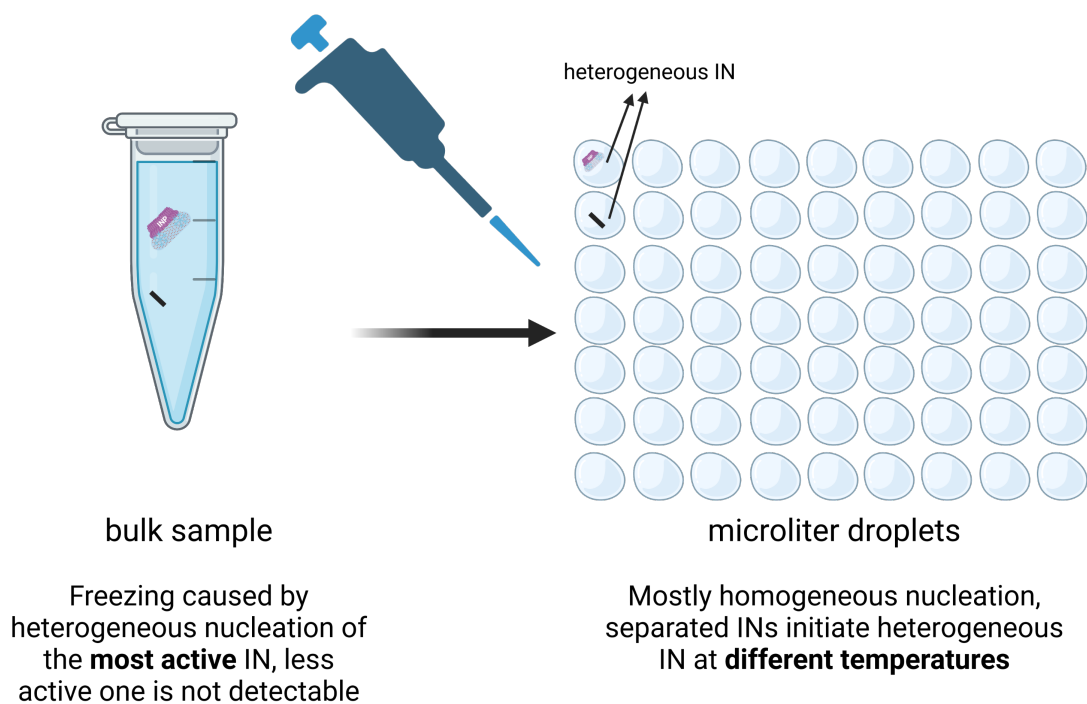
Figure 2.1: Ice nucleation in bulk samples compared to microliter droplet experiments. Minimizing the sample volume enables the determination of homogeneous ice nucleation temperature. In bulk samples even single IN lead to freezing of the whole. Pipetting the sample to a large number of microliter droplets enables the determination of both, heterogeneous and homogeneous ice nucleation temperatures.

2.2 Twin-plate Ice Nucleation Assay (TINA)

The central method of this thesis is a droplet freezing assay that allows accurate determination of ice nucleation efficiency over a wide range of concentrations.

The twin-plate ice nucleation assay (TINA) is a fully-automated droplet freezing assay which was developed to investigate the heterogeneous nucleation efficiency of biological samples.[43] Two 384-well plates enable the characterization and analysis of ice nucleators with high statistics by simultaneously determining hundreds of freezing events per experiment of up to eight concentrations. In a standard high-throughput experiment, the well plates containing seven 10-fold dilutions of the sample and one solvent reference are cooled with a rate of –1 K/min by two independently cooled aluminum blocks. The phase transformation is determined using two IR cameras that track the latent heat release of all 96 3 μL-droplet per sample simultaneously.

Calculating the fraction of ice f_{ice} temperature dependently gives direct insights into the heterogeneous nucleation properties of the sample. f_{ice} is the number of frozen

droplets s divided by the total number of droplets per sample, which is 96 in our experiments.

$$f_{ice} = \frac{s}{96} \tag{2.1}$$

Valis quantitative evaluation of heterogeneous freezing nucleation enables the conversion of fractions of ice (see figure 2.2 B) in a number of active IN in a certain temperature range per mass unit (see figure 2.2 C), assuming ice nucleation as a time independent process.

$$\frac{\Delta N_m}{\Delta T}(T) = -ln(1 - \frac{s}{a - \sum_{i=0}^{j} s}) \cdot \frac{c}{\Delta T} \qquad ; \qquad 0 \le j \le a \tag{2.2}$$

where s is the number of freezing events in bins of $\Delta T = 0.1$ K, a is the total number of droplets, m is the sample mass in the initial solution or suspension. The concentration c is calculated using the volume of the initial sample V_{wash}, the volume of the droplets V_{drop} and the dilution factor d. [43, 44]

$$c = \frac{V_{wash}}{V_{drop}} \cdot \frac{d}{m} \tag{2.3}$$

The cumulative number of active IN per mass unit is calculated by equation 2.4

$$N_m(T) = -ln(1 - \frac{\sum_{i=0}^{j} s}{a}) \cdot c \qquad ; \qquad 0 \le j \le a \tag{2.4}$$

The TINA setup as well as the plotted fractions of ice and corresponding cumulative number of active IN are illustrated in Figure 2.2.
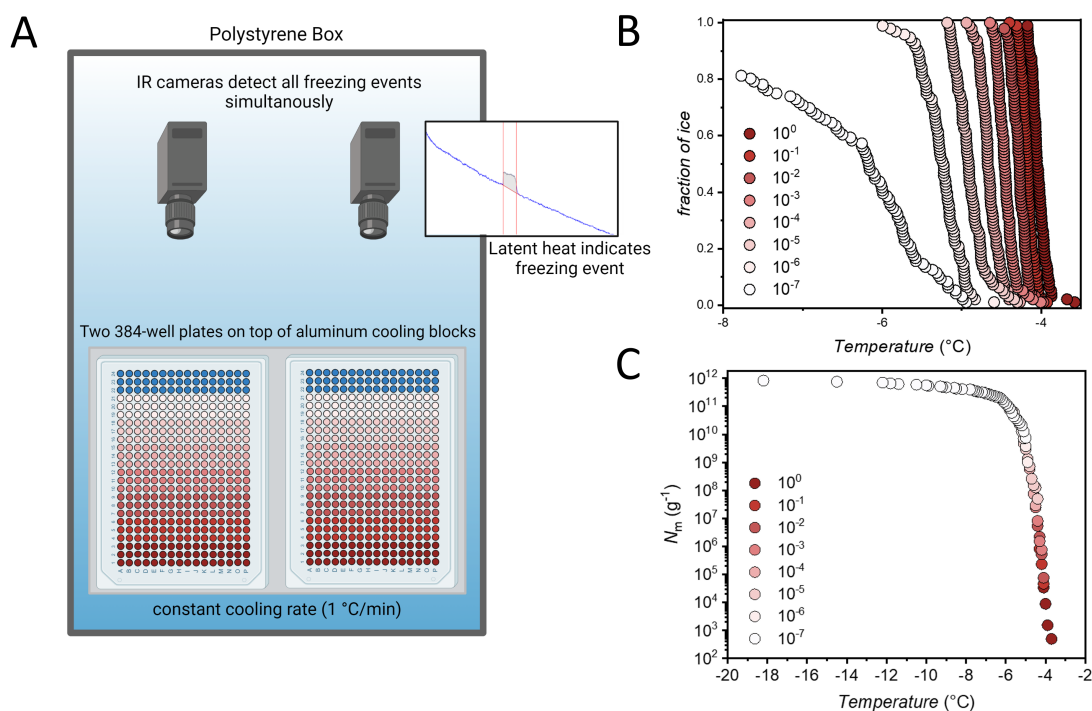
Figure 2.2: A: Schematic representation of the TINA-setup. Two 384-well plates on top of two independent aluminum cooling blocks are cooled with a constant cooling rate of –1 K/min. The freezing events are tracked by two IR-cameras. B: Temperature-dependent fraction of ice plotted for a wide concentration range. Each dot represents one frozen droplet of a certain concentration of *Fusarium acuminatum*. The samples were diluted 10-fold. C: Cumulative number of active ice nucleators per gram of *Fusarium acuminatum*, calculated using Vali equation.

2.3 Ice-Affinity Purification

The IBPs studied in this thesis are components of biological samples. However, these organisms contain several other molecular components that complicate the targeted analysis of IBP. To remove non-ice-binding components and extract the IBP from the biological samples, the ice affinity of the macromolecules described in section 1.3 is used.

The principle of the method was first published by Kuiper *et al.* in 2003 and has been established for the extraction of ice-binding molecules.[45] The two methods used for this work are based on the publications of Marshall *et al..* (see Figure 2.3 A) and Adar *et al..* (see Figure 2.3B).[46, 47]

While the ice shell purification according to Marshall *et al.* was developed for the milligram range in a round flask, the falling water ice purification developed by Adar *et al.* allows for efficient purification of large amounts of IBPs starting from 2.5 L of crude extract using a commercially available ice cube machine.[46]

Ice Affinity Purification to extract all Ice-binding Molecules
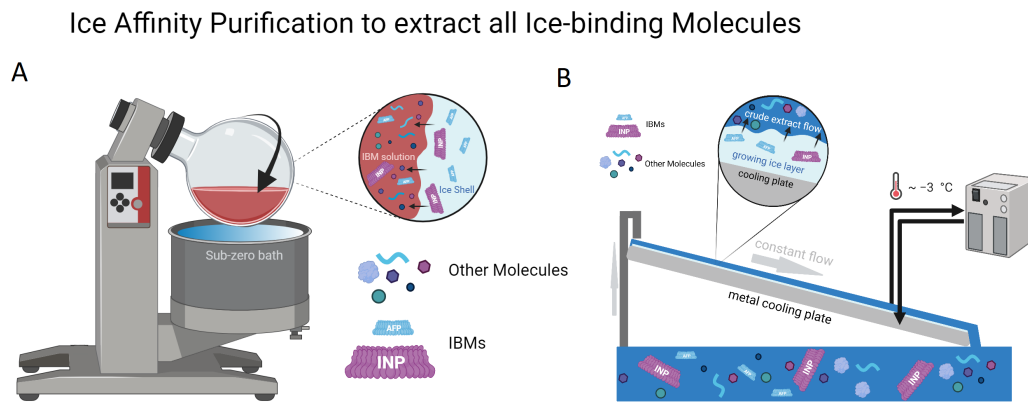
Figure 2.3: Schematic illustrations of ice-affinity purification methods. A: Ice Shell Purification B: Falling Water Ice Affinity Purification

Starting from a crude extract of a biological sample containing IBP, controlled ice growth is initiated by a cooling plate. Based on the structural similarity of IBP and ice, and the resulting ice affinity of INP and AFP, these proteins and all other ice-binding molecules, bind irreversibly to the forming ice.[48, 49] A purification process lasts until 30% to 50% of the crude extract is frozen. The ice is then separated from the extract and lyophilized to obtain IBP.

3 Results & Conclusions

My research resulted in five first-author (thereof two shared first author) and two second author publications in peer-reviewed scientific journals as well as one second-author book-chapter. Two more publications and one patent are in preparation and close to submission. The results are summarized in this chapter.

During my dissertation, I investigated the unique property of biological ice nucleators to initiate a freezing process in even the smallest droplets of pure water at temperatures below the melting point.

The phase transition from liquid water to ice is kinetically inhibited due to surface effects at the interface of water and ice. Embryonic ice crystals formed of water clusters of a critical size are crucial for the freezing process. If a water cluster in a ice-like structure reaches the critical size, the ice crystal continues to grow. Smaller water clusters decay spontaneously. In droplets of microliter to picoliter size, the probability for the random formation of embryonic ice crystals is low due to the strongly limited number of water molecules, which enables supercooling to temperatures down to –38 °C. Organisms such as bacteria and fungi, can support the clustering of water molecules in aqueous solutions and therefore initiate freezing process in droplets. The focus of my research has been on INPs of the bacterium *P. syringae*, which is the most-efficient IN known and is commercially available as a fragmented and freeze-dried product Snomax.

3.1 Environmentally-relevant effects: pH, Ions & Temperature

Climatic conditions, pollution, and other compounds present in the environment can influence ice nucleation activity in organisms.Because the INPs of interest originate from biological sources, it was relevant to investigate concentration dependent IN activity of Snomax in

varying environmental conditions. Activity was measured at altered pH and temperature, as well as in the presence of various salts.[50, 51, 52]

When ice nucleation activity was measured at different pH-values, it was observed that the activity decreases in both the acidic and alkaline range. However, the change in activity induced by the acidic pH-range is much more significant than at basic pH-values. Under acidid conditions, only highly-active INP aggregates were inhibited. The activity of smaller, less active IN was not reduced until extreme pH-values were reached. In this collaborative study, surface sensitive SFG spectroscopy was used to study the protein-initiated alignment of water molecules at the water-air interface. Here, the alignment of the molecules correlates with the charge of the protein. The ice nucleation activity has been shown to correlate with the alignment of the water molecules and thus the charge of the protein. At the isoelectric point, the active IN is inhibited. It was concluded that for the formation of highly-active IN aggregates, the charges of the functional groups are crucial. If the functional groups in the protein are protonated or deprotonated by changing the pH, the formation of functional aggregates associated with an increase in IBS is inhibited. Even if activity partially recovers upon neutralization, maximum activity is not regained. For details of the study see appendix A.1.

Biological ice nucleation activity can also be affected by ions, which are omnipresent in organisms. Ion–protein interactions have been described by the Hofmeister series. In a recent study, the effects of a series of salts on the ice nucleation activity of *P. syringae* were described. The study provided information that bacterial ice nucleation also follows the trend of the Hofmeister series. However, weakly hydrated anions such as perchlorate can cause denaturation of the protein and thus inhibition of the activity. For details of the study see appendix A.4.

In a temperature-dependent study, the arrangement of water at the interface was investigated using SFG spectroscopy. Previous studies had shown that INP-initiated ordering of water molecules at the interface increases with decreasing temperature. In this study, we denatured and inactivated proteins of the bacterium *P. syringae* by heat so that ice nucleation activity was no longer present. The change in secondary structure caused by denaturation was shown by CD spectroscopy and surface sensitive SFG experiments. Proteins were subsequently purified by IAP. The heat-treated INP and untreated INP were then examined by temperature-dependent SFG measurements. No significant difference was found between the samples, so a correlation between SFG signal and ice nucleation activity can be excluded. For details of the study see appendix A.3.

3.2 Effects of AFPs on INPs of *P. syringae*

We investigated whether AFPs can inhibit the activity of INPs.[53] INPs mimic embryonic ice crystals which initiate ice growth, while AFPs bind to crystals to block further growth. Inhibition could be caused by direct binding of AFPs to the INPs IBS or by binding to the initiated embryonic ice crystal. Five different AFPs, which belong to the major classes of AFPs, were investigated in the study. In addition, the effect of BSA as a reference protein and the impacts of inactivated AFPs on INP were investigated. The study clearly showed that the inhibition of INPs by AFPs is not a general effect. Inhibition by AFP1 and enhancement by AFGP1-5 were speculated to be specific membrane-protein interactions, as membrane interactions for these AFPs have been published previously. For details of the study see appendix A.2.

3.3 Ice nucleation active components in *P. syringae*

To investigate which components of the bacterium contribute to the ice nucleation activity, the INP was separated from the membrane by Folch extraction and subsequently purified by IAP.[54] The INA of each component was determined. In addition, various lipids as well as cholesterol, which is present in the membrane, were analyzed. However, the INA of the original system was not observed for any of the components. The highly active Class A with IN temperatures of -2 °C could not be determined. The results are in agreement with previous considerations that see aggregate formation as the cause of Class A. An intact membrane is necessary for the formation of large aggregates. Further measurements in deuterium-water mixtures also indicated that aggregates are larger in deuterated water. For details of the study see appendix A.6.

3.4 Ice Nucleation Activity of Perfluorinated Organic Acids

Perfluorinated acids (PFAs) are persistent and widespread anthropogenic compounds that have been detected in remote regions. In this study, PFAs were tested for ice nucleation activity to understand whether transport pathways via the atmosphere are possible.[55] The results clearly show that PFAs can nucleate ice. By correlating surface tension and ice nucleation activity, a surface-induced nucleation process was concluded. For details of the study see appendix A.5.

3.5 Current work (in preparation)

In a study that is close to submission, we investigated whether INPs are large proteins or aggregates of smaller subunits. The study was performed with INPs from the fungi *Fusarium acuminatum*. In contrast to bacterial INPs from *P. syringae* the samples from *F. acuminatum* contain only one ice nucleator. Filtration experiments and TINA measurements were used to determine the INA of different size fractions. Filtrate and supernatant were characterized and showed no significant differences in composition. Amino acid determinations showed a high content of threonine, serine and aspartic and glutamic acid. Even the *Fusarium acuminatum* filtrates containing INPs below 30 kDa showed ice nucleation at temperatures of approximately –5 °C. It was concluded that the INA of *F. acuminatum* is not caused by large INPs but rather by aggregation of smaller subunits. The decreased ice nucleation activity was attributed to a lower concentration of subunits remaining after filtration, which corresponded to dilution of the original sample by the filtering process. For details of the study see appendix B.2.

Our previous study shows aggregation as a cause of highly efficient IN in fungal INPs. For bacterial INPs from *P. syringae*, aggregation was suggested as key for class A nucleators. As such, it was investigated whether class A aggregates of bacterial INPs can be targeted using polyols. Addition of polyols such as ethylene glycol, glycerol or PVA to bacterial INPs from *P. syringae* in PBS revealed significant differences in the equilibrium between class A and C. Hence, addition of polyols in PBS enables the successful conversion of all INPs into highly active class A INPs. For details of the study see appendix B.1.

Bibliography

[1] P. Ball. Water as an active constituent in cell biology. *Chemical reviews*, 108(1):74–108, 2008.

[2] E. Brini, C. J. Fennell, M. Fernandez-Serra, B. Hribar-Lee, M. Lukšič, and K. A. Dill. How water's properties are encoded in its molecular structure and energies. *Chemical Reviews*, 117(19):12385–12414, 2017.

[3] B. Zobrist, C. Marcolli, T. Peter, and T. Koop. Heterogeneous ice nucleation in aqueous solutions: the role of water activity. *The Journal of Physical Chemistry A*, 112(17):3965–3975, 2008.

[4] V. F. Petrenko and R. W. Whitworth. *Physics of ice*. Oxford University Press Oxford, 1999.

[5] J. P. Costanzo, R. E. Lee, and P. H. Lortz. Glucose concentration regulates freeze tolerance in the wood frog rana sylvatica. *Journal of Experimental Biology*, 181(1):245–255, 1993.

[6] A. L. DeVries and D. E. Wohlschlag. Freezing resistance in some antarctic fishes. *Science*, 163(3871):1073–1075, 1969.

[7] L. R. Maki, Elizabeth L. G., M. Chang-Chien, and D. R. Caldwell. Ice nucleation induced by pseudomonas syringae. *Applied microbiology*, 28(3):456–459, 1974.

[8] A. S. Oude Vrielink, A. Aloi, L. L. C. Olijve, and I. K. Voets. Interaction of ice binding proteins with ice, water and ions. *Biointerphases*, 11(1):018906, 2016.

[9] C. A. Knight, A. L. DeVries, and L. D. Oolman. Fish antifreeze protein and the freezing and recrystallization of ice. *Nature*, 308(5956):295–296, 1984.

[10] C. A. Knight, J. Hallett, and A. L. DeVries. Solute effects on ice recrystallization: an assessment technique. *Cryobiology*, 25(1):55–60, 1988.

[11] J. A. Raymond, C. Fritsen, and K. Shen. An ice-binding protein from an antarctic sea ice bacterium. *FEMS microbiology ecology*, 61(2):214–221, 2007.

[12] A. Hudait, N. Odendahl, Y. Qiu, F. Paesani, and V. Molinero. Ice-nucleating and antifreeze proteins recognize ice through a diversity of anchored clathrate and ice-like motifs. *Journal of the American Chemical Society*, 140(14):4905–4912, 2018.

[13] J. A. Raymond. Glycerol is a colligative antifreeze in some northern fishes. *Journal of Experimental Zoology*, 262(3):347–352, 1992.

[14] R. A. Ring and D. Tesar. Adaptations to cold in canadian arctic insects. *Cryobiology*, 18(2):199–211, 1981.

[15] G. L. Fletcher, C. L. Hew, and P. L. Davies. Antifreeze proteins of teleost fishes. *Annual review of physiology*, 63(1):359–390, 2001.

[16] J. G. Duman. Antifreeze and ice nucleator proteins in terrestrial arthropods. *Annual Review of Physiology*, 63(1):327–357, 2001.

[17] S. L. Wilson, D. L. Kelley, and V. K. Walker. Ice-active characteristics of soil bacteria selected by ice-affinity. *Environmental microbiology*, 8(10):1816–1824, 2006.

[18] H. Kawahara, Y. Nakano, K. Omiya, N. Muryoi, J. Nishikawa, and H. Obata. Production of two types of ice crystal-controlling proteins in antarctic bacterium. *Journal of bioscience and bioengineering*, 98(3):220–223, 2004.

[19] T. Koop. Homogeneous ice nucleation in water and aqueous solutions. *Zeitschrift für physikalische Chemie*, 218(11):1231–1258, 2004.

[20] L. M. Kozloff, M. A. Schofield, and M. Lute. Ice nucleating activity of pseudomonas syringae and erwinia herbicola. *Journal of bacteriology*, 153(1):222–231, 1983.

[21] A. T. Kunert, M. L. Pöhlker, K. Tang, C. S. Krevert, C. Wieder, K. R. Speth, L. E. Hanson, C. E. Morris, David G. Schmale III, U. Pöschl, and J. Fröhlich-Nowoisky. Macromolecular fungal ice nuclei in fusarium: effects of physical and chemical processing. *Biogeosciences*, 16(23):4647–4659, 2019.

[22] B. G. Pummer, H. Bauer, J. Bernardi, S. Bleicher, and H. Grothe. Suspendable macromolecules are responsible for ice nucleation activity of birch and conifer pollen. *Atmospheric Chemistry and Physics*, 12(5):2541–2550, 2012.

[23] S. Huang, W. Hu, J. Chen, Z. Wu, D. Zhang, and P. Fu. Overview of biological ice nucleating particles in the atmosphere. *Environment International*, 146:106197, 2021.

[24] D. Turnbull and J. C. Fisher. Rate of nucleation in condensed systems. *The Journal of chemical physics*, 17(1):71–73, 1949.

[25] L. Ickes, A. Welti, C. Hoose, and U. Lohmann. Classical nucleation theory of homogeneous freezing of water: thermodynamic and kinetic parameters. *Physical Chemistry Chemical Physics*, 17(8):5514–5537, 2015.

[26] T. Koop and B. J. Murray. A physically constrained classical description of the homogeneous nucleation of ice in water. *The Journal of chemical physics*, 145(21):211915, 2016.

[27] D. M. Murphy and T. Koop. Review of the vapour pressures of ice and supercooled water for atmospheric applications. *Quarterly Journal of the Royal Meteorological Society: A journal of the atmospheric sciences, applied meteorology and physical oceanography*, 131(608):1539–1565, 2005.

[28] M. Bar Dolev, I. Braslavsky, and P. L. Davies. Ice-binding proteins and their function. *Annual review of biochemistry*, 85:515–542, 2016.

[29] A. L. DeVries, S. K. Komatsu, and R. E. Feeney. Chemical and physical properties of freezing point-depressing glycoproteins from antarctic fishes. *Journal of Biological Chemistry*, 245(11):2901–2908, 1970.

[30] K. E. Zachariassen and J. A. Husby. Antifreeze effect of thermal hysteresis agents protects highly supercooled insects. *Nature*, 298(5877):865–867, 1982.

[31] J. G. Duman and T. M. Olsen. Thermal hysteresis protein activity in bacteria, fungi, and phylogenetically diverse plants. *Cryobiology*, 30(3):322–328, 1993.

[32] Peter L Davies and Brian D Sykes. Antifreeze proteins. *Current opinion in structural biology*, 7(6):828–834, 1997.

[33] Y. Qiu, A. Hudait, and V. Molinero. How size and aggregation of ice-binding proteins control their ice nucleation efficiency. *Journal of the American Chemical Society*, 141(18):7439–7452, 2019.

[34] L. R. Maki and K. J. Willoughby. Bacteria as biogenic sources of freezing nuclei. *Journal of Applied Meteorology and Climatology*, 17(7):1049–1053, 1978.

[35] S. E. Lindow, D. C. Arny, and C. D. Upper. Erwinia herbicola: a bacterial ice nucleus active in increasing frost injury to corn. *Phytopathology*, 68(3):523–527, 1978.

[36] J. Zhao and C. S. Orser. Conserved repetition in the ice nucleation gene inax from xanthomonas campestris pv. translucens. *Molecular and General Genetics MGG*, 223(1):163–166, 1990.

[37] Z. Wu, L. Qin, and V. K. Walker. Characterization and recombinant expression of a divergent ice nucleation protein from 'pseudomonas borealis'. *Microbiology*, 155(4):1164–1169, 2009.

[38] P. K. Wolber. Bacterial ice nucleation. *Advances in microbial physiology*, 34:203–237, 1993.

[39] D. Schmid, D. Pridmore, G. Capitani, R. Battistutta, J. Neeser, and A. Jann. Molecular organisation of the ice nucleation protein inav from pseudomonas syringae. *FEBS letters*, 414(3):590–594, 1997.

[40] R. L. Green and G. J. Warren. Physical and functional repetition in a bacterial ice nucleation gene. *Nature*, 317(6038):645–648, 1985.

[41] A. Hudait, D. R. Moberg, Y. Qiu, N. Odendahl, F. Paesani, and V. Molinero. Preordering of water is not needed for ice recognition by hyperactive antifreeze proteins. *Proceedings of the National Academy of Sciences*, 115(33):8266–8271, 2018.

[42] M. A. Turner, F. Arellano, and L. M. Kozloff. Three separate classes of bacterial ice nucleation structures. *Journal of bacteriology*, 172(5):2521–2526, 1990.

[43] A. T. Kunert, M. Lamneck, F. Helleis, U. Pöschl, M. L. Pöhlker, and J. Fröhlich-Nowoisky. Twin-plate ice nucleation assay (tina) with infrared detection for high-throughput droplet freezing experiments with biological ice nuclei in laboratory and field samples. *Atmospheric Measurement Techniques*, 11(11):6327–6337, 2018.

[44] G. Vali. Quantitative evaluation of experimental results an the heterogeneous freezing nucleation of supercooled liquids. *Journal of Atmospheric Sciences*, 28(3):402–409, 1971.

[45] M. J. Kuiper, C. Lankin, S. Y. Gauthier, V. K. Walker, and P. L. Davies. Purification of antifreeze proteins by adsorption to ice. *Biochemical and biophysical research communications*, 300(3):645–648, 2003.

[46] C. Adar, V. Sirotinskaya, M. Bar Dolev, T. Friehmann, and I. Braslavsky. Falling water ice affinity purification of ice-binding proteins. *Scientific reports*, 8(1):1–9, 2018.

[47] C. J. Marshall, K. Basu, and P. L. Davies. Ice-shell purification of ice-binding proteins. *Cryobiology*, 72(3):258–263, 2016.

[48] K. Meister, A. L. DeVries, H. J. Bakker, and R. Drori. Antifreeze glycoproteins bind irreversibly to ice. *Journal of the American Chemical Society*, 140(30):9365–9368, 2018.

[49] Y. Celik, R. Drori, N. Pertaya-Braun, A. Altan, T. Barton, M. Bar-Dolev, A. Groisman, P. L. Davies, and I. Braslavsky. Microfluidic experiments reveal that antifreeze proteins bound to ice crystals suffice to prevent their growth. *Proceedings of the National Academy of Sciences*, 110(4):1309–1314, 2013.

[50] M. Lukas, R. Schwidetzky, A. T. Kunert, U. Pöschl, J. Fröhlich-Nowoisky, M. Bonn, and K. Meister. Electrostatic interactions control the functionality of bacterial ice nucleators. *Journal of the American Chemical Society*, 142(15):6842–6846, 2020.

[51] M. Lukas, R. Schwidetzky, A. T. Kunert, E. H. G. Backus, U. Pöschl, J. Fröhlich-Nowoisky, M. Bonn, and K. Meister. Interfacial water ordering is insufficient to explain ice-nucleating protein activity. *The Journal of Physical Chemistry Letters*, 12(1):218–223, 2021.

[52] R. Schwidetzky, M. Lukas, A. YazdanYar, A. T. Kunert, U. Pöschl, K. F. Domke, J. Fröhlich-Nowoisky, M. Bonn, T. Koop, Y. Nagata, and K. Meister. Specific ion–protein interactions influence bacterial ice nucleation. *Chemistry–A European Journal*, 27(26):7402–7407, 2021.

[53] R. Schwidetzky, A. T. Kunert, M. Bonn, U. Pöschl, H. Ramløv, A. L. DeVries, J. Fröhlich-Nowoisky, and K. Meister. Inhibition of bacterial ice nucleators is not an intrinsic property of antifreeze proteins. *The Journal of Physical Chemistry B*, 124(24):4889–4895, 2020.

[54] R. Schwidetzky, P. Sudera, A. T. Backes, U. Pöschl, M. Bonn, J. Fröhlich-Nowoisky, and K. Meister. Membranes are decisive for maximum freezing efficiency of bacterial ice nucleators. *The Journal of Physical Chemistry Letters*, 12(44):10783–10787, 2021.

[55] R. Schwidetzky, Y. Sun, J. Fröhlich-Nowoisky, A. T. Kunert, M. Bonn, and K. Meister. Ice nucleation activity of perfluorinated organic acids. *The Journal of Physical Chemistry Letters*, 12(13):3431–3435, 2021.

A Publications

A.1 Lukas *et al.*, J. Am. Chem. Soc., 2019

Electrostatic Interactions Control the Functionality of Bacterial Ice Nucleators

M. Lukas[1], R. Schwidetzky[1], A. T. Kunert[2], U. Pöschl[2], J. Fröhlich-Nowoisky[2], M. Bonn[1], and K. Meister[1,3]

[1] Max-Planck-Institute for Polymer Research, 55128 Mainz, Germany
[2] Max-Planck-Institute for Chemistry, 55128 Mainz, Germany
[3] University of Alaska Southeast, Juneau, Alaska 99801, United States

Author contributions:

R.S. performed the freezing experiments and contributed to analyzing and discussing the results as well as writing the manuscript.

Electrostatic Interactions Control the Functionality of Bacterial Ice Nucleators

M. Lukas, R. Schwidetzky, A. T. Kunert, U. Pöschl, J. Fröhlich-Nowoisky, M. Bonn, and K. Meister*

ACCESS | 📊 Metrics & More | 📰 Article Recommendations | SI Supporting Information

ABSTRACT: Bacterial ice-nucleating proteins (INPs) promote heterogeneous ice nucleation more efficiently than any other material. The details of their working mechanism remain elusive, but their high activity has been shown to involve the formation of functional INP aggregates. Here we reveal the importance of electrostatic interactions for the activity of INPs from the bacterium *Pseudomonas syringae* by combining a high-throughput ice nucleation assay with surface-specific sum-frequency generation spectroscopy. We determined the charge state of nonviable *P. syringae* as a function of pH by monitoring the degree of alignment of the interfacial water molecules and the corresponding ice nucleation activity. The net charge correlates with the ice nucleation activity of the INP aggregates, which is minimal at the isoelectric point. In contrast, the activity of INP monomers is less affected by pH changes. We conclude that electrostatic interactions play an essential role in the formation of the highly efficient functionally aligned INP aggregates, providing a mechanism for promoting aggregation under conditions of stress that prompt the bacteria to nucleate ice.

Ice formation is the most important liquid-to-solid phase transition on earth and is strongly affected by the presence of nucleators that initiate heterogeneous ice nucleation at temperatures above −40 °C. There is a large variety of compounds that can act as ice nucleators, and their efficiency strongly differs.[1−5] The most efficient ice nucleators are bacteria from *Pseudomonas syringae,* which can initiate the crystallization of water at temperatures as high as −2 °C.[6,7] The ability of bacteria to nucleate ice is caused by specialized ice-nucleating proteins (INPs) that are anchored in the outer membrane on the bacterial cell wall.[8] Bacterial INPs contain a large central-repeat domain that has been proposed to be the active site and which is responsible for ice nucleation through a mechanism that likely involves the preordering of water.[9,10] Apart from the specific ice-binding site, the high ice nucleation activity of INPs has been shown to depend on the size of the nucleation size and the ability to aggregate into larger protein clusters.[11−15] INPs have repeatedly been shown to aggregate in the bacterial outer membranes,[5,8,15−17] and both the number of INPs in the aggregate and the sub-angstrom distance between the INPs affect the ice nucleation efficiency.[11] Based on their activity, the INP aggregates are typically divided into classes as shown in Figure 1.[12] Class A consists of large aggregates (>50 INPs) that are responsible for freezing at temperatures between −2 and −4 °C.[12] Class B consists of smaller aggregates that induce freezing at −5 to −6.5 °C, and class C consists of mostly monomeric INPs that induce ice formation between −7 to −12 °C.[12] In nature, the aggregation of INPs occurs under conditions of stress, which require the bacteria to nucleate ice.[7] The INP aggregation mechanism and whether INP aggregation in cell membranes is promoted by a change in chemistry is unknown. Notably, lowering the pH to acidic values has been shown to reduce the ice nucleation activity of bacterial INPs.[12,18−20] In contrast, changing the pH

to alkaline values did not affect the nucleation activity.[12] The molecular origin for this pH sensitivity is unknown, but a better understanding would provide needed insights into the driving forces of INP aggregation. Moreover, it would have direct implications for understanding biological ice nucleation in the atmosphere, where pH levels are oftentimes acidic due to anthropogenic activities.[18]

Figure 1 shows the results of ice nucleation measurements of the bacterial ice nucleator Snomax at three pH values. Snomax is a commonly used model system for biological and atmospheric ice nucleation studies,[20−22] and it consists of a preparation of inactivated bacteria cells of *P. syringae*. The initial Snomax solutions in water had a concentration of 0.1 mg/mL and a pH of ∼6.2. The samples were then serially diluted, resulting in concentrations from 1 ng/mL to 1 mg/mL. The cumulative ice nucleator number concentration (N_m) was calculated using Vali's formula, and it represents the number of ice nucleators per unit weight that are active above a certain temperature.[23]

For the bacterial ice nucleator solution in water (pH ∼6.2), the spectrum shows two strong increases in $N_m(T)$ around ∼−2.9 °C and ∼−7.5 °C with plateaus between ∼−4.5 °C and ∼−7 °C and above ∼−9.5 °C. The two rises in the spectrum reveal that the ice nucleation activity of *P. syringae* stems from two classes of ice nucleators with different activation temperatures. The plateaus at temperatures T below each
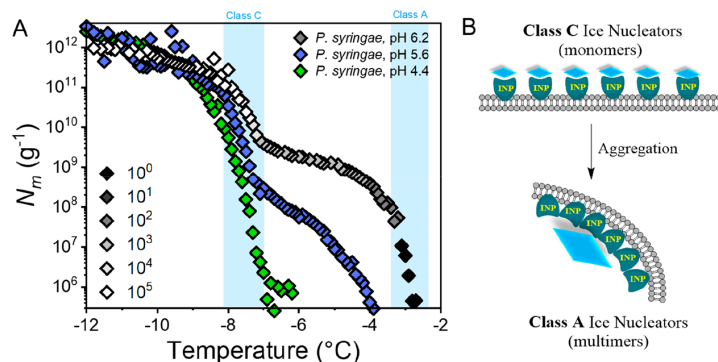
Figure 1. Freezing experiments of aqueous solutions of Snomax containing bacterial ice nucleators from *P. syringae* in water and at different pH values. (A) Shown is the cumulative number of ice nucleators (N_m) per unit mass of Snomax vs temperature. Numbers in the legend denote dilution factors. The temperature ranges for class A and C bacterial ice nucleators are shaded in blue.[12] (B) Schematic structure of class A and C nucleators in a membrane. Class C refers to mostly monomeric INPs, which aggregate to form the highly efficient class A nucleators. Both the number of INPs in the aggregate and the sub-angstrom distance between INPs affect the ice nucleation efficiency.
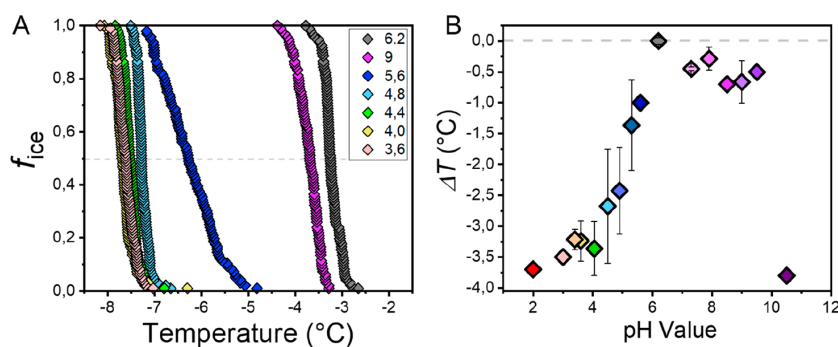

Figure 2. Freezing experiments of aqueous solutions of Snomax containing bacterial ice nucleators from *P. syringae* at different pH values. (A) Fraction of frozen droplets (f_{ice}) for highly concentrated (0.1 mg/mL) Snomax solutions. (B) Temperature shifts ΔT induced by different pH values. Shifts represent the difference at f_{ice} = 0.5 between Snomax in water (pH ∼6.2) and at different pH values. Error bars represent the standard deviation for multiple independent measurements.

increase of $N_m(T)$ arise when fewer ice nucleators at these temperatures are present.[21] We attribute the observed rises at ∼−2.9 °C and ∼−7.5 °C to class A and C ice nucleators, respectively.

For lower pH solutions, the trend looks markedly different. At pH 5.6 the rise at ∼− 2.9 °C is absent; instead, we observe a rise at ∼−4.5 °C. Further, the second rise at ∼−7.5 °C is slightly shifted by ∼−0.5 °C. Evidently, lowering the pH influences the ability of the ice-nucleating proteins to form the more efficient class A aggregates. Further lowering the pH fortifies this effect, and at a pH of ∼4.4, the class C nucleators have disappeared; apparently, class A nucleators were converted into class C. While class A nucleators are very pH-sensitive, class C nucleators are only weakly affected by pH variations.

To obtain a more detailed picture of the effect of the pH, we conducted a comprehensive evaluation of pH values of 2−10.5, as shown in Figure 2. We find that the change of pH gives rise to different effects, as shown in Figure 2B: (i) Lowering the pH to acidic values shifts the freezing point of class A to lower temperatures. This trend increases until pH ∼4, where the resulting freezing temperature ∼−7 °C closely resembles that of class C nucleators. The more acidic conditions clearly prevent the formation of highly efficient class A aggregates,

reducing the activity of class A to that of class C. (ii) Raising the pH to basic conditions has a small effect on class A ice nucleators, and the resulting response looks similar to that of bacteria in water, only shifted by ∼0.6 °C to lower temperatures (Figures 2B and S1). (iii) Raising the pH to extreme basic conditions shifts the freezing point by ∼3.5 °C to lower temperatures. The resulting freezing temperature of ∼− 7 °C resembles that of class C nucleators.

To investigate the molecular origin of the strong pH dependence of bacterial INP's ice nucleation efficiency, we conducted sum-frequency generation (SFG) spectroscopic experiments of Snomax adsorbed to the air−water interface at different pH values. SFG is a surface-specific method that can be used to probe interfacial water of biomolecules.[24,25] In this technique, an infrared and a visible pulse are combined at a surface to generate light at the sum frequency of the two incident fields. The technique is bulk-forbidden in isotropic media, and only ensembles of molecules with a net orientation, e.g., at an interface, can generate a detectable signal. The SFG signal intensity depends on the number of aligned molecules at the interface.

At charged surfaces, the surface field can align the water dipoles. Such charge-induced enhanced ordering of the interfacial water molecules causes the signal intensity in the
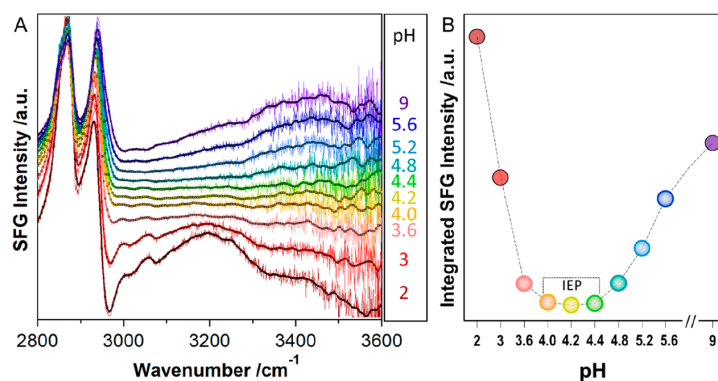
Figure 3. (A) SFG spectra of aqueous solutions of Snomax containing bacterial ice nucleators from *P. syringae* at the air−water interface as a function of bulk pH. The bulk concentration of Snomax was 0.1 mg/mL. (B) Integrated SFG intensity of the frequency region from 3100 to 3600 cm^{-1} for Snomax (*P. syringae*) at different bulk pH values.

O−H stretching region (3150−3600 cm^{-1}) to increase, and, inversely, the SFG signal intensity can be used to quantify the amount of charge at the electrified surface (Figure S2). This concept has previously been applied to determine the isoelectric point (IEP) of proteins.[26−29] Figure 3A shows pH-dependent SFG spectra of aqueous solutions of Snomax adsorbed to the air−water interface. In the frequency region from 2800 to 3100 cm^{-1}, the SFG spectra show strong signals from C−H stretching vibrations. At frequencies above 3100 cm^{-1}, the spectrum shows a broad response from the O−H stretching band of interfacial water molecules. The SFG intensity of the CH and OH groups shows substantial changes when the solution pH is altered. We find that at pH values of ∼4.2, the intensity of the O−H stretching signals is close to zero, whereas, at values below and above, the intensity of the O−H bands increases markedly and dominates the SFG spectrum of *P. syringae*. The observed changes in the C−H region can be explained with interferences with the O−H resonances.[27,28] To more accurately determine the IEP of *P. syringae*, we integrated the SFG signal in the frequency region of ∼3100−3600 cm^{-1}. Figure 3B shows the pH dependence of the integrated intensity of the O−H stretching region. The lowest value for *P. syringae* was found at pH ∼4.2, which corresponds to the point of no net charge or IEP of the bacteria. The interfacial IEP of ∼4.2 is similar to the bulk IEP of 4.0 that was previously reported for *P. syringae*[30] and consistent with the bulk IEP between 3 and 4 that we infer from zeta-potential measurements (Figure S3).

Ice nucleation bacteria are being studied extensively due to their important roles in precipitation and frost injury of plants.[31] Elucidating the impact of environmental factors such as the pH is essential for understanding not only atmospheric ice nucleation processes but also the functionality of INP aggregates. Electrostatic properties are governed by the distribution and ratio of charged and polar residues within protein structures and are among the most important factors that determine the functionality, stability, and interactions of proteins. We demonstrate that acidic pH values reduce the ice-nucleating activity of nonviable *P. syringae* bacteria and that the effect arises from the inactivation of the highly efficient class A aggregates active at high subzero temperatures. In contrast, we find no significant influence of mild basic pH values on the ice nucleation activity. The effect of acidic pH on the ice nucleation activity of *P. syringae* has previously been observed,

and those results are consistent with our findings.[6,12,18,19] Turner et al. proposed that the acidic pH denatures the larger class A INP complexes and that this process is irreversible.[12] Unlike Turner et al., we observe that the ice nucleation activity of the class A INP aggregates can be partially recovered upon raising the pH back to neutral values (Figures S4−S6). Combined, the pH-dependent SFG and droplet freezing experiments revealed that eliminating the net negative charge of *P. syringae* correlates with the decrease of the ice nucleation activity from the large class A INP aggregates. We explain these observations with the formation of misfolded INP aggregates as a result of the decreased charge repulsion. Upon lowering the pH toward pH 4.2, negatively charged amino acids are protonated, and the net charge is reduced. The large numbers of glutamic acid residues contained in INPs of *P. syringae* are likely candidates for protonation.[10] As a result of the protonation, the charge repulsion between INP monomers is absent, and hydrophobic interactions cause the INPs to misfold. These newly formed INP aggregates differ substantially from the precisely aligned functional class A INP aggregates (Figures S7 and S8) and lack the ice nucleation activity at high subzero temperatures. Consequently, only single INPs or smaller aggregates, i.e. class C nucleators, remain active at acidic pH, which is in line with our experimental observations. The finding that the ice nucleation activity can be recovered by going back to neutral pH further provides evidence that no irreversible denaturation of INPs occurs. In contrast, the drop of the freezing point at extremely basic conditions can not be recovered, which we explain with (partial) irreversible denaturation of the INP aggregates (Figure S9). In nature, the aggregation of INPs occurs in the cell membrane of ice-nucleating bacteria under conditions of stress that require them to nucleate ice.[7] The alteration of the pH in the system would provide a means to trigger INP aggregation in the cell membrane.

■ ASSOCIATED CONTENT

Ⓢ Supporting Information

The Supporting Information is available free of charge at https://pubs.acs.org/doi/10.1021/jacs.9b13069.

> Experimental setups, experimental methods, effect of alkaline pH on ice nucleation activity, effect of reversibility of acidic and alkaline pH change, Supporting Figures S1−S9 (PDF)

■ AUTHOR INFORMATION

Corresponding Author

K. Meister − *Max Planck Institute for Polymer Research, 55128 Mainz, Germany; University of Alaska Southeast, Juneau, Alaska 99801, United States;* ⓞ orcid.org/0000-0002-6853-6325; Email: meisterk@mpip-mainz.mpg.de

Authors

M. Lukas − *Max Planck Institute for Polymer Research, 55128 Mainz, Germany*

R. Schwidetzky − *Max Planck Institute for Polymer Research, 55128 Mainz, Germany*

A. T. Kunert − *Max Planck Institute for Chemistry, 55128 Mainz, Germany*

U. Pöschl − *Max Planck Institute for Chemistry, 55128 Mainz, Germany;* ⓞ orcid.org/0000-0003-1412-3557

J. Fröhlich-Nowoisky − *Max Planck Institute for Chemistry, 55128 Mainz, Germany;* ⓞ orcid.org/0000-0002-1278-0054

M. Bonn − *Max Planck Institute for Polymer Research, 55128 Mainz, Germany;* ⓞ orcid.org/0000-0001-6851-8453

Complete contact information is available at:
https://pubs.acs.org/10.1021/jacs.9b13069

Notes

The authors declare no competing financial interest.

■ REFERENCES

(1) Murray, B. J.; O'Sullivan, D.; Atkinson, J. D.; Webb, M. E. Ice nucleation by particles immersed in supercooled cloud droplets. *Chem. Soc. Rev.* **2012**, *41* (19), 6519−6554.

(2) Pummer, B. G.; Budke, C.; Augustin-Bauditz, S.; Niedermeier, D.; Felgitsch, L.; Kampf, C. J.; Huber, R. G.; Liedl, K. R.; Loerting, T.; Moschen, T.; Schauperl, M.; Tollinger, M.; Morris, C. E.; Wex, H.; Grothe, H.; Pöschl, U.; Koop, T.; Fröhlich-Nowoisky, J. Ice nucleation by water-soluble macromolecules. *Atmos. Chem. Phys.* **2015**, *15* (8), 4077−4091.

(3) Kunert, A. T.; Pöhlker, M. L.; Krevert, C. S.; Wieder, C.; Speth, K. R.; Hanson, L. E.; Morris, C. E.; Schmale, D. G., III; Pöschl, U.; Fröhlich-Nowoisky, J. Highly active and stable fungal ice nuclei are widespread among Fusarium species. *Biogeosciences* **2019**, *16* (23), 4647−4659.

(4) Mueller, G. M.; Wolber, P. K.; Warren, G. J. Clustering of ice nucleation protein correlates with ice nucleation activity. *Cryobiology* **1990**, *27* (4), 416−422.

(5) Schmid, D.; Pridmore, D.; Capitani, G.; Battistutta, R.; Neeser, J.-R.; Jann, A. J. F. l. Molecular organisation of the ice nucleation protein InaV from Pseudomonas syringae. *FEBS Lett.* **1997**, *414* (3), 590−594.

(6) Kozloff, L. M.; Schofield, M. A.; Lute, M. Ice nucleating activity of Pseudomonas syringae and Erwinia herbicola. *J. Bacteriol.* **1983**, *153* (1), 222−231.

(7) Maki, L. R.; Galyan, E. L.; Chang-Chien, M. M.; Caldwell, D. R. Ice nucleation induced by pseudomonas syringae. *Appl. Microbiol.* **1974**, *28* (3), 456−459.

(8) Govindarajan, A. G.; Lindow, S. E. Size of bacterial ice-nucleation sites measured in situ by radiation inactivation analysis. *Proc. Natl. Acad. Sci. U. S. A.* **1988**, *85* (5), 1334−8.

(9) Garnham, C. P.; Campbell, R. L.; Walker, V. K.; Davies, P. L. Novel dimeric beta-helical model of an ice nucleation protein with bridged active sites. *BMC Struct. Biol.* **2011**, *11*, 36.

(10) Pandey, R.; Usui, K.; Livingstone, R. A.; Fischer, S. A.; Pfaendtner, J.; Backus, E. H. G.; Nagata, Y.; Fröhlich-Nowoisky, J.; Schmüser, L.; Mauri, S.; Scheel, J. F.; Knopf, D. A.; Pöschl, U.; Bonn, M.; Weidner, T. Ice-nucleating bacteria control the order and dynamics of interfacial water. *Science Advances* **2016**, *2* (4), No. e1501630.

(11) Gurian-Sherman, D.; Lindow, S. E. Bacterial ice nucleation: significance and molecular basis. *FASEB J.* **1993**, *7* (14), 1338−43.

(12) Turner, M. A.; Arellano, F.; Kozloff, L. M. Three separate classes of bacterial ice nucleation structures. *J. Bacteriol.* **1990**, *172* (5), 2521−2526.

(13) Qiu, Y.; Hudait, A.; Molinero, V. How Size and Aggregation of Ice-Binding Proteins Control Their Ice Nucleation Efficiency. *J. Am. Chem. Soc.* **2019**, *141* (18), 7439−7452.

(14) Liu, K.; Wang, C.; Ma, J.; Shi, G.; Yao, X.; Fang, H.; Song, Y.; Wang, J. Janus effect of antifreeze proteins on ice nucleation. *Proc. Natl. Acad. Sci. U. S. A.* **2016**, *113* (51), 14739−14744.

(15) Bai, G.; Gao, D.; Liu, Z.; Zhou, X.; Wang, J. Probing the critical nucleus size for ice formation with graphene oxide nanosheets. *Nature* **2019**, *576* (7787), 437−441.

(16) Southworth, M. W.; Wolber, P. K.; Warren, G. J. Nonlinear relationship between concentration and activity of a bacterial ice nucleation protein. *J. Biol. Chem.* **1988**, *263* (29), 15211−15216.

(17) Mueller, G. M.; Wolber, P. K.; Warren, G. J. J. C. Clustering of ice nucleation protein correlates with ice nucleation activity. *Cryobiology* **1990**, *27* (4), 416−422.

(18) Attard, E.; Yang, H.; Delort, A. M.; Amato, P.; Pöschl, U.; Glaux, C.; Koop, T.; Morris, C. E. Effects of atmospheric conditions on ice nucleation activity of *Pseudomonas*. *Atmos. Chem. Phys.* **2012**, *12* (22), 10667−10677.

(19) Kawahara, H.; Tanaka, Y.; Obata, H. Isolation and Characterization of a Novel Ice-nucleating Bacterium, Pseudomonas sp. KUIN-4, Which Has Stable Activity in Acidic Solution. *Biosci., Biotechnol., Biochem.* **1995**, *59* (8), 1528−1532.

(20) Wex, H.; Augustin-Bauditz, S.; Boose, Y.; Budke, C.; Curtius, J.; Diehl, K.; Dreyer, A.; Frank, F.; Hartmann, S.; Hiranuma, N.; Jantsch, E.; Kanji, Z. A.; Kiselev, A.; Koop, T.; Möhler, O.; Niedermeier, D.; Nillius, B.; Rösch, M.; Rose, D.; Schmidt, C.; Steinke, I.; Stratmann, F. Intercomparing different devices for the investigation of ice nucleating particles using Snomax® as test substance. *Atmos. Chem. Phys.* **2015**, *15* (3), 1463−1485.

(21) Budke, C.; Koop, T. BINARY: an optical freezing array for assessing temperature and time dependence of heterogeneous ice nucleation. *Atmos. Meas. Tech.* **2015**, *8* (2), 689−703.

(22) Kunert, A. T.; Lamneck, M.; Helleis, F.; Pöschl, U.; Pöhlker, M. L.; Fröhlich-Nowoisky, J. Twin-plate Ice Nucleation Assay (TINA) with infrared detection for high-throughput droplet freezing experiments with biological ice nuclei in laboratory and field samples. *Atmos. Meas. Tech.* **2018**, *11* (11), 6327−6337.

(23) Vali, G. Quantitative Evaluation of Experimental Results and the Heterogeneous Freezing Nucleation of Supercooled Liquids. *J. Atmos. Sci.* **1971**, *28* (3), 402−409.

(24) Meister, K.; Strazdaite, S.; DeVries, A. L.; Lotze, S.; Olijve, L. L. C.; Voets, I. K.; Bakker, H. J. Observation of ice-like water layers at an aqueous protein surface. *Proc. Natl. Acad. Sci. U. S. A.* **2014**, *111* (50), 17732−17736.

(25) Meister, K.; Paananen, A.; Speet, B.; Lienemann, M.; Bakker, H. J. Molecular Structure of Hydrophobins Studied with Site-Directed Mutagenesis and Vibrational Sum-Frequency Generation Spectroscopy. *J. Phys. Chem. B* **2017**, *121* (40), 9398−9402.

(26) Devineau, S.; Inoue, K.-i.; Kusaka, R.; Urashima, S.-h.; Nihonyanagi, S.; Baigl, D.; Tsuneshige, A.; Tahara, T. Change of the isoelectric point of hemoglobin at the air/water interface probed by the orientational flip-flop of water molecules. *Phys. Chem. Chem. Phys.* **2017**, *19* (16), 10292−10300.

(27) Engelhardt, K.; Peukert, W.; Braunschweig, B. Vibrational sum-frequency generation at protein modified air-water interfaces: Effects of molecular structure and surface charging. *Curr. Opin. Colloid Interface Sci.* **2014**, *19* (3), 207−215.

31

(28) Strazdaite, S.; Meister, K.; Bakker, H. J. Orientation of polar molecules near charged protein interfaces. *Phys. Chem. Chem. Phys.* **2016**, *18* (10), 7414−7418.

(29) Guckeisen, T.; Hosseinpour, S.; Peukert, W. Isoelectric Points of Proteins at the Air/Liquid Interface and in Solution. *Langmuir* **2019**, *35* (14), 5004−5012.

(30) Horká, M.; Horký, J.; Matoušková, H.; Šlais, K. Free flow and capillary isoelectric focusing of bacteria from the tomatoes plant tissues. *Journal of Chromatography A* **2009**, *1216* (6), 1019−1024.

(31) Morris, C. E.; Conen, F.; Alex Huffman, J.; Phillips, V.; Poschl, U.; Sands, D. C. Bioprecipitation: a feedback cycle linking earth history, ecosystem dynamics and land use through biological ice nucleators in the atmosphere. *Global change biology* **2014**, *20* (2), 341−51.

Supporting Information:

Electrostatic Interactions Control the Functionality of

Bacterial Ice Nucleators

Authors: Max Lukas[1], Ralph Schwidetzky[1], Anna Theresa Kunert[2], Ulrich Pöschl[2], Janine Fröhlich-Nowoisky[2], Mischa Bonn[1], and Konrad Meister[1]

Affiliations:

[1]Max Planck Institute for Polymer Research, 55128 Mainz, Germany

[2]Max Planck Institute for Chemistry, 55128 Mainz, Germany

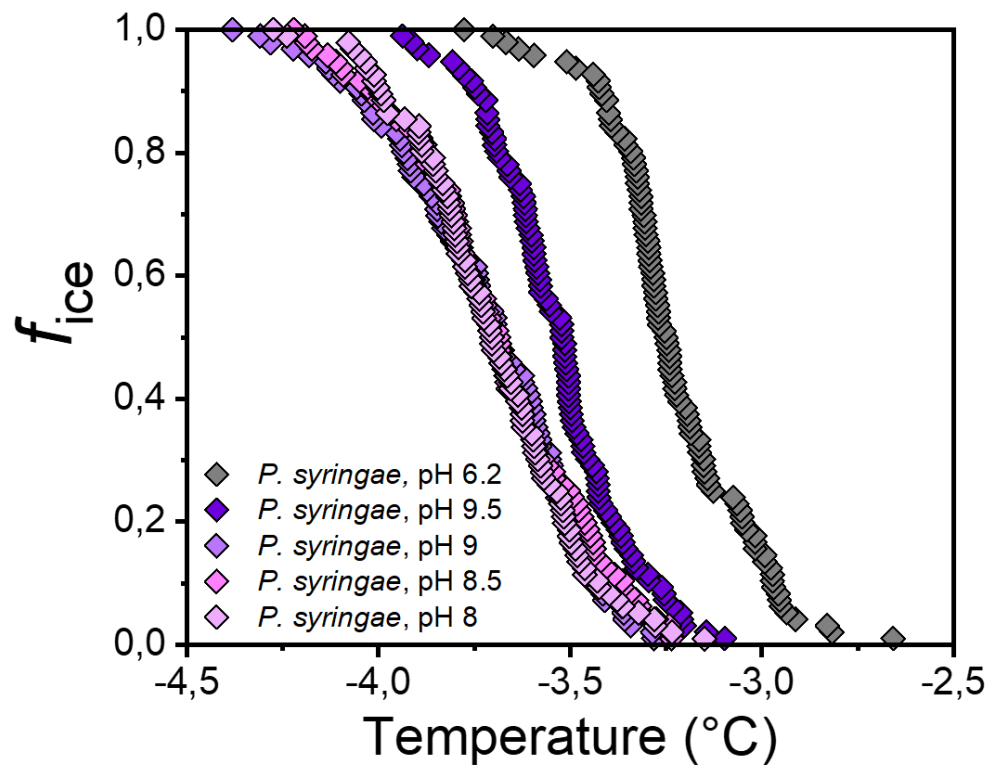[3]University of Alaska Southeast, 99801 Juneau, AK, United States

Figure S1: Freezing experiments of aqueous solutions of Snomax containing bacterial ice nucleators from *P. syringae* at alkaline pH values. Fraction of frozen droplets (f_{ice}) for highly concentrated (0.1 mg/mL samples) Snomax (*P. syringae*) solutions.
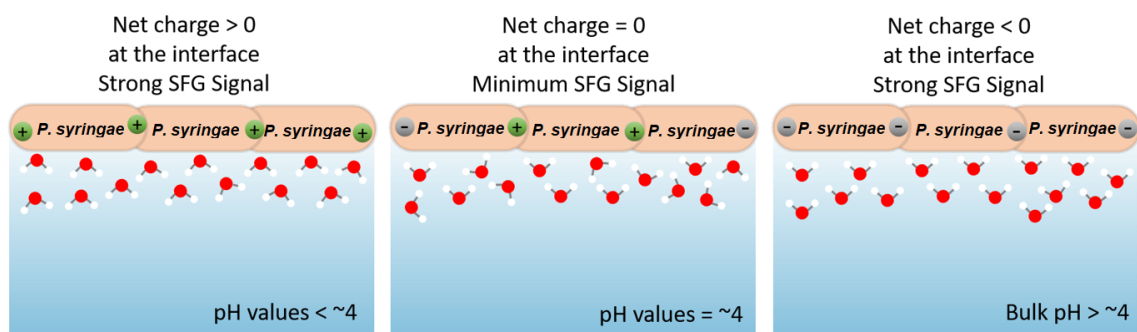
Figure S2: Schematic representation of the orientation of interfacial water molecules next to *P. syringae* as a function of pH.
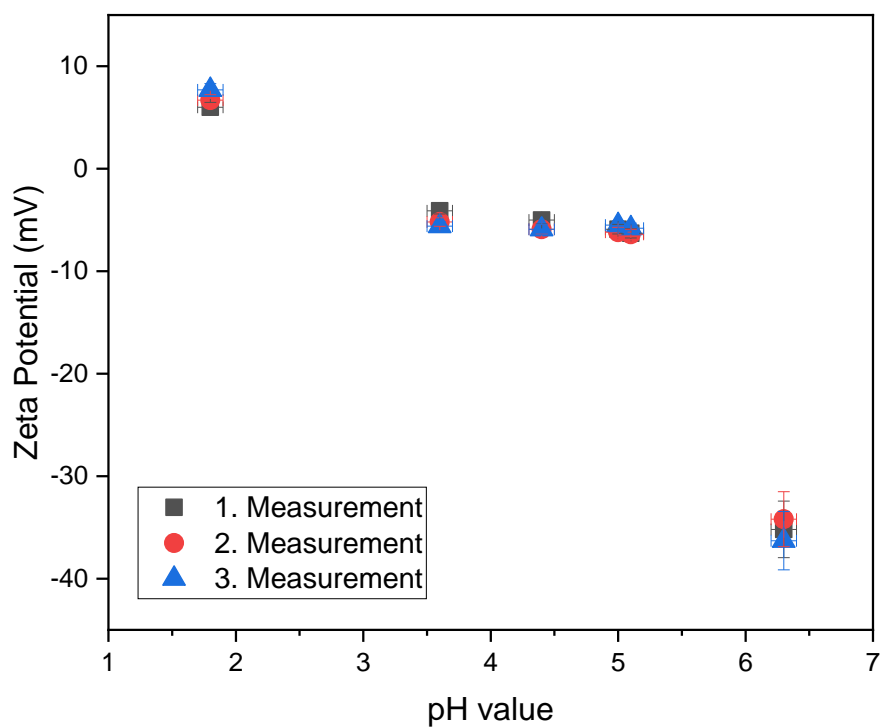
Figure S3: Zeta potential measurements of aqueous solutions of Snomax containing bacterial ice nucleators from *P. syringae*, measured in 0.1 g/L solutions. From this plot, the isoelectric point was estimated to be between 3 and 3.5.

S4

Figure S4: Freezing experiments of aqueous solutions of Snomax containing bacterial ice nucleators from *P. syringae* as a function of pH values. Fraction of frozen droplets (f_{ice}) for highly concentrated (0.1 mg/mL) Snomax (*P. syringae)* solutions, in which the pH was first decreased using HCl and then increased using NaOH.
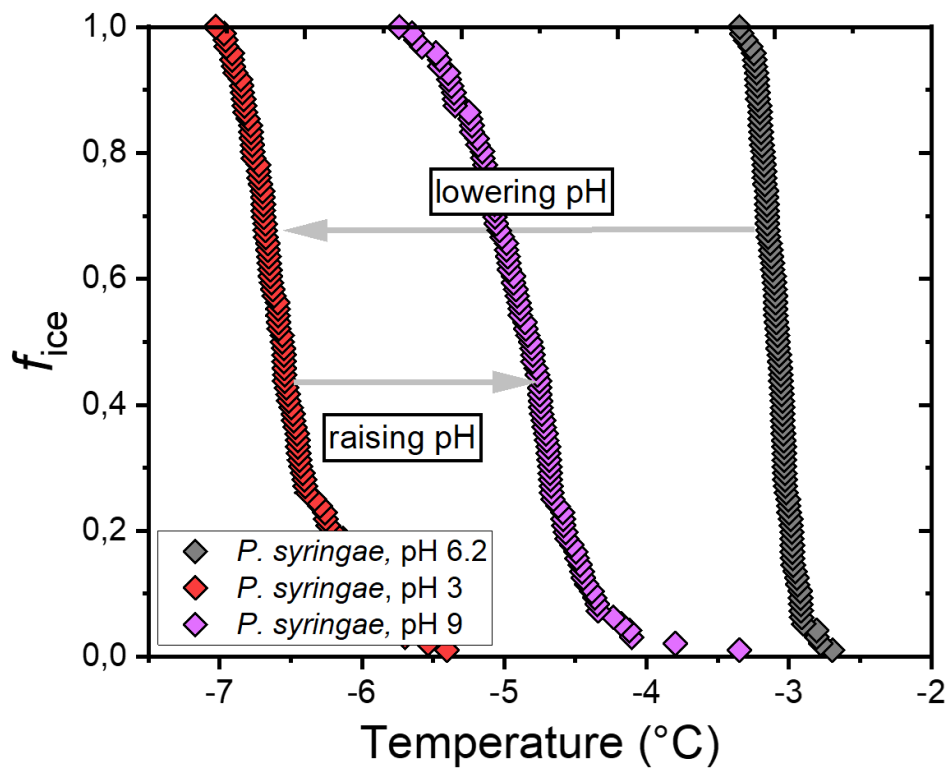
S5

Figure S5: Freezing experiments of aqueous solutions of Snomax containing bacterial ice nucleators from *P. syringae* as a function of pH values. Fraction of frozen droplets (f_{ice}) for highly concentrated (0.1 mg/mL) Snomax (*P. syringae)* solutions, in which the pH was first decreased using HCl and then increased using NaOH.
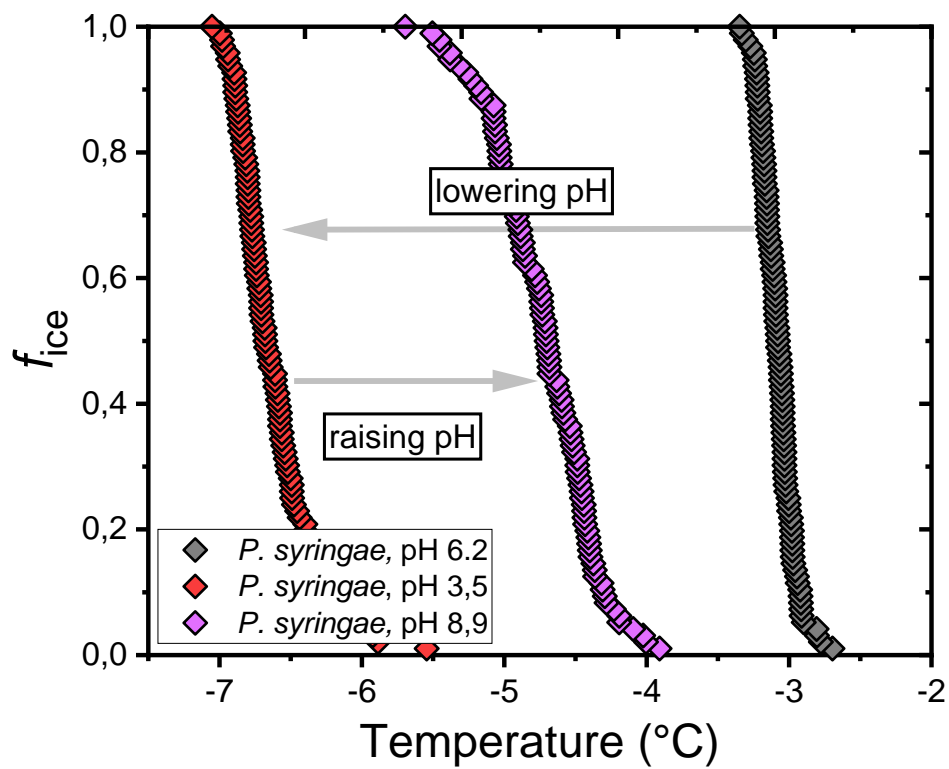
Figure S6: Freezing experiments of aqueous solutions of Snomax containing bacterial ice nucleators from *P. syringae* as a function of pH values. Fraction of frozen droplets (f_{ice}) for highly concentrated (0.1 mg/mL) Snomax (*P. syringae)* solutions, in which the pH was first decreased and then increased using acetate buffer.

S7
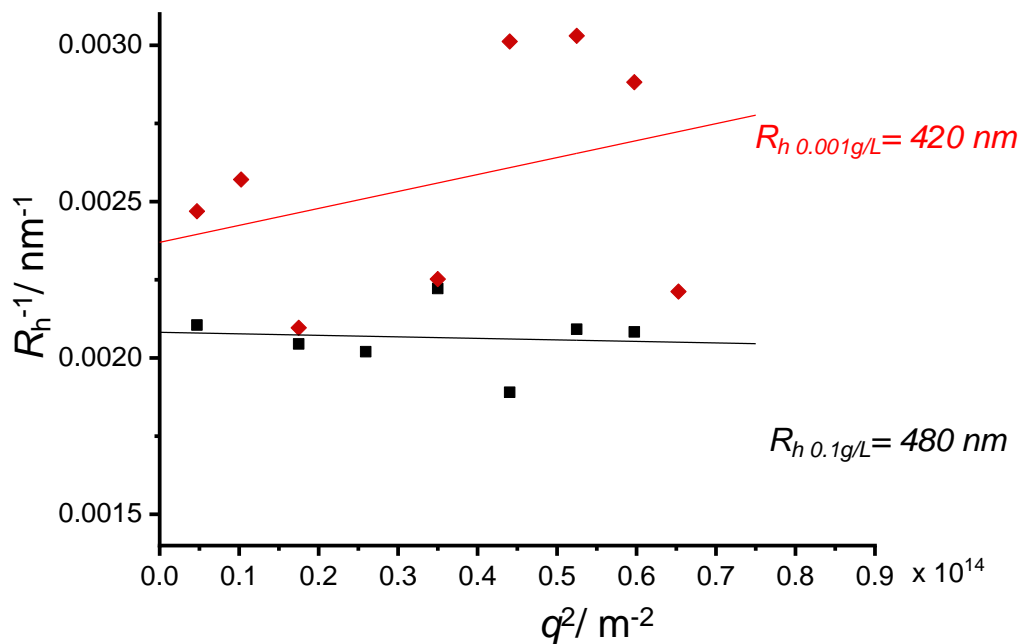
Figure S7: Hydrodynamic radii of Snomax containing bacterial ice nucleators from *P. syringae* at 0.1 g/L and at 0.001 g/L. The radii at higher concentration are larger, suggestsing that larger aggregates are present in the solution.

S8
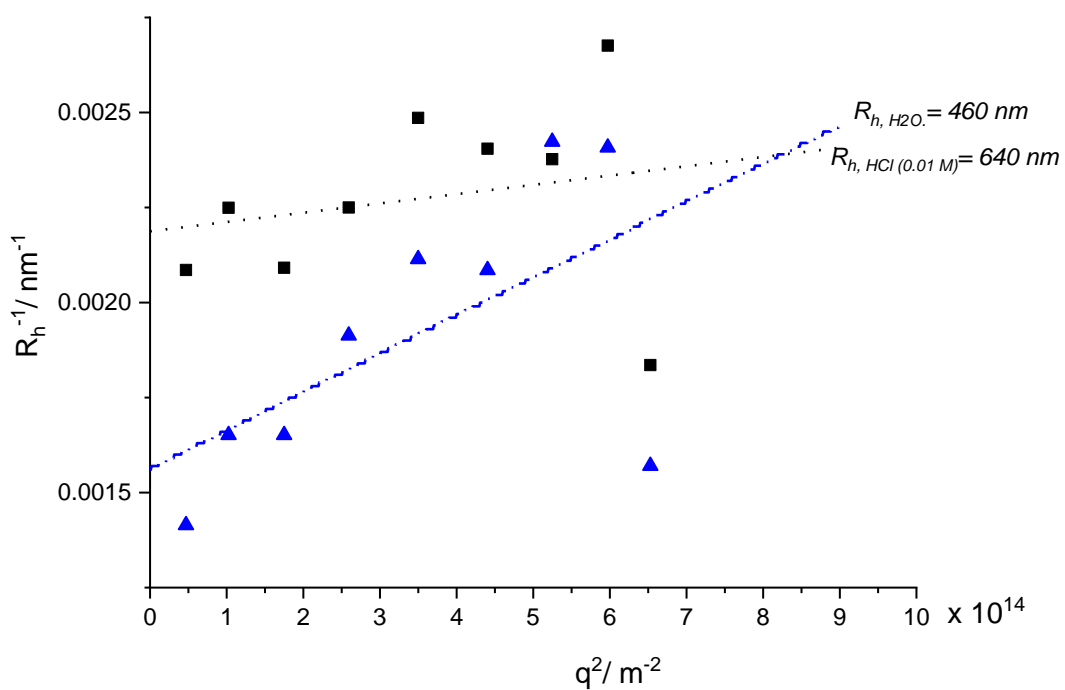
Figure S8: Hydrodynamic radii of Snomax containing bacterial ice nucleators from *P. syringae* at 0.1 g/L in water (pH ~6.2) and in 0.01 M HCl (pH ~3.6). The radii at lower pH are significantly larger, which shows that larger aggregates are present in the solution.
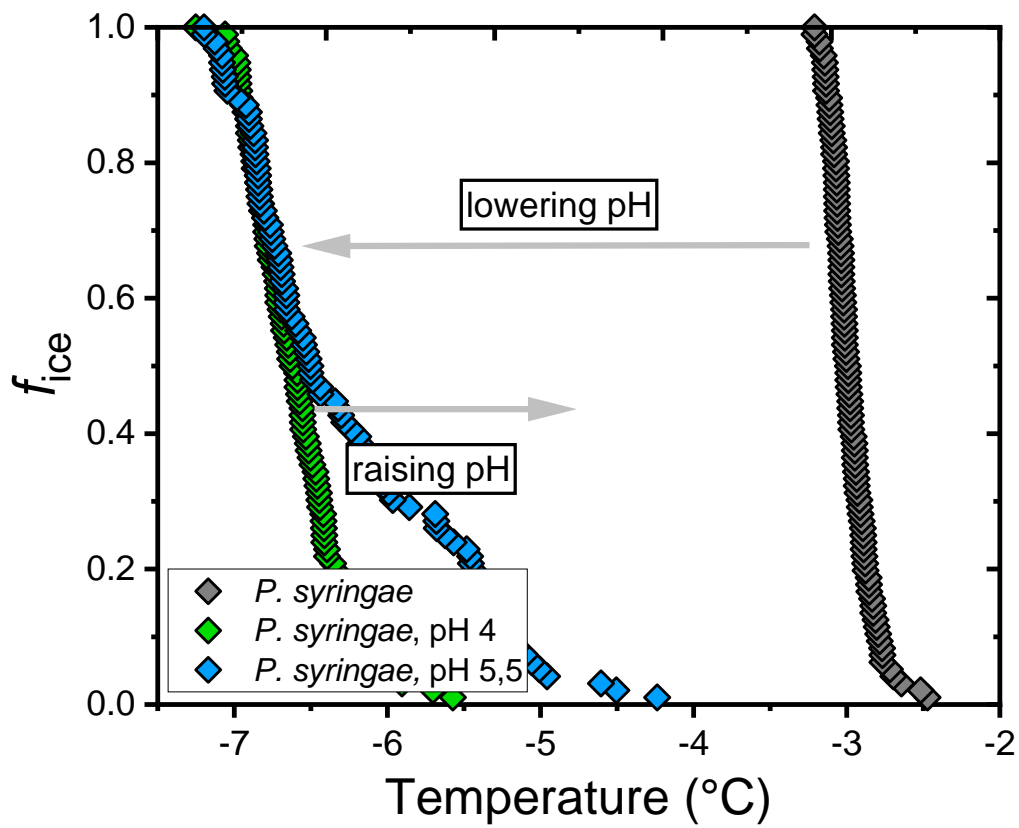
S9
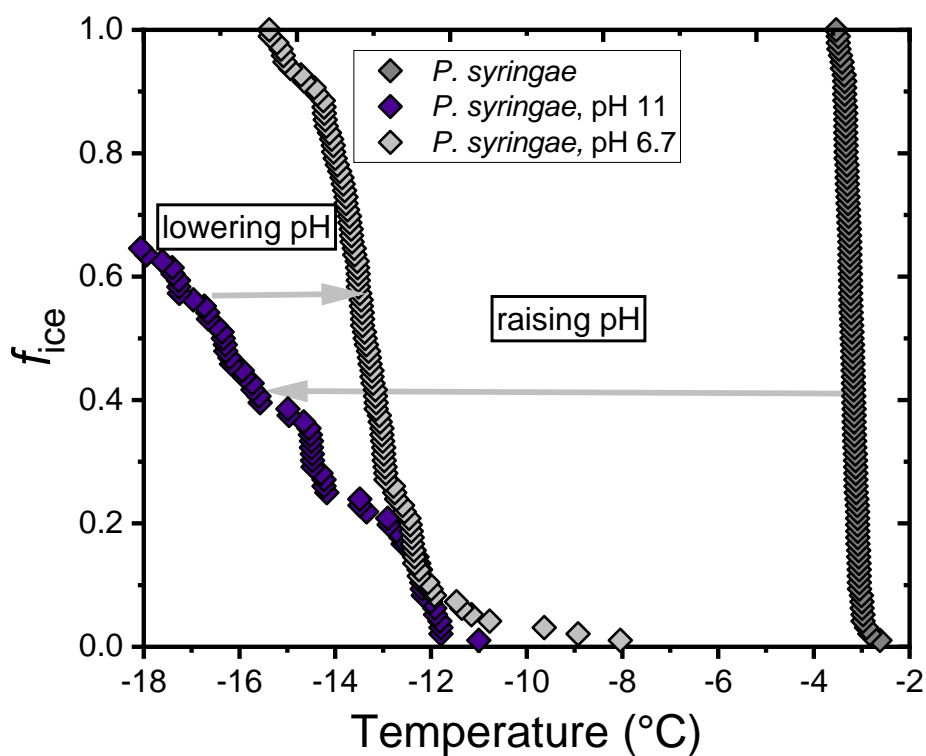
Figure S9: Freezing experiments of aqueous solutions of Snomax containing bacterial ice nucleators from *P. syringae* as a function of pH values. Fraction of frozen droplets (f_{ice}) for highly concentrated (0.1 mg/mL) Snomax (*P. syringae)* solutions, in which the pH was first raised to pH 11 and then lowered to pH 6.7.

Materials and Methods

Samples: Pure water was prepared as described elsewhere[1]. Snomax was obtained from SMI Snow Makers AG (Thun, Switzerland) and contains a preparation of freeze-dried, irradiated bacteria cells of *Pseudomonas syringae*. Buffer materials (Tris, PBS, acetate) as well as NaOH and HCl were obtained from Sigma Aldrich (Darmstadt, Germany). The concentration of Snomax was 0.1 mg/mL, and the pH value in pure water was 6.2 +/- 0.2. The SFG experiments and TINA experiments were performed in either pure water or in 0.1 M buffer solution (acetate, PBS, Tris,) of the respected pH. The ionic strength of the solutions was 0.1 M and adjusted by adding NaCl. The pH values of all samples were controlled before each measurement.

TINA Experiments. Ice nucleation experiments were performed using the high-throughput Twin-plate Ice Nucleation Assay (TINA)[1]. The details of the instrument have been described recently[1]. In a typical experiment, the investigated ice nucleator sample was serially diluted 10-fold by a liquid handling station (epMotion ep5073, Eppendorf, Hamburg, Germany). 96 droplets (3 µL) per dilution were placed on two 384-well plates and tested with a continuous cooling-rate of 1 °C/min from 0 °C to -20 °C. The droplet-freezing was determined by two infrared cameras (Seek Therman Compact XR, Seek Thermal Inc., Santa Barbara, CA, USA). The uncertainty in the temperature of the setup was ±0.2 °C. The obtained fraction of frozen droplets were used to calculate the cumulative number of ice nucleators using the Vali formula[1]. Experiments were performed 3-6 times on independent samples.

DLS measurements. The hydrodynamic radii (R_h) of 0.1 g/L and 0.001 g/L Snomax in ultrapure water and 0.1 g/L in 0.01 M HCl were determined using dynamic light scattering (DLS). Light scattering measurements were performed on an ALV spectrometer consisting of a goniometer and an ALV-5004 multiple-tau full-digital correlator (320 channels), which allows measurements over an angular range from 30° to 150°. A He-Ne laser (wavelength of 632.8 nm) was used as light source. Measurements were performed at 20 °C at 9 angles ranging from 30° to 150°.

Zeta potential. The Zeta potential measurements were performed using a Zetasizer (Malvern, UK) and a sample volume of 1 mL. The pH of the Snomax solutions was altered using NaOH and HCl.

Sum-Frequency Generation Spectroscopy Experiments. The details of the experimental setup have been described previously[2]. For the SFG intensity spectra, we used a conventional SFG setup in reflection geometry. A broadband IR (~ 5 µJ, full width half maximum (FWHM) of ~ 450 cm^{-1}) and a narrowband VIS (~ 13 µJ, centered at ~ 800 nm, FWHM of ~ 15 cm^{-1}) beam were focused and spatially and temporally overlapped on the sample surface, with incident angles of 36° (VIS) and 41° (IR) with respect to the surface normal. The spectra presented in this study were simultaneously recorded in the C-H and O-H-stretch region. The spectral resolution was limited by the bandwidth of the VIS. The generated SFG signal was collimated by a lens, directed and focused onto a spectrograph (*Acton SP 300i, Princeton Instruments*) and detected by a camera (*Newton 970, Andor Instruments*). All spectra were obtained in the ssp-polarization combination (s-polarized SFG, s-polarized VIS, p-polarized IR). Background spectra where taken with a blocked IR beam and all spectra were normalized to reference spectra from z-cut quartz. The SFG measurements were performed in a custom-made Teflon trough at room temperature. The Snomax (*P. syringae*) solutions were measured at a concentration of 0.1 g/L. Samples were allowed to equilibrate for two hours before measurements. The equilibration of the samples at the interface was complete, when the surface pressure was constant and the SFG spectra did not change within one hour.

Colligative effects. We exclude significant contributions of colligative effects on our results, since we performed measurements in buffer systems or by adjusting the pH value using NaOH and HCl. The ionic strength was kept constant at 0.1 M for all solutions and adjusted by adding NaCl. The maximum theoretical shift due to colligative effects in the TINA measurements would be ~ 0.4 °C which is less than the observed shifts.

1.   Kunert, A. T.; Lamneck, M.; Helleis, F.; Pöschl, U.; Pöhlker, M. L.; Fröhlich-Nowoisky, J., Twin-plate Ice Nucleation Assay (TINA) with infrared detection for high-throughput droplet freezing experiments with biological ice nuclei in laboratory and field samples. *Atmos. Meas. Tech.* **2018,** *11* (11), 6327-6337.
2.   Dreier, L. B.; Wolde-Kidan, A.; Bonthuis, D. J.; Netz, R. R.; Backus, E. H. G.; Bonn, M., Unraveling the Origin of the Apparent Charge of Zwitterionic Lipid Layers. *The Journal of Physical Chemistry Letters* **2019,** *10* (20), 6355-6359.

A.2 Schwidetzky *et al.*, J. Phys. Chem. B., 2020

Inhibition of Bacterial Ice Nucleators Is Not an Intrinsic Property of Antifreeze Proteins

R. Schwidetzky[1], A. T. Kunert[2], M. Bonn[1], U. Pöschl[2], Hans Ramløv[3], A. L. DeVries[4], J. Fröhlich-Nowoisky[2], and K. Meister[1,5]

[1] Max-Planck-Institute for Polymer Research, 55128 Mainz, Germany

[2] Max-Planck-Institute for Chemistry, 55128 Mainz, Germany

[3] Roskilde University, 4000 Roskilde, Denmark

[4] University of Illinois at Urbana– Champaign, Urbana, Illinois 61801, United States

[5] University of Alaska Southeast, Juneau, Alaska 99801, United States

Author contributions:

R.S. performed the freezing experiments and contributed to analyzing and discussing the results as well as writing the manuscript.

Article

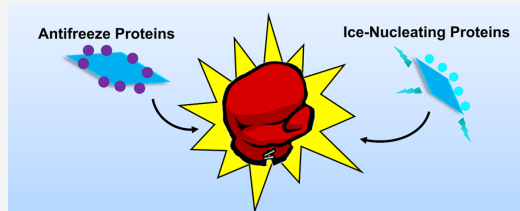# Inhibition of Bacterial Ice Nucleators Is Not an Intrinsic Property of Antifreeze Proteins

Ralph Schwidetzky, Anna T. Kunert, Mischa Bonn, Ulrich Pöschl, Hans Ramløv, Arthur L. DeVries, Janine Fröhlich-Nowoisky, and Konrad Meister*

Cite This: *J. Phys. Chem. B* 2020, 124, 4889−4895

Read Online

ACCESS | Metrics & More | Article Recommendations | Supporting Information

ABSTRACT: Cold-adapted organisms use antifreeze proteins (AFPs) or ice-nucleating proteins (INPs) for the survival in freezing habitats. AFPs have been reported to be able to inhibit the activity of INPs, a property that would be of great physiological relevance. The generality of this effect is not understood, and for the few known examples of INP inhibition by AFPs, the molecular mechanisms remain unclear. Here, we report a comprehensive evaluation of the effects of five different AFPs on the activity of bacterial ice nucleators using a high-throughput ice nucleation assay. We find that bacterial INPs are inhibited by certain AFPs, while others show no effect. Thus, the ability to inhibit the activity of INPs is not an intrinsic property of AFPs, and the interactions of INPs and different AFPs proceed through protein-specific rather than universal molecular mechanisms.

INTRODUCTION

Ice formation is the most important liquid-to-solid phase transition on earth and is critical for fields as diverse as cryobiology, geology, and climate science.[1] The crystallization of water into ice and the process of ice recrystallization upon thawing are further major contributors to cell death and lethal to most organisms.[2] Ice-nucleation-active bacteria are a primary cause of frost damage to plants, and in the earth's atmosphere, they can contribute to the formation of snow and rain.[3] The formation of ice is thermodynamically favored in water at temperatures below 0 °C, but the initial crystallization is kinetically hindered.[4] As a result, pure water can be supercooled to temperatures as low as −46 °C, below which homogeneous ice nucleation occurs.[5] Freezing of water in biological systems is a heterogeneous process, facilitated by the presence of ice-nucleating agents of biological and abiotic origins.[6] The most efficient biological ice nucleators are ice-nucleating proteins (INPs) from bacteria such as *Pseudomonas syringae* and *Erwinia herbicola*, which can initiate ice formation at temperatures close to 0 °C.[7] Most known bacterial ice nucleators consist of large proteins with an estimated weight of 150−180 kDa that are anchored in the outer cell membranes. INPs are typically present as monomers but have repeatedly been shown to aggregate in the bacterial outer membranes.[8] The ice nucleation induced by bacteria generally occurs in the ranges of −2 to −4 °C, −5 to −7 °C, and below −7 °C and is associated with INP subpopulations of different sizes with the monomers and small assemblies being the least and larger aggregates being the most efficient.[9] Based on their activity in droplet freezing experiments, the bacterial INP aggregates are usually grouped into classes A, B, and C.[9b] Class A represents

large protein oligomers of up to a hundred INPs,[8a] and class C consists of a few single proteins.[8a,10] However, up to now, the details of the structure and functionality of the INP aggregates remain the object of active research. On the molecular scale, INPs are believed to function by organizing water into icelike patterns, which increase in size as the temperature decreases until they are large enough to form a stable embryonic crystal, which leads to ice growth.[11] Potent biological ice nucleators have also been identified in freeze-tolerant organisms, i.e., insects that survive the freezing of a fraction of their body fluids, pollen, and fungi, as integral parts of their freeze-tolerance strategy in nature.[6c,12]

Freeze-avoiding organisms have evolved an opposite approach to ensure survival in subzero environments. They produce antifreeze proteins (AFPs) or antifreeze glycoproteins (AFGPs) that are able to bind to embryonic ice crystals and arrest their macroscopic growth.[6c,13] The success of AF(G)Ps as efficient protection against freezing can be witnessed by their wide distribution among organisms of different kingdoms, phyla, and species.[6c] The AF(G)Ps found in different organisms show a remarkable diversity in structures[14] but share the same capability of binding to ice and the lowering of the temperatures of ice growth.[13b] Despite having diametrically opposite functions, INPs resemble AF(G)Ps in many respects.
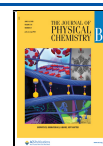
Both classes of proteins can interact with ice, and molecular simulations suggest that active ice-binding surfaces and adjacent interfacial water of INPs are similar to AF(G)Ps, just on a much larger scale.[10,15] In fact, there is increasing experimental evidence that AF(G)Ps have ice-nucleating activity[16] but at temperatures much lower than those of INPs.

Interestingly, AF(G)Ps have frequently been reported to also inhibit the activity of biological ice nucleators.[17] Such an effect would be of physiological importance and could explain why some cold-adapted organisms produce both AFPs and INPs.[6c,12a] However, the mechanism of the inhibition of INPs by AFPs remains largely unknown and is highly debated.[17,18] For instance, Parody-Morreale et al. reported that antifreeze glycoproteins (AFGPs) from *Dissostichus mawsoni* inhibited the ice-nucleating activity of the bacteria *Erwinia herbicola* and *P. syringae*,[19] whereas Holt et al. found that in the presence of AFGPs, the ice-nucleating activity of *P. syringae* was slightly enhanced.[18] Olsen and Duman reported that AFPs from the beetle *Dendroides canadensis* inhibited the activity of the bacteria *Pseudomonas fluorescens* but not the INPs from the crane fly *Tipula trivittata*.[20] While the above studies clearly demonstrate the importance of the subject, the reported experiments focused on a limited number of antifreeze proteins and left many open questions. Here, we investigate the effect of five types of AFPs and the non-AFP bovine serum albumin (BSA) on bacterial ice nucleators using a high-throughput twin-plate ice nucleation assay (TINA).[21] TINA enables the simultaneous measurement of a complete dilution series with high statistics, enabling the analysis and characterization of the efficiency of biological ice nuclei and their inhibitors with high accuracy.[21]

■ METHODS

Snomax was obtained from SMI Snow Makers AG (Thun, Switzerland) and contains a preparation of fragmented freeze-dried, irradiated bacteria cells of *P. syringae*. AFP-1 was purified from winter flounder *Pseudopleuronectes americanus*.[22] AFGP$_{1-5}$ and AFGP$_{7-8}$ were purified from the Antarctic toothfish *D. mawsoni*.[23] *Rm*AFP was obtained by recombinant protein expression as described elsewhere.[24] AFP-3 was purified from the Antarctic eelpout (*Lycodichthys dearborni*) or obtained by recombinant protein expression, including the mutant T18N.[4] In this mutant, the threonine residue at position 18 is replaced by asparagine, which causes the complete loss of antifreeze activity.[14] For the AFGP$_{1-5}$ variant, we oxidized the C-6 hydroxyl groups of the galactose moieties to carboxylic acids as described previously.[25] Only AF(G)P samples with tested antifreeze activity were used, and the activity was determined prior to the experiments using nanoliter cryoscopy. BSA was obtained from Sigma-Aldrich and was used without further purification. Pure water was prepared as described elsewhere.[21] *Fusarium acuminatum* from USDA-ARS, Michigan State University (Linda E. Hanson, East Lansing, MI) was cultivated on full-strength potato dextrose agar (VWR International GmbH, Darmstadt, Germany) first at room temperature for 1 week and then at 6 °C for about 4 weeks. An aqueous extract containing proteinaceous IN from spores and mycelial surfaces was prepared as described elsewhere.[12d]

Ice nucleation experiments were performed using a high-throughput droplet freezing assay. The details of the instrument have been described previously.[21] In a typical experiment, a 0.1 mg/mL solution of Snomax (*P. syringae*) in pure water was serially diluted 10-fold by a liquid handling

station (epMotion ep5073, Eppendorf, Hamburg, Germany) with either a solution of AF(G)Ps (0.1 mg/mL) or pure water. For each dilution, 96 droplets (3 μL) per dilution were placed on two 384-well-plates and tested with a continuous cooling rate of 1 °C/min from 0 to −30 °C. The freezing of droplets was determined by two infrared cameras (Seek Therman Compact XR, Seek Thermal Inc., Santa Barbara, CA). The uncertainty in the temperature of the setup was ±0.2 °C. The obtained fraction of frozen droplets and the counting error were used to calculate the cumulative number of ice nucleators with the associated error using the Vali formula and the Gaussian error propagation.[21,26] The pH values of all samples were controlled before TINA measurements and were ∼6−7. Samples were measured at least three times in independent experiments except for the variants that were measured twice.

The hydrodynamic radii (R_h) of 0.1 and 0.001 g/L of Snomax in ultrapure water were determined using dynamic light scattering (DLS). Light scattering measurements were performed on an ALV spectrometer consisting of a goniometer and an ALV-5004 multiple-tau full-digital correlator (320 channels), which allows measurements over an angular range from 30 to 150°. A He−Ne laser (wavelength of 632.8 nm) was used as a light source. Measurements were performed at 20 °C at nine angles ranging from 30 to 150°.

■ RESULTS

Figure 1 shows the results of TINA measurements of a dilution series of bacterial ice nucleators from *P. syringae* (Snomax).
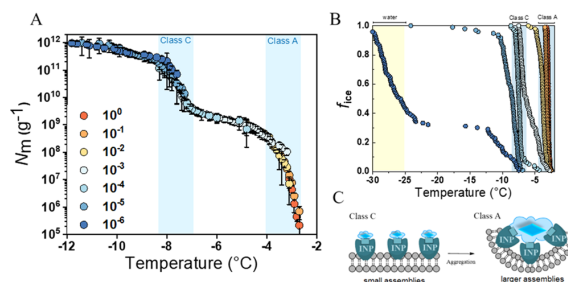

Figure 1. Freezing experiments of aqueous solutions of Snomax containing bacterial ice nucleators from *P. syringae*. (A) Cumulative number of ice nucleators (N_m) per unit mass of *P. syringae* vs temperature for various dilutions indicated in the legend, starting with 0.1 mg/mL. The error bars were calculated using the counting error and the Gaussian error propagation. (B) Fraction of frozen droplets (f_{ice}) for different *P. syringae* dilutions. Symbol colors indicate data from droplets with different concentrations and are identical to (A). The temperature ranges for classes A and C nucleators are shaded in light blue. The yellow-shaded region presents the temperature range in which pure water freezes in our system.[21] (C) Schematic structure of classes C and A nucleators. Class C consists of monomeric and small INP assemblies, which aggregate to form the highly efficient class A (larger aggregates). The INPs are shown with their active ice-binding site and preordered water patterns in their vicinity.

Snomax is widely used as a model and reference system for biological and atmospheric ice nucleation studies[21,27] and contains a preparation of freeze-dried irradiated bacteria cells of *P. syringae*. The initial mass concentration was 0.1 mg/mL and was then serially diluted 10-fold, over six orders of magnitude, with pure water using an automated liquid handling station. The resulting ice nucleator concentration ranged from 0.1 mg/mL to 0.1 ng/mL, per 3 μL of droplet.

The cumulative ice nucleator number concentration (N_m) was calculated using Vali's formula and represents the total number of ice nucleators that are active above a certain temperature.[26]

For the pure bacterial ice nucleator solution, the spectrum shows two strong increases in $N_m(T)$ around ~−2.9 and ~−7.5 °C with distinct plateaus between ~−4.5 and ~−7 °C and above ~−9.5 °C (Figure 1). These values are reproducible (Supporting Information, Figure S1) and consistent with previous studies.[21,27] The two distinct rises in the spectrum indicate that the ice nucleation activity of *P. syringae* stems from two distinct subpopulations of ice nucleators with different activation temperatures. These subpopulations have previously been assigned to isolated (~−7.5 °C) and aggregated (~−2.5 °C) INPs.[9b] Aggregation of INPs occurs in the cell membrane of *P. syringae* under conditions of stress as schematically shown in Figure 1C.[7b] The aggregation of the INPs effectively increases the size of the ice-binding surface, which increases the ice nucleation activity though cooperative effects.[28] The plateaus at temperatures below the two increases of $N_m(T)$ indicate that there are no or few additional ice nucleators active at different temperatures in the investigated droplets.[27b] The presence of two predominant ice nucleators becomes apparent when comparing the droplet freezing statistics of the different dilutions, as shown in Figure 1B. The two main bacterial ice nucleators with activities around ~−2.5 and ~−7.5 °C are apparent, as well as a third rise at ~−25 °C. We assign the observed rise at ~−2.5 °C to the highly efficient nucleators of class A and the less-efficient ice nucleators that cause nucleation around ~−7.5 °C to class C.[9b] Protein complexes of class B were not clearly observed in our measurements, which is in agreement with others.[21,27b] The third rise at ~−25 °C corresponds to the freezing point of pure water in our system.[21] At high Snomax concentrations, intermolecular interactions between INPs and different bacterial fragments of Snomax (*P. syringae*) occur, which results in aggregation and the formation of class A. Diluting the samples reduces the probability of such interactions and hence the formation of larger aggregates (Supporting Information, Figure S2). At very high dilution, there are no more ice nucleators present and, eventually, the curve resembles that of pure water.

Figure 2 shows the effect of BSA, the fish antifreeze proteins type 1 (AFP-1), type 3 (AFP-3), the insect antifreeze protein from *Rhagium mordax* (*Rm*AFP), and the small antifreeze glycoproteins (AFGP$_{7-8}$) and larger AFGP$_{1-5}$ isoforms on the ice-nucleating activity of *P. syringae*. The investigated proteins vary significantly in terms of three-dimensional structures, putative ice-binding planes, and antifreeze activities.[14] The freezing assay experiments were performed at a fixed AF(G)P concentration of 0.1 mg/mL and the same dilution range for INP as that shown in Figure 1, which results in varying AF(G)P/INP ratios spanning from 1:1 (wt %) to a vast excess of AF(G)Ps (Supporting Information, Table S1).

The most efficient bacterial class A ice nucleators are predominantly present in concentrated Snomax (*P. syringae*) solutions. The addition of different proteins to the concentrated *P. syringae* solutions gives rise to three types of effect: (i) the addition of AFGP$_{1-5}$ has no effect on the freezing curve, and the freezing statistics are indistinguishable from that of Snomax (*P. syringae*) in water. AFGP$_{1-5}$ is known to stabilize membranes,[29] so that the aggregation of proteins in membrane structures (Figure 1B) is preserved and IN activity retained; (ii) AFP-3, AFGP$_{7-8}$, *Rm*AFP, and BSA have similar and rather small effects on the class A ice nucleators: the resulting response is comparable to that of the pure bacteria, only shifted by ~0.7 °C to lower temperatures (Figure 2A). This minor inhibition of the class A nucleators is statistically insignificant, but it should be noted that f_{ice} at 0.5 was consistently found to be at lower temperatures compared to Snomax. This could indicate a slight inhibition that originates from nonspecific interactions of the different proteins with the outer cell membrane of *P. syringae*. Such interactions would perturb the formation of the precisely aligned INP aggregates that give rise to the high freezing temperatures, and, as a consequence, freezing occurs at lower temperatures. This inhibition mechanism is independent of antifreeze activities, explaining why AFPs and non-AFPs show similar activities. (iii) The addition of AFP-1 shifts the freezing point by ~3.5 °C to lower temperatures. The resulting freezing temperature around ~−7 °C closely resembles that of class C nucleators. AFP-1 is known to insert and disturb model cell membranes[29b,30] and evidently has the ability to prevent the formation of highly efficient class A aggregates, reducing the activity of class A to that of class C.

Additionally, we examined the effect of the AF(G)Ps on the class C ice nucleators of *P. syringae*, where the INPs are predominantly present as smaller aggregates and monomers. We find that some AF(G)Ps inhibit ice nucleation activity and shift the freezing point to lower temperatures. Interestingly, the degree of the inhibition is markedly different from that observed for class A. For class C, *Rm*AFP is the most efficient inhibitor, and AFP-1, the most efficient class A inhibitor, only shows moderate counter activity. We further find that BSA shows no effect on class C, which is in line with previous studies that observed no inhibitory effect of non-AFPs on class C nucleators.[17a]

Interestingly, we find that the larger isoform AFGP$_{1-5}$ shows no inhibition but a moderate enhancement of the activity of class C nucleators, while the smaller isoform AFGP$_{7-8}$ inhibits the INPs. The enhancement of ice nucleation by the addition of AFGP$_{1-5}$ is interesting since bacterial nucleators are very potent ice nucleators on their own. We rank the inhibition efficiency in the order *Rm*AFP ≫ AFP-1 = AFGP$_{7-8}$ = AFP-3 = BSA > AFGP$_{1-5}$. This ranking does not reflect the efficiency of the antifreeze activity of the proteins, except for *Rm*AFP, which is the most active AFP known.
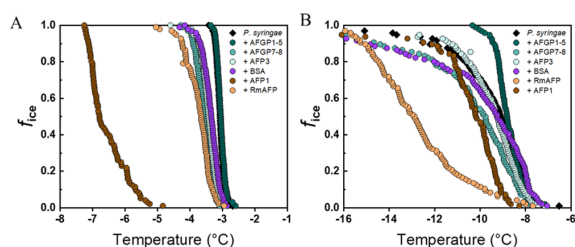

Figure 2. Freezing experiments of aqueous solutions of Snomax containing ice nucleators from *P. syringae* in the presence of a variety of AF(G)Ps. Fraction of frozen droplets (f_{ice}) for concentrated (0.1 mg/mL, A) and diluted (1 ng/mL, B) Snomax (*P. syringae*) solutions in the presence of different AF(G)Ps at a fixed 0.1 mg/mL concentration. The high-concentration Snomax (*P. syringae*) solutions predominately contain INP aggregates (class A), while lower-concentration solutions are mostly monomeric INPs (class C).

To further explore the relationship between the inhibition of the INPs and antifreeze activity, we studied inactive mutants of AFP-3 and AFGP$_{1-5}$. In the AFP-3* variant, the threonine 18 residue was replaced by asparagine, which results in the elimination of antifreeze activity.[14] In the AFGP$_{1-5}$* variant, we oxidized the C-6 hydroxyls of the galactose moieties to carboxylic acids, which results in the elimination of >80% of the antifreeze activity.[25] In Figure 3, we compare the true
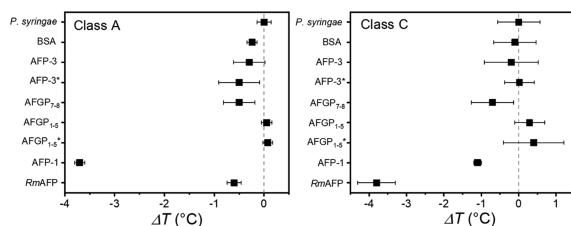

Figure 3. Ice nucleation inhibition efficiency of AF(G)Ps and non-AFP on classes A (aggregates) and C (monomer) bacterial ice nucleators solutions. Shifts represent the difference of f_{ice} at 0.5 between *P. syringae* and added AF(G)P. Each experiment was performed at least three times, and the error bars represent the standard deviation between the individual measurements.

supercooling of all of the AFPs and different variants at high and low Snomax (*P. syringae*) concentrations. Supercooling values ΔT represent the temperature difference at $f_{ice} = 0.5$ between Snomax (*P. syringae*) with and without the added protein at high (left panel) and low (right panel) Snomax (*P. syringae*) concentrations. All proteins were measured at least three times. For both AFP-3s, we find no significant difference between active and inactive variants on the class A or C ice nucleators. For the modified AFGP-Carboxyl variant, we likewise observe no significant change relative to the natural AFGP$_{1-5}$. AFP-1 and *Rm*AFP both inhibit ice nucleation, yet each with marked and opposite efficiencies for class A and class C INPs.

■ DISCUSSION

Freeze-avoiding organisms extend their supercooling abilities by the accumulation of colligative solutes, by the removal of ice nucleators, by inhibiting the activity of ice nucleators present, or alternately by inactivating embryonic ice crystals.[6c] The importance of biological macromolecules that inhibit ice nucleators has been recognized, but there have been no systematic studies with sufficiently robust analytical methods.[31] AF(G)Ps were among the most studied systems due to their known properties to recognize and bind ice crystals inhibiting their growth.[17] However, the generality of such inhibition of INPs by AF(G)P is not well supported, and for the few reported examples of inhibition by AF(G)Ps, the mechanism is unknown. Previous studies speculated that AF(G)Ps can inhibit the activity of INPs via (i) inhibiting the growth of newly formed ice embryos or (ii) via masking the active sites of INPs.[17]

Our results provide clear evidence that some AF(G)Ps can inhibit the activity of bacterial INPs, while others show no effect. The finding that some AF(G)Ps do not affect bacterial INPs excludes an inhibition mechanism based on the inhibition of newly formed ice crystals since otherwise, all AF(G)Ps should exhibit activity. Our results suggest that AF(G)Ps can inhibit the bacterial ice nucleators in a specific

manner that depends on the AF(G)Ps and the size of the INP aggregate.

Bacterial INPs have been suggested to form preordered "icelike" interfacial water domains at their putative ice-binding sites.[11b] Likewise, AFPs like *Rm*AFP are known to use preordered icelike interfacial water domains for the recognition and subsequent attachment to ice.[16b,32] We speculate that the preordered water domains of the AFPs will have a high affinity for similar icelike water domains and, therefore, for the preordered water of the INPs.[32a] Consequently, upon diffusion of AFPs into the vicinity of INPs, they will remain longer in the hydration shell of INPs and thereby disturb the interfacial water arrangement required for a nucleation event. This form of inhibition would be dependent on the similarity of the structure and hydration motifs of AFPs and INPs and on the antifreeze activity of the AFPs, which has been related to the extent of their preordered interfacial water domains.[32c] Bacterial INPs from *P. syringae* and hyperactive insect AFPs like *Rm*AFP are proposed to bind ice though a flat array of TxT repeats, where T is threonine and x a nonconserved amino acid.[15] Hence, the hyperactive *Rm*AFP shows strong inhibition of class C. We explain the reduced inhibition of class A INPs with larger aggregates that could disturb these specific interactions due to steric hindrances. Non-AFPs and inactive AFP variants will also randomly diffuse through the preordered water domains of INPs but lack the affinity for preordered interfacial water and therefore fail to mask the INPs. This hypothetical mechanism is schematically shown in Figure 4.

AFGPs are unique because of their highly flexible solution structure, multiple ice-binding sites, and the capability to
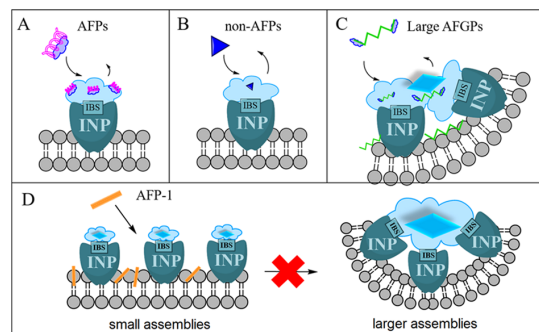

Figure 4. Proposed mechanism of the inhibition of ice nucleators from *P. syringae* by AF(G)Ps. INPs are shown with their active ice-binding sites (IBS) and preordered icelike water patterns in their vicinity (blue clouds). (A) Hyperactive AFPs like *Rm*AFP use preordered water domains to bind ice. They also have structural similarity to the INPs of *P. syringae*,[15] and the preordered water domains of *Rm*AFP will have an affinity for the preordered interfacial water domains of the bacterial INPs. Hence, *Rm*AFP will disturb the preordering of the interfacial water that is needed for ice nucleation and masks the bacterial ice-nucleating sites. (B) Non-AFPs have no preordered water domains (no blue cloud) and therefore no affinity for the interfacial water domains of INPs. (C) Large AFGP isoforms can stabilize and link INPs to form larger aggregates that nucleate at higher temperatures. (D) AFP-1 interacts with the cell membranes of the bacteria to prevent the functional aggregation of the INP monomers, which then give rise to the highly efficient class A nucleators. Mechanisms that involve direct interactions with the growing ice can be excluded since not all AFPs show inhibition activity.

stabilize membranes.[29a,33] Our observations that the larger AFGP$_{1-5}$ isoforms do not inhibit bacterial INPs but rather show no effect or even a slight enhancement are in agreement with Holt et al.[18] We speculate that larger AFGPs can stabilize INPs in the membranes and potentially link INPs to form larger aggregates that nucleate at higher temperatures, and that this stabilization outcompetes any occurring inhibition activity of AFGPs.

Our results further demonstrate that the highly efficient class A nucleators are more vulnerable to inhibition. For the most active inhibitor AFP-1, we propose a mechanism in which the proteins interact with the cell membrane of the bacteria to prevent the aggregation of the INP monomers, thereby preventing the formation of the highly efficient class A nucleators. Mechanisms that would involve direct interaction of AFP-1 with the growing ice front or the ice-nucleating site of the INPs can be excluded since class C ice nucleators were less inhibited, and fungal INPs were not inhibited at all by AFP-1 (Supporting Information, Figure S3).

This mechanism is in line with findings that AFP-1 directly inserts into model cell membranes, whereas AFGPs and other AFPs interact weaker and show fewer effects on the membrane.[29b,30]

The different mechanisms underlying the inhibition of bacterial INPs by AF(G)Ps are likely highly specific with different specific efficiencies. Thus, we conclude that the inhibition of INPs is not an intrinsic property of AF(G)Ps, and no universal INP inhibition mechanism through AFPs exists. This is further supported by the findings that AFP-1, the best inhibitor of bacterial INPs, had no effect on fungal INPs (Supporting Information, Figure S3). Ice nucleation can be promoted by a range of properties, including charge,[34] lattice matching,[35] hydrophobicity,[36] or morphology.[37] In such cases, it is not apparent that AF(G)Ps will show inhibitory activity.

ASSOCIATED CONTENT

Supporting Information

The Supporting Information is available free of charge at https://pubs.acs.org/doi/10.1021/acs.jpcb.0c03001.

Ice nucleation measurements of Snomax; dynamic light scattering measurements; ice nucleation measurements of fungal ice nucleators (Figures 1−3); molar ratios of AF(G)Ps (Table 1) (PDF)

AUTHOR INFORMATION

Corresponding Author

Konrad Meister − Max Planck Institute for Polymer Research, 55128 Mainz, Germany; University of Alaska Southeast, Juneau, Alaska 99801, United States; orcid.org/0000-0002-6853-6325; Email: meisterk@mpip-mainz.mpg.de

Authors

Ralph Schwidetzky − Max Planck Institute for Polymer Research, 55128 Mainz, Germany

Anna T. Kunert − Max Planck Institute for Chemistry, 55128 Mainz, Germany

Mischa Bonn − Max Planck Institute for Polymer Research, 55128 Mainz, Germany; orcid.org/0000-0001-6851-8453

Ulrich Pöschl − Max Planck Institute for Chemistry, 55128 Mainz, Germany; orcid.org/0000-0003-1412-3557

Hans Ramløv − Roskilde University, 4000 Roskilde, Denmark

Arthur L. DeVries − University of Illinois at Urbana—Champaign, Urbana, Illinois 61801, United States

Janine Fröhlich-Nowoisky − Max Planck Institute for Chemistry, 55128 Mainz, Germany; orcid.org/0000-0002-1278-0054

Complete contact information is available at:
https://pubs.acs.org/10.1021/acs.jpcb.0c03001

Notes

The authors declare no competing financial interest.

REFERENCES

(1) (a) Vergara-Temprado, J.; Miltenberger, A. K.; Furtado, K.; Grosvenor, D. P.; Shipway, B. J.; Hill, A. A.; Wilkinson, J. M.; Field, P. R.; Murray, B. J.; Carslaw, K. S. Strong control of Southern Ocean cloud reflectivity by ice-nucleating particles. Proc. Natl. Acad. Sci. U.S.A. 2018, 115, 2687−2692. (b) Mazur, P. Cryobiology: the freezing of biological systems. Science 1970, 168, 939−949.

(2) Ramløv, H. Aspects of natural cold tolerance in ectothermic animals. Hum. Reprod. 2000, 15, 26−46.

(3) (a) Morris, C. E.; Conen, F.; Alex Huffman, J.; Phillips, V.; Poschl, U.; Sands, D. C. Bioprecipitation: a feedback cycle linking earth history, ecosystem dynamics and land use through biological ice nucleators in the atmosphere. Global Change Biol. 2014, 20, 341−351. (b) Failor, K. C.; Schmale, D. G.; Vinatzer, B. A.; Monteil, C. L. Ice nucleation active bacteria in precipitation are genetically diverse and nucleate ice by employing different mechanisms. ISME J. 2017, 11, 2740−2753. (c) Joly, M.; Amato, P.; Deguillaume, L.; Monier, M.; Hoose, C.; Delort, A. Direct quantification of total and biological ice nuclei in cloud water. Atmos. Chem. Phys. Discuss. 2014, 14, 3707−3731.

(4) Murray, B. J.; Broadley, S. L.; Wilson, T. W.; Bull, S. J.; Wills, R. H.; Christenson, H. K.; Murray, E. J. Kinetics of the homogeneous freezing of water. Phys. Chem. Chem. Phys. 2010, 12, 10380−10387.

(5) Kim, K. H.; Späh, A.; Pathak, H.; Perakis, F.; Mariedahl, D.; Amann-Winkel, K.; Sellberg, J. A.; Lee, J. H.; Kim, S.; Park, J.; Nam, K. H.; Katayama, T.; Nilsson, A. Maxima in the thermodynamic response and correlation functions of deeply supercooled water. Science 2017, 358, 1589−1593.

(6) (a) Zachariassen, K. E.; Kristiansen, E.; Pedersen, S. A.; Hammel, H. T. Ice nucleation in solutions and freeze-avoiding insects—homogeneous or heterogeneous? Cryobiology 2004, 48, 309−321. (b) Fröhlich-Nowoisky, J.; Kampf, C. J.; Weber, B.; Huffman, J. A.; Pöhlker, C.; Andreae, M. O.; Lang-Yona, N.; Burrows, S. M.; Gunthe, S. S.; Elbert, W.; Su, H.; Hoor, P.; Thines, E.; Hoffmann, T.; Després, V. R.; Pöschl, U. Bioaerosols in the Earth system: Climate, health, and ecosystem interactions. Atmos. Res. 2016, 182, 346−376. (c) Duman, J. G. Antifreeze and ice nucleator proteins in terrestrial arthropods. Annu. Rev. Physiol. 2001, 63, 327−357.

(7) (a) Kozloff, L. M.; Schofield, M. A.; Lute, M. Ice nucleating activity of Pseudomonas syringae and Erwinia herbicola. J. Bacteriol. 1983, 153, 222−231. (b) Maki, L. R.; Galyan, E. L.; Chang-Chien, M. M.; Caldwell, D. R. Ice nucleation induced by Pseudomonas syringae. Appl. Microbiol. 1974, 28, 456−459.

(8) (a) Govindarajan, A. G.; Lindow, S. E. Size of bacterial ice-nucleation sites measured in situ by radiation inactivation analysis. Proc. Natl. Acad. Sci. U.S.A. 1988, 85, 1334−1338. (b) Southworth, M. W.; Wolber, P. K.; Warren, G. J. Nonlinear relationship between concentration and activity of a bacterial ice nucleation protein. J. Biol. Chem. 1988, 263, 15211−15216. (c) Mueller, G. M.; Wolber, P. K.; Warren, G. J. J. C. Clustering of ice nucleation protein correlates with

ice nucleation activity. *Cryobiology* **1990**, *27*, 416−422. (d) Schmid, D.; Pridmore, D.; Capitani, G.; Battistutta, R.; Neeser, J.-R.; Jann, A. J. F. l. Molecular organisation of the ice nucleation protein InaV from *Pseudomonas syringae*. *FEBS Lett.* **1997**, *414*, 590−594.

(9) (a) Yankofsky, S. A.; Levin, Z.; Bertold, T.; Sandlerman, N. Some Basic Characteristics of Bacterial Freezing Nuclei. *J. Appl. Meteorol.* **1981**, *20*, 1013−1019. (b) Turner, M. A.; Arellano, F.; Kozloff, L. M. Three separate classes of bacterial ice nucleation structures. *J. Bacteriol.* **1990**, *172*, 2521−2526.

(10) Garnham, C. P.; Campbell, R. L.; Walker, V. K.; Davies, P. L. Novel dimeric beta-helical model of an ice nucleation protein with bridged active sites. *BMC Struct. Biol.* **2011**, *11*, No. 36.

(11) (a) Knight, C. A. The Freezing of Supercooled Liquids. *Am. J. Phys.* **1968**, *36*, 466−467. (b) Hudait, A.; Moberg, D. R.; Qiu, Y.; Odendahl, N.; Paesani, F.; Molinero, V. Preordering of water is not needed for ice recognition by hyperactive antifreeze proteins. *Proc. Natl. Acad. Sci. U.S.A.* **2018**, *115*, 8266−8271.

(12) (a) Dreischmeier, K.; Budke, C.; Wiehemeier, L.; Kottke, T.; Koop, T. Boreal pollen contain ice-nucleating as well as ice-binding 'antifreeze' polysaccharides. *Sci. Rep.* **2017**, *7*, No. 41890. (b) Fröhlich-Nowoisky, J.; Hill, T. C. J.; Pummer, B. G.; Yordanova, P.; Franc, G. D.; Pöschl, U. Ice nucleation activity in the widespread soil fungus *Mortierella alpina*. *Biogeosciences* **2015**, *12*, 1057−1071. (c) Pummer, B. G.; Budke, C.; Augustin-Bauditz, S.; Niedermeier, D.; Felgitsch, L.; Kampf, C. J.; Huber, R. G.; Liedl, K. R.; Loerting, T.; Moschen, T.; Schauperl, M.; Tollinger, M.; Morris, C. E.; Wex, H.; Grothe, H.; Pöschl, U.; Koop, T.; Fröhlich-Nowoisky, J. Ice nucleation by water-soluble macromolecules. *Atmos. Chem. Phys.* **2015**, *15*, 4077−4091. (d) Kunert, A. T.; Pöhlker, M. L.; Krevert, C. S.; Wieder, C.; Speth, K. R.; Hanson, L. E.; Morris, C. E.; Schmale III, D. G.; Pöschl, U.; Fröhlich-Nowoisky, J. Macromolecular fungal ice nuclei in Fusarium: effects of physical and chemical processing, Biogeosciences **2019**, *16*, 4647−4659.

(13) (a) DeVries, A. L. Glycoproteins as biological antifreeze agents in antarctic fishes. *Science* **1971**, *172*, 1152−1155. (b) Raymond, J. A.; DeVries, A. L. Adsorption inhibition as a mechanism of freezing resistance in polar fishes. *Proc. Natl. Acad. Sci. U.S.A.* **1977**, *74*, 2589−2593.

(14) Olijve, L. L. C.; Meister, K.; DeVries, A. L.; Duman, J. G.; Guo, S.; Bakker, H. J.; Voets, I. K. Blocking rapid ice crystal growth through nonbasal plane adsorption of antifreeze proteins. *Proc. Natl. Acad. Sci. U.S.A.* **2016**, *113*, 3740−3745.

(15) Hudait, A.; Odendahl, N.; Qiu, Y.; Paesani, F.; Molinero, V. Ice-Nucleating and Antifreeze Proteins Recognize Ice through a Diversity of Anchored Clathrate and Ice-like Motifs. *J. Am. Chem. Soc.* **2018**, *140*, 4905−4912.

(16) (a) Eickhoff, L.; Dreischmeier, K.; Zipori, A.; Sirotinskaya, V.; Adar, C.; Reicher, N.; Braslavsky, I.; Rudich, Y.; Koop, T. Contrasting Behavior of Antifreeze Proteins: Ice Growth Inhibitors and Ice Nucleation Promoters. *J. Phys. Chem. Lett.* **2019**, *10*, 966−972. (b) Liu, K.; Wang, C.; Ma, J.; Shi, G.; Yao, X.; Fang, H.; Song, Y.; Wang, J. Janus effect of antifreeze proteins on ice nucleation. *Proc. Natl. Acad. Sci. U.S.A.* **2016**, *113*, 14739−14744. (c) Wilson, P. W.; Osterday, K. E.; Heneghan, A. F.; Haymet, A. D. J. Type I Antifreeze Proteins Enhance Ice Nucleation above Certain Concentrations. *J. Biol. Chem.* **2010**, *285*, 34741−34745.

(17) (a) Tomalty, H. E.; Walker, V. K. Perturbation of bacterial ice nucleation activity by a grass antifreeze protein. *Biochem. Biophys. Res. Commun.* **2014**, *452*, 636−641. (b) Wilson, P. W.; Leader, J. P. Stabilization of supercooled fluids by thermal hysteresis proteins. *Biophys. J.* **1995**, *68*, 2098−2107.

(18) Holt, C. B. The effect of antifreeze proteins and poly(vinyl alcohol) on the nucleation of ice: A preliminary study. *Cryoletters* **2003**, *24*, 323−330.

(19) Parody-Morreale, A.; Murphy, K. P.; Cera, E. D.; Fall, R.; DeVries, A. L.; Gill, S. J. Inhibition of bacterial ice nucleators by fish antifreeze glycoproteins. *Nature* **1988**, *333*, 782−783.

(20) Olsen, T. M.; Duman, J. G. Maintenance of the supercooled state in the gut fluid of overwintering pyrochroid beetle larvae,

Dendroides canadensis: role of ice nucleators and antifreeze proteins. *J. Comp. Physiol., B* **1997**, *167*, 114−122.

(21) Kunert, A. T.; Lamneck, M.; Helleis, F.; Pöschl, U.; Pöhlker, M. L.; Fröhlich-Nowoisky, J. Twin-plate Ice Nucleation Assay (TINA) with infrared detection for high-throughput droplet freezing experiments with biological ice nuclei in laboratory and field samples. *Atmos. Meas. Tech.* **2018**, *11*, 6327−6337.

(22) Duman, J. G.; DeVries, A. L. Isolation, characterization, and physical properties of protein antifreezes from the winter flounder, *Pseudopleuronectes americanus*. *Comp. Biochem. Physiol., B: Comp. Biochem.* **1976**, *54*, 375−380.

(23) Evans, C. W.; Gubala, V.; Nooney, R.; Williams, D. E.; Brimble, M. A.; Devries, A. L. How do Antarctic notothenioid fishes cope with internal ice? A novel function for antifreeze glycoproteins. *Antarct. Sci.* **2011**, *23*, 57−64.

(24) Friis, D. S.; Kristiansen, E.; von Solms, N.; Ramløv, H. Antifreeze activity enhancement by site directed mutagenesis on an antifreeze protein from the beetle *Rhagium mordax*. *FEBS Lett.* **2014**, *588*, 1767−1772.

(25) Shier, W. T.; Lin, Y.; De Vries, A. L. Structure and mode of action of glycoproteins from an antarctic fish. *Biochim. Biophys. Acta, Protein Struct.* **1972**, *263*, 406−413.

(26) Vali, G. Quantitative Evaluation of Experimental Results an the Heterogeneous Freezing Nucleation of Supercooled Liquids. *J. Atmos. Sci.* **1971**, *28*, 402−409.

(27) (a) Wex, H.; Augustin-Bauditz, S.; Boose, Y.; Budke, C.; Curtius, J.; Diehl, K.; Dreyer, A.; Frank, F.; Hartmann, S.; Hiranuma, N.; Jantsch, E.; Kanji, Z. A.; Kiselev, A.; Koop, T.; Möhler, O.; Niedermeier, D.; Nillius, B.; Rösch, M.; Rose, D.; Schmidt, C.; Steinke, I.; Stratmann, F. Intercomparing different devices for the investigation of ice nucleating particles using Snomax as test substance. *Atmos. Chem. Phys.* **2015**, *15*, 1463−1485. (b) Budke, C.; Koop, T. BINARY: an optical freezing array for assessing temperature and time dependence of heterogeneous ice nucleation. *Atmos. Meas. Tech.* **2015**, *8*, 689−703.

(28) Qiu, Y.; Hudait, A.; Molinero, V. How Size and Aggregation of Ice-Binding Proteins Control Their Ice Nucleation Efficiency. *J. Am. Chem. Soc.* **2019**, *141*, 7439−7452.

(29) (a) Huelsz-Prince, G.; DeVries, A. L.; Bakker, H. J.; van Zon, J. S.; Meister, K. Effect of Antifreeze Glycoproteins on Organoid Survival during and after Hypothermic Storage. *Biomolecules* **2019**, *9*, No. 110. (b) Tomczak, M. M.; Hincha, D. K.; Estrada, S. D.; Wolkers, W. F.; Crowe, L. M.; Feeney, R. E.; Tablin, F.; Crowe, J. H. A mechanism for stabilization of membranes at low temperatures by an antifreeze protein. *Biophys. J.* **2002**, *82*, 874−881.

(30) (a) Garner, J.; Inglis, S. R.; Hook, J.; Separovic, F.; Harding, M. M. A solid-state NMR study of the interaction of fish antifreeze proteins with phospholipid membranes. *Eur. Biophys. J.* **2008**, *37*, 1031−1038. (b) Kar, R. K.; Mroue, K. H.; Kumar, D.; Tejo, B. A.; Bhunia, A. Structure and Dynamics of Antifreeze Protein−Model Membrane Interactions: A Combined Spectroscopic and Molecular Dynamics Study. *J. Phys. Chem. B* **2016**, *120*, 902−914.

(31) Fujikawa, S.; Kuwabara, C.; Kasuga, J.; Arakawa, K. Super-cooling-Promoting (Anti-ice Nucleation) Substances. *Adv. Exp. Med. Biol.* **2018**, *1081*, 289−320.

(32) (a) Meister, K.; Strazdaite, S.; DeVries, A. L.; Lotze, S.; Olijve, L. L. C.; Voets, I. K.; Bakker, H. J. Observation of ice-like water layers at an aqueous protein surface. *Proc. Natl. Acad. Sci. U.S.A.* **2014**, *111*, 17732−17736. (b) Kozuch, D. J.; Stillinger, F. H.; Debenedetti, P. G. Combined molecular dynamics and neural network method for predicting protein antifreeze activity. *Proc. Natl. Acad. Sci. U.S.A.* **2018**, *115*, 13252−13257. (c) Meister, K.; Ebbinghaus, S.; Xu, Y.; Duman, J. G.; DeVries, A.; Gruebele, M.; Leitner, D. M.; Havenith, M. Long-range protein−water dynamics in hyperactive insect antifreeze proteins. *Proc. Natl. Acad. Sci. U.S.A.* **2013**, *110*, 1617−1622. (d) Meister, K.; Moll, C. J.; Chakraborty, S.; Jana, B.; DeVries, A. L.; Ramløv, H.; Bakker, H. J. Molecular structure of a hyperactive antifreeze protein adsorbed to ice. *J. Chem. Phys.* **2019**, *150*, No. 131101.

(33) (a) Giubertoni, G.; Meister, K.; DeVries, A. L.; Bakker, H. J. Determination of the Solution Structure of Antifreeze Glycoproteins Using Two-Dimensional Infrared Spectroscopy. *J. Phys. Chem. Lett.* **2019**, *10*, 352−357. (b) Hays, L. M.; Feeney, R. E.; Crowe, L. M.; Crowe, J. H.; Oliver, A. E. Antifreeze glycoproteins inhibit leakage from liposomes during thermotropic phase transitions. *Proc. Natl. Acad. Sci. U.S.A.* **1996**, *93*, 6835−6840.

(34) Hudait, A.; Molinero, V. Ice Crystallization in Ultrafine Water−Salt Aerosols: Nucleation, Ice-Solution Equilibrium, and Internal Structure. *J. Am. Chem. Soc.* **2014**, *136*, 8081−8093.

(35) Pruppacher, H. R. On the growth of ice crystals in supercooled water and aqueous solution drops. *Pure Appl. Geophys.* **1967**, *68*, 186−195.

(36) Li, K.; Xu, S.; Chen, J.; Zhang, Q.; Zhang, Y.; Cui, D.; Zhou, X.; Wang, J.; Song, Y. Viscosity of interfacial water regulates ice nucleation. *Appl. Phys. Lett.* **2014**, *104*, No. 101605.

(37) Zhang, Z.; Liu, X.-Y. Control of ice nucleation: freezing and antifreeze strategies. *Chem. Soc. Rev.* **2018**, *47*, 7116−7139.

52

Supporting Information:

Inhibition of Bacterial Ice Nucleators is Not an Intrinsic Property of Antifreeze Proteins

Authors: Ralph Schwidetzky[1], Anna T. Kunert[2], Mischa Bonn[1], Ulrich Pöschl[2], Hans Ramløv[3], Arthur L. DeVries[4], Janine Fröhlich-Nowoisky[2] and Konrad Meister*[1,5]

Affiliations:

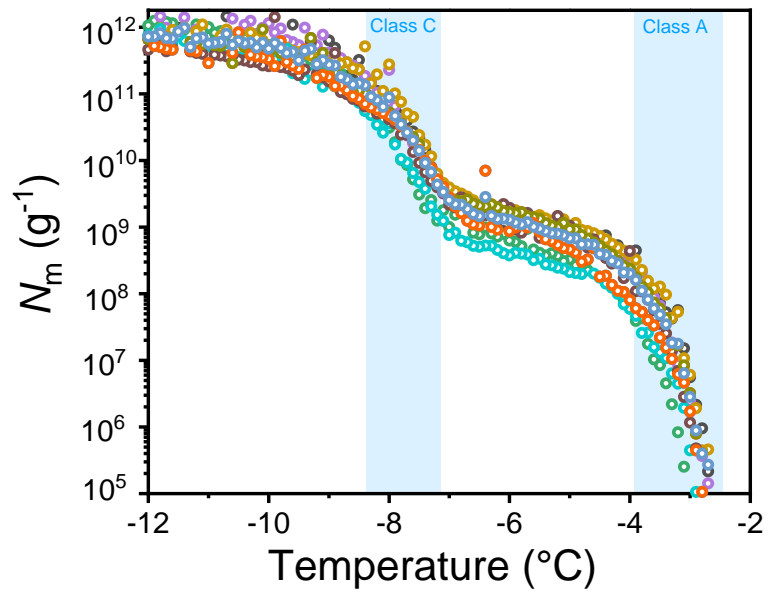[1]Max Planck Institute for Polymer Research, 55128 Mainz, Germany

[2]Max Planck Institute for Chemistry, 55128 Mainz, Germany

[3]Roskilde University, 4000 Roskilde, Denmark

[4]University of Illinois at Urbana–Champaign, Urbana, IL, 61801, USA

[5]University of Alaska Southeast, Juneau, AK, 99801, USA

*Correspondence to: meisterk@mpip-mainz.mpg.de

Supporting Figure 1: Freezing experiments of aqueous solutions of Snomax® containing bacterial ice nucleators from *P. syringae*. Shown are the cumulative number of ice nucleators per unit mass of *P. syringae* vs. temperature for eleven independent experiments. The temperature ranges for class A and class C INPs are shaded in light blue[9].
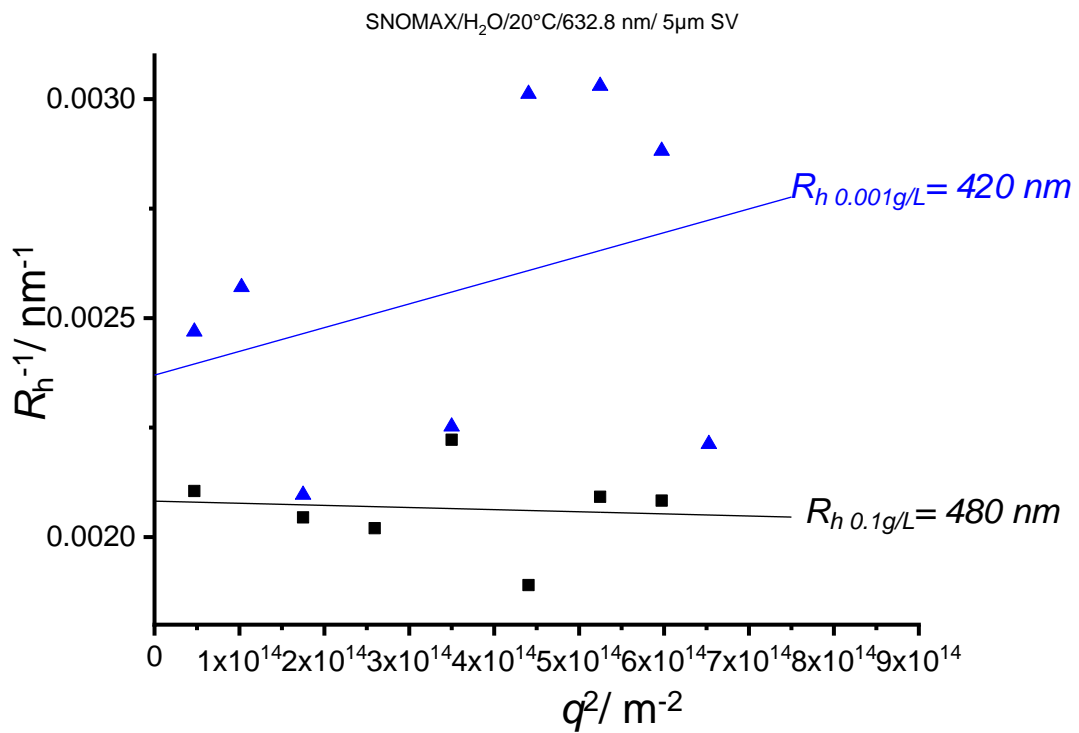
Supporting Figure 2: Hydrodynamic radii of Snomax® containing bacterial ice nucleators from *P. syringae* at 0.1 g/L and at 0.001 g/L. The radii at higher concentration are larger, which suggests that larger aggregates are present in the solution.
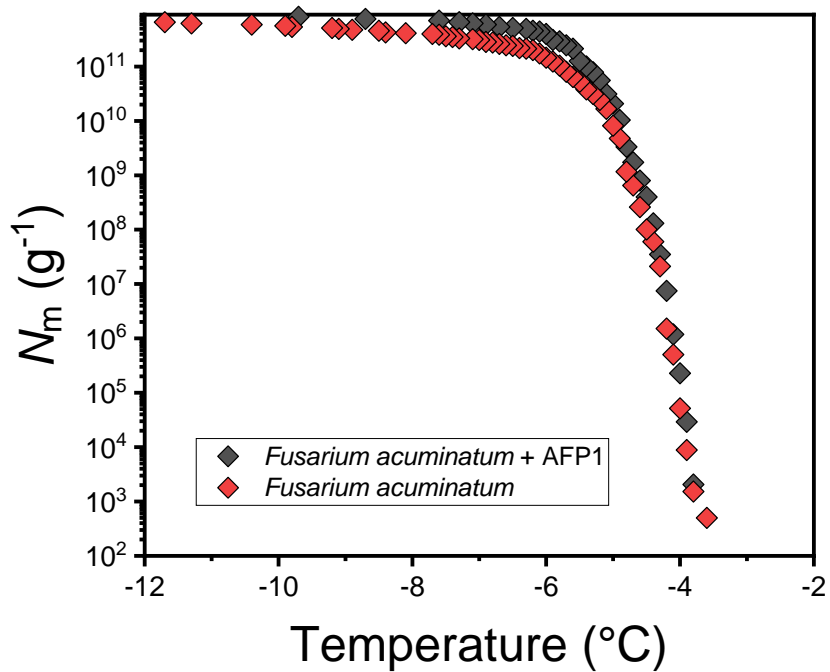
Supporting Figure 3: Freezing experiments of aqueous extracts from *Fusarium acuminatum* containing fungal ice nucleating proteins and in the presence of AFP-1. Shown is the cumulative number of ice nucleators (N_m) per gram of mycelium plotted against the temperature (T).

S4

Supporting Table 1: Molar ratios of the INP:AF(G)Ps at the different dilution steps of the freezing experiments.

Dilution Step	INP (mg/mL)	AF(G)P (mg/mL)	Molar ratio AFGP$_{1-5}$: INP	Molar ratio AFGP$_{7-8}$: INP	Molar ratio AFP-1 : INP	Molar ratio AFP-3 : INP	Molar ratio RmAFP : INP
1	0.1	0.1	7.5	$6.2*10^1$	$4.3*10^1$	$2.5*10^1$	$1.6*10^1$
2	0.01	0.1	$7.5*10^1$	$6.2*10^2$	$4.3*10^2$	$2.5*10^2$	$1.6*10^2$
3	$1*10^{-3}$	0.1	$7.5*10^2$	$6.2*10^3$	$4.3*10^3$	$2.5*10^3$	$1.6*10^3$
4	$1*10^{-4}$	0.1	$7.5*10^3$	$6.2*10^4$	$4.3*10^4$	$2.5*10^4$	$1.6*10^4$
5	$1*10^{-5}$	0.1	$7.5*10^4$	$6.2*10^5$	$4.3*10^5$	$2.5*10^5$	$1.6*10^5$
6	$1*10^{-6}$	0.1	$7.5*10^5$	$6.2*10^6$	$4.3*10^6$	$2.5*10^6$	$1.6*10^6$
7	$1*10^{-7}$	0.1	$7.5*10^6$	$6.2*10^7$	$4.3*10^7$	$2.5*10^7$	$1.6*10^7$
8	$1*10^{-8}$	0.1	$7.5*10^7$	$6.2*10^8$	$4.3*10^8$	$2.5*10^8$	$1.6*10^8$

A.3 Lukas *et al.*, J. Phys. Chem. Lett., 2021

Interfacial Water Ordering is Insufficient to Explain Ice-Nucleating Protein Activity

M. Lukas[*,1], R. Schwidetzky[*,1], A. T. Kunert[2], E.H.G. Backus[1,3], U. Pöschl[2], J. Fröhlich-Nowoisky[2], M. Bonn[1], and K. Meister[1,4]

[*] These authors contributed equally to this work.
[1] Max-Planck-Institute for Polymer Research, 55128 Mainz, Germany
[2] Max-Planck-Institute for Chemistry, 55128 Mainz, Germany
[3] University of Vienna, 1090 Vienna, Austria
[4] University of Alaska Southeast, Juneau, Alaska 99801, United States

Author contributions:

R.S. performed the freezing experiments and contributed to analyzing and discussing the results as well as writing the manuscript.

Letter

Interfacial Water Ordering Is Insufficient to Explain Ice-Nucleating Protein Activity

Max Lukas,*,[⊥] Ralph Schwidetzky,[⊥] Anna T. Kunert, Ellen H.G. Backus, Ulrich Pöschl,
Janine Fröhlich-Nowoisky, Mischa Bonn, and Konrad Meister*

Read Online

ACCESS | Metrics & More | Article Recommendations | Supporting Information

ABSTRACT: Ice-nucleating proteins (INPs) found in bacteria are the most effective ice
nucleators known, enabling the crystallization of water at temperatures close to 0 °C. Although
their function has been known for decades, the underlying mechanism is still under debate. Here,
we show that INPs from *Pseudomonas syringae* in aqueous solution exhibit a defined solution
structure and show no significant conformational changes upon cooling. In contrast, irreversible
structural changes are observed upon heating to temperatures exceeding ∼55 °C, leading to a loss
of the ice-nucleation activity. Sum-frequency generation (SFG) spectroscopy reveals that active
and heat-inactivated INPs impose similar structural ordering of interfacial water molecules upon
cooling. Our results demonstrate that increased water ordering is not sufficient to explain INPs'
high ice-nucleation activity and confirm that intact three-dimensional protein structures are
critical for bacterial ice nucleation, supporting a mechanism that depends on the INPs'
supramolecular interactions.
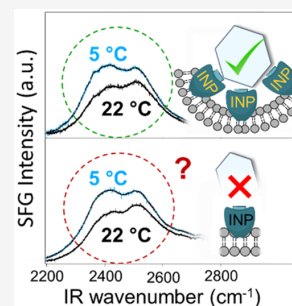
The formation of ice is thermodynamically favored in water
at temperatures below 0 °C, but the crystallization is
kinetically hindered owing to the energy barrier associated with
creating the initial ice seed.[1] As a result, pure water droplets
can, depending on their size and cooling rate, be supercooled
to temperatures as low as −38 °C.[2] Ice crystals can be formed
either by homogeneous nucleation at lower temperatures or by
heterogeneous nucleation catalyzed by compounds that serve
as ice nucleators (IN). The most effective biological IN known
are ice-nucleating proteins from bacteria such as *Pseudomonas
syringae*.[3,4] Bacterial INPs can have different sizes but are
typically large macromolecules that are anchored to the outer
cell membrane of the bacterial cell wall. They are typically
present as monomers but have repeatedly been shown to
aggregate in the bacterial outer membranes.[5−8] Large INP
aggregates are thought to be responsible for freezing at
temperatures between −2 and −4 °C and smaller INP
aggregates at temperatures between −7 and −12 °C.[9]

Computer-based homology modeling proposed the bacterial
INP structure to be *β*-helical (Figure 1A) with similarities to
hyperactive insect antifreeze proteins (AFPs).[10] More recent
models based on molecular dynamic simulations further
suggest that a highly conserved threonine-X-threonine motif
is used to interact with ice, which again is similar to some
AFPs.[11] On the molecular scale, the INPs are believed to work
by organizing water into preordered patterns, which increase in
size as the temperature decreases until they are large enough to
form a stable embryonic crystal, leading to ice growth.[12]
However, the role of the INP structure, the interaction of INPs
with water, and the underlying working mechanism remain
largely unknown. Here, we study the effects of temperature on

the structure, hydration shell, and ice-nucleation efficiency of
purified proteinaceous IN of *P. syringae*.

We performed purification of fragmented *P. syringae*
(Snomax) solutions using falling water ice affinity and rotary
ice-shell purification (see the Supporting Information (SI) for
details).[13,14] Both purification methods use the unique
property of the INPs to interact with ice and have previously
been used to purify AFPs from natural sources.[15] The
purification process involved the incorporation of the INPs
into the slowly growing ice phase and the exclusion of other
biomolecules and impurities. Using this ice-affinity purification,
we obtained a mixture of all the INPs present in *P. syringae*,
including residual protein-associated lipids. The success of the
purification was assessed by determining the ice-nucleation
activity of the purified INPs using the high-throughput Twin-
plate Ice Nucleation Assay (TINA) (Figure 1 and Figure
S2).[16] In the following, we will refer to these purified samples
as "purified INPs".

Figure 1B shows typical statistical freezing curves of aqueous
solutions of fragmented *P. syringae* and purified INPs with
0.1 mg/mL, while Figure 1C compares their freezing behaviors
inferred from freezing curves recorded for concentrations
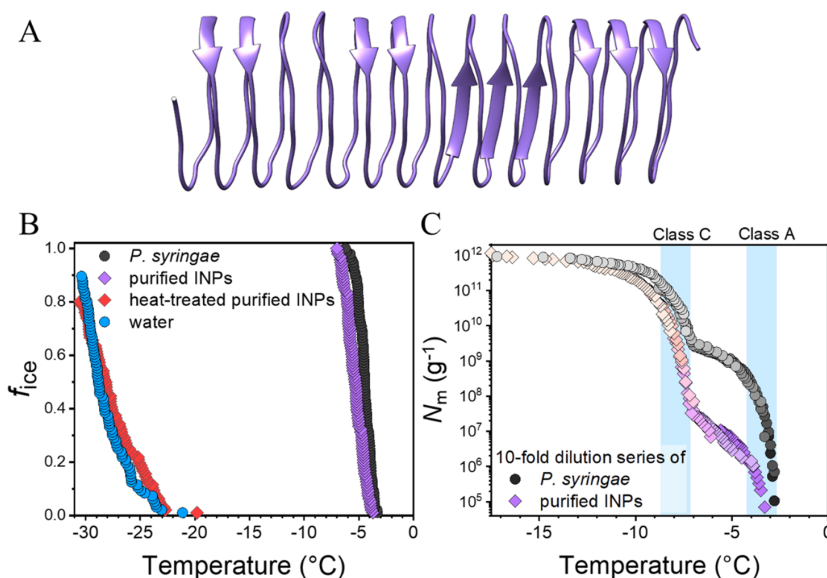spanning from 0.1 mg/mL to 1 ng/mL (see also Figure S3).

Figure 1. Structure and ice-nucleation activity of the proteinaceous ice nucleators from *P. syringae*. (A) Model structure of the INP from *P. syringae*, possessing a β-helical fold. (B) Statistical freezing curves of aqueous *P. syringae* solutions and their purified INPs, compared to the heat-inactivated INPs and the freezing curve of pure water in our system. Shown is the fraction of frozen 3 μL droplets (f_{ice}) vs temperature for the highest concentrations (0.1 mg/mL) of the utilized dilution series. (C) Freezing spectra of aqueous dilutions (10^{-1} mg/mL to 10^{-6} mg/mL) of *P. syringae* and their purified INPs. Shown are the cumulative numbers of active IN (N_m) per unit mass vs temperature. The temperature ranges for class A and class C bacterial IN in water are shaded in blue.

The curve of *P. syringae* shows two substantial increases in the cumulative number of IN per unit mass, $N_m(T)$ (Figure 1C) around −3.0 and −7.5 °C with plateaus between −4.5 and −7.0 °C and below −9.5 °C. At the plateaus, at temperatures below each increase of $N_m(T)$, fewer IN are active.[17] The two rises in the curve reveal that the ice-nucleation activity stems from two distinct classes of IN with different activation temperatures. We attribute the observed rise at −3.0 °C to large assemblies of INPs (class A IN) and the rise at −7.5 °C to smaller assemblies of INPs (class C IN) in accordance with previous studies.[18−23] The freezing curve of the purified INPs looks similar to the nonpurified INP solution, with a change in the ratio of the INP number in the two classes at −3.0 and −7.5 °C (see also Figure S2). Clearly, the purification process was successful and yielded active INPs. The reduction of class A IN activity for the purified sample indicates that the purification reduced the number of the larger INP aggregates compared to the nonpurified solution. This observation is in line with the hypothesis that the bacterial membranes are involved in the formation of larger functional INP aggregates,[5,10,24−28] and we expect bacterial membrane fragments to have no ice affinity.

Heat-treated INP solutions (see the SI for details on heat treatment) behave fundamentally differently. As apparent from comparing the droplet freezing statistics of the highest dilution concentrations shown in Figure 1B, the rises at −3.0 and −7.5 °C are completely absent. Instead, we observe activity only around −25 °C, which corresponds to background freezing of pure water in our system. Evidently, the heat treatment of the purified INPs completely inactivates their ice-nucleation abilities.

Using SFG spectroscopy, Pandey et al. reported that fragmented *P. syringae* bacteria (Snomax) show an increased capability to order water in their vicinity when cooled to

temperatures close to the melting point of deuterated water.[29] Control experiments using misfolded and denatured INP fragments, lipids, and the protein lysozyme did not show this effect. The alignment of water into an ordered structure was concluded to be a condition that will promote interfacial ice nucleation.

Here, we conducted further SFG experiments with active and heat-inactivated INPs to determine whether there is a direct causal correlation between enhanced SFG water signals at low temperatures and bacterial ice-nucleation activity. In SFG, a broadband infrared pulse resonant with the probed molecular vibrations and a visible pulse are combined at a surface to generate light at the sum frequency of the two incident fields. The SFG process is bulk-forbidden in isotropic media, and only ensembles of molecules with a net orientation, e.g., at an interface, can generate a detectable signal.

Figure 2A shows the temperature-dependent SFG spectra of aqueous solutions of purified INPs. The broad response from the O−D stretching bands of interfacial water molecules appears at frequencies below 2700 cm^{-1} and is affected by their interactions with the INPs adsorbed to the air−liquid interface. In the frequency region of 2800−3000 cm^{-1}, the SFG spectra show strong signals that we attribute to C−H stretching vibrations.

The SFG intensity of the O−D bands strongly increases upon lowering the temperature close to the melting temperature (3.82 °C for D$_2$O), indicating an increase in the structural order of the interfacial water molecules. This effect is completely reversible, as evident from the integrals of the water (O−D) bands for two cycles shown in the insets. The observed effect is also significantly larger than the effect observed for pure water (insets in Figure 2 and Figure S4).[30] In contrast, the signal intensity of the C−H stretching vibrations remains constant upon lowering the temperature.
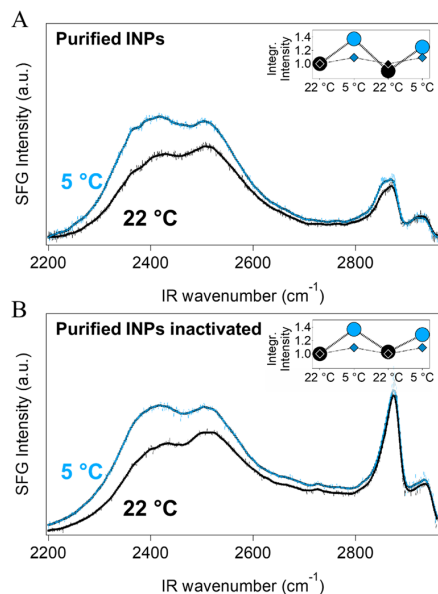
Figure 2. Temperature-dependent SFG measurements of aqueous solutions of active and heat-inactivated proteinaceous ice nucleators purified from *P. syringae*. (A) SFG spectra of the active INPs at the air−liquid interface in D_2O at 22 and 5 °C, respectively. (B) SFG spectra of the heat-inactivated INPs at the air−liquid interface in D_2O at 22 and 5 °C, respectively. The bulk INP concentrations were 0.1 mg/mL. The insets show the integrated SFG intensities in the O−D stretching frequency region of ∼2200−2700 cm^{-1} for two temperature cycles (circles) compared to pure D_2O (squares), normalized to the respective first value at 22 °C.

Figure 2B shows temperature-dependent SFG spectra of aqueous solutions of heat-inactivated INPs. Interestingly, we find that the completely inactive INPs adsorbed to the air−liquid interface cause a comparably strong increase in the SFG intensity of the O−D signals upon lowering the temperature. Thus, we conclude that the enhanced interfacial water ordering at low temperatures cannot be directly associated with the presence of ice-nucleation active sites.

Interestingly, while the water response is indistinguishable between the active and inactivated INPs, marked changes occur in the C−H stretching region. Although we cannot precisely assign the manifold C−H stretching contributions in the SFG spectra, these changes indicate that there is a substantial change in the protein structure after inactivation.

Figure 3A shows SFG spectra in the amide I region, which is sensitive to the secondary structure and orientation of proteins.[31,32] The amide I SFG spectra at room temperature and close to the melting temperature look very similar and show a strong signal at ∼1645 cm^{-1} and a weak signal at ∼1710 cm^{-1}. We assign the signal at 1645 cm^{-1} to the protein backbone of the INPs[33−35] and the weak signal at 1710 cm^{-1} to carbonyl groups in lipid molecules (see also Figure S5).[36−38] The lipid signal presumably originates from membrane lipids that remain protein-associated during the purification, which is in line with the presence of class A aggregates in our freezing experiments (Figure 1B). The observation that the amide I SFG spectra do not change upon cooling suggests no structural or conformational changes of the INPs upon approaching biologically relevant working temperatures. These conclusions
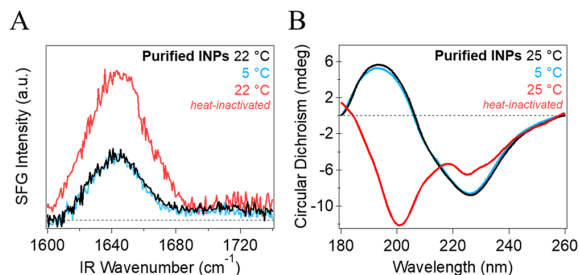

Figure 3. Amide I SFG and CD spectra of purified INPs derived from *P. syringae*. (A) SFG spectra of purified INPs in D_2O, measured in the amide I region. The spectra of the active INP at 22 and 5 °C look similar, with signals at ∼1640 and 1710 cm^{-1}. The heat-inactivated INPs (red) show a considerably increased signal at ∼1640 cm^{-1}. (B) CD spectra of purified INPs in water at 25 and 5 °C, as well as at 25 °C after heat-inactivation (red). Dashed lines indicate zero in both panels.

are supported by temperature-dependent CD spectra that also show very little change upon lowering the temperature (Figure 3B).

Upon heating of the purified INPs, the amide I SFG response and the CD spectrum undergo marked changes, as evident from Figures 3A and 3B. Figure 3A shows that the interfacial protein backbone SFG signal at ∼1645 cm^{-1} of heat-inactivated INPs is increased, while the lipid signal at ∼1710 cm^{-1} appears unaffected. The CD spectrum of the active INPs in Figure 3B shows a maximum molar ellipticity at 195 nm and a minimum at 228 nm, after which there is a gradual return to zero from 230 to 260 nm. Increasing the temperature reduces the molar ellipticity at 195 nm, and the minimum at 228 nm is reduced (see also Figure S7). These spectral changes following heating above ∼55 °C suggest significant, irreversible alterations in the secondary structure contents of the INPs. We propose that the observed irreversible conformational changes cause a loss of the proteins' native functional structure and are the origin of the complete elimination of the INP's ice-nucleation activity after heat treatment.

The CD spectrum of the purified INPs (Figure 4A) looks unusual, and its deconvolution using the structural database does not allow a clear distinction into the common secondary structures of α-helix, β-turn, β-strand, or random coil.[41] The spectral shape, however, shows similarities with those of AFPs derived from *Marinomonas primoryensis* (*Mp*AFP) and *Rhagium inquisitor* (*Ri*AFP) (Figure 4B, 4C) but with slightly shifted peak positions. Both AFPs have β-helical folds,[41] which is in agreement with the current theoretical model of the INP as shown in Figure 1A and the inset of Figure 4A.[42] The negligible changes in CD spectra at low temperatures are further consistent with temperature-dependent measurements of structurally similar β-helical AFPs.[43]

In summary, we purified INPs from *P. syringae* using ice-affinity methods and report experimental evidence that the purified INPs are ice-nucleation active and that they adopt defined solution structures, which show resemblance with β-helical AFP spectra.[41] We further show that enhanced interfacial water ordering at temperatures close to the melting point of ice is found not only for active but also for completely inactivated INPs. While protein-induced enhanced interfacial water ordering likely constitutes an essential part of INPs'
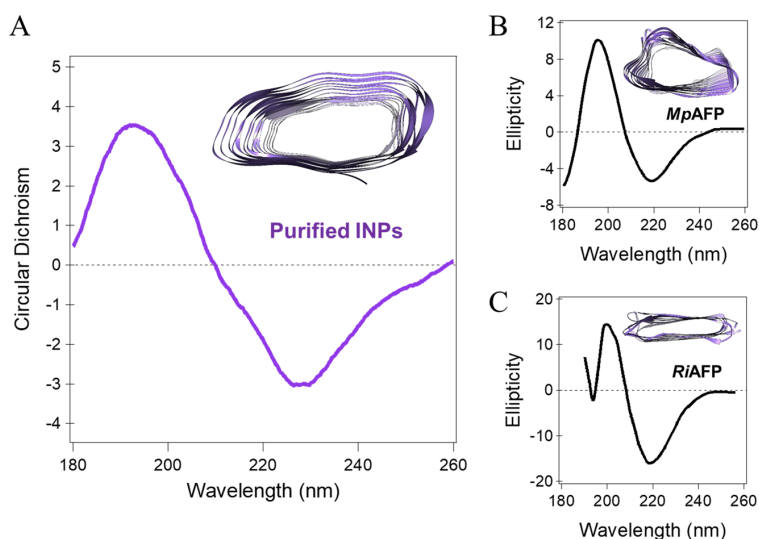
Figure 4. Circular dichroism spectrum of purified INPs compared to the spectra of two AFPs. (A) CD spectra of purified INPs derived from fragmented *P. syringae* at 25 °C in water [circular dichroism (mdeg)]. (B) CD spectrum of an AFP derived from *Marinomonas primoryensis* (*Mp*AFP) [ellipticity (mdeg)]. Data obtained from Garnham et al.[39] (C) CD spectrum of an AFP derived from *Rhagium inquisitor* (*Ri*AFP) [mean residue ellipticity (deg cm^{-2}/dmol × 10^{-3})]. Data obtained from Hakim et al.[40] Dashed lines indicate zero in all panels. The insets show cross sections of the proteins with the β-sheets highlighted in purple.

working mechanism, our results reveal that increased water ordering observed with SFG spectroscopy is, by itself, not a sufficient condition for INP activity. Instead, our results highlight that the intact three-dimensional fold is essential for the ice-nucleation activity of INPs. This observation, combined with the similarity of the protein structure of the INPs from *P. syringae* and other ice-binding proteins, suggests that supramolecular interactions and ordering are key to the exceptional ice-nucleation activity of bacterial INPs.[42] We hypothesize that the completely intact native structure of the INP is required for the formation of the functional aggregates that allow the formation of ice nuclei or embryos large enough to enable freezing at −2 °C (∼10^4 kDa).[23−25] Specifically, if the observed water ordering effect plays a role in bacterial ice nucleation, we can surmise that some secondary structures of the INPs remain at least partially intact, inducing a similar degree of order. However, the breakdown of higher-order structures (tertiary, quaternary) leads to the loss of the collective alignment of INP units that explains the substantial loss in effectiveness.[24] This hypothesis would predict a freezing behavior of the inactivated INPs comparable to structurally similar antifreeze proteins and will be tested in future studies.

ASSOCIATED CONTENT

Supporting Information
The Supporting Information is available free of charge at https://pubs.acs.org/doi/10.1021/acs.jpclett.0c03163.

Experimental details, experimental methods, and supporting Figures S1−S7: Coomassie blue-stained SDS PAGE analysis of ice-affinity purifications of the INPs; freezing experiments of aqueous solutions of *P. syringae* (A) and purified INPs (B); fraction of frozen droplets for *P. syringae* and purified INP solutions corresponding to data shown in Figure 1; temperature-dependent sum-frequency generation measurements of pure D$_2$O at 22 and 5 °C; SFG spectra in the amide I region; SFG

spectra of Snomax (gray) and purified INPs (black) as well as inactive INPs (red); CD spectra of purified INPs derived from *P. syringae* at temperatures from 25 to 75 °C in water as well as an autoclaved sample (121 °C) (A), and the melting curve of the protein obtained from the circular dichroism values at 222 nm (B); and CD spectra of purified INPs and fragmented *P. syringae* (Snomax), normalized to the highest local maximum, respectively (PDF)

AUTHOR INFORMATION

Corresponding Authors
Max Lukas − *Max Planck Institute for Polymer Research, 55128 Mainz, Germany;* ⓞ orcid.org/0000-0001-6949-8423; Email: lukas@mpip-mainz.mpg.de

Konrad Meister − *Max Planck Institute for Polymer Research, 55128 Mainz, Germany; University of Alaska Southeast, Juneau, Alaska 99801, United States;* ⓞ orcid.org/0000-0002-6853-6325; Email: meisterk@mpip-mainz.mpg.de

Authors
Ralph Schwidetzky − *Max Planck Institute for Polymer Research, 55128 Mainz, Germany*

Anna T. Kunert − *Max Planck Institute for Chemistry, 55128 Mainz, Germany*

Ellen H.G. Backus − *Max Planck Institute for Polymer Research, 55128 Mainz, Germany; Department of Physical Chemistry, University of Vienna, 1090 Vienna, Austria;* ⓞ orcid.org/0000-0002-6202-0280

Ulrich Pöschl − *Max Planck Institute for Chemistry, 55128 Mainz, Germany;* ⓞ orcid.org/0000-0003-1412-3557

Janine Fröhlich-Nowoisky − *Max Planck Institute for Chemistry, 55128 Mainz, Germany;* ⓞ orcid.org/0000-0002-1278-0054

Mischa Bonn − *Max Planck Institute for Polymer Research, 55128 Mainz, Germany;* ◉ orcid.org/0000-0001-6851-8453

Complete contact information is available at:
https://pubs.acs.org/10.1021/acs.jpclett.0c03163

Author Contributions

[⊥]These authors contributed equally.

Notes

The authors declare no competing financial interest.

■ REFERENCES

(1) Murray, B. J.; Broadley, S. L.; Wilson, T. W.; Bull, S. J.; Wills, R. H.; Christenson, H. K.; Murray, E. J. Kinetics of the Homogeneous Freezing of Water. *Phys. Chem. Chem. Phys.* **2010**, *12* (35), 10380−10387.

(2) Koop, T.; Luo, B.; Tsias, A.; Peter, T. Water Activity as the Determinant for Homogeneous Ice Nucleation in Aqueous Solutions. *Nature* **2000**, *406* (6796), 611−614.

(3) Kozloff, L. M.; Schofield, M. A.; Lute, M. Ice Nucleating Activity of Pseudomonas Syringae and Erwinia Herbicola. *J. Bacteriol.* **1983**, *153* (1), 222−231.

(4) Maki, L. R.; Galyan, E. L.; Chang-Chien, M.-M.; Caldwell, D. R. Ice Nucleation Induced by Pseudomonas Syringae1. *Appl. Microbiol.* **1974**, *28* (3), 456−459.

(5) Govindarajan, A. G.; Lindow, S. E. Size of Bacterial Ice-Nucleation Sites Measured in Situ by Radiation Inactivation Analysis. *Proc. Natl. Acad. Sci. U. S. A.* **1988**, *85*, 1334.

(6) Southworth, M. W.; Wolber, P. K.; Warren, G. J. Nonlinear Relationship between Concentration and Activity of a Bacterial Ice Nucleation Protein. *J. Biol. Chem.* **1988**, *263* (29), 15211−15216.

(7) Mueller, G. M.; Wolber, P. K.; Warren, G. J. J. C. Clustering of Ice Nucleation Protein Correlates with Ice Nucleation Activity. *Cryobiology* **1990**, *27* (4), 416−422.

(8) Schmid, D.; Pridmore, D.; Capitani, G.; Battistutta, R.; Neeser, J. R.; Jann, A. Molecular Organisation of the Ice Nucleation Protein Inav from Pseudomonas Syringae. *FEBS Lett.* **1997**, *414* (3), 590−594.

(9) Turner, M. A.; Arellano, F.; Kozloff, L. M. Three Separate Classes of Bacterial Ice Nucleation Structures. *J. Bacteriol.* **1990**, *172* (5), 2521−2526.

(10) Garnham, C. P.; Campbell, R. L.; Walker, V. K.; Davies, P. L. Novel Dimeric Beta-Helical Model of an Ice Nucleation Protein with Bridged Active Sites. *BMC Struct. Biol.* **2011**, *11* (1), 36.

(11) Hudait, A.; Moberg, D. R.; Qiu, Y.; Odendahl, N.; Paesani, F.; Molinero, V. Preordering of Water Is Not Needed for Ice Recognition by Hyperactive Antifreeze Proteins. *Proc. Natl. Acad. Sci. U. S. A.* **2018**, *115* (33), 8266−8271.

(12) Duman, J. G. Antifreeze and Ice Nucleator Proteins in Terrestrial Arthropods. *Annu. Rev. Physiol.* **2001**, *63* (1), 327−357.

(13) Adar, C.; Sirotinskaya, V.; Bar Dolev, M.; Friehmann, T.; Braslavsky, I. Falling Water Ice Affinity Purification of Ice-Binding Proteins. *Sci. Rep.* **2018**, *8* (1), 11046.

(14) Marshall, C. J.; Basu, K.; Davies, P. L. Ice-Shell Purification of Ice-Binding Proteins. *Cryobiology* **2016**, *72* (3), 258−263.

(15) Tomalty, H. E.; Graham, L. A.; Eves, R.; Gruneberg, A. K.; Davies, P. L. Laboratory-Scale Isolation of Insect Antifreeze Protein for Cryobiology. *Biomolecules* **2019**, *9* (5), 180.

(16) Kunert, A. T.; Lamneck, M.; Helleis, F.; Pöschl, U.; Pohlker, M. L.; Fröhlich-Nowoisky, J. Twin-Plate Ice Nucleation Assay (Tina) with Infrared Detection for High-Throughput Droplet Freezing Experiments with Biological Ice Nuclei in Laboratory and Field Samples. *Atmos. Meas. Tech.* **2018**, *11* (11), 6327−6337.

(17) Budke, C.; Koop, T. Binary: An Optical Freezing Array for Assessing Temperature and Time Dependence of Heterogeneous Ice Nucleation. *Atmos. Meas. Tech.* **2015**, *8* (2), 689−703.

(18) Maki, L. R.; Galyan, E. L.; Chang-Chien, M. M.; Caldwell, D. R. Ice Nucleation Induced by Pseudomonas Syringae. *Appl. Microbiol.* **1974**, *28* (3), 456−459.

(19) Yankofsky, S. A.; Levin, Z.; Bertold, T.; Sandlerman, N. Some Basic Characteristics of Bacterial Freezing Nuclei. *J. Appl. Meteorol.* **1981**, *20* (9), 1013−1019.

(20) Turner, M. A.; Arellano, F.; Kozloff, L. M. Three Separate Classes of Bacterial Ice Nucleation Structures. *J. Bacteriol.* **1990**, *172* (5), 2521−2526.

(21) Kozloff, L. M.; Turner, M. A.; Arellano, F. Formation of Bacterial Membrane Ice-Nucleating Lipoglycoprotein Complexes. *J. Bacteriol.* **1991**, *173* (20), 6528−6536.

(22) Schwidetzky, R.; Kunert, A. T.; Bonn, M.; Pöschl, U.; Ramløv, H.; DeVries, A. L.; Fröhlich-Nowoisky, J.; Meister, K. Inhibition of Bacterial Ice Nucleators Is Not an Intrinsic Property of Antifreeze Proteins. *J. Phys. Chem. B* **2020**, *124* (24), 4889−4895.

(23) Lukas, M.; Schwidetzky, R.; Kunert, A. T.; Pöschl, U.; Fröhlich-Nowoisky, J.; Bonn, M.; Meister, K. Electrostatic Interactions Control the Functionality of Bacterial Ice Nucleators. *J. Am. Chem. Soc.* **2020**, *142* (15), 6842−6846.

(24) Qiu, Y.; Hudait, A.; Molinero, V. How Size and Aggregation of Ice-Binding Proteins Control Their Ice Nucleation Efficiency. *J. Am. Chem. Soc.* **2019**, *141* (18), 7439−7452.

(25) Pummer, B. G.; Budke, C.; Augustin-Bauditz, S.; Niedermeier, D.; Felgitsch, L.; Kampf, C. J.; Huber, R. G.; Liedl, K. R.; Loerting, T.; Moschen, T.; et al. Ice Nucleation by Water-Soluble Macromolecules. *Atmos. Chem. Phys.* **2015**, *15* (8), 4077−4091.

(26) Ling, M. L.; Wex, H.; Grawe, S.; Jakobsson, J.; Londahl, J.; Hartmann, S.; Finster, K.; Boesen, T.; Santl-Temkiv, T. Effects of Ice Nucleation Protein Repeat Number and Oligomerization Level on Ice Nucleation Activity. *J. Geophys. Res.: Atmos.* **2018**, *123* (3), 1802−1810.

(27) Bonechi, C.; Tamasi, G.; Pardini, A.; Donati, A.; Volpi, V.; Leone, G.; Consumi, M.; Magnani, A.; Rossi, C. Ordering Effect of Protein Surfaces on Water Dynamics: Nmr Relaxation Study. *Biophys. Chem.* **2019**, *249*, 106149.

(28) Burke, M. J.; Lindow, S. E. Surface-Properties and Size of the Ice Nucleation Site in Ice Nucleation Active Bacteria - Theoretical Considerations. *Cryobiology* **1990**, *27* (1), 80−84.

(29) Pandey, R.; Usui, K.; Livingstone, R. A.; Fischer, S. A.; Pfaendtner, J.; Backus, E. H.; Nagata, Y.; Fröhlich-Nowoisky, J.; Schmuser, L.; Mauri, S.; et al. Ice-Nucleating Bacteria Control the Order and Dynamics of Interfacial Water. *Sci. Adv.* **2016**, *2* (4), No. e1501630.

(30) Moberg, D. R.; Straight, S. C.; Paesani, F. Temperature Dependence of the Air/Water Interface Revealed by Polarization Sensitive Sum-Frequency Generation Spectroscopy. *J. Phys. Chem. B* **2018**, *122* (15), 4356−4365.

(31) Meister, K.; Roeters, S. J.; Paananen, A.; Woutersen, S.; Versluis, J.; Szilvay, G. R.; Bakker, H. J. Observation of Ph-Induced Protein Reorientation at the Water Surface. *J. Phys. Chem. Lett.* **2017**, *8* (8), 1772−1776.

(32) Roeters, S. J.; van Dijk, C. N.; Torres-Knoop, A.; Backus, E. H.; Campen, R. K.; Bonn, M.; Woutersen, S. Determining in Situ Protein Conformation and Orientation from the Amide-I Sum-Frequency Generation Spectrum: Theory and Experiment. *J. Phys. Chem. A* **2013**, *117* (29), 6311−6322.

(33) Fu, L.; Wang, Z.; Psciuk, B. T.; Xiao, D.; Batista, V. S.; Yan, E. C. Characterization of Parallel Beta-Sheets at Interfaces by Chiral Sum Frequency Generation Spectroscopy. *J. Phys. Chem. Lett.* **2015**, *6* (8), 1310−1315.

(34) Chen, X.; Wang, J.; Sniadecki, J. J.; Even, M. A.; Chen, Z. Probing Alpha-Helical and Beta-Sheet Structures of Peptides at Solid/Liquid Interfaces with Sfg. *Langmuir* **2005**, *21* (7), 2662−2664.

(35) Golbek, T. W.; Franz, J.; Elliott Fowler, J.; Schilke, K. F.; Weidner, T.; Baio, J. E. Identifying the Selectivity of Antimicrobial Peptides to Cell Membranes by Sum Frequency Generation Spectroscopy. *Biointerphases* **2017**, *12* (2), 02D406.

(36) Dreier, L. B.; Bonn, M.; Backus, E. H. G. Hydration and Orientation of Carbonyl Groups in Oppositely Charged Lipid Monolayers on Water. *J. Phys. Chem. B* **2019**, *123* (5), 1085−1089.

(37) Blume, A.; Hubner, W.; Messner, G. Fourier Transform Infrared Spectroscopy of 13c = O-Labeled Phospholipids Hydrogen Bonding to Carbonyl Groups. *Biochemistry* **1988**, *27* (21), 8239−8249.

(38) Mantsch, H. H.; Mcelhaney, R. N. Phospholipid Phase-Transitions in Model and Biological-Membranes as Studied by Infrared-Spectroscopy. *Chem. Phys. Lipids* **1991**, *57* (2−3), 213−226.

(39) Garnham, C. P.; Gilbert, J. A.; Hartman, C. P.; Campbell, R. L.; Laybourn-Parry, J.; Davies, P. L. A Ca2+-Dependent Bacterial Antifreeze Protein Domain Has a Novel Beta-Helical Ice-Binding Fold. *Biochem. J.* **2008**, *411* (1), 171.

(40) Hakim, A.; Thakral, D.; Zhu, D. F.; Nguyen, J. B. Expression, Purification, Crystallization and Preliminary Crystallographic Studies of Rhagium Inquisitor Antifreeze Protein. *Acta Crystallogr., Sect. F: Struct. Biol. Cryst. Commun.* **2012**, *68* (5), 547−550.

(41) Basu, K.; Graham, L. A.; Campbell, R. L.; Davies, P. L. Flies Expand the Repertoire of Protein Structures That Bind Ice. *Proc. Natl. Acad. Sci. U. S. A.* **2015**, *112* (3), 737−742.

(42) Hudait, A.; Odendahl, N.; Qiu, Y.; Paesani, F.; Molinero, V. Ice-Nucleating and Antifreeze Proteins Recognize Ice through a Diversity of Anchored Clathrate and Ice-Like Motifs. *J. Am. Chem. Soc.* **2018**, *140* (14), 4905−4912.

(43) Li, N.; Kendrick, B. S.; Manning, M. C.; Carpenter, J. F.; Duman, J. G. Secondary Structure of Antifreeze Proteins from Overwintering Larvae of the Beetle Dendroides Canadensis. *Arch. Biochem. Biophys.* **1998**, *360* (1), 25−32.

64

Supporting Information:

Interfacial Water Ordering is Insufficient to Explain Ice-Nucleating Protein Activity

Max Lukas[#,†,*], Ralph Schwidetzky[#,†], Anna T. Kunert[‡], Ellen H.G. Backus[†,∥], Ulrich Pöschl[‡], Janine Fröhlich-Nowoisky[‡], Mischa Bonn[†] and Konrad Meister[†,⊥,*]

[†]Max Planck Institute for Polymer Research, 55128 Mainz, Germany

[‡]Max Planck Institute for Chemistry, 55128 Mainz, Germany

[∥]University of Vienna, 1090 Vienna, Austria

[⊥]University of Alaska Southeast, 99801 Juneau, AK, United States

[#]Authors contributed equally

AUTHOR INFORMATION

Corresponding Authors

M. Lukas − Max Planck Institute for Polymer Research, 55128 Mainz, Germany; orcid.org/0000-0001-6949-8423; Email: lukas@mpip-mainz.mpg.de

K. Meister − Max Planck Institute for Polymer Research, 55128 Mainz, Germany; University of Alaska Southeast, Juneau, Alaska 99801, United States; orcid.org/0000-0002-6853-6325; Email: meisterk@mpip-mainz.mpg.de

Methods:

Ice Affinity Purification

Falling water ice-affinity purification and rotary ice-shell purification were used to purify the INPs of the bacteria *P. syringae*. Details of the purification method have been described elsewhere.[1,2] We purified fragmented *P. syringae* cells obtained as the commercial product Snomax. For falling water ice-affinity purification, a commercially available ice-making machine (K20, Whirlpool, USA) was used to pump an aqueous Snomax solution (750 mg in 2.5 L H_2O) to the top of a metal plate. As the temperature of the metal plate is cooled down to subzero temperatures, nucleation occurs. The constant *P. syringae* solution circulation leads to the adsorption of the weakly ice-binding INPs to the ice-surface. During the purification, ~30% of the solution gradually froze. The obtained ice was melted and freeze-dried to obtain a mixture of all present INPs from *P. syringae*. The large size of the INPs, the presence of protein-associated lipids and the tendency of aggregation and formation of assemblies makes the quantification of the purification challenging. We first assessed the success of the INP purification by determining the ice nucleation activity of the purified INP samples using TINA measurements. We further performed gel electrophoresis experiments to track the removal of impurities of the purified solution. Supporting Figure 1B shows that at similar mass concentrations, the purified and ice-active INP samples do not show several of the protein bands that were found for the fragmented *P. syringae* cells. We also do not expect a strong singular bond of an INP in the gel since *P. syringae* produces variants of INPs which can have many different sizes. Moreover, Coomassie blue has been shown to only weakly bind to a protein with a similar structure and amino acid composition.[3]

For the preparation of our INP samples, we chose the more efficient falling water ice-affinity purification to obtain the needed large amounts of lyophilized INP samples for SFG and TINA experiments. We further compared the results of the falling water ice-affinity purification with results obtained from rotary ice-shell purification.[1] Here, in a 500 mL flask, 20–30 mL water was used to form an ice-shell using a dry ice-ethanol bath for 30–60 s. The flask was rotated in a temperature-controlled ethylene glycol bath, and the temperature of the bath was set to −2 °C. 100 mL precooled Snomax solution (0.5 mg/mL) was added, and the flask rotated continuously in the bath until 30% of the solution were frozen. The flask was removed from the motor, and the liquid phase was separated from the ice phase. The ice-phase contained INPs from

P. syringae and was melted. The obtained solution was then used to confirm the similarity of CD spectra of INPs purified with this method and the falling water ice-affinity method.

Heat Treatment/Inactivation

Heat treatments were performed to inactivate the bacterial IN. For this, a 0.1 mg/mL Snomax solution was autoclaved at 121 °C for 20 min (Laboklav 25). The autoclaved solutions did not show any indication for lowered protein concentrations (visual observation) due to precipitation. Additionally, surface tension measurements of the untreated and heat-treated samples conducted during the Amide I SFG experiments also revealed no significant changes or indications for the formation of precipitates.

TINA Experiments

Ice nucleation experiments were performed using the high-throughput Twin-plate Ice Nucleation Assay (TINA), which has been described in detail elsewhere.[4] In a typical experiment, the investigated IN sample was serially diluted 10-fold by a liquid handling station (epMotion ep5073, Eppendorf, Hamburg, Germany). 96 droplets (3 µL) per dilution were placed on two 384-well plates and tested with a continuous cooling-rate of 1 °C/min from 0 °C to −20 °C with a temperature uncertainty of ±0.2 °C. The droplet-freezing was determined by two infrared cameras (Seek Therman Compact XR, Seek Thermal Inc., Santa Barbara, CA, USA). The obtained fraction of frozen droplets was used to calculate the cumulative number of ice nucleators using the Vali formula.[5] All experiments were performed multiple times with independent samples, as shown in SFig 2. Background freezing of pure (autoclaved MilliQ) water in our system occurred at around −25 °C and is likely caused by remaining impurities or the supporting surface of the utilized well plates.

Sum-Frequency Generation Spectroscopy

The details of the experimental setup have been described elsewhere.[6] SFG intensity spectra were obtained using a conventional SFG setup in reflection geometry. Broadband infrared (IR) (~ 5 µJ pulse energy) and a narrowband visible (VIS, ~ 13 µJ, centered at ~ 800 nm) fs-pulses were focused and spatially and temporally overlapped on the sample surface, with incident angles of 36° (VIS) and 41° (IR) with respect to the surface normal. The spectra presented in this study were simultaneously recorded in the C-H and O-D -stretch (IR ~2000–3100 cm^{-1}) or in the Amide I (IR ~1600–1700 cm^{-1}) region. The bandwidths were determined by the

respective bandwidths of the IR pulses. The spectral resolution was limited by the bandwidth of the VIS pulses (FWHM ~ 15 cm^{-1}). The generated SFG signals were collimated by a lens, directed and focused onto a spectrograph (*Acton SP 300i, Princeton Instruments*) and detected by an EMCCD camera (*Newton 970, Andor Instruments*). Spectra were obtained in the SSP polarization combination (S-polarized SFG, S-polarized VIS, P-polarized IR) or in the SPS polarization combination (S-polarized SFG, P-polarized VIS, S-polarized IR). Background spectra were taken with blocked IR and unblocked VIS beam, and all spectra were normalized to nonresonant reference spectra from z-cut quartz. The SFG measurements were performed in a custom-made, temperature controllable PTFE-coated aluminum trough. We conducted measurements at 22 °C and 5 °C. The INP and Snomax (*P. syringae*) solutions were measured at a concentration of 0.1 mg/mL. Samples were allowed to equilibrate for at least two hours before measurements. The equilibration of the samples at the interface was complete, when the simultaneously measured surface tension (Wilhelmy plate method, *DeltaPi/Dyne Probes, Kibron Inc.*) was constant and the SFG spectra did not change within one hour. Calibration of the surface tension measurements was conducted using pure D_2O (Sigma Aldrich 99.9%) before each SFG experiment. The sample box was purged with nitrogen during the experiments. Comparison of Amide I SFG measurements in two different polarization combinations did not reveal any indication for protein reorientation on the surface.

CD spectroscopy

The purified INPs were analyzed at a concentration of 0.5 mg/mL in MilliQ water. The sample was measured in a 350 µL quartz cuvette (Hellma Analytics) with a path length of 1 mm. Measurements were conducted using a *JASCO 1500* circular dichroism spectrometer. Temperatures were controlled and maintained by a *PTC-510* Peltier temperature-controlled sample holder in combination with an external cryogenic bath. Equilibration time for every sample before each set of measurements was 15 min. Spectra were background subtracted and processed using the Spectra Manager Analysis program from JASCO.

INP Model

The INP model consists of a 16-amino acid ring (GYGSTQTSGSESSLTA), which was repeated 14 times, along the x-axis. The initial structure for INP was taken from Hudait *et al.* 2018.[7]

S4
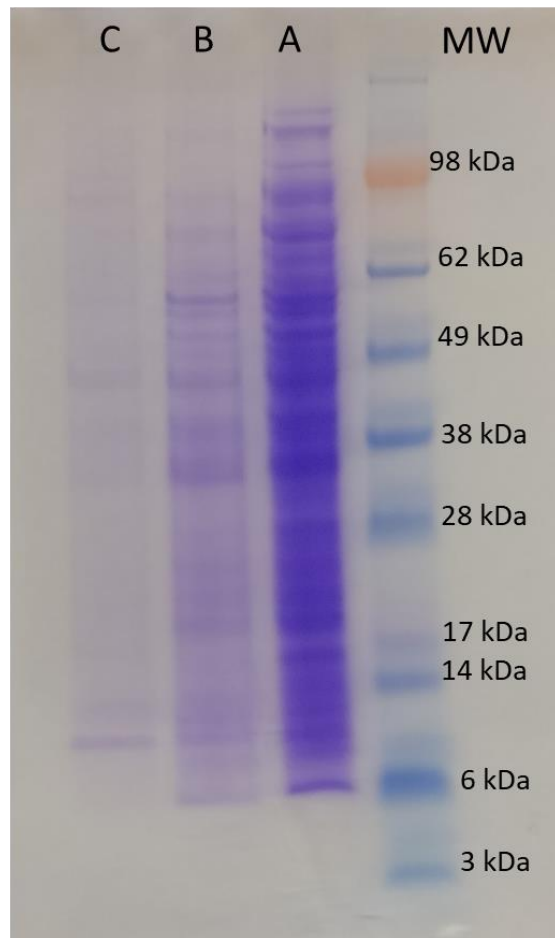
Supporting Figure 1: Coomassie blue-stained SDS-PAGE analysis of ice-affinity purifications of the INPs. Lanes were loaded with fractions on an equal volume basis relative to the starting material. Samples shown in each lane correspond to protein markers, original *P. syringae* culture (A) and purified sample after the first (B) and second round (C) of falling water ice-affinity purification.

S5
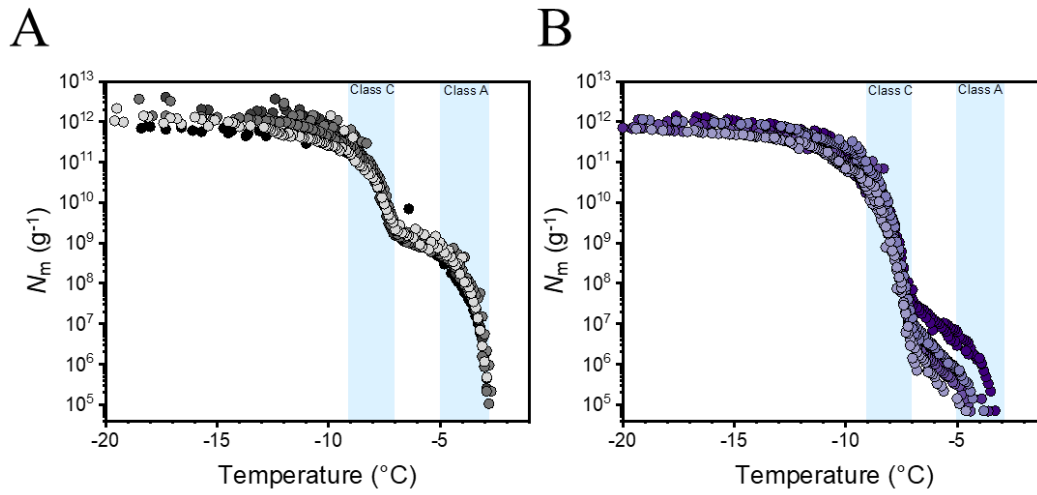
Supporting Figure 2: Freezing experiments of aqueous solutions of *P. syringae* (A) and purified INPs (B). Shown are the cumulative number of active ice nucleators per unit mass of *P. syringae* vs. temperature for five independent experiments. The temperature ranges for class A and class C INPs are shaded in light blue.
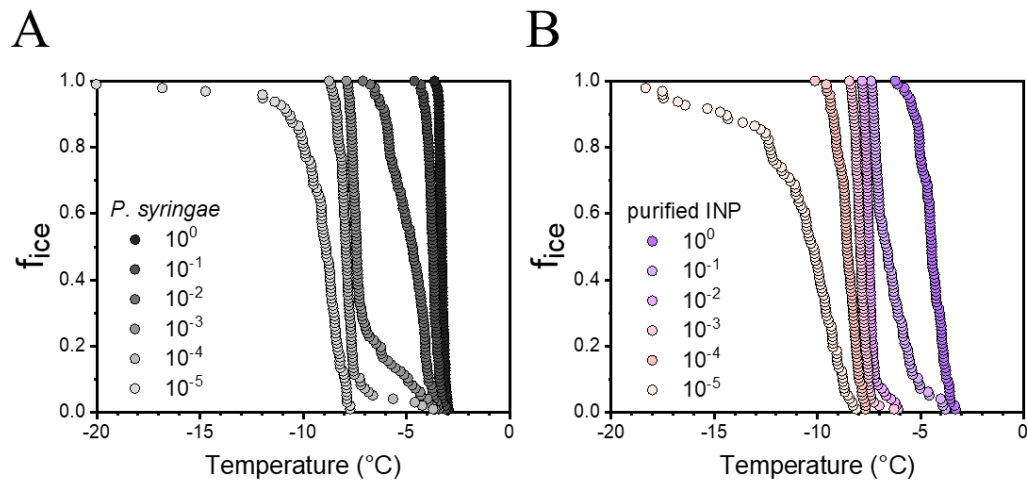
Supporting Figure 3: Fraction of frozen droplets for *P. syringae* and purified INP solutions corresponding to data shown in Figure 1. The initial concentration of 10^{-1} mg/mL is diluted down to 10^{-6} mg/mL.
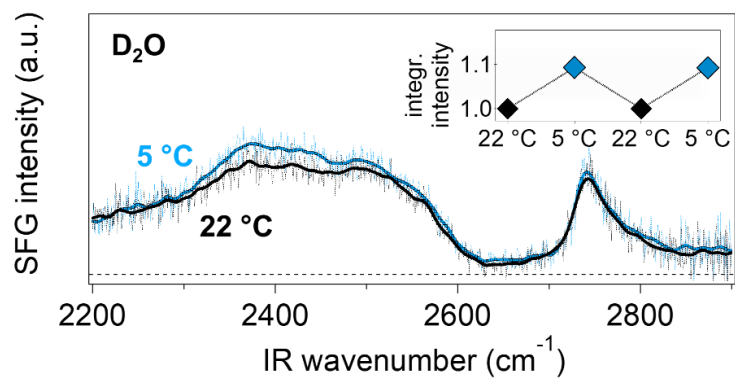
Supporting Figure 4: Temperature-dependent sum-frequency generation measurements of pure D_2O at 22 and 5 °C. The peak at ~2720 cm^{-1} stems from the free O-D stretching mode which arises from non-hydrogen-bonded deuterium atoms at the surface. The free O-D disappears upon surface coverage with sample molecules. The inset shows the integrated SFG intensities of the O-D stretching frequency region ~2200–2700 cm^{-1} for two temperature cycles.
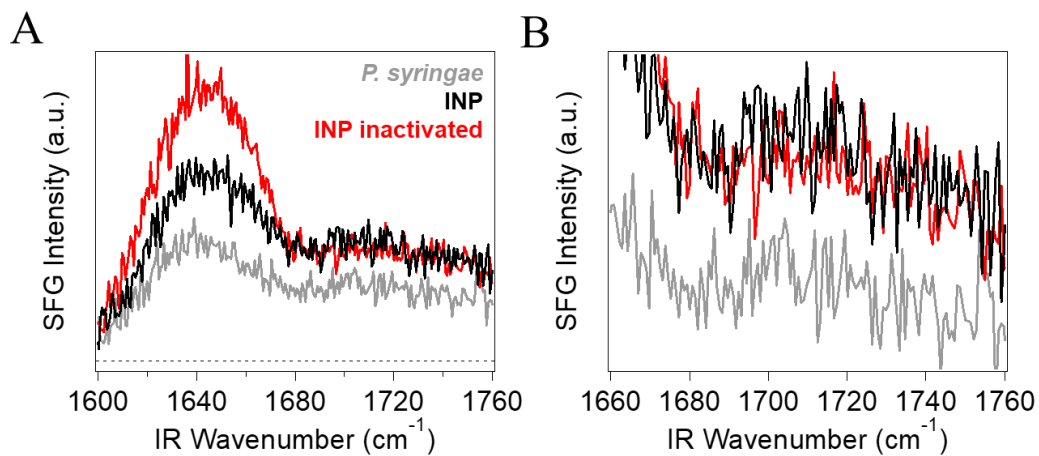
Supporting Figure 5: SFG spectra in the amide I region. (A) *P. syringae* (grey), purified INPs derived from *P. syringae* (black) and heat-treated INPs, all measured at room temperature in H₂O. The dashed line indicates zero. (B) Magnification of the carbonyl region, which reveals weak lipid signals. As a result of the purification, the protein signals of the INP samples is increased compared to that of the bacteria.
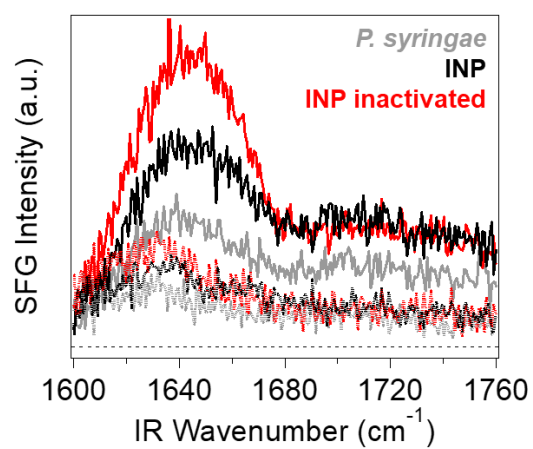
Supporting Figure 6: SFG spectra of Snomax (grey) and purified INPs (black) as well as inactive INPs (red). Measurements were performed in the SSP (solid lines) and PSP (dotted lines) polarization configuration.

S10
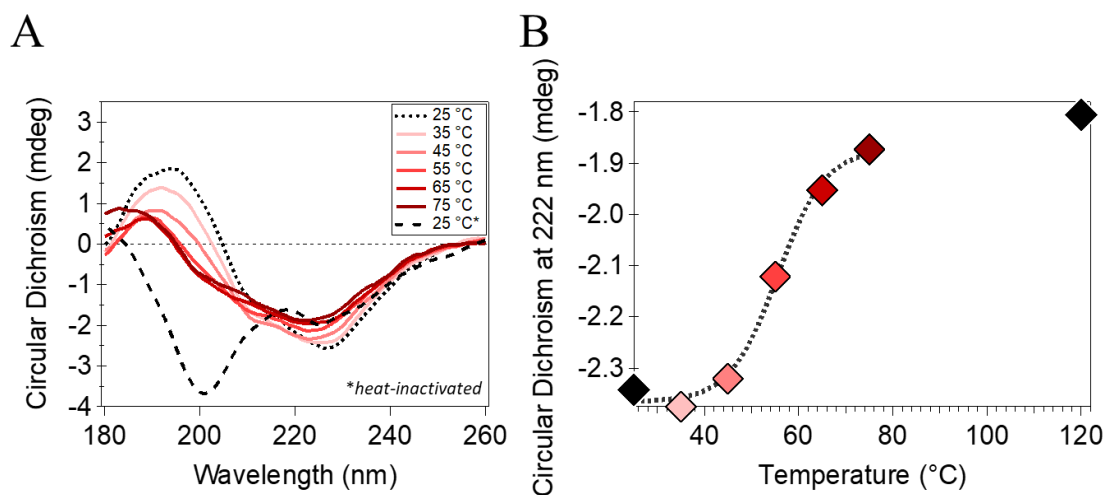
Supporting Figure 7: CD spectra of purified INPs derived from *P. syringae* at temperatures from 25 to 75 °C in water as well as an autoclaved sample (heated to 121°C, measured at 25 °C) (A), and melting curve of the protein obtained from the circular dichroism values at 222 nm (B). The dashed line is a guide for the eye. The melting point is estimated to be at around 55 °C.

S11
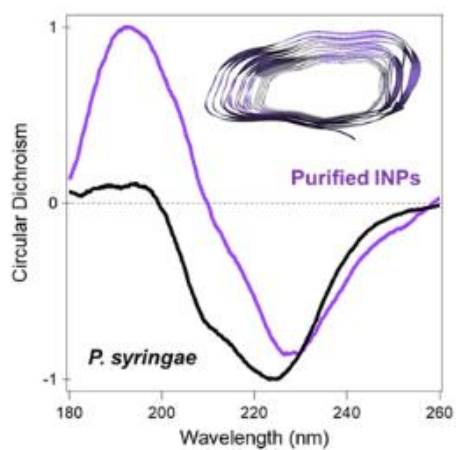
Supporting Figure 8: CD spectra of purified INPs and fragmented *P. syringae* (Snomax), normalized to the highest local maximum, respectively.

REFERENCES

(1)   Marshall, C. J.; Basu, K.; Davies, P. L. Ice-Shell Purification of Ice-Binding Proteins. *Cryobiology* **2016,** *72* (3), 258-263.

(2)   Adar, C.; Sirotinskaya, V.; Bar Dolev, M.; Friehmann, T.; Braslavsky, I. Falling Water Ice Affinity Purification of Ice-Binding Proteins. *Sci Rep* **2018,** *8* (1), 11046.

(3)   Tomalty, H. E.; Graham, L. A.; Eves, R.; Gruneberg, A. K.; Davies, P. L. Laboratory-Scale Isolation of Insect Antifreeze Protein for Cryobiology. *Biomolecules* **2019,** *9* (5), 180.

(4)   Kunert, A. T.; Lamneck, M.; Helleis, F.; Pöschl, U.; Pöhlker, M. L.; Fröhlich-Nowoisky, J. Twin-Plate Ice Nucleation Assay (Tina) with Infrared Detection for High-Throughput Droplet Freezing Experiments with Biological Ice Nuclei in Laboratory and Field Samples. *Atmos. Meas. Tech.* **2018,** *11* (11), 6327-6337.

(5)   Reischel, M. T.; Vali, G. Freezing Nucleation in Aqueous Electrolytes. *Tellus* **1975,** *27* (4), 414-427.

(6)   Dreier, L. B.; Wolde-Kidan, A.; Bonthuis, D. J.; Netz, R. R.; Backus, E. H. G.; Bonn, M. Unraveling the Origin of the Apparent Charge of Zwitterionic Lipid Layers. *J Phys Chem Lett* **2019,** *10* (20), 6355-6359.

(7)   Hudait, A.; Odendahl, N.; Qiu, Y.; Paesani, F.; Molinero, V. Ice-Nucleating and Antifreeze Proteins Recognize Ice through a Diversity of Anchored Clathrate and Ice-Like Motifs. *J. Am. Chem. Soc.* **2018,** *140* (14), 4905-4912.

A.4 Schwidetzky *et al.*, Chem. Eu. J, 2021

Specific Ion–Protein Interactions Influence Bacterial Ice Nucleation

R. Schwidetzky[*,1], M. Lukas[*,1], A. YazdanYar[*,1], A. T. Kunert[2], U. Pöschl[2], K. F. Dohmke[1], J. Fröhlich-Nowoisky[2], M. Bonn[1], T. Koop[3], Y. Nagata[1] and K. Meister[1,4]

[*] These authors contributed equally to this work.

[1] Max-Planck-Institute for Polymer Research, 55128 Mainz, Germany

[2] Max-Planck-Institute for Chemistry, 55128 Mainz, Germany

[3] Bielefeld University, 33615 Bielefeld, Germany

[4] University of Alaska Southeast, Juneau, Alaska 99801, United States

Author contributions:

R.S. performed the freezing experiments and contributed to analyzing and discussing the results as well as writing the manuscript.

▌Membrane Proteins

Specific Ion–Protein Interactions Influence Bacterial Ice Nucleation

Ralph Schwidetzky[+],*[a] Max Lukas[+],[a] Azade YazdanYar[+],[a] Anna T. Kunert,[b] Ulrich Pöschl,[b] Katrin F. Domke,[a] Janine Fröhlich-Nowoisky,[b] Mischa Bonn,[a] Thomas Koop,[c] Yuki Nagata,[a] and Konrad Meister*[a, d]

Abstract: Ice nucleation-active bacteria are the most efficient ice nucleators known, enabling the crystallization of water at temperatures close to 0 °C, thereby overcoming the kinetically hindered phase transition process at these conditions. Using highly specialized ice-nucleating proteins (INPs), they can cause frost damage to plants and influence the formation of clouds and precipitation in the atmosphere. In nature, the bacteria are usually found in aqueous environments containing ions. The impact of ions on bacterial ice nucleation efficiency, however, has remained elusive. Here, we demonstrate that ions can profoundly influence the efficiency of bacterial ice nucleators in a manner that follows the Hofmeister series. Weakly hydrated ions inhibit bacterial ice nucleation whereas strongly hydrated ions apparently facilitate ice nucleation. Surface-specific sum-frequency generation spectroscopy and molecular dynamics simulations reveal that the different effects are due to specific interactions of the ions with the INPs on the surface of the bacteria. Our results demonstrate that heterogeneous ice nucleation facilitated by bacteria strongly depends upon the nature of the ions, and specific ion–protein interactions are essential for the complete description of heterogeneous ice nucleation by bacteria.

Introduction

At ambient conditions, the formation of ice from water is thermodynamically favored at temperatures below 0 °C, however, this crystallization process is kinetically hindered. As a result, pure water can be supercooled to temperatures as low as −38 °C, below which homogenous ice nucleation occurs.[1] In natural systems, water freezes in a heterogeneous process, facilitated by the presence of ice-nucleating substances of biological and abiotic origins.[2] Ice nucleation-active bacteria from *Pseudomonas syringae* are the best ice nucleators (IN) known,

[a] R. Schwidetzky,[+] M. Lukas,[+] Dr. A. YazdanYar,[+] Dr. K. F. Domke, Prof. Dr. M. Bonn, Dr. Y. Nagata, Prof. Dr. K. Meister
Max Planck Institute for Polymer Research, 55128 Mainz (Germany)
E-mail: schwidetzkyr@mpip-mainz.mpg.de
meisterk@mpip-mainz.mpg.de

[b] Dr. A. T. Kunert, Prof. Dr. U. Pöschl, Dr. J. Fröhlich-Nowoisky
Max Planck Institute for Chemistry, 55128 Mainz (Germany)

[c] Prof. Dr. T. Koop
Bielefeld University, 33615 Bielefeld (Germany)

[d] Prof. Dr. K. Meister
University of Alaska Southeast, 99801 Juneau, AK (USA)

[+] These authors contributed equally to this work.

Supporting Information and the ORCID identification number(s) for the author(s) of this article can be found under:
https://doi.org/10.1002/chem.202004630.

and their ability to induce ice formation at high sub-zero temperatures has direct impacts on agriculture, microbial ecology, geology and precipitation patterns.[3] The ability to nucleate ice is attributed to ice-nucleating proteins (INPs). INPs are monomeric but have repeatedly been shown to form functional aggregates in the bacterial outer membranes, and the largest INP aggregates ($>$50 INPs) are thought to be responsible for enabling freezing close to 0 °C.[4] INP-induced ice nucleation usually takes place in ionic solutions, because ions are omnipresent in the environment. Therefore, the effect of salts on the INP-mediated freezing of water is of fundamental interest. For homogenous ice nucleation, it is established that ice formation depends on the water activity of the given aqueous solution, independently of the nature of the present ions.[1] In contrast, the effect of ions on heterogeneous ice formation facilitated by bacteria has remained largely elusive.[3b, 5]

The interaction of ions with proteins can be categorized by the Hofmeister series and has been observed for numerous processes.[6] In the 1880s, Franz Hofmeister ranked ions based on their ability to precipitate proteins from solution.[7] The work resulted in the following rankings for anions: $SO_4^{2-} > HPO_4^{2-} > CH_3COO^- > Cl^- > Br^- > I^- > SCN^-$ and for cations: $[C(NH_2)_3]^+$ (Gdm^+) $> Mg^{2+} > Ca^{2+} > Li^+ > Na^+ > NH_4^+ > N(CH_3)_4^+$, respectively.[8] Ions on the left side of the series stabilize and salt out proteins, whereas ions on the right denature and solubilize proteins. It is generally accepted that the Hofmeister series is an interfacial phenomenon, in which direct protein-ion-water interactions are of central significance.[6a, 9] Here, we investigate the effects of different ions on the ice nu-

Chemistry–A European Journal

Full Paper
doi.org/10.1002/chem.202004630

Chemistry Europe
European Chemical
Societies Publishing

cleation activity of the proteinaceous IN from *Pseudomonas syringae* (*P. syringae*).[10]

Results and Discussion

Figure 1 A shows the results of freezing experiments of a dilution series of the bacterial IN (Snomax) in water and in aqueous solutions containing either 0.5 mol kg^{-1} NaCl, NH$_4$Cl, NaSCN or MgSO$_4$. The freezing spectra of the bacterial IN in water and in the presence of MgSO$_4$ look similar and show two increases in the cumulative number of IN per unit mass of bacteria, N_m (T), at $-2.9\,°C$ and $-7.5\,°C$ with plateaus between $-4.5\,°C$ and $-7\,°C$ and below $-9.5\,°C$. The two increases reveal that the ice nucleation activity of *P. syringae* is caused by two classes of IN with different activation temperatures, and we attribute them to class A and C IN, respectively.[11] Class C IN is usually attributed to individual INPs or small assemblies in the bacterial membrane, and class A IN is thought to originate from larger clusters of class C IN, as shown in Figure 1 B.

In the presence of NaCl, the freezing spectrum is identical to the one of *P. syringae* in pure water, with a ~2°C shift of the INP-mediated freezing curve to lower temperatures. This observed shift is in line with the expected shift of $-1.86\,°C$ based on the colligative melting point depression properties of a 0.5 mol kg^{-1} NaCl solution (see Supporting Information, Figure S1).[12] For NH$_4$Cl and NaSCN solutions, the trends are markedly different from those of *P. syringae* in pure water or NaCl solution. In the presence of NH$_4$Cl, the class A-related increase at about $-2.9\,°C$ is absent; instead, we observe a small increase at $-7\,°C$. Further, the second increase is observed at $-9\,°C$, which again is ~2°C lower than that in water and which is similar to the shift observed on adding NaCl. For NaSCN, we observe only a single increase centered at $-11.5\,°C$. Evidently,

the four salts influence the efficiency of the INP-mediated freezing points differently.

We examined whether different water activities in the investigated salt solutions may be the origin of the observed ion-specific effects on bacterial ice nucleation. Accounting for the effects of water activity, we found that they do not alter the respective observed influence of the salts on the INP-mediated freezing point (Figure S2). In fact, NaCl, NH$_4$Cl, and NaSCN all have nearly identical water activities at 0.5 mol kg^{-1}. Yet, they differ significantly in their effect on the bacterial ice nucleation activity. Clearly, the effect of salts on heterogeneous ice nucleation facilitated by bacterial INPs is not simply determined by water activity, as holds for homogeneous nucleation, and requires further investigations.

We conducted a comprehensive experimental evaluation of seventeen salts of the Hofmeister series to obtain more details of the specific effects of ions on the bacterial activities of the INPs. The experimentally determined freezing points in the salt solutions shown in Figure 2 were corrected for their respective water activity by taking the shifted melting points into account (see Supporting Information).

Four major categories can be identified from the plotted salt induced shifts in freezing temperatures: (i) NaSCN influences both bacterial IN classes A and C and lowers their respective freezing temperatures; (ii) NH$_4$Cl lowers the freezing temperature of class A, but does not affect class C; (iii) NaCl has negligible effects on both freezing temperatures; and (iv) MgSO$_4$ increases the freezing temperatures of classes A and C. Interestingly, the effects of the salts on the INP-mediated freezing temperatures follows the individual position of the anions in the Hofmeister series. Weakly hydrated ions such as SCN$^-$ lower the INP-mediated freezing temperatures, whereas salts that have no effects, or apparently facilitate freezing, are more strongly hydrated ions such as Cl$^-$ or SO$_4^{2-}$.
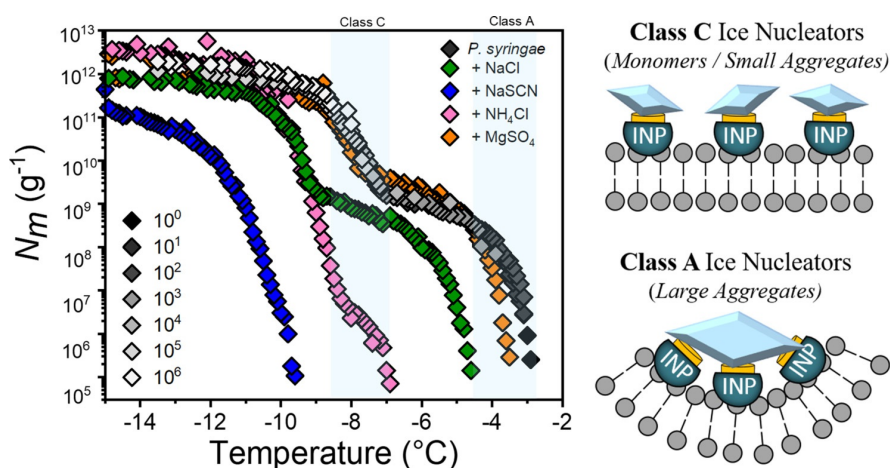

Figure 1. Freezing experiments of bacterial ice nucleators from *P. syringae* in aqueous solutions: (A) Results for IN in pure water (grey) and in aqueous solutions of 0.5 mol kg^{-1} NaCl (green), NH$_4$Cl (magenta), NaSCN (blue), and MgSO$_4$ (orange). Plotted is the cumulative number of IN per unit mass of *P. syringae* vs. temperature for various degrees of dilution, starting with 0.1 mg mL^{-1}. Numbers and grey shades in the legend denote dilution factors and are shown for *P. syringae* in pure water only. The temperature ranges for class A and C bacterial IN in water are shaded in blue. (B) Proposed schematic illustration of class C and A IN structures. The high activity of bacterial IN relies on INPs, which assemble into larger functional protein clusters. The most effective IN clusters are termed class A, consisting of large INP assemblies. Class C IN are less active and consist of smaller INP assemblies.
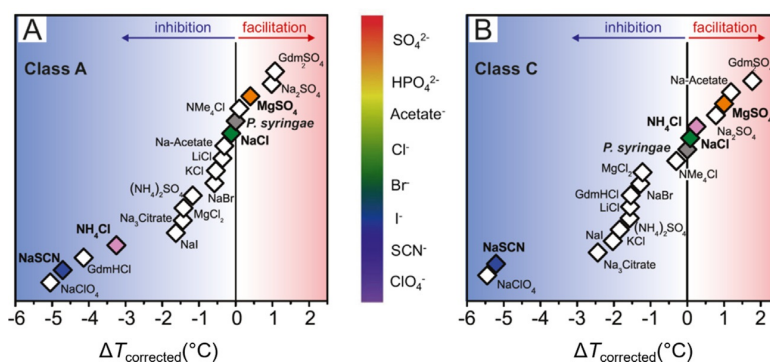
Chemistry–A European Journal

Full Paper
doi.org/10.1002/chem.202004630

Chemistry
Europe
European Chemical
Societies Publishing

Figure 2. Effects of salts on the activity of bacterial IN from *P. syringae*: Shown are the temperature shifts (ΔT) induced by different salts on the freezing temperatures of class A and class C IN in water (grey diamonds). Vertically, the salts are ordered by the appearance of their anions in the Hofmeister series. The shifts represent the temperature difference for a frozen fraction of 50% of investigated samples ($f_{ice} = 0.5$) between *P. syringae* in water and in the respective 0.5 mol kg^{-1} salt solution, the latter corrected for their water-activity effect (see Supporting Information). The concentration of *P. syringae* was 0.1 mg mL^{-1} for class A IN (A) and 10^{-6} mg mL^{-1} for class C IN (B). The corresponding anion Hofmeister series is shown in the inset.

How can the different effects of the ions on the ice nucleation properties of the bacteria be explained? Different ions affect the local water structure, having different hydrogen-bond-forming and -breaking capabilities.[6a] Ions can, however, also alter protein conformations, and we surmise that both effects could alter the freezing behavior of INPs.[6a] Clearly, molecular-level information is required to explore both possibilities. The combination of sum-frequency generation (SFG) vibrational spectroscopy experiments and molecular dynamics (MD) simulations is ideally suited for elucidating biomolecular conformations and biomolecule-water interactions.[4c, 9b, 13]

SFG is a surface-specific method in which an infrared and a visible pulse are combined at a surface to generate light at the sum-frequency of the two incident fields. The selection rule of this spectroscopy dictates that only ensembles of molecules with a net orientation, for example, at an interface, can generate a detectable signal. The SFG signal intensity depends on

the number of aligned molecules at the interface. Changes in the solution pH was shown to strongly affect the SFG spectral response of bacterial ice nucleators. Therefore, all SFG experiments were performed in PBS buffer since the addition of salts can affect the solution pH in an ion-specific manner.[14] At charged surfaces, the surface field can align the water dipoles, as illustrated in Figure 3A. Such charge-induced enhanced ordering of the interfacial water molecules causes the SFG signal intensity in the O–H stretching region (IR wavenumber ~3100–3600 cm^{-1}) to increase, and inversely, the SFG signal intensity can be used to quantify the amount of charge at the electrified surface. This concept has been used previously to investigate the effect of ions on biomolecules.[6b, 9b, 14, 15]

Figure 3B shows the SFG spectra of aqueous solutions of *P. syringae* adsorbed to the air–liquid interface in PBS buffer and in the presence of salts. The signals in the frequency region from 2800–3100 cm^{-1} originate from C–H stretching vi-
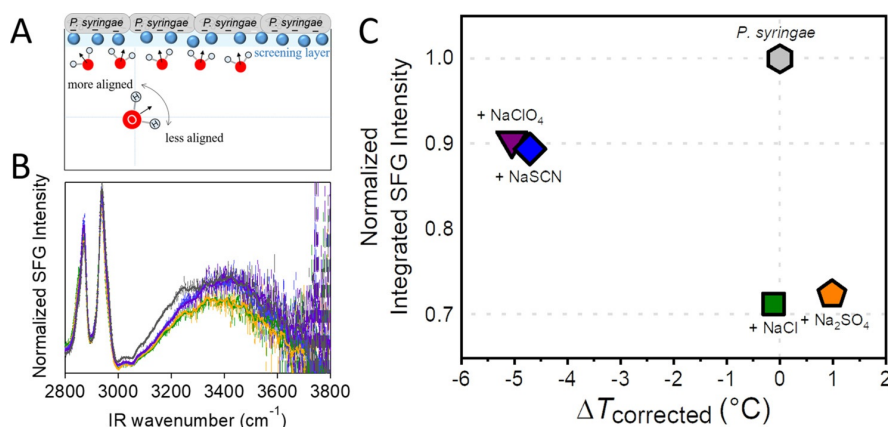

Figure 3. Sum-frequency generation spectroscopy measurements of bacterial ice nucleators from *P. syringae* in aqueous salt solutions: (A) Schematic representation of the orientation of interfacial water molecules next to *P. syringae* (grey) possessing a negative net charge. The straight arrows indicate the direction of the water dipoles and the blue spheres depict ions. The curved arrow indicates possible disruptions of the alignment due to the presence of salts. (B) SFG spectra of *P. syringae* layers at the air–liquid interface of a phosphate-buffered saline (PBS) solution (grey) and in the presence of NaCl (green), NaSCN (blue), NaClO$_4$ (purple) and Na$_2$SO$_4$ (orange). The bulk concentration of *P. syringae* was 0.1 mg mL^{-1}, and the salt concentrations were chosen to have identical ionic strength. (C) Normalized integrated SFG intensities of the frequency region from 3100–3600 cm^{-1} for *P. syringae* in PBS and in the presence of salts plotted against the respective class A temperature shifts observed in the freezing experiments (Figure 2A).

brations. The broad signal between 3100–3600 cm^{-1} is assigned to the O—H stretching band of interfacial water molecules. We integrated the SFG signal in the frequency region of 3100–3600 cm^{-1} to allow for a direct quantitative comparison of the effects of the salts as shown in Figure 3 C. The SFG intensity is highest in PBS buffer and decreases upon the addition of salts. This observation can be explained as follows: The cations of the salts screen the net negative charge of *P. syringae*, which in turn reduces the water molecules' alignment and causes the O—H stretch signal to decrease.[15] Interestingly, the salts show different efficiencies in screening the net charge despite having identical ionic strengths. The weakly hydrated anions decrease the SFG intensity less than strongly hydrated anions like SO$_4^{2-}$. One explanation for this observation is the preferred adsorption of weakly hydrated anions to the *P. syringae* surface, rendering it more negative and, in turn, causing more water alignment and increasing the O-H signal intensity compared to strongly hydrated anions, which prefer to stay solvated (Scenario 1). A second explanation is that the ions can change the INP conformation, thereby affecting the charge distribution of the protein, which would alter the water alignment and thus the SFG signal (Scenario 2).

To distinguish between both scenarios, we performed MD simulations of the solvated INP in the presence of ions. The INP structure consists of fourteen repetitions of the amino acid sequence GYGSTQTSGSESSLTA as shown in Figure 4 A. The INP model adapts a β-helical structure, in excellent agreement with

our circular dichroism spectrum of the purified INP (Figure S3). We particularly focused on the water orientation and ionic distribution near the proposed active sites of the INP[16] and considered simulation settings, in which we kept the INP structure either flexible or fixed (see Experimental Section).

We analyzed the water orientation ($\langle \cos\theta \rangle$) relative to the IN planes of the INP in the presence of the different salts (Figure S4), where θ is the angle between the water molecule's bisector and the plane normal of the active sites (see Experimental Section). We can directly compare the experimental and computational findings by obtaining the square of the integrated $\rho\langle \cos\theta \rangle$ (ρ is the density of water), which is approximately proportional to the SFG intensity.[17]

The comparison of the SFG intensities and the square of $\rho\langle \cos\theta \rangle$ (calculated SFG intensities) for the INP samples, presented in Figure 4 B, reveals that the simulations reproduce the experimental trend and capture the effects of the different ions on the water orientation near the INP well. In agreement with the experiments, we observe that weakly hydrated ions are found near the INP surface, rendering the protein more negative and enhancing water orientation relative to the active IN planes, while strongly hydrated ions show a gradual increase in the population when moving away from the INP surface to the bulk water (Figure 4 C). This finding is in line with Scenario 1 and consistent with the Hofmeister series. The depth profiles of the different ion species along the surface normal of the IN planes are further largely different (Fig-
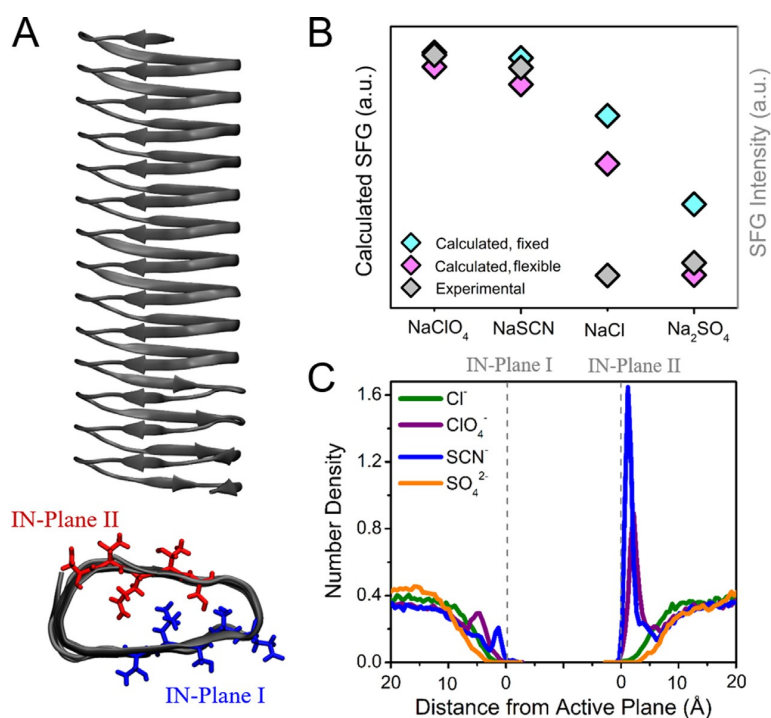

Figure 4. Molecular dynamics simulations of the INP from *P. syringae*: (A) Model of the INP from *P. syringae*, consisting of 14 repeats and forming a β-helical structure. The two ice-nucleating planes are highlighted in red and blue, respectively. (B) Calculated and experimental SFG intensities in the presence of four different salts. In the simulations, the INP structure was kept in either a fixed (cyan) or a flexible (magenta) geometry. (C) Distribution of the anions with respect to the two active ice-nucleating planes for the flexible geometry of the INP.

Chemistry–A European Journal

Full Paper
doi.org/10.1002/chem.202004630

Chemistry Europe
European Chemical
Societies Publishing

ure 4 C), underlining the different ion interactions with the protein.

To elucidate the possible effect of the protein conformation on the water orientation and ion distributions (Scenario 2), we computed the water orientation near the INP by fixing the protein geometry in the MD simulation (see Experimental Section). The fixed structure of the INP shows the same trend for the ions, but the extent of the effects on the water orientation is reduced (Figure 4 B). We also examined the depth profile of the ion distributions for the fixed geometry (Figure S5), and, compared to the flexible geometry, the weakly hydrated anions approach the fixed INP much less. Coming back to the two scenarios, these observations manifest, that the change of the INP conformation and the propensity of the ions affect the water ordering property as competing scenarios.

Conclusions

The above investigations suggest that ions affect the conformation and aggregation behavior of biomolecules in aqueous solutions very specifically, in addition to nonspecific electrostatic interactions. Our study provides unique insights into how different ions influence protein stability, aggregation, and, ultimately, the biological function of an organism. We provide clear evidence that the effect of ions on bacterial ice nucleation is not independent of the nature of the ion but is due to specific ion–protein interactions that follow the trend of the Hofmeister series.

Weakly hydrated anions like perchlorate can directly interact with individual INP units and change their conformations and disable their individual IN sites (Figure 4, Figure S3). The change in INP conformation further leads to the loss of the formation of the functional aggregates and collective alignment of INP units that enable freezing at $-2\,°C$ (Figure 1). We also note that ion addition can affect the pH value of the aqueous solutions in an ion-specific manner. Such pH changes strongly influence the ice nucleation activity of *P. syringae* as shown before,[3b, 14] and those results are consistent with the observations made for NH_4Cl in this work. Hence, the observed ion-specific inhibitory effect of NH_4Cl is entirely due to the change of the solution pH (Figure S6).

Strongly hydrated ions enhance bacterial ice nucleation slightly. Sulfate ions were reported to decrease the reorientation time of water at the ice-binding site of antifreeze proteins[18] and can create low-mobility water regions next to the active IN sites of the INP (see Experimental Section, Figures S7, S8). We speculate that such low-mobility regions may facilitate ice nucleation, in line with a recent MD simulation showing that low-mobility regions are the origin of seeds in homogenous ice nucleation.[19]

Undoubtedly, fully intact ice-nucleating protein (INP) structures and a precise sub-Ångström arrangement of INPs and water molecules are required for the extraordinary ice nucleation ability of INPs. The large variety of the salts investigated here, together with the different types of mechanisms by which ions affect bacterial IN, suggest that the general water activity-based ice nucleation criterion is not sufficient for a de-

tailed description of the effects of solutes on bacterial IN. The water-activity approach is valid for those cases, where the solutes do not directly affect the surfaces of ice nucleators, which is clearly not the case for the bacterial INPs studied here. We note that several of the salts studied here have direct biological and atmospheric relevance and are found at similar concentrations in the environment, for example, in natural cloud condensation nuclei.[5a, 20] As bacterial ice nucleation efficiency is controlled by complex and mutually interacting environmental variables such as the presence of co-solutes or pH value, these all must be taken into account for a complete understanding and a validated environmental application of bacterial ice nucleators' properties.

Conflict of interest

The authors declare no conflict of interest.

[1] T. Koop, B. P. Luo, A. Tsias, T. Peter, *Nature* **2000**, *406*, 611–614.
[2] a) P. W. Wilson, A. F. Heneghan, A. D. Haymet, *Cryobiology* **2003**, *46*, 88–98; b) L. R. Maki, K. J. Willoughby, *J. Appl. Meteorol.* **1978**, *17*, 1049–1053; c) K. Liu, C. Wang, J. Ma, G. Shi, X. Yao, H. Fang, Y. Song, J. Wang, *Proc. Natl. Acad. Sci. USA* **2016**, *113*, 14739–14744; d) G. Bai, D. Gao, Z. Liu, X. Zhou, J. Wang, *Nature* **2019**, *576*, 437–441.
[3] a) C. Morris, D. Georgakopoulos, D. Sands in *Journal de Physique IV (Proceedings), Vol. 121*, EDP sciences, **2004**, pp. 87–103; b) E. Attard, H. Yang, A.-M. Delort, P. Amato, U. Pöschl, C. Glaux, T. Koop, C. Morris, *Atmos. Chem. Phys.* **2012**, *12*, 10667–10677.
[4] a) A. G. Govindarajan, S. E. Lindow, *Proc. Natl. Acad. Sci. USA* **1988**, *85*, 1334–1338; b) C. P. Garnham, R. L. Campbell, V. K. Walker, P. L. Davies, *BMC Struct. Biol.* **2011**, *11*, 36; c) R. Pandey, K. Usui, R. A. Livingstone, S. A. Fischer, J. Pfaendtner, E. H. Backus, Y. Nagata, J. Fröhlich-Nowoisky, L. Schmuser, S. Mauri, J. F. Scheel, D. A. Knopf, U. Pöschl, M. Bonn, T. Weidner, *Sci Adv* **2016**, *2*, e1501630.
[5] a) M. T. Reischel, G. Vali, *Tellus* **1975**, *27*, 414–427; b) T. Koop, B. Zobrist, *Phys. Chem. Chem. Phys.* **2009**, *11*, 10839–10850.
[6] a) P. Jungwirth, P. S. Cremer, *Nat. Chem.* **2014**, *6*, 261–263; b) X. Chen, T. Yang, S. Kataoka, P. S. Cremer, *J. Am. Chem. Soc.* **2007**, *129*, 12272–12279; c) D. J. Tobias, J. C. Hemminger, *Science* **2008**, *319*, 1197–1198.
[7] F. Hofmeister, *Arch. Exp. Pathol. Pharmakol.* **1888**, *24*, 247–260.
[8] H. I. Okur, J. Hladilkova, K. B. Rembert, Y. Cho, J. Heyda, J. Dzubiella, P. S. Cremer, P. Jungwirth, *J. Phys. Chem. B* **2017**, *121*, 1997–2014.
[9] a) K. D. Collins, M. W. Washabaugh, *Q Rev Biophys* **1985**, *18*, 323–422; b) E. E. Bruce, P. T. Bui, B. A. Rogers, P. S. Cremer, N. F. A. van der Vegt, *J. Am. Chem. Soc.* **2019**, *141*, 6609–6616.
[10] a) H. Wex, S. Augustin-Bauditz, Y. Boose, C. Budke, J. Curtius, K. Diehl, A. Dreyer, F. Frank, S. Hartmann, N. Hiranuma, E. Jantsch, Z. A. Kanji, A. Ki-

selev, T. Koop, O. Möhler, D. Niedermeier, B. Nillius, M. Rösch, D. Rose, C. Schmidt, I. Steinke, F. Stratmann, *Atmos. Chem. Phys.* **2015**, *15*, 1463–1485; b) C. Budke, T. Koop, *Atmos. Meas. Tech.* **2015**, *8*, 689–703; c) A. T. Kunert, M. Lamneck, F. Helleis, U. Pöschl, M. L. Pöhlker, J. Fröhlich-Nowoisky, *Atmos. Meas. Tech.* **2018**, *11*, 6327–6337.

[11] M. A. Turner, F. Arellano, L. M. Kozloff, *J. Bacteriol.* **1990**, *172*, 2521–2526.

[12] A. A. Zavitsas, *J. Phys. Chem. B* **2001**, *105*, 7805–7817.

[13] K. Meister, S. Strazdaite, A. L. DeVries, S. Lotze, L. L. Olijve, I. K. Voets, H. J. Bakker, *Proc. Natl. Acad. Sci. USA* **2014**, *111*, 17732–17736.

[14] M. Lukas, R. Schwidetzky, A. T. Kunert, U. Pöschl, J. Fröhlich-Nowoisky, M. Bonn, K. Meister, *J. Am. Chem. Soc.* **2020**, *142*, 6842–6846.

[15] a) S. Nihonyanagi, S. Yamaguchi, T. Tahara, *J. Am. Chem. Soc.* **2014**, *136*, 6155–6158; b) X. Chen, S. C. Flores, S. M. Lim, Y. Zhang, T. Yang, J. Kherb, P. S. Cremer, *Langmuir* **2010**, *26*, 16447–16454.

[16] A. Hudait, N. Odendahl, Y. Q. Qiu, F. Paesani, V. Molinero, *J. Am. Chem. Soc.* **2018**, *140*, 4905–4912.

[17] F. Tang, T. Ohto, S. Sun, J. R. Rouxel, S. Imoto, E. H. G. Backus, S. Mukamel, M. Bonn, Y. Nagata, *Chem. Rev.* **2020**, *120*, 3633–3667.

[18] K. Meister, J. G. Duman, Y. Xu, A. L. DeVries, D. M. Leitner, M. Havenith, *J. Phys. Chem. B* **2014**, *118*, 7920–7924.

[19] M. Fitzner, G. C. Sosso, S. J. Cox, A. Michaelides, *Proc. Natl. Acad. Sci. USA* **2019**, *116*, 2009–2014.

[20] T. F. Whale, M. A. Holden, T. W. Wilson, D. O'Sullivan, B. J. Murray, *Chem. Sci.* **2018**, *9*, 4142–4151.

84

Chemistry–A European Journal

Supporting Information

Specific Ion–Protein Interactions Influence Bacterial Ice Nucleation

Ralph Schwidetzky[+],*[a] Max Lukas[+],[a] Azade YazdanYar[+],[a] Anna T. Kunert,[b] Ulrich Pöschl,[b] Katrin F. Domke,[a] Janine Fröhlich-Nowoisky,[b] Mischa Bonn,[a] Thomas Koop,[c] Yuki Nagata,[a] and Konrad Meister*[a, d]

Author Contributions

R.S., J.F.-N., Y.N. and K.M. designed research. R.S. and M.L. performed the experiments, A.Y.Y. and Y.N. performed the MD simulation. K.M. supervised the project. All authors analyzed and discussed the results and wrote the manuscript.

Contents

1

Experimental Procedures

Samples

Pure water was prepared as described elsewhere.[1] PBS-Buffer, the different salts, NaOH, and HCl were obtained from Sigma Aldrich (Darmstadt, Germany). Snomax® was purchased from SMI Snow Makers AG (Thun, Switzerland) and consists of a preparation of inactivated bacteria cells of *P. syringae*. The Snomax® concentration was 0.1 mg/mL, and the pH value in pure water was 6.2 +/- 0.2. SFG and TINA experiments were performed in pure water or in 0.15 M PBS buffer. The pH values of all samples were measured before each measurement.

Colligative Melting Point Depression

The theoretical melting point depression of the salts was calculated according to the formula:

$$\Delta T_f = n \cdot c \cdot E_f = n \cdot c \cdot (-1.86 \; \frac{K \cdot kg}{mol})$$

where *c* is the molality of the salt, *n* is the number of ions of the completely dissociated salt and E_f is the cryoscopic constant of water.[2]

Melting Point Correction

The reported shifts in ice nucleation temperature between *P. syringae* in pure water and in the different salt solutions in Figure 2 were corrected for the change in ice melting point due to the presence of the salt. The ice melting point of each salt solution at 0.5 mol/kg was determined as follows: For those salts for which ice melting point data as a function of salt concentration were available, these data were fitted and the interpolated ice melting point at 0.5 mol/kg was obtained. For the remaining salts, we used data of the osmotic coefficient at 0.5 mol/kg (at 25 °C) to determine the water activity of the solution.[2-3] The water activity can then be used to determine the ice melting point using a previously established parameterization (assuming a temperature-independent water activity of the solution).[4] The latter procedure was checked with NaCl, and the two results agreed very well.

TINA Experiments

Ice nucleation experiments were performed using the high-throughput Twin-plate Ice Nucleation Assay (TINA), which has been described recently.[1] In a typical experiment, the investigated sample was serially diluted 10-fold by a liquid handling station (epMotion ep5073, Eppendorf, Hamburg, Germany), and 96 droplets (3 μL) per dilution were placed on two 384-well plates. The experiment was run with a continuous cooling-rate of 1 °C/min from 0 °C to -20 °C (temperature uncertainty < 0.2 °C), and droplet freezing was determined by two infrared cameras (Seek Therman Compact XR, Seek Thermal Inc., Santa Barbara, CA, USA). The obtained fraction of frozen droplets was used to calculate the cumulative number of IN using the Vali formula.[5] Experiments were performed multiple times on independent samples. To quantify and compare the data, we used the T_{50} value of class A (0.1 mg/mL) and class C (10^{-6} mg/mL) dilutions, respectively. The T_{50} value is defined as the temperature at which 50% of the investigated droplets are frozen.

CD Spectroscopy

Circular dichroism experiments were performed on a Jasco-1500 CD-Spectrometer. Measurements were performed at an INP concentration of ~0.01 mg/mL in pure water or in 0.5 mol/kg salt solutions. Samples were measured in a quartz cuvette at room temperature and the scan rate was 5 nm/min and the scan range was from 180 - 260 nm with data pitch

0.2 nm and data integration time 2s. INPs of *P. syringae* (Snomax) were purified using rotary ice-affinity purification as described elsewhere.[6]

Sum-Frequency Generation Spectroscopy Experiments

The details of the experimental setup have been described previously.[7] For the SFG intensity spectra, we used a conventional SFG setup in reflection geometry. A broadband IR (~ 5 µJ, full width half maximum (FWHM) of ~ 450 cm^{-1}) and a narrowband VIS (~ 13 µJ, centered at ~ 800 nm, FWHM of ~ 15 cm^{-1}) beam were focused and spatially and temporally overlapped on the sample surface, with incident angles of 36° (VIS) and 41° (IR) with respect to the surface normal. The spectra presented in this study were simultaneously recorded in the C-H and O-H-stretch region. The spectral resolution was limited by the bandwidth of the VIS. The generated SFG signal was collimated by a lens, directed and focused onto a spectrograph (*Acton SP 300i, Princeton Instruments*) and detected by a camera (*Newton 970, Andor Instruments*). All spectra were obtained in the ssp-polarization combination (s-polarized SFG, s-polarized VIS, p-polarized IR). Background spectra were taken with a blocked IR beam and all spectra were normalized to reference spectra from z-cut quartz. The SFG measurements were performed in a custom-made Teflon trough at room temperature. The Snomax (*P. syringae*) solutions were measured at a concentration of 0.1 mg/mL. Samples were allowed to equilibrate for two hours before measurements. The equilibration of the samples at the interface was complete, when the SFG spectra did not change within one hour. The concentrations of the salts were adjusted to obtain identical ionic strengths (molalities: 0.5 mol/kg for NaCl, NaSCN, NaClO$_4$; 0.16 mol/kg for Na$_2$SO$_4$). The pH-values of all samples were kept constant by measuring in PBS buffer.

MD Simulations

INP Model and Active Ice-nucleating Sites

Force field-based all-atom molecular dynamics simulations were performed using the Gromacs package. The INP model consists of a 16-amino acid ring (GYGSTQTSGSESSLTA), which was repeated 14 times, along the x-axis (Figure 4A). The initial structure for INP was taken from Hudait et *al.*,[8] and its intra- and intermolecular interactions were parameterized using the OPLS-AA force field.[9]

The active ice-nucleating sites were chosen based on the previous findings where STQTS and ESSLT sequences were found to induce ice nucleation with comparable efficiency.[8] These two sequences lie on opposite sides of the INP (Figure 4A). We define two active ice-nucleating sites based on the ESSLT sequences on one side of the INP, as well as the STQTS sequence on the opposite side of the INP (IN-plane I and II, respectively). These planes are defined based on the atomic positions.

To define a plane, we used two vectors that lie in the plane (V1 and V2). For the STQTS active plane, V1 was defined between the two Ser residues on the two sides of the sequence (STQTS). Since INP has 14 rings, V1 was averaged over these 14 rings. V2 was defined between the alpha carbon of GLN (Q) in the second and one before the last ring in INP. For the ESSLTA active plane, V1 was averaged over the 14 rings between GLU and ALA residues, while V2 was defined for the LEU residues.

Analysis of water orientation was performed based on the angle of water molecules bisectors $(\overrightarrow{OH_1} + \overrightarrow{OH_2})$ and the plane normal of the active ice-nucleating sites.

Simulation Protocols

We ran the molecular dynamics simulations for five systems, with an initial dimension of $80 \times 55 \times 55$ Å^3, and periodic boundary conditions. All systems contained the solvated INP in water (modelled by the SPC/E water model), and 14 sodium ions to neutralize the net charge of INP. One of the systems did not contain any additional ions. The other systems each contained an ionic solution of Na-Cl, Na-ClO$_4$, Na-SCN, and Na$_2$-SO$_4$, with an ionic concentration of ~0.8 M, where the number of cationic species was twice for Na$_2$-SO$_4$ compared to the mono-valent anions. A position restraint was applied to the alpha carbon atom of all the Gly residues in INP (42 atoms in total) to stabilize its conformation, and results were compared to simulation, for which all the backbone atoms were under the position restraint. We refer to the former as the flexible and to the latter as the fixed INP geometry.

Before the production molecular dynamics runs of 50 ns in using the NPT ensemble at 300 K, all the systems were stabilizing by minimizing the total energy of the systems. Sequently, we increased the temperature gradually to 300 K during 2 ns, and we ran molecular dynamics simulation at 300 K for an additional 3 ns using the velocity rescaling through canonical ensemble method, followed by an NPT equilibration step of 5 ns, and a production run of 50 ns at 300

3

K. The pressure of the system was controlled by the Berendsen barostat. A time step of 1 fs was used to integrate the equations of motion and the atomic positions were stored every 10 ps. A cutoff radius of 10 Å was used for short-range van der Waals interactions. Long-range electrostatic interactions were treated by the Fast smooth Particle-Mesh Ewald (SPME) algorithm.

Ionic Species

The intra- and intermolecular force field parameters and the atomic charges for the ionic species are presented in table S1.

Hydrogen Bond Lifetimes

To explore the hydrogen bond dynamics in the systems, and understand the effect of salts on the dynamics, we computed the autocorrelation time function of hydrogen bonds. The data are displayed in Figure S7 and S8. The hydrogen bond kinetics are not a single-step process[10], and should be interpreted considering various mechanisms. In fact, with fitting the hydrogen bond lifetime autocorrelation to a function in the form of

$$a \exp\left(-\frac{t}{\tau_1}\right) + b \exp\left(-\frac{t}{\tau_2}\right) + c_0,$$

we can correlate the two relaxation times to the breaking and re-formation of bonds, and to the fact that the movement of a molecule, will require collective rearrangement of the neighboring molecules.[11] The former is responsible for fast dynamics in the system, and the fast decay of the autocorrelation function (Fig. S8), while the latter is responsible for the slow dynamics in the system.[11a, 12] Previous molecular dynamics simulations found that the lifetime of hydrogen bonds grows by ~180 times close to the ice nucleation temperature[13] and leads to very slow dynamics in the system. Results for the two relaxation times are presented in Table S2, for the flexible and the fixed INP geometry. Corresponding error bars can be seen in Fig. S8. We observe that for both relaxation times, the system which contains sulfate shows a longer relaxation time for hydrogen bonds, suggesting that this anion causes the dynamics to slow down. Furthermore, the effect of the different salts on the relaxation times is reduced when the fixed geometry of INP is considered (Fig. S8), highlighting that the conformation of the INP affects the interaction of the ions with the INP.
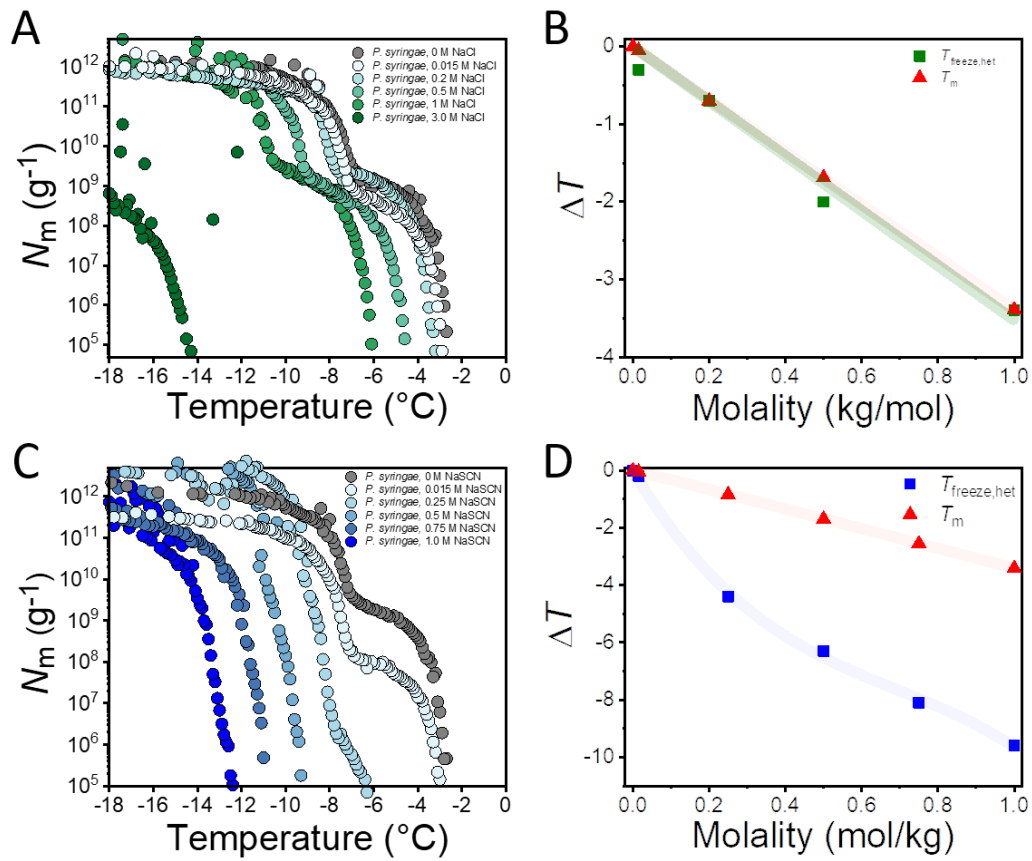
4

Figure S1: (A) Freezing experiments of aqueous solutions containing bacterial ice nucleators from *P. syringae* in pure water (grey) and in different NaCl solutions (green). Plotted is the cumulative number of ice nucleators per unit mass (N_m) of *P. syringae* vs. temperature for various degrees of dilution, starting with 0.1 mg/mL. (B) Temperature shifts of the heterogeneous ice nucleation temperature (green squares) induced at different NaCl concentrations. Shifts represent the difference at $f_{ice} = 0.5$ between *P. syringae* in water and in NaCl solutions. The red line represents a linear fit of the ice melting temperatures (red triangles) and the green line is a linear fit of the experimental data. (C) Freezing experiments of aqueous solutions containing bacterial ice nucleators from *P. syringae* in pure water (grey) and in different NaSCN solutions (blue). (D) Temperature shifts of the heterogeneous ice nucleation temperature (blue squares) induced at different NaSCN concentrations. The red line represents a linear fit of the ice melting temperatures and the blue line is a cubic fit of the experimental data.
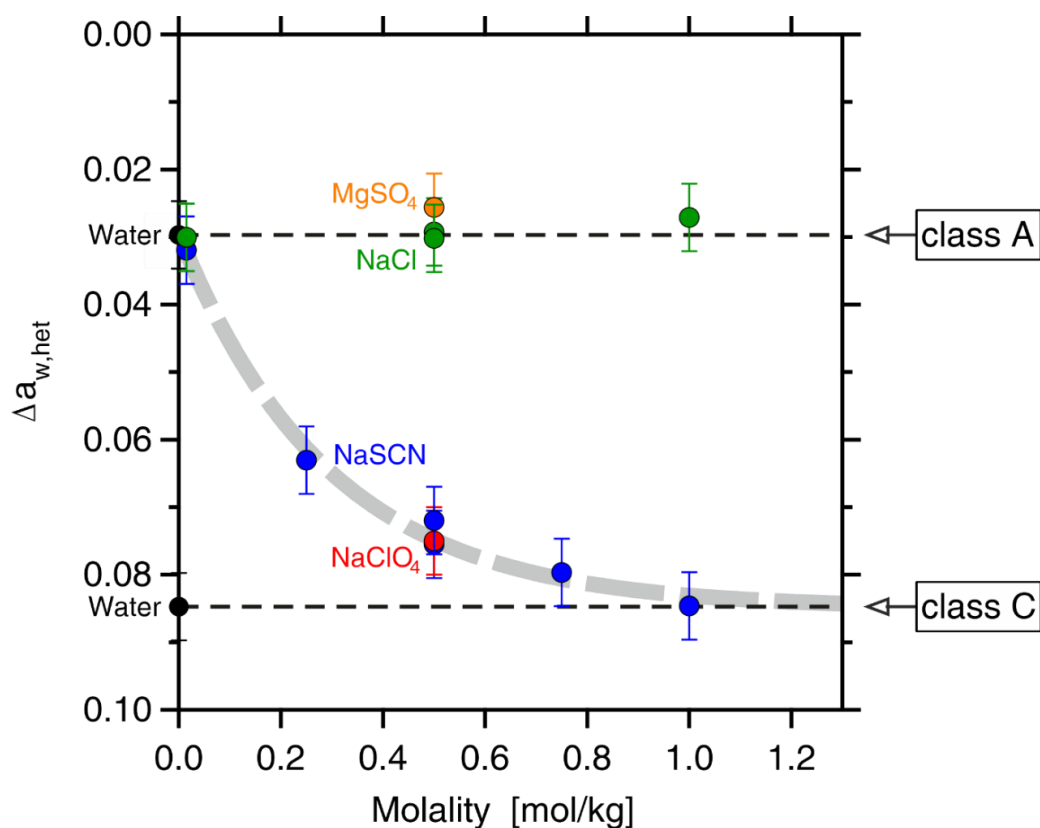
Figure S2: Water activity dependence of the freezing temperature of *P. syringae* in water and at different salt concentration. Plotted is the relative change $\Delta a_{w,het}$ between the water activity of the investigated salt solution (a_w) and that at the ice melting point ($a_{w,ice}$), both at the experimentally observed freezing temperature (T_{50}), as a function of the salt molality. $\Delta a_{w,het}$ was calculated from $\Delta a_{w,het}(T_{50}) = a_w(T_{50}) - a_{w,ice}(T_{50})$. The value of a_w of the different salt solutions was obtained from their ice melting points using a parameterizations from the literature.[4] The black data points are the $\Delta a_{w,het}$ values in pure water for class A and class C ice nucleators, obtained from the T_{50} freezing temperatures at *P. syringae* concentrations of 0.1 mg/mL and 10^{-6} mg/mL, respectively. A constant $\Delta a_{w,het}$ as a function of salt molality (black dashed lines) indicates that the salt has a negligible effect on the efficiency of the particular ice nucleator, as is the case for NaCl (green). In contrast, the data for NaSCN (blue) and NaClO$_4$ (red) show an increase in $\Delta a_{w,het}$ with increasing salt molality, implying an inhibition of the particular class A ice nucleator. An exponential fit to these data (grey dashed line) approaches the $\Delta a_{w,het}$ value of the class C ice nucleator, implying that that the class A INP aggregates are inhibited, while the individual class C INPs appear not to be affected.
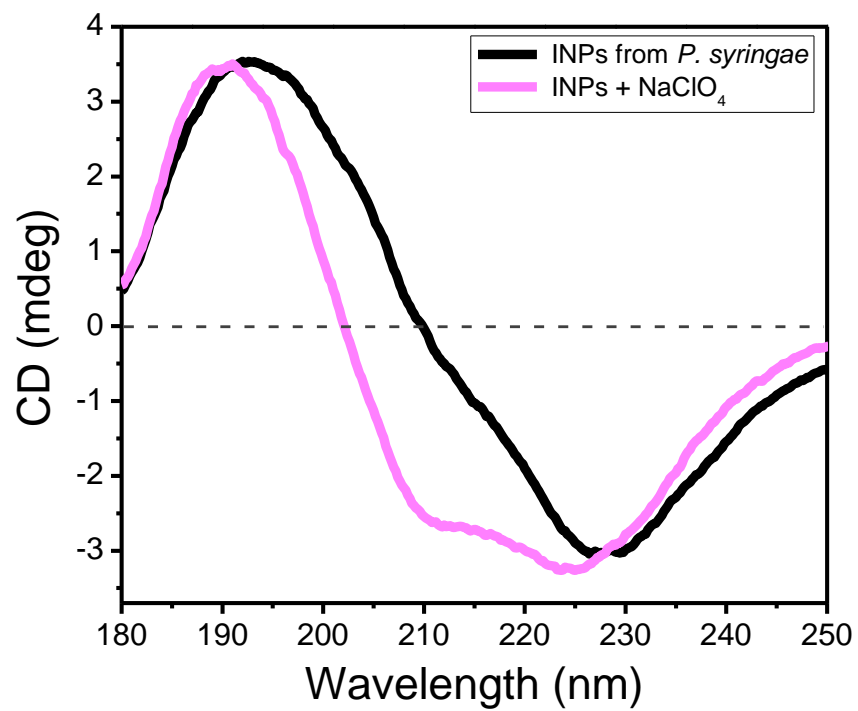
6

Figure S3: Circular dichroism spectra of the ice-nucleating proteins from *P. syringae* in water (black) and in a 0.5 mol/kg NaClO$_4$ solution (magenta).

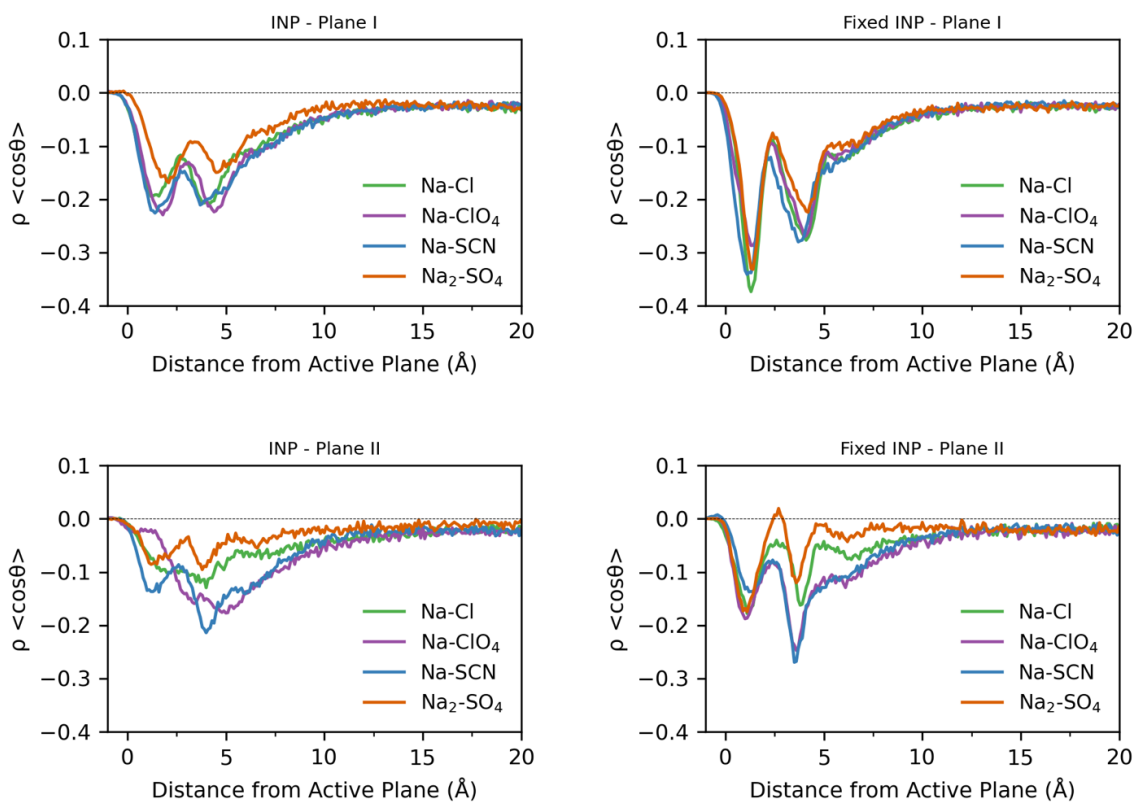**Figure S4:** Density profile of $\rho\langle\cos\theta\rangle$, where ρ is the density of water, and θ is the angle between water molecule's bisector and the plane normal, with respect to INP plane I and II, for INP in its fixed geometry.

8

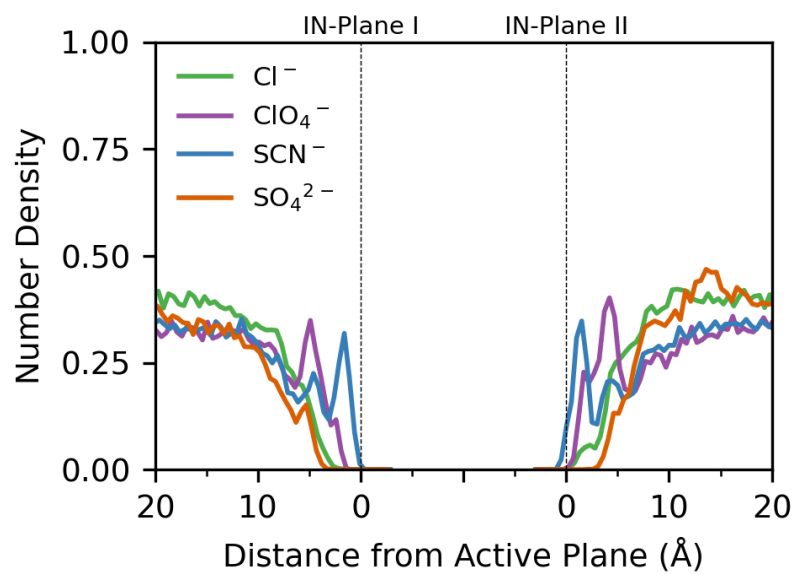**Figure S5:** Anionic distribution with respect to the active sites for the fixed geometry of the INP.

9

Figure S6: (A) Freezing experiments of aqueous solutions of Snomax containing bacterial ice nucleators from *P. syringae* in pure water (grey), in NH₄Cl and in NH₄Cl with PBS buffer solutions. Plotted is the cumulative number of ice nucleators per unit mass of *P. syringae, N_m* vs. temperature for various degrees of dilution, starting with 0.1 mg/mL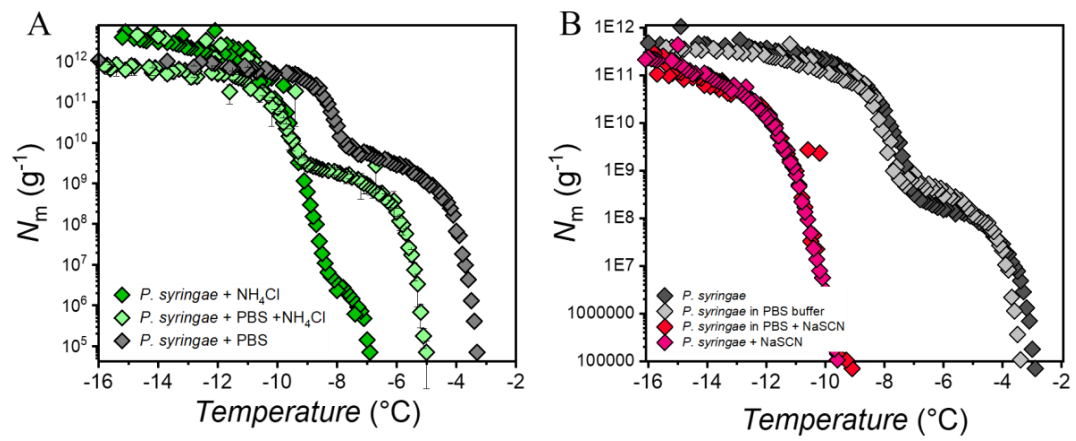. (B) Freezing experiments of aqueous solutions of Snomax containing bacterial ice nucleators from *P. syringae* in pure water (grey), in NaSCN and in NaSCN with PBS buffer solutions.

10
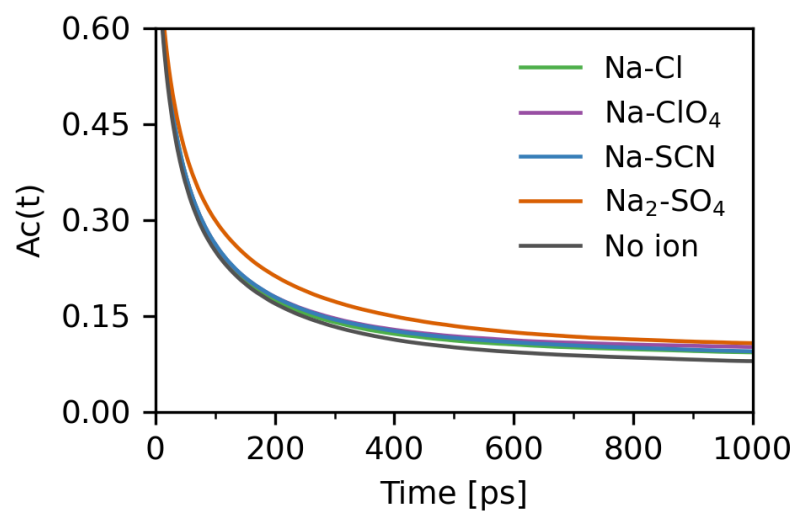
Figure S7: Hydrogen bond lifetime autocorrelation function for the INP in the presence of different salts. Water, and groups involved in both active sites were considered to define hydrogen bonds. For each system, five tests were performed with a simulation time of 2 ns, where the trajectory was outputted every 50 fs.

11

Figure S8: Relaxation times of the hydrogen bonds obtained from fitting the hydrogen bond lifetime autocorrelation function (Figure S6) to $a \exp\left(-\frac{t}{\tau_1}\right) + b \exp\left(-\frac{t}{\tau_2}\right) + c_0$. Values are shown with their standard error bars for the flexible and fixed INP, in the presence of different salts.

12

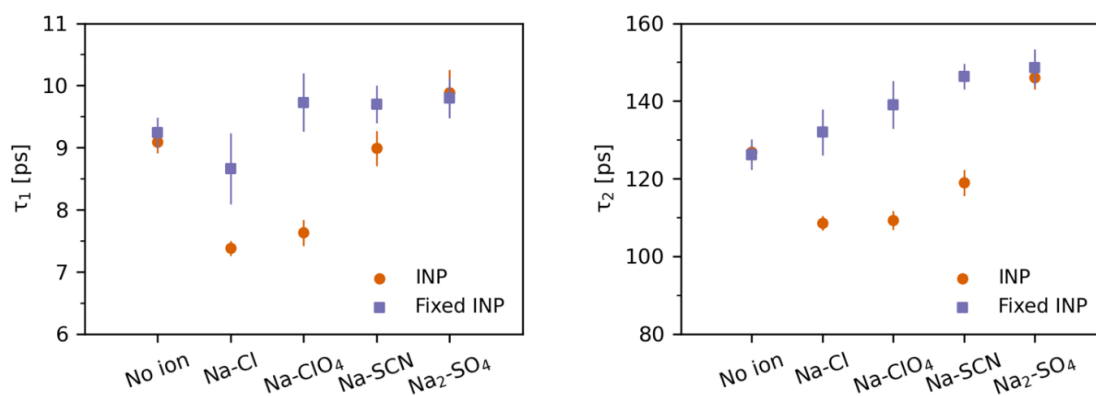Table S1: Charges, inter- and intramolecular parameters for the ionic species. The references are given in parentheses.

Ion		q [e]	ϵ [$kJ.mol^{-1}$]	σ [Å]	r [Å]	Bonds k [$kJ.mol^{-1}.nm^{-2}$]	α [D]	Angles k [$kJ.mol^{-1}.Rad^{-2}$]
Na⁺ (1)		1.0	0.011598	3.33045	-	-	-	-
Cl⁻ (1)		-1.0	0.492833	4.41724	-	-	-	-
ClO₄⁻ (2)	Cl	1.176	0.493712	3.5	1.506	636384.0	109.5	1746.36
	O	-0.544	0.87864	2.9				
SCN⁻ (3)	S	-0.573	1.523	3.83	(S-C) 1.66	577080.0		
	C	0.483	0.425	3.35			179.8	1308.72
	N	-0.910	0.310	3.7	(C-N) 1.19	2453640.0		
SO₄²⁻	S	1.716 (5)	1.05 (4)	3.563 (4)	1.516 (5)	454524.0 (4)	109.43 (5)	626.64 (4)
	O	-0.929 (5)	0.882 (4)	2.960 (4)				

1 Jorgensen et al.[9] , 2 Doherty et al. [14], 3 Tesei et al. [15] , 4 GAFF [16], 5 in-house Gaussian and AIMD calculations.

13

Table S2: Relaxation time of hydrogen bonds.

	τ_1 [ps]		τ_2 [ps]	
	INP	Fixed INP	INP	Fixed INP
No ions	9.09	9.24	126.90	126.21
Na-Cl	7.38	8.66	108.58	131.98
Na-ClO$_4$	7.63	9.73	109.29	139.06
Na-SCN	8.99	9.70	118.96	146.33
Na$_2$-SO$_4$	9.89	9.80	146.05	148.56

References

[1]   A. T. Kunert, M. Lamneck, F. Helleis, U. Pöschl, M. L. Pöhlker, J. Fröhlich-Nowoisky, *Atmos. Meas. Tech.* **2018**, *11*, 6327-6337.

[2]   D. R. Lide, *CRC handbook of chemistry and physics, 89th edition (Internet version)*, Taylor & Francis, **2009**.

[3]   aO. Bonner, *The Journal of Chemical Thermodynamics* **1976**, *8*, 1167-1172; bA. Kumar, *Fluid phase equilibria* **2001**, *180*, 195-204; cG. Scatchard, S. Prentiss, P. Jones, *Journal of the American Chemical Society* **1934**, *56*, 805-807.

[4]   T. Koop, B. Zobrist, *Physical Chemistry Chemical Physics* **2009**, *11*, 10839-10850.

[5]   M. T. REISCHEL, G. VALI, *Tellus* **1975**, *27*, 414-427.

[6]   H. E. Tomalty, L. A. Graham, R. Eves, A. K. Gruneberg, P. L. Davies, *Biomolecules* **2019**, *9*, 180.

[7]   L. B. Dreier, A. Wolde-Kidan, D. J. Bonthuis, R. R. Netz, E. H. G. Backus, M. Bonn, *The Journal of Physical Chemistry Letters* **2019**, *10*, 6355-6359.

[8]   A. Hudait, N. Odendahl, Y. Qiu, F. Paesani, V. Molinero, *Journal of the American Chemical Society* **2018**, *140*, 4905-4912.

[9]   W. L. Jorgensen, D. S. Maxwell, J. Tirado-Rives, *Journal of the American Chemical Society* **1996**, *118*, 11225-11236.

[10]   a A. Luzar, D. Chandler, *Nature* **1996**, *379*, 55-57; b A. Striolo, *Nano letters* **2006**, *6*, 633-639.

[11]   a D. van der Spoel, P. J. van Maaren, P. Larsson, N. Tîmneanu, *The Journal of Physical Chemistry B* **2006**, *110*, 4393-4398; b F. W. Starr, J. K. Nielsen, H. E. Stanley, *Physical Review E* **2000**, *62*, 579.

[12]   V. Balos, S. Imoto, R. R. Netz, M. Bonn, D. J. Bonthuis, Y. Nagata, J. Hunger, *Nature Communications* **2020**, *11*, 1611.

[13]   M. Matsumoto, S. Saito, I. Ohmine, *Nature* **2002**, *416*, 409-413.

[14]   B. Doherty, X. Zhong, S. Gathiaka, B. Li, O. Acevedo, *Journal of chemical theory and computation* **2017**, *13*, 6131-6145.

[15]   G. Tesei, V. Aspelin, M. Lund, *The Journal of Physical Chemistry B* **2018**, *122*, 5094-5105.

[16]   W. Wang, R. Wolf, DA *Journal of Computational Chemistry* **2004**, *25*, 1157-1174.

Author contributions

15

A.5 Schwidetzky *et al.*, J. Phys. Chem. Lett., 2021

Ice Nucleation Activity of Perfluorinated Organic Acids

R. Schwidetzky[1], Y. Sun[1], J. Fröhlich-Nowoisky[2], A. T. Kunert[2], M. Bonn[1], and K. Meister[1,4]

[1] Max-Planck-Institute for Polymer Research, 55128 Mainz, Germany
[2] Max-Planck-Institute for Chemistry, 55128 Mainz, Germany
[3] University of Alaska Southeast, Juneau, Alaska 99801, United States

Author contributions:

R.S. performed the freezing experiments and contributed to analyzing and discussing the results as well as writing the manuscript.

Ice Nucleation Activity of Perfluorinated Organic Acids

Ralph Schwidetzky, Yuling Sun, Janine Fröhlich-Nowoisky, Anna T. Kunert, Mischa Bonn, and Konrad Meister*
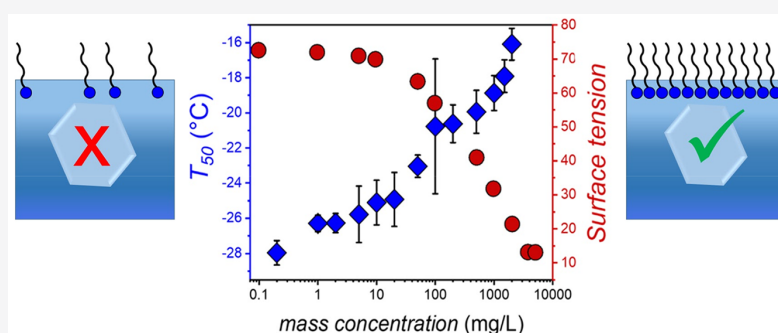
Read Online

ACCESS | Metrics & More | Article Recommendations | Supporting Information

ABSTRACT: Perfluorinated acids (PFAs) are widely used synthetic chemical compounds, highly resistant to environmental degradation. The widespread PFA contamination in remote regions such as the High Arctic implies currently not understood long-range atmospheric transport pathways. Here, we report that perfluorooctanoic acid (PFOA) initiates heterogeneous ice nucleation at temperatures as high as −16 °C. In contrast, the eight-carbon octanoic acid, perfluorooctanesulfonic acid, and deprotonated PFOA showed poor ice nucleating capabilities. The ice nucleation ability of PFOA correlates with the formation of a PFOA monolayer at the air−water interface, suggesting a mechanism in which the aligned hydroxyl groups of the carboxylic acid moieties provide a lattice matching to ice. The ice nucleation capabilities of fluorinated compounds like PFOA might be relevant for cloud glaciation in the atmosphere and the removal of these persistent pollutants by wet deposition.

Perfluorinated acids (PFAs) such as perfluorooctanoic acid (PFOA) or perfluorooctanesulfonic acid (PFOS) are anthropogenically generated compounds that have emerged as significant global environmental pollutants with persistent, bioaccumulative, and toxic properties.[1,2] The adverse environmental effects of PFAs have led to their addition to annexe A of the Stockholm Convention for persistent organic pollutants, and PFOS and related chemicals were voluntarily removed from the market.[3] Despite the efforts to stop the environmental release, products containing PFAs remain in use and continue to contribute to environmental contamination. Of the perfluorinated acids, PFOA is the most ubiquitous pollutant due to its extensive usage in the fluoropolymer industry and high total emissions.[4,5] PFOA has been observed in different air and water sources (rain, snow, sea) and was detected in regions as remote as the High Arctic.[6,7] Since there are no primary sources of PFOA in remote locations that could contribute to contamination, questions arise regarding the sources and transport pathways of this concerning pollutant.[7,8] The currently suggested long-range transport pathways of PFOAs are hydrospheric and atmospheric, with the latter being more relevant for remote locations and the Arctic.[9,10] This can be witnessed by high PFA and PFOA concentrations in the

Arctic atmosphere and ongoing detection of PFOA and PFAs in Arctic snow samples.[7,11]

Within the atmosphere, perfluorinated compounds can undergo atmospheric oxidation and react with Criegee intermediates,[12] but they could also interact with clouds,[13] which are important for weather effects due to cloud glaciation and precipitation. Pure water droplets do not freeze homogeneously until ∼ −38 °C owing to the energy barrier associated with creating the initial crystallization nucleus.[14] In cloud droplets, water typically freezes in a heterogeneous process, facilitated by the presence of particles that serve as ice nucleators (IN). Common abiotic IN include clay, dust, minerals, or carbonaceous materials.[15] Biogenic IN consist of biomolecules derived from bacteria, fungi, insects, or pollen.[16] Among the abiotic ice-nucleating surfaces, monolayers of long-chain alcohols have been shown to be particularly effective,

while fatty acids with similar chain lengths are significantly less so.[17] Here, we report that PFOA is an efficient IN, much more so than the structurally similar PFOS and octanoic acid (OA). These compounds consist of a hydrophobic tail and a hydrophilic headgroup, and are known to accumulate and form monolayers at the air−water interface (Figure 1).[18] The
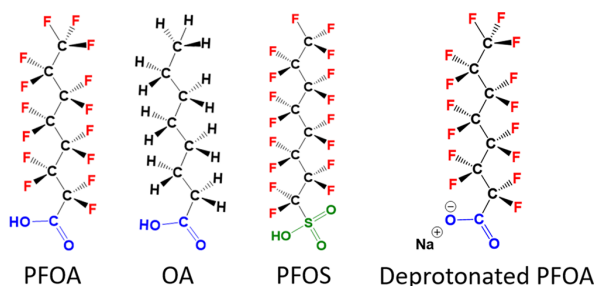

Figure 1. Chemical structures of the investigated perfluorooctanoic acid (PFOA), octanoic acid (OA), perfluorooctanesulfonic acid (PFOS), and deprotonated PFOA.

ice nucleation activities of the (fluoro)surfactants are investigated using the high-throughput Twin-plate Ice Nucleation Assay (TINA).[19] TINA enables the simultaneous measurement of a complete dilution series with each series composed of hundreds of droplets of a few microliters with high statistics, enabling the analysis and characterization of the efficiency of particles with high accuracy.[20−22]

Figure 2A shows the results of statistical freezing curves of aqueous PFOA solutions with concentrations between 0 and 2000 mg/L, while Figure 2B shows the T_{50} values of PFOA solutions as a function of concentration. The T_{50} values are defined as the temperatures at which 50% of the droplets are frozen. PFOA shows considerable ice nucleating activity, in a manner highly dependent on the solution concentration.

At PFOA concentrations up to 0.02 mg/L, the ice nucleation activity is negligible, with freezing occurring at T_{50} = ∼ −28 °C, comparable to pure water in our experimental setup. Increasing the concentration above 0.02 mg/L results in freezing temperatures that are higher than that of pure water. We find that for 200 mg/L PFOA solutions T_{50} = ∼ −21 °C, and for 2000 mg/L solutions, T_{50} increases up to ∼ −16 °C.

While the maximal determined T_{50} value is ∼ −16 °C, it is also worth mentioning that we occasionally observed high initial freezing temperatures of up to −5 °C even at low concentrations (Figure 2A).

Interestingly, the T_{50} values of the droplet freezing statistics do not simply increase linearly with higher concentration. Instead, the data for PFOA shows resemblance with a Langmuir adsorption model with an initial rapid increase in T_{50} up to ∼200 mg/L and a subsequent slower increase and leveling off of the ice nucleation activity until 2000 mg/L.

Next, we determined the ice nucleation activity of OA, PFOS, and deprotonated PFOA to unravel which properties of PFOA give rise to its ice nucleation efficiency. The activities of OA, deprotonated PFOA, and PFOS were determined over different concentration ranges owing to their respective solubilities in water.

Figure 3 shows the T_{50} values of OA, deprotonated PFOA, and PFOS solutions plotted as a function of concentration in aqueous solution. We find that, similar to PFOA, the T_{50} plots of all three compounds resemble Langmuir adsorption models. However, in contrast to PFOA, the maximal ice nucleation activities were significantly lower for all three (fluoro)-surfactants. For OA, we found that the maximal ice nucleation activity is at ∼ −24 °C, which is only slightly higher than the freezing temperature of pure water in our setup. Apparently, the perhydrogenated fatty acid is a significantly poorer ice nucleator than perfluorinated PFOA (Figure S1). For PFOS, the maximal ice nucleation activity was ∼ −20.5 °C, but at 20 times higher concentration than PFOA. Deprotonation of the carboxylic acid headgroup of PFOA eliminates most ice nucleation activity with a maximum of ∼ −26.5 °C. It seems that both changing the hydrophilic headgroup of PFOA or the hydrophobicity of the tail suppresses the ice nucleation activities of the respective (fluoro)surfactants. We performed dynamic light scattering and calorimetric measurements to examine whether different water activities or solution aggregates may be the origin of the observed differences in the ice nucleation capabilities. Neither the melting points of the compounds nor their aggregate sizes were found to differ notably (Table S1, Figure S2), eliminating explanations involving different water activities or aggregate sizes in solution as the origins for the observed differences in ice nucleation activity.
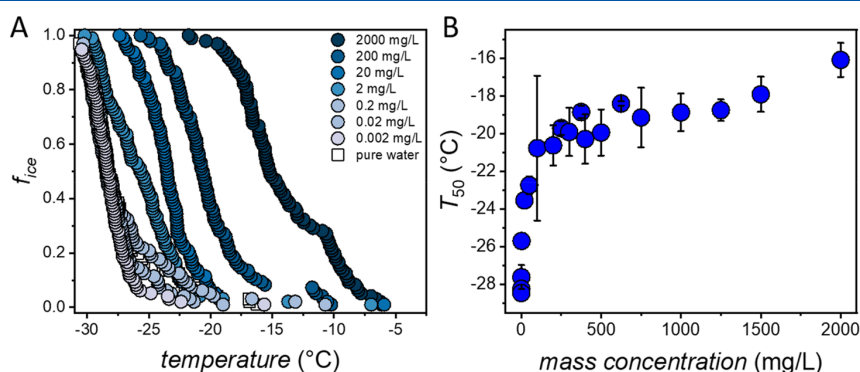
Figure 2. Ice nucleation activity of PFOA. (A) Freezing curves of aqueous PFOA solutions from concentrations ranging from 0 to 2000 mg/L. Shown are the fraction of frozen 3 μL droplets vs temperature. The point at which 50% of the droplets are frozen (f_{ice} = 0.5) represents the T_{50} value. (B) T_{50} values of aqueous PFOA solutions as a function of concentration. Error bars represent the standard deviation of 3−8 independent measurements.
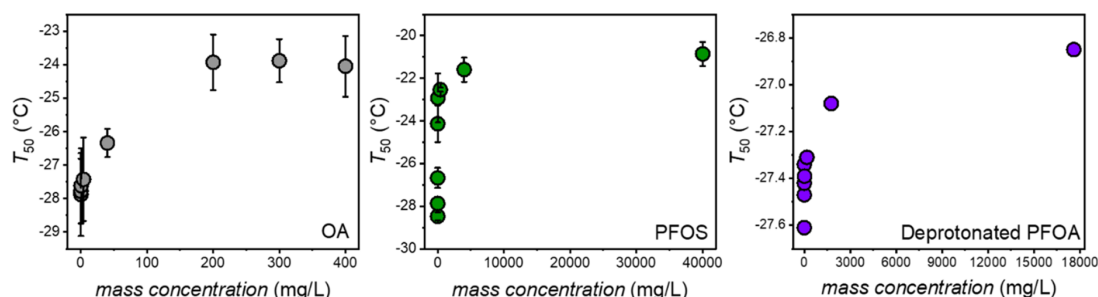
Figure 3. Ice nucleation activity, quantified through T_{50} values, of OA (gray circles), PFOS (green circles), and deprotonated PFOA (purple circles) solutions as a function of concentration. Error bars represent the standard deviation of 3−5 independent measurements.

PFOA and other fluorosurfactants are known to accumulate and form monolayers at the air−water interface,[18] with a maximum surface excess of ∼2 mg/m² for aqueous concentrations exceeding 100 mg/L. In the TINA droplet freezing experiments, the surface pressure cannot be controlled and is a function of the amount of PFOA at the surface and the temperature. Interestingly, we find that the observed ice nucleation activities of PFOA and the other surfactants directly correlate with their surface tensions, implying that their ice nucleation activities are linked to the buildup of the (fluoro)surfactant monolayers (Figure 4B, Figure S3). We
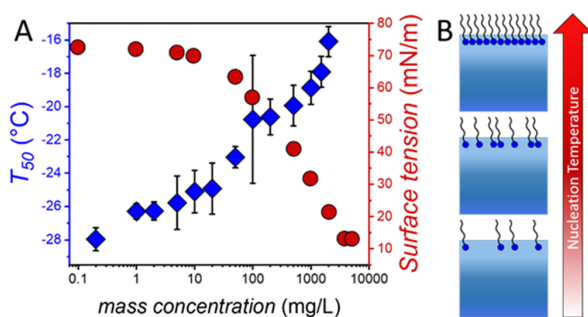

Figure 4. Surface tension and ice nucleation of PFOA. (A) The ice nucleation activity of PFOA is concentration dependent and follows the trend of the surface tension. Surface tension values were derived from Lyu et al.[26] (B) Schematic representation of the buildup of a PFOA monolayer, which correlates with the increase of the ice nucleation activity (nucleation temperature) of PFOA.

exclude the possibility that multilayered structures or micelles form or coexist underneath the PFOA monolayer, since we observe no changes in aggregate size in DLS measurements (Figure S4). The critical micelle concentration for PFOA also falls below the solubility limit, and X-ray reflectivity measurements showed that the thickness of a perfluorinated carboxylic acid layer corresponds to a monolayer state of the film.[23]

Previously, monolayers of *n*-alkyl alcohols have been shown to be particularly effective in nucleating ice and that their freezing temperatures increased with the length of the hydrocarbon tail.[17] These monolayers expose hydroxyl groups to water in a manner that resembles the basal plane of ice. Hence, it was suggested that the structural lattice matching with ice governs their ice-nucleating efficiency. Interestingly, fatty acid monolayers, which also expose hydroxyl groups to water, are very poor ice nucleators, with solid fatty acid crystals showing more promise.[24] Molecular simulations have

previously suggested that the discrepancy between the alcohol and fatty acid layers was due to differences in the monolayer's compactness and the resulting structural match to ice, which are key for determining the ice nucleation ability of organic surfaces that expose hydroxyl groups to ice.[25]

Upon fluorination, hydrophobic chains will undergo structural and conformational changes that directly affect the packing of the monolayer. Structurally, perfluorinated chains display a larger footprint (∼0.28 nm²) than hydrogenated chains (∼0.19 nm²) and thus lower interfacial densities and molar volumes than hydrogenated chains with the same number of carbon atoms.[27] There are also conformational differences. For perfluorinated chains, the dihedral angle at minimum energy is not exactly 180°, as it is for hydrogenated ones. Consequently, perfluorinated chains adopt a characteristic helical conformation, while hydrogenated chains tend to be in an all-*trans* planar zigzag form.[28−30] Moreover, the energy barrier for internal rotation of perfluorinated chains is appreciably higher than for hydrogenated chains, which induce a rigid character, in contrast with the flexible character of hydrogenated chains.[29]

Altogether, the Langmuir monolayers of fluorinated molecules will have a higher crystallinity than their hydrocarbon counterparts. In fact, grazing incidence X-ray diffraction studies of monolayers of perfluorinated carboxylic acids have revealed tight hexagonal packing of molecules with their long axes nearly perpendicular to the water surface and the coexistence of crystalline and dilute disordered phases.[23,31]

We conclude that upon fluorination, the morphology and packing within the monolayer allow for a better alignment of the carboxylic acid groups with less structural fluctuations, thereby providing a better ice template and enabling enhanced nucleation properties. This hypothesis is supported by additional measurements of perfluorodecanoic acid, which also shows good ice nucleation abilities (Figure S5). Our conclusion is also in line with previous suggestions based on MD simulations and experimental findings that solid fatty acid particles are better INs than fatty acid monolayers.[24,25] Irrespective of the precise molecular mechanism, the finding that PFAs have high ice nucleation activity may have direct implications for the transport and environmental fate of these persistent organic pollutants, as they could get distributed to remote environments by actively being involved in cloud glaciation.

While the local concentration at the anthropogenic point of origin may be high, once it becomes distributed in the environment, average concentrations found in the atmosphere are significantly lower than the ones reported here (∼15 pg/

m³),[32] and the deprotonated PFOA form is likely prevalent, which has low ice nucleation activity.[33] Our results suggest that increasing the crystallinity and order of monolayers through perfluorination will also affect the ice nucleation abilities of other perfluorinated compounds such as long-chain alcohols, potentially rendering them from good to exceptional ice nucleators with direct atmospheric implications.[13,17] The possible ice nucleation synergy between hydrogenated and perfluorinated long-chain alcohols and the interplay of PFAs with other ice-nucleating particles found in the atmosphere are yet to be investigated.

■ ASSOCIATED CONTENT

ⓢ Supporting Information

The Supporting Information is available free of charge at https://pubs.acs.org/doi/10.1021/acs.jpclett.1c00604.

> Experimental details and supporting Figures S1−S5 (PDF)

■ AUTHOR INFORMATION

Corresponding Author

Konrad Meister − *Max Planck Institute for Polymer Research, 55128 Mainz, Germany; University of Alaska Southeast, Juneau, Alaska 99801, United States;* ⓞ orcid.org/0000-0002-6853-6325; Email: meisterk@mpip-mainz.mpg.de

Authors

Ralph Schwidetzky − *Max Planck Institute for Polymer Research, 55128 Mainz, Germany*

Yuling Sun − *Max Planck Institute for Polymer Research, 55128 Mainz, Germany*

Janine Fröhlich-Nowoisky − *Max Planck Institute for Chemistry, 55128 Mainz, Germany;* ⓞ orcid.org/0000-0002-1278-0054

Anna T. Kunert − *Max Planck Institute for Chemistry, 55128 Mainz, Germany;* ⓞ orcid.org/0000-0002-2163-8973

Mischa Bonn − *Max Planck Institute for Polymer Research, 55128 Mainz, Germany;* ⓞ orcid.org/0000-0001-6851-8453

Complete contact information is available at:
https://pubs.acs.org/10.1021/acs.jpclett.1c00604

Notes

The authors declare no competing financial interest.

■ ACKNOWLEDGMENTS

■ REFERENCES

(1) Liu, W.; Wu, J.; He, W.; Xu, F. A review on perfluoroalkyl acids studies: Environmental Behaviors, Toxic Effects, and Ecological and Health Risks. *Ecosystem Health and Sustainability* **2019**, *5* (1), 1−19.

(2) Martin, J. W.; Smithwick, M. M.; Braune, B. M.; Hoekstra, P. F.; Muir, D. C. G.; Mabury, S. A. Identification of Long-Chain Perfluorinated Acids in Biota from the Canadian Arctic. *Environ. Sci. Technol.* **2004**, *38* (2), 373−380.

(3) Kim, S.-K.; Kannan, K. Perfluorinated Acids in Air, Rain, Snow, Surface Runoff, and Lakes: Relative Importance of Pathways to Contamination of Urban Lakes. *Environ. Sci. Technol.* **2007**, *41* (24), 8328−8334.

(4) Song, X.; Vestergren, R.; Shi, Y.; Huang, J.; Cai, Y. Emissions, Transport, and Fate of Emerging Per- and Polyfluoroalkyl Substances from One of the Major Fluoropolymer Manufacturing Facilities in China. *Environ. Sci. Technol.* **2018**, *52* (17), 9694−9703.

(5) Wang, Z.; Cousins, I. T.; Scheringer, M.; Buck, R. C.; Hungerbühler, K. Global Emission Inventories for C4-C14 Perfluoroalkyl Carboxylic Acid (PFCA) Homologues from 1951 to 2030, Part II: The Remaining Pieces of the Puzzle. *Environ. Int.* **2014**, *69*, 166−76.

(6) Young, C. J.; Furdui, V. I.; Franklin, J.; Koerner, R. M.; Muir, D. C. G.; Mabury, S. A. Perfluorinated Acids in Arctic Snow: New Evidence for Atmospheric Formation. *Environ. Sci. Technol.* **2007**, *41* (10), 3455−3461.

(7) Muir, D.; Bossi, R.; Carlsson, P.; Evans, M.; De Silva, A.; Halsall, C.; Rauert, C.; Herzke, D.; Hung, H.; Letcher, R.; et al. Levels and Trends of Poly- and Perfluoroalkyl Substances in the Arctic Environment - An update. *Emerging Contaminants* **2019**, *5*, 240−271.

(8) MacInnis, J. J.; Lehnherr, I.; Muir, D. C. G.; St. Pierre, K. A.; St. Louis, V. L.; Spencer, C.; De Silva, A. O. Fate and Transport of Perfluoroalkyl Substances from Snowpacks into a Lake in the High Arctic of Canada. *Environ. Sci. Technol.* **2019**, *53* (18), 10753−10762.

(9) Stemmler, I.; Lammel, G. Pathways of PFOA to the Arctic: Variabilities and Contributions of Oceanic Currents and Atmospheric Transport and Chemistry Sources. *Atmos. Chem. Phys.* **2010**, *10* (20), 9965−9980.

(10) Armitage, J. M.; MacLeod, M.; Cousins, I. T. Modeling the Global Fate and Transport of Perfluorooctanoic Acid (PFOA) and Perfluorooctanoate (PFO) Emitted from Direct Sources Using a Multispecies Mass Balance Model. *Environ. Sci. Technol.* **2009**, *43* (4), 1134−1140.

(11) Yeung, L. W. Y.; Dassuncao, C.; Mabury, S.; Sunderland, E. M.; Zhang, X.; Lohmann, R. Vertical Profiles, Sources, and Transport of PFASs in the Arctic Ocean. *Environ. Sci. Technol.* **2017**, *51* (12), 6735−6744.

(12) Taatjes, C. A.; Khan, M. A. H.; Eskola, A. J.; Percival, C. J.; Osborn, D. L.; Wallington, T. J.; Shallcross, D. E. Reaction of Perfluorooctanoic Acid with Criegee Intermediates and Implications for the Atmospheric Fate of Perfluorocarboxylic Acids. *Environ. Sci. Technol.* **2019**, *53* (3), 1245−1251.

(13) Ellis, D. A.; Martin, J. W.; Mabury, S. A.; Hurley, M. D.; Sulbaek Andersen, M. P.; Wallington, T. J. Atmospheric Lifetime of Fluorotelomer Alcohols. *Environ. Sci. Technol.* **2003**, *37* (17), 3816−3820.

(14) Koop, T.; Luo, B.; Tsias, A.; Peter, T. Water Activity as the Determinant for Homogeneous Ice Nucleation in Aqueous Solutions. *Nature* **2000**, *406* (6796), 611−614.

(15) Lupi, L.; Hudait, A.; Molinero, V. Heterogeneous Nucleation of Ice on Carbon Surfaces. *J. Am. Chem. Soc.* **2014**, *136* (8), 3156−3164.

(16) Pummer, B. G.; Budke, C.; Augustin-Bauditz, S.; Niedermeier, D.; Felgitsch, L.; Kampf, C. J.; Huber, R. G.; Liedl, K. R.; Loerting, T.; Moschen, T.; et al. Ice nucleation by Water-Soluble Macromolecules. *Atmos. Chem. Phys.* **2015**, *15* (8), 4077−4091.

(17) Gavish, M.; Popovitz-Biro, R.; Lahav, M.; Leiserowitz, L. Ice Nucleation by Alcohols Arranged in Monolayers at the Surface of Water Drops. *Science* **1990**, *250* (4983), 973−975.

(18) Costanza, J.; Arshadi, M.; Abriola, L. M.; Pennell, K. D. Accumulation of PFOA and PFOS at the Air-Water Interface. *Environ. Sci. Technol. Lett.* **2019**, *6* (8), 487−491.

(19) Kunert, A. T.; Lamneck, M.; Helleis, F.; Pöschl, U.; Pöhlker, M. L.; Fröhlich-Nowoisky, J. Twin-plate Ice Nucleation Assay (TINA) with Infrared Detection for High-Throughput Droplet Freezing Experiments with Biological Ice Nuclei in Laboratory and Field Samples. *Atmos. Meas. Tech.* **2018**, *11* (11), 6327−6337.

(20) Lukas, M.; Schwidetzky, R.; Kunert, A. T.; Backus, E. H. G.; Pöschl, U.; Fröhlich-Nowoisky, J.; Bonn, M.; Meister, K. Interfacial Water Ordering Is Insufficient to Explain Ice-Nucleating Protein Activity. *J. Phys. Chem. Lett.* **2021**, *12* (1), 218−223.

(21) Schwidetzky, R.; Kunert, A. T.; Bonn, M.; Pöschl, U.; Ramløv, H.; DeVries, A. L.; Fröhlich-Nowoisky, J.; Meister, K. Inhibition of Bacterial Ice Nucleators Is Not an Intrinsic Property of Antifreeze Proteins. *J. Phys. Chem. B* **2020**, *124* (24), 4889−4895.

(22) Lukas, M.; Schwidetzky, R.; Kunert, A. T.; Pöschl, U.; Fröhlich-Nowoisky, J.; Bonn, M.; Meister, K. Electrostatic Interactions Control the Functionality of Bacterial Ice Nucleators. *J. Am. Chem. Soc.* **2020**, *142* (15), 6842−6846.

(23) Fontaine, P.; Filipe, E. J. M.; Fauré, M.-C.; Rego, T.; Taßler, S.; Alves, A. C.; Silva, G. M. C.; Morgado, P.; Goldmann, M. Structure of Langmuir Monolayers of Perfluorinated Fatty Acids: Evidence of a New 2D Smectic C Phase. *Molecules* **2019**, *24* (19), 3590.

(24) DeMott, P. J.; Mason, R. H.; McCluskey, C. S.; Hill, T. C. J.; Perkins, R. J.; Desyaterik, Y.; Bertram, A. K.; Trueblood Jonathan, V.; Grassian, V. H.; Qiu, Y.; et al. Ice Nucleation by Particles Containing Long-Chain Fatty Acids of Relevance to Freezing by Sea Spray Aerosols. *Environmental Science: Processes & Impacts* **2018**, *20* (11), 1559−1569.

(25) Qiu, Y.; Odendahl, N.; Hudait, A.; Mason, R.; Bertram, A. K.; Paesani, F.; DeMott, P. J.; Molinero, V. Ice Nucleation Efficiency of Hydroxylated Organic Surfaces Is Controlled by Their Structural Fluctuations and Mismatch to Ice. *J. Am. Chem. Soc.* **2017**, *139* (8), 3052−3064.

(26) Lyu, Y.; Brusseau, M. L.; Chen, W.; Yan, N.; Fu, X.; Lin, X. Adsorption of PFOA at the Air-Water Interface during Transport in Unsaturated Porous Media. *Environ. Sci. Technol.* **2018**, *52* (14), 7745−7753.

(27) Kirsch, P. *Modern Fluoroorganic Chemistry*; Wiley-VCH: 2004.

(28) Bunn, C. W.; Howells, E. R. Structures of Molecules and Crystals of Fluoro-Carbons. *Nature* **1954**, *174* (4429), 549−551.

(29) Jang, S. S.; Blanco, M.; Goddard, W. A.; Caldwell, G.; Ross, R. B. The Source of Helicity in Perfluorinated N-Alkanes. *Macromolecules* **2003**, *36* (14), 5331−5341.

(30) Monde, K.; Miura, N.; Hashimoto, M.; Taniguchi, T.; Inabe, T. Conformational Analysis of Chiral Helical Perfluoroalkyl Chains by VCD. *J. Am. Chem. Soc.* **2006**, *128* (18), 6000−6001.

(31) Als-Nielsen, J.; Jacquemain, D.; Kjaer, K.; Leveiller, F.; Lahav, M.; Leiserowitz, L. Principles and Applications of Grazing Incidence X-ray and Neutron Scattering from Ordered Molecular Monolayers at the Air-Water Interface. *Phys. Rep.* **1994**, *246* (5), 251−313.

(32) Liu, B.; Zhang, H.; Yao, D.; Li, J.; Xie, L.; Wang, X.; Wang, Y.; Liu, G.; Yang, B. Perfluorinated Compounds (PFCs) in the Atmosphere of Shenzhen, China: Spatial Distribution, Sources and Health Risk Assessment. *Chemosphere* **2015**, *138*, 511−8.

(33) Burns, D. C.; Ellis, D. A.; Li, H.; McMurdo, C. J.; Webster, E. Experimental pKa Determination for Perfluorooctanoic Acid (PFOA) and the Potential Impact of pKa Concentration Dependence on Laboratory-Measured Partitioning Phenomena and Environmental Modeling. *Environ. Sci. Technol.* **2008**, *42* (24), 9283−9288.

Supporting Information:

Ice Nucleation Activity of Perfluorinated Organic Acids

Ralph Schwidetzky[#,†], Yuling Sun[†], Janine Fröhlich-Nowoisky[§], Anna T. Kunert[§], Mischa Bonn[†] and Konrad Meister[†, ⊥,]*

[†]Max Planck Institute for Polymer Research, 55128 Mainz, Germany

[§]Max Planck Institute for Chemistry, 55128 Mainz, Germany

[⊥]University of Alaska Southeast, 99801 Juneau, AK, United States

Corresponding Authors

K. Meister − Max Planck Institute for Polymer Research, 55128 Mainz, Germany; University of Alaska Southeast, Juneau, Alaska 99801, United States; orcid.org/0000-0002-6853-6325; Email: meisterk@mpip-mainz.mpg.de

Materials and Methods

Samples: PFOA, PFDeA OA, and PFOS were obtained from Sigma Aldrich. TINA experiments were performed in ultrapure water, which was prepared as described elsewhere[1]. Deprotonated PFOA was obtained by dissolving PFOA in 0.1 M sodium hydroxide (Roth).

TINA Experiments. Ice nucleation experiments were performed using a high-throughput droplet freezing assay. The details of the instrument have been described recently[1]. In a typical experiment, 96 droplets (3 µL) of the investigated solutions were placed on two 384-well-plates by a liquid handling station (epMotion ep5073, Eppendorf, Hamburg, Germany) and tested with a continuous cooling-rate of 1 °C/min from 0 °C to −30 °C. The droplet-freezing was determined by two infrared cameras (Seek Therman Compact XR, Seek Thermal Inc., Santa Barbara, CA, USA). The uncertainty in the temperature of the setup was ±0.2 °C. Samples were measured several times with independent samples (PFOA 8 times, OA 3 times, PFOS 2 times, deprotonated PFOA 2 times).

DSC Measurements. Differential Scanning Calorimetry (DSC 822 with sample robot by Mettler Toledo) was used to determine the melting points. All samples were measured in a range from −60 to 20 °C (heating rate: 1 K/min, cooling rate: −10 K/min). Measurements consisted of two cooling/heating cycles and the corresponding melting points were averaged.

DLS Measurements. Dynamic light scattering (DLS, Submicron Particle Sizer Nicomp 380 with a fixed scattering angle of 90°, laser wavelength $\lambda = 632.8$ nm) was used to determine the sizes of any solution aggregates of the (fluoro)surfactants. DLS measurements were typically performed at concentrations of 0.2 mg/mL.

Surface Tension Measurements. Surface tension was measured using Du Noüy rings (DCAT, DataPhysics Instruments GmbH) and SCAT 32 software. Each concentration was measured twice, and all measurements were performed at 22 °C.
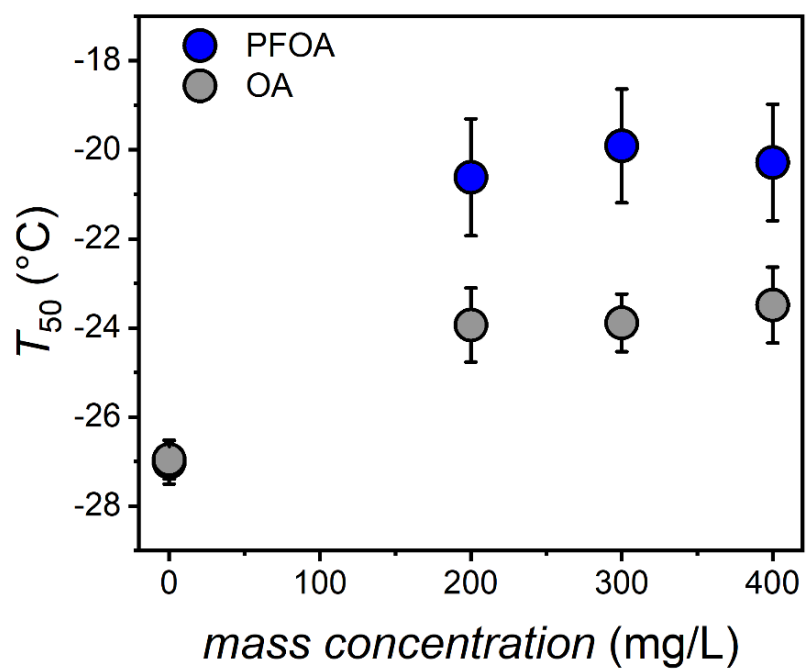
Figure S1: Comparative representation of the ice nucleation activity of PFOA (blue) and OA (grey). The values represent the average of three independent experiments.
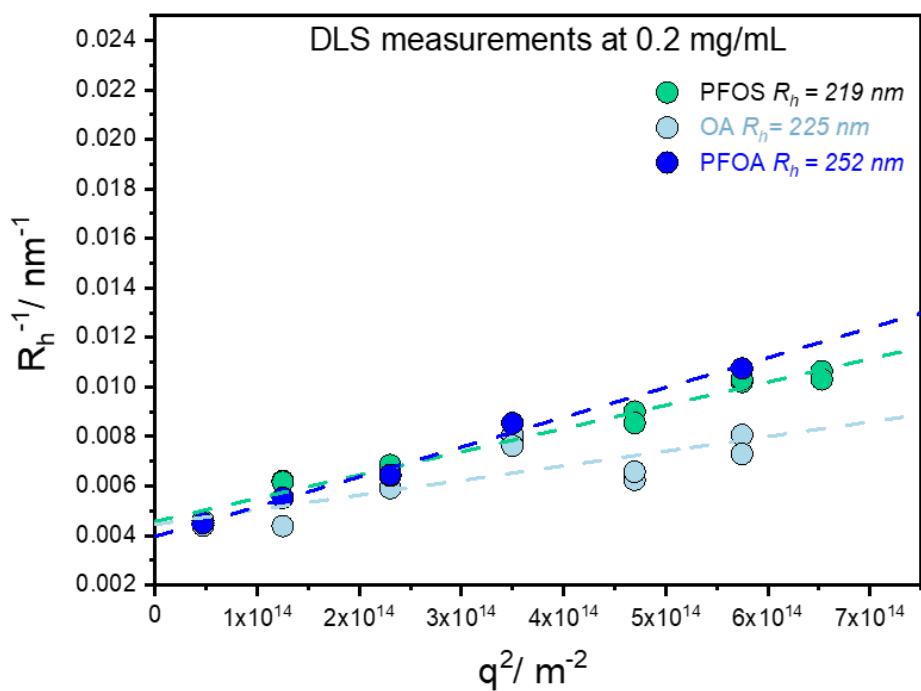
Figure S2: Particle sizes of PFOA, OA and PFOS in aqueous solution at concentrations of 0.2 mg/mL as determined by DLS measurements.
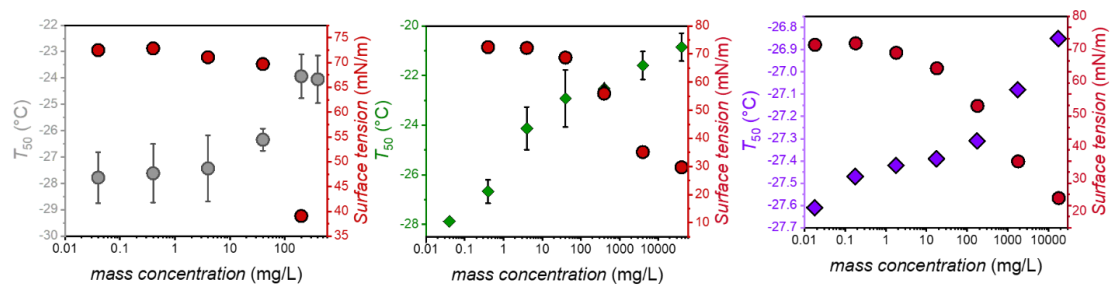
Figure S3*: Surface dependence of OA (grey), PFOS (green) and deprotonated PFOA (purple). The ice nucleation activity of the three compounds is concentration-dependent and follows the trend of the surface tension (red) similar to PFOA.
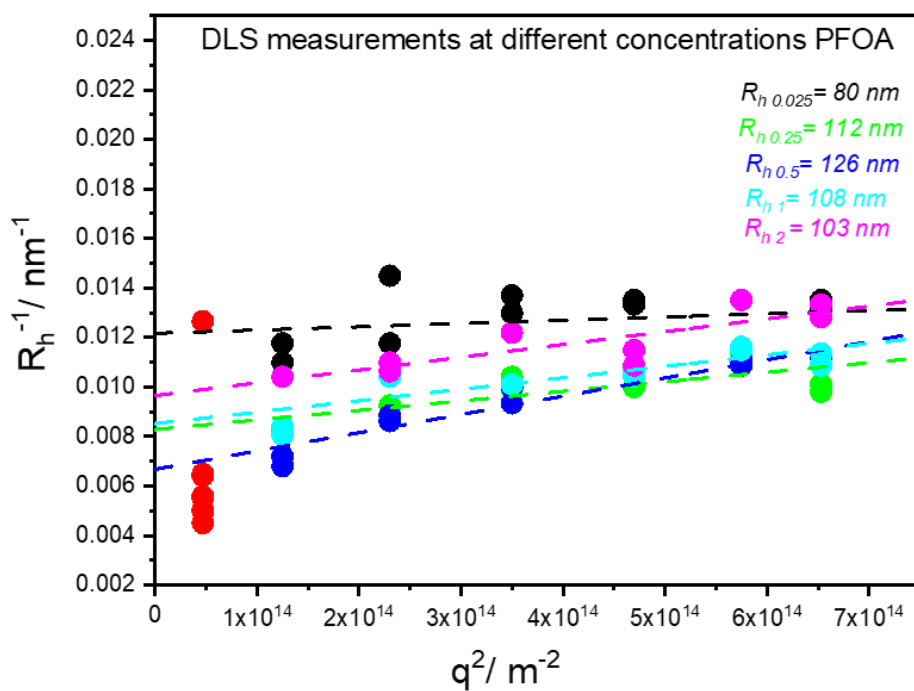
Figure S4: Particle sizes of PFOA in aqueous solution at concentrations spanning from 0.025 mg/mL to 2 mg/mL as determined by DLS measurements.
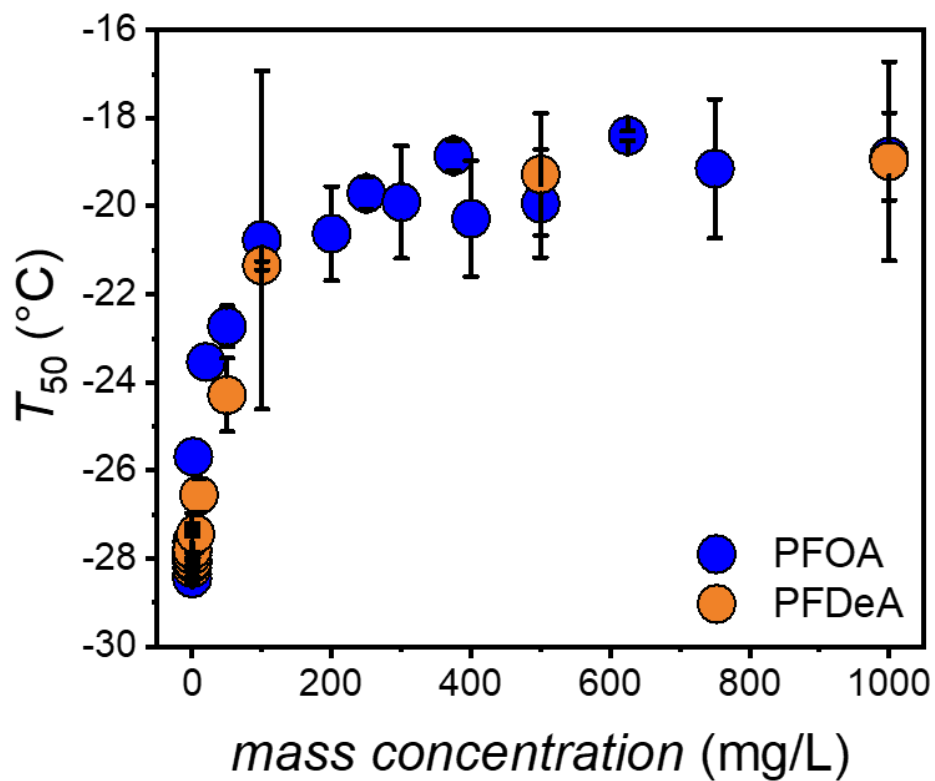
Figure S5: Comparative representation of the ice nucleation activity of PFOA (blue) and perfluorodecanoic acid (PFDeA, orange).

Table S1: Melting Points of PFOA, OA and PFOS at concentrations of 0.2 mg/mL in water as determined by DSC measurements.

Sample	Melting Point (°C)
PFOA	0.06°C
OA	0.09°C
PFOS	0.01°C

References

(1.)   Kunert, A. T.; Lamneck, M.; Helleis, F.; Pöschl, U.; Pöhlker, M. L.; Fröhlich-Nowoisky, J. Twin-Plate Ice Nucleation Assay (TINA) with Infrared Detection for High-Throughput Droplet Freezing Experiments with Biological Ice Nuclei in Laboratory and Field Samples. *Atmos. Meas. Tech.* **2018,** *11* (11), 6327-6337.

A.6 Schwidetzky *et al.*, J. Phys. Chem. Lett., 2021

Membranes Are Decisive for Maximum Freezing Efficiency of Bacterial Ice Nucleators

R. Schwidetzky[1], P. Suderna[1], A. T. Backes[2], U. Pöschl[2], M. Bonn[1], J. Fröhlich-Nowoisky[2], and K. Meister[1,3]

[1] Max-Planck-Institute for Polymer Research, 55128 Mainz, Germany
[2] Max-Planck-Institute for Chemistry, 55128 Mainz, Germany
[3] University of Alaska Southeast, Juneau, Alaska 99801, United States

Author contributions:

R.S. performed the freezing experiments and contributed to analyzing and discussing the results as well as writing the manuscript.

Letter

Membranes Are Decisive for Maximum Freezing Efficiency of Bacterial Ice Nucleators

R. Schwidetzky, P. Sudera, A. T. Backes, U. Pöschl, M. Bonn, J. Fröhlich-Nowoisky, and K. Meister*

Read Online

ACCESS | Metrics & More | Article Recommendations | SI Supporting Information

ABSTRACT: Ice-nucleating proteins (INPs) from *Pseudomonas syringae* are among the most active ice nucleators known, enabling ice formation at temperatures close to the melting point of water. The working mechanisms of INPs remain elusive, but their ice nucleation activity has been proposed to depend on the ability to form large INP aggregates. Here, we provide experimental evidence that INPs alone are not sufficient to achieve maximum freezing efficiency and that intact membranes are critical. Ice nucleation measurements of phospholipids and lipopolysaccharides show that these membrane components are not part of the active nucleation site but rather enable INP assembly. Substantially improved ice nucleation by INP assemblies is observed for deuterated water, indicating stabilization of assemblies by the stronger hydrogen bonds of D_2O. Together, these results show that the degree of order/disorder and the assembly size are critically important in determining the extent to which bacterial INPs can facilitate ice nucleation.
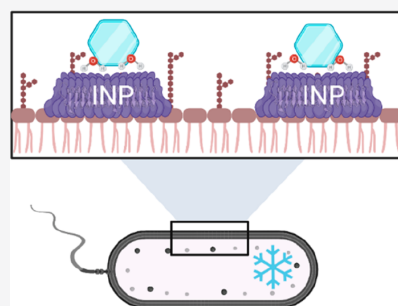
The formation of ice is thermodynamically favored at temperatures below 0 °C, but the crystallization is kinetically hindered. As a result, pure water can be supercooled to temperatures as low as −38 °C, below which homogeneous ice nucleation occurs.[1] Nature provides extraordinary examples of how to induce ice formation at much warmer temperatures. Certain ice nucleation active microbes enable ice formation at temperatures close to 0 °C, better than other organic or inorganic material.[2,3] Ice nucleation active bacteria cause frost damage to plants, and in the atmosphere, they may glaciate clouds and influence precipitation patterns.[4,5] The best characterized biological ice nucleators (INs) are from the plant-associated bacteria *Pseudomonas syringae*.[2,6] The ability of *P. syringae* to facilitate ice nucleation is attributed to specialized ice-nucleating proteins (INPs) anchored to the outer bacterial cell membrane.[7,8] The functional structure of the INPs has been reported to contain a hydrophobic N-terminal domain, a hydrophilic C-terminal domain, and a large central repeat domain presumably acting as ice nucleation sites.[9] The proposed nucleation sites consist of arrays of STQT and ESSLT motifs, where threonine and serine are most conserved.[10] Apart from the structural properties of the active site, the exceptional activity of bacterial INs has been reported to critically depend on the ability of the INPs to assemble into large clusters.[10−12] Based on their activity in droplet freezing experiments, the bacterial INs are oftentimes grouped into classes A−C.[13] Class A INs consist of large aggregates (>30 INPs) and are responsible for freezing between ∼−2 and ∼−4 °C, whereas C INs consist of smaller aggregates that induce freezing at ∼−7.5 °C.[10,13] Class B INs are less common and responsible for freezing between ∼-5 and ∼−7 °C. The INPs

are localized in the outer bacterial membrane, as demonstrated by fractionating experiments and the isolation of ice-nucleating vesicles shed from the membrane.[8,14] The leaflet of the outer membrane of Gram-negative bacteria like *P. syringae* consists of phospholipids and complex lipopolysaccharides (Figure 1). Turner et al. suggested that phosphatidylinositol (PI) is important for ice nucleation activity as a part of the ice nucleation site and to serve as an anchor for INPs.[15,16] In contrast, Schmid et al. reported that INPs cannot be anchored to the membrane via PI. Govindarajan et al. further showed that delipidating membranes abolished the activity of class C INs and that the addition of lipids reconstituted activity.[7] A number of studies also revealed that chemicals that disrupt the fluidity of the membrane reduced ice nucleation activity.[2,7,17] Recent studies further showed that environmental factors (pH, salts, antifreeze proteins) can have very different effects on class A and class C INs.[11,18−20] Here, we use the high-throughput twin-plate ice nucleation assay (TINA) to investigate the ice nucleation activity of the lipids 1,2-dimyristoyl-3-trimethylammonium−propane (DPTAP), 1,2-dipalmitoyl-*sn*-glycero-3-phosphoglycerol (sodium counterion) (DPPG), 1,2-dipalmitoyl-*sn*-glycero-3-phosphorylethanol-amine (chloride counterion) (DPPE), phosphatidylinositol
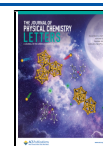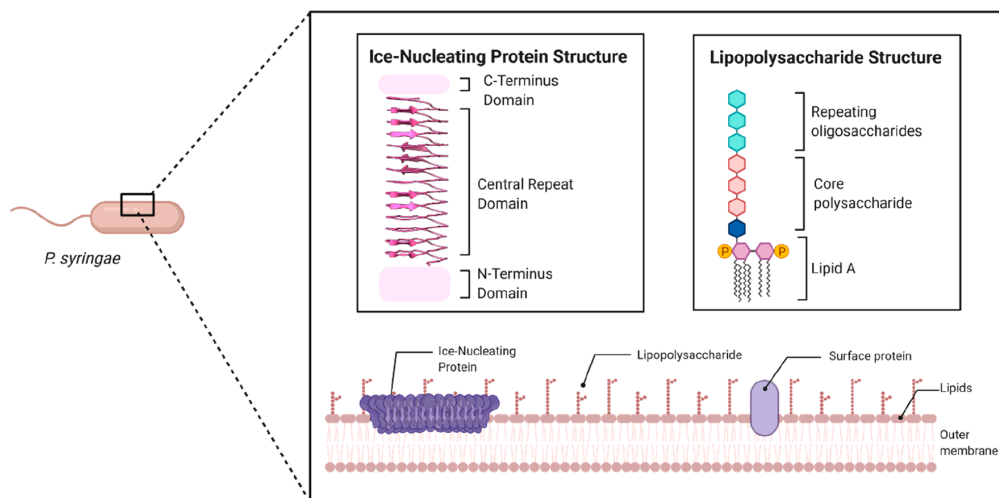
Figure 1. Schematic representation of the Gram-negative, rod-shaped bacterium *P. syringae*, the modeled structures of an ice-nucleating protein, and a lipopolysaccharide, as well as their location in the outer bacterial cell membrane.
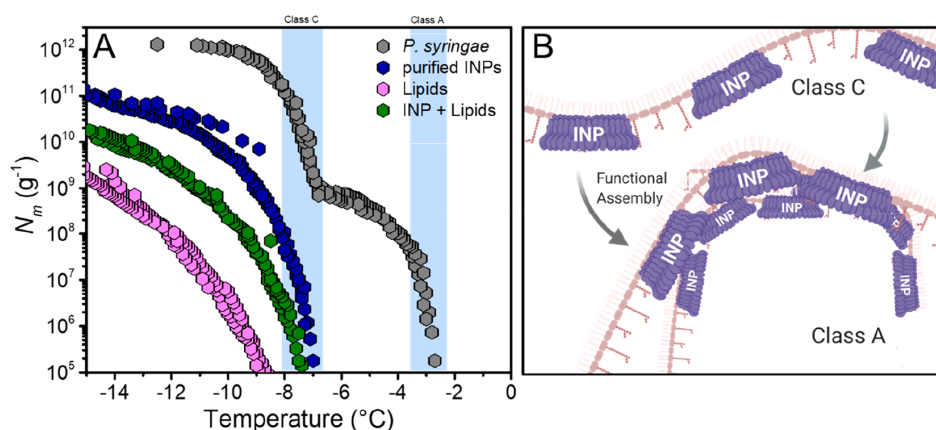

Figure 2. Freezing experiments with aqueous solutions of *P. syringae,* purified INPs, extracted lipids, and a combination of purified INPs and lipids in water. (A) Cumulative number of ice nucleators per unit mass of sample (N_m) plotted against temperature. The temperature ranges for class A and C bacterial ice nucleators in water are shaded in blue. (B) Hypothetical representation of class A and C ice nucleators in a membrane. Class C refers to small INP assemblies and class A to larger, highly efficient INP assemblies.

(PI), lipopolysaccharides, and the effects of deuterated water, heat, and delipidation on the ice nucleation activity of *P. syringae*.[21]

Figure 2a shows the results of ice nucleation measurements of the bacterial INs Snomax in water. Snomax consists of inactivated cells of *P. syringae* and is widely used as a model for bacterial ice nucleation studies.[22] The initial *P. syringae* solutions had a concentration of 0.1 mg/mL and were then serially diluted 10-fold, resulting in concentrations from 1 ng/mL to 0.1 mg/mL. The cumulative ice nucleator number concentration (N_m) was calculated using Vali's formula and represents the number of ice nucleators per unit weight that are active above a certain temperature.[23] For the bacterial IN solution in water, the spectrum shows two strong increases in $N_m(T)$ around $\sim$−2.9 and $\sim$−7.5 °C with plateaus between $\sim$−4.5 and $\sim$−7 °C and below $\sim$−9.5 °C. The two rises in the spectrum reveal the presence of two classes of IN with different activation temperatures. We attribute the observed rises at

$\sim$−2.9 and $\sim$−7.5 °C to class A and C IN, respectively. Class A IN supposedly consist of large INP assemblies and the less active class C IN consist of smaller INP assemblies. We purified the INPs of *P. syringae* using Folch extraction (FE) and ice affinity purification (IAP). FE is based on the partitioning of lipids in a biphasic mixture of chloroform and methanol and causes a separation of lipid and protein components.[24] IAP uses the ability of INPs to bind to ice, and the purification process involves the incorporation of INPs into the growing ice phase and the exclusion of impurities.[20,25] We will refer to the purified samples as "lipid" (FE extraction) and "purified INP" (FE extraction and subsequent IAP) fractions. Figure 2 shows that the freezing spectra of both the lipid and purified INP fractions of *P. syringae* look different than the spectrum of *P. syringae* in water. For both fractions, we observe that the class A related increase at $\sim$−2.9 °C is absent and that the total number of INs is reduced. For the purified INPs, we observe an increase at $\sim$−7 °C, and for the
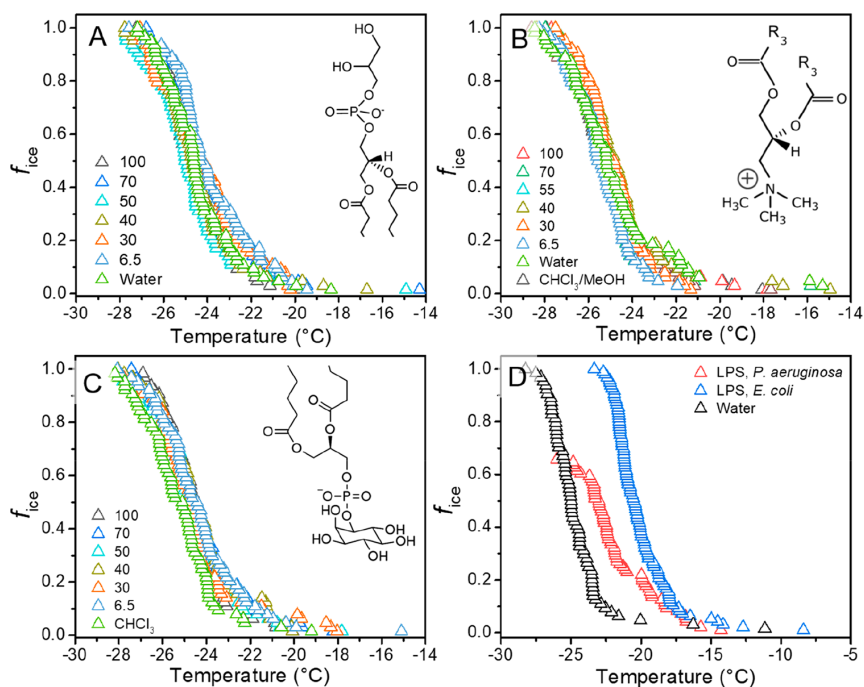
Figure 3. Droplet freezing experiments of phospholipids and LPS. Parts A−C show the fraction of frozen 1 μL droplets plotted against temperature, for the lipids DPPE, DPPG, and PI, respectively. Lipids were dissolved in 9:1 chloroform:methanol and measurements were performed with surface coverages ranging from 6.5 to 100 Å^2/molecule on water. (D) Freezing curves of aqueous LPS solutions (5 mg/mL) extracted from ice-nucleation active and nonactive bacteria. Insets show the chemical structure of the lipid headgroups.
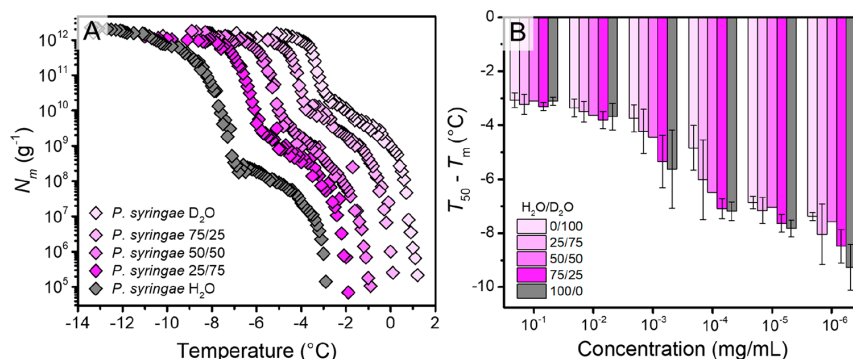

Figure 4. Freezing experiments of aqueous solutions of *P. syringae* in water, deuterated water, and mixtures of the two. (A) Cumulative number of ice nucleators (N_m) per unit mass of sample vs temperature. (B) T_{50} values of *P. syringae* in water and D$_2$O mixtures, corrected for their respective melting points. T_{50} values are defined as the temperatures at which 50% of the droplets are frozen.

lipid fraction, an increase at ∼−8 °C. Apparently, the removal of the lipids keeps the class C INs largely intact, but it prevents the formation of the highly efficient class A INs. Interestingly, the lipid fraction retained significant activity. Ice nucleation activity of lipids alone can be excluded, as demonstrated by Figure 3, which shows a lack of IN activity for different lipids and lipopolysaccharides (LPS). We thus explain this observation with remaining INPs in the lipid fraction. Figure 2 also shows the results of combining the purified INPs with the lipid fraction. We find that the freezing spectra of the combined INP+lipid fractions show an increase at ∼−7 °C corresponding to class C INs and no increase at ∼−2.9 °C. *P. syringae* samples that underwent delipidation treatment but

were not separated also only showed an increase at ∼−7 °C corresponding to class C INs and no increase at ∼−2.9 °C (Figure S1).

Clearly, the loss of activity of class A INs upon delipidation is irreversible, and reintroducing a lipid matrix is insufficient to restore activity of class A INs.

Figure 3 shows the results of statistical freezing curves of the lipids DPPE, DPTAP, PI, DPPG (Figure S2), and LPS. The activities of the lipids were determined in aqueous solutions with different surface coverages (for details, see methods). We find that all of the lipids show negligible ice nucleation activity. The observed T_{50} values of ∼−25 °C are similar to those of pure water in our setup. T_{50} values are defined as the

temperatures at which 50% of the droplets are frozen. These observations are in line with previous findings that long-chain fatty acids and surfactants are poor INs.[26,27]

LPS is another major component of the outer layer of the cell membrane of Gram-negative bacteria. LPS molecules are often associated with membrane proteins and are in direct contact with the environment. Figure 3d shows freezing spectra of LPS extracts from the ice nucleation-active bacteria *Pseudomonas aeruginosa*[28] and the nonactive bacteria *Escherichia coli*. At maximal LPS concentrations of 5 mg/mL, the ice nucleation activity is weak, with freezing occurring at T_{50} = ~−22.5 °C for *P. aeruginosa* and ~−20 °C for *E. coli*. LPS has previously been reported to have moderate ice-nucleating abilities, which agrees with our findings.[29,30] We conclude that LPS might play minor roles in ice nucleation, but since LPS derived from the nonactive bacteria showed higher activity, this role is likely not crucial for the class A IN that enables maximum freezing efficiency.

Having established that lipids and LPS are not active components of the ice nucleation site, we hypothesized whether the role of the membrane might be to serve as a functional assembly matrix for the highly efficient class A IN. Figure 4 shows the results of ice nucleation measurements of the bacterial IN in water, deuterated water (D$_2$O), and in mixtures of the two. For *P. syringae* in pure D$_2$O, the freezing spectrum looks similar to that of *P. syringae* in water, with a ~4 °C shift of the INP-mediated freezing curve to warmer temperatures. The observed shift is consistent with the expected shift of ~3.82 °C based on the higher melting point of D$_2$O. Turner et al. previously described a third intermediate class B INs, active at around ~−5 °C, and that examining the effects of substituting D$_2$O for H$_2$O allows for differentiation of the different classes on the basis of their isotope-induced shifts in nucleation threshold.[13] As apparent from Figure 4, the freezing spectra did not show an additional increase assignable to a third class of INs. However, we did observe some differences in the freezing curves of *P. syringae* in H$_2$O and D$_2$O. We explain the observed differences with higher rigidities of INPs in D$_2$O and fewer structural fluctuations of the INP-assemblies due to the stronger intramolecular D-bonds.[31,32] In fact, at a macroscopic level, there is some evidence suggesting that D$_2$O is a worse solvent than water and that proteins tend to reduce the surface area in contact with D$_2$O by forming larger aggregates.[33,34] Thus, especially small INP aggregates, present at lower concentrations, tend to increase their size and thereby the ice nucleation efficiency as shown in Figure 4B

INPs are localized in the outer bacterial membrane, suggesting that lipids might be required for ice nucleation activity as part of the active nucleation site or by enabling precise INP assembly. The fact that we did not observe ice nucleation activity of lipids and LPS components of the membrane implies that they are not part of the nucleation site. Interestingly, PI was previously reported to be an important component in ice nucleation sites of bacteria and insects.[15,16,35] In these studies, the presence of borate compounds was further shown to dramatically reduce the ice nucleation activity of *P. syringae*, which was explained by the complexation of the hydroxyl groups of the inositol.[6,36] We find that PI shows no ice nucleation activity, and the presence of borate compounds also did not reduce the ice nucleation activity of *P. syringae* (Figure S3). Our findings further support the interpretation that class C and class A INs from *P. syringae* do not differ in the

structure of their INP building blocks but solely in their assembly size and supramolecular ordering. After delipidation experiments, the purified INPs displayed ice nucleation activity that could be assigned to class C INs, while class A activity was completely removed. We conclude that class C IN only consists of small INP assemblies that do not require lipids for functionality, whereas class A aggregates require an intact membrane environment for functional alignment and aggregation. Using different H$_2$O/D$_2$O ratios, we were able to show that the extent of the assembly of INPs and the corresponding amount of class A and class C INs can be altered depending on the solvent mixture. Our results unambiguously prove that maximum ice nucleation activity observed in bacteria results from the association of INPs within the membrane. Hence, studies that take only the bacterial INPs into consideration have to be taken with a caveat, as they do not resemble the bacterial system and their highly efficient INs. Our data is consistent with a mechanism, in which bacteria have to exert precise control over (1) the distance between the INP monomers at the sub-Ångstrom level, and (2) the size of the protein assemblies to achieve high ice nucleation activities.[10] This mechanism explains the high sensitivity of class A INs to temperature as well as chemicals[7,11,17,19] that modify the properties of the cell membrane or the aggregation behavior of proteins. Given that highly active class A INs have also been observed in mutated *E. coli* cells[12] suggests that INP assembly is robust toward variations in exact membrane composition.

■ ASSOCIATED CONTENT

ⓢ Supporting Information

The Supporting Information is available free of charge at https://pubs.acs.org/doi/10.1021/acs.jpclett.1c03118.

> Experimental methods; Figure S1, effect of Folch extraction on bacterial INs; Figure S2, droplet freezing experiments of the phospholipid DPPG; Figure S3, effect of borate compounds (0.3 M) on bacterial INs (PDF)

■ AUTHOR INFORMATION

Corresponding Author

K. Meister − *Max Planck Institute for Polymer Research, 55128 Mainz, Germany; University of Alaska Southeast, Juneau, Alaska 99801, United States;* ⓞ orcid.org/0000-0002-6853-6325; Email: meisterk@mpip-mainz.mpg.de

Authors

R. Schwidetzky − *Max Planck Institute for Polymer Research, 55128 Mainz, Germany*

P. Sudera − *Max Planck Institute for Polymer Research, 55128 Mainz, Germany*

A. T. Backes − *Max Planck Institute for Chemistry, 55128 Mainz, Germany*

U. Pöschl − *Max Planck Institute for Chemistry, 55128 Mainz, Germany;* ⓞ orcid.org/0000-0003-1412-3557

M. Bonn − *Max Planck Institute for Polymer Research, 55128 Mainz, Germany;* ⓞ orcid.org/0000-0001-6851-8453

J. Fröhlich-Nowoisky − *Max Planck Institute for Chemistry, 55128 Mainz, Germany;* ⓞ orcid.org/0000-0002-1278-0054

Complete contact information is available at:
https://pubs.acs.org/10.1021/acs.jpclett.1c03118

REFERENCES

(1) Koop, T.; Luo, B.; Tsias, A.; Peter, T. Water activity as the determinant for homogeneous ice nucleation in aqueous solutions. *Nature* **2000**, *406* (6796), 611−614.

(2) Kozloff, L M; Schofield, M A; Lute, M Ice nucleating activity of Pseudomonas syringae and Erwinia herbicola. *J. Bacteriol.* **1983**, *153* (1), 222−231.

(3) Pouleur, S.; Richard, C.; Martin, J. G.; Antoun, H. Ice Nucleation Activity in Fusarium acuminatum and Fusarium avenaceum. *Appl. Environ. Microbiol.* **1992**, *58* (9), 2960−4.

(4) Schnell, R. C.; Vali, G. Atmospheric Ice Nuclei from Decomposing Vegetation. *Nature* **1972**, *236* (5343), 163−165.

(5) Lindow, S. E.; Arny, D. C.; Upper, C. D. Bacterial Ice Nucleation: A Factor in Frost Injury to Plants 1. *Plant Physiol.* **1982**, *70* (4), 1084−1089.

(6) Kozloff, L. M.; Schofield, M. A.; Lute, M. Ice nucleating activity of Pseudomonas syringae and Erwinia herbicola. *J. Bacteriol.* **1983**, *153* (1), 222−231.

(7) Govindarajan, A. G.; Lindow, S. E. Phospholipid requirement for expression of ice nuclei in Pseudomonas syringae and in vitro. *J. Biol. Chem.* **1988**, *263* (19), 9333−8.

(8) Govindarajan, A. G.; Lindow, S. E. Size of bacterial ice-nucleation sites measured in situ by radiation inactivation analysis. *Proc. Natl. Acad. Sci. U. S. A.* **1988**, *85* (5), 1334−1338.

(9) Wolber, P.; Warren, G. Bacterial ice-nucleation proteins. *Trends Biochem. Sci.* **1989**, *14* (5), 179−182.

(10) Qiu, Y.; Hudait, A.; Molinero, V. How Size and Aggregation of Ice-Binding Proteins Control Their Ice Nucleation Efficiency. *J. Am. Chem. Soc.* **2019**, *141* (18), 7439−7452.

(11) Lukas, M.; Schwidetzky, R.; Kunert, A. T.; Pöschl, U.; Fröhlich-Nowoisky, J.; Bonn, M.; Meister, K. Electrostatic Interactions Control the Functionality of Bacterial Ice Nucleators. *J. Am. Chem. Soc.* **2020**, *142* (15), 6842−6846.

(12) Mueller, G. M.; Wolber, P. K.; Warren, G. J. Clustering of ice nucleation protein correlates with ice nucleation activity. *Cryobiology* **1990**, *27* (4), 416−422.

(13) Turner, M. A.; Arellano, F.; Kozloff, L. M. Three separate classes of bacterial ice nucleation structures. *J. Bacteriol.* **1990**, *172* (5), 2521−2526.

(14) Phelps, P.; Giddings, T. H.; Prochoda, M.; Fall, R. Release of cell-free ice nuclei by Erwinia herbicola. *J. Bacteriol.* **1986**, *167* (2), 496−502.

(15) Duman, J. G. Antifreeze and Ice Nucleator Proteins in Terrestrial Arthropods. *Annu. Rev. Physiol.* **2001**, *63* (1), 327−357.

(16) Kozloff, L. M.; Lute, M.; Westaway, D. Phosphatidylinositol as a Component of the Ice Nucleating Site of Pseudomonas syringae and Erwinia herbiola. *Science* **1984**, *226* (4676), 845−6.

(17) Turner, M. A.; Arellano, F.; Kozloff, L. M. Components of ice nucleation structures of bacteria. *J. Bacteriol.* **1991**, *173* (20), 6515−6527.

(18) Schwidetzky, R.; Kunert, A. T.; Bonn, M.; Pöschl, U.; Ramløv, H.; DeVries, A. L.; Fröhlich-Nowoisky, J.; Meister, K. Inhibition of Bacterial Ice Nucleators Is Not an Intrinsic Property of Antifreeze Proteins. *J. Phys. Chem. B* **2020**, *124* (24), 4889−4895.

(19) Schwidetzky, R.; Lukas, M.; YazdanYar, A.; Kunert, A. T.; Pöschl, U.; Domke, K. F.; Fröhlich-Nowoisky, J.; Bonn, M.; Koop, T.; Nagata, Y.; et al. Specific Ion−Protein Interactions Influence Bacterial Ice Nucleation. *Chem. - Eur. J.* **2021**, *27* (26), 7402−7407.

(20) Lukas, M.; Schwidetzky, R.; Kunert, A. T.; Backus, E. H. G.; Pöschl, U.; Fröhlich-Nowoisky, J.; Bonn, M.; Meister, K. Interfacial Water Ordering Is Insufficient to Explain Ice-Nucleating Protein Activity. *J. Phys. Chem. Lett.* **2021**, *12* (1), 218−223.

(21) Kunert, A. T.; Lamneck, M.; Helleis, F.; Pöschl, U.; Pöhlker, M. L.; Fröhlich-Nowoisky, J. Twin-plate Ice Nucleation Assay (TINA) with infrared detection for high-throughput droplet freezing experiments with biological ice nuclei in laboratory and field samples. *Atmos. Meas. Tech.* **2018**, *11* (11), 6327−6337.

(22) Budke, C.; Koop, T. BINARY: an optical freezing array for assessing temperature and time dependence of heterogeneous ice nucleation. *Atmos. Meas. Tech.* **2015**, *8* (2), 689−703.

(23) Vali, G. Quantitative Evaluation of Experimental Results an the Heterogeneous Freezing Nucleation of Supercooled Liquids. *J. Atmos. Sci.* **1971**, *28* (3), 402−409.

(24) Eggers, L. F.; Schwudke, D. Liquid Extraction: Folch. In *Encyclopedia of Lipidomics*; Wenk, M. R., Ed.; Springer Netherlands: Dordrecht, The Netherlands, 2016; pp 1−6.

(25) Tomalty, H. E.; Graham, L. A.; Eves, R.; Gruneberg, A. K.; Davies, P. L. Laboratory-Scale Isolation of Insect Antifreeze Protein for Cryobiology. *Biomolecules* **2019**, *9* (5), 180.

(26) DeMott, P. J.; Mason, R. H.; McCluskey, C. S.; Hill, T. C. J.; Perkins, R. J.; Desyaterik, Y.; Bertram, A. K.; Trueblood, J. V.; Grassian, V. H.; Qiu, Y.; et al. Ice nucleation by particles containing long-chain fatty acids of relevance to freezing by sea spray aerosols. *Environmental Science: Processes & Impacts* **2018**, *20* (11), 1559−1569.

(27) Schwidetzky, R.; Sun, Y.; Fröhlich-Nowoisky, J.; Kunert, A. T.; Bonn, M.; Meister, K. Ice Nucleation Activity of Perfluorinated Organic Acids. *J. Phys. Chem. Lett.* **2021**, *12* (13), 3431−3435.

(28) Hazra, A.; Saha, M.; De, U. K.; Mukherjee, J.; Goswami, K. Study of ice nucleating characteristics of Pseudomonas aeruginosa. *J. Aerosol Sci.* **2004**, *35* (11), 1405−1414.

(29) Maeda, M.; Lee, W. J.; Taga, N. Distribution of lip-opolysaccharide, an indicator of bacterial biomass, in subtropical areas of the sea. *Mar. Biol.* **1983**, *76* (3), 257−262.

(30) Mael, L. E.; Busse, H.; Grassian, V. H. Measurements of Immersion Freezing and Heterogeneous Chemistry of Atmospherically Relevant Single Particles with Micro-Raman Spectroscopy. *Anal. Chem.* **2019**, *91* (17), 11138−11145.

(31) Cioni, P.; Strambini, G. B. Effect of Heavy Water on Protein Flexibility. *Biophys. J.* **2002**, *82* (6), 3246−3253.

(32) Scheiner, S.; Čuma, M. Relative Stability of Hydrogen and Deuterium Bonds. *J. Am. Chem. Soc.* **1996**, *118* (6), 1511−1521.

(33) Maybury, R. H.; Katz, J. J. Protein Denaturation in Heavy Water. *Nature* **1956**, *177* (4509), 629−630.

(34) Chakrabarti, G.; Kim, S.; Gupta, M. L.; Barton, J. S.; Himes, R. H. Stabilization of Tubulin by Deuterium Oxide. *Biochemistry* **1999**, *38* (10), 3067−3072.

(35) Kozloff, L. M.; Turner, M. A.; Arellano, F.; Lute, M. Phosphatidylinositol, a phospholipid of ice-nucleating bacteria. *J. Bacteriol.* **1991**, *173* (6), 2053−60.

(36) Bäumer, A.; Duman, J. G.; Havenith, M. Ice nucleation of an insect lipoprotein ice nucleator (LPIN) correlates with retardation of the hydrogen bond dynamics at the myo-inositol ring. *Phys. Chem. Chem. Phys.* **2016**, *18* (28), 19318−19323.

Supporting Information

Title: Membranes Are Decisive for Maximum Freezing Efficiency of Bacterial Ice Nucleators

Authors: R. Schwidetzky[1], P. Sudera[1], A. T. Backes[2], U. Pöschl[2], M. Bonn[1], J. Fröhlich-Nowoisky[2], and K. Meister[1,3]

Affiliations:

[1]Max Planck Institute for Polymer Research, 55128 Mainz, Germany

[2]Max Planck Institute for Chemistry, 55128 Mainz, Germany

[3]University of Alaska Southeast, 99801 Juneau, AK, United States

Methods:

Materials. Pure water was obtained from Millipore Milli-Q® Integral 3 water purification system (Merck Chemicals GmbH, Darmstadt, Germany), autoclaved at 121 °C for 15 min, and filtered through a 0.1 µm bottle top filtration unit (VWR International GmbH, Darmstadt, Germany). Deuterated water, lipids, and lipopolysaccharide extracts were purchased from Sigma Aldrich. Snomax® was purchased from SMI Snow Makers AG (Thun, Switzerland) and consists of a preparation of inactivated bacteria cells of *P. syringae*.

Folch Extraction. Folch extraction was performed by a protocol adapted from Wessel *et al*[37]. In short, *P. syringae* was dissolved in water at a concentration of 10 mg/mL. 5 mL of the solution was pipetted in a 50 mL falcon tube, 20 mL methanol was added, and the mixture was vortexed thoroughly. Then, 10 mL chloroform was added, and the solution was vortexed again. After the addition of 15 mL water, the mixture was generously vortexed and centrifuged at 13,000 g for 1 min. The resulting sample contained a large aqueous layer on top, a circular flake of protein in the interphase, and a smaller chloroform layer at the bottom. The upper layer was carefully removed, 15 mL methanol was added, vortexed, and centrifuged at 13,000 g for 2 min. All samples were dried under vacuum.

Ice Affinity Purification. Rotary ice-shell purification was used to purify the ice-nucleating biomolecules of Snomax. Details of the purification method have been described elsewhere[20, 25]. In short, ~20–30 mL of water was used in a 500 mL flask to form an ice-shell using a dry ice-ethanol bath for 30–60 s. The flask was then rotated in a temperature-controlled ethylene glycol bath, and the temperature of the bath was set to −2 °C. 50 mL precooled bacterial IN solution was added, and the flask rotated continuously in the bath until 30% of the solution was frozen. The obtained ice was melted and freeze-dried to obtain a mixture of present ice-binding proteins from *P. syringae*.

TINA Experiments. Ice nucleation experiments were performed using the high-throughput Twin-plate Ice Nucleation Assay (TINA), which has been described in detail elsewhere[21]. In a typical experiment, the investigated IN sample was serially diluted 10-fold by a liquid handling station (epMotion ep5073, Eppendorf, Hamburg, Germany). 96 droplets (3 µL) per dilution were placed on two 384-well plates and tested with a continuous cooling-rate of 1 °C/min from 0 °C to −30 °C in H_2O and 5 °C to -25 °C in D_2O with a temperature uncertainty of ±0.2 °C. The droplet-freezing was determined by two infrared cameras (Seek Therman Compact XR, Seek Thermal Inc., Santa Barbara, CA, USA). The obtained fraction of frozen droplets was used to calculate the cumulative number of ice nucleators using the Vali formula[23]. Experiments were performed multiple times with independent samples. The exact number of independent measurements were Figure 2 (INP extract: six experiments, lipid extract: three experiments, INP + lipid: three experiments); Figure 3 (all experiments were performed in duplicates); Figure 4 (100% D_2O: three experiments, 100%: H_2O three experiments, mixtures: two experiments). Background freezing of pure water in our system occurred at ∼−25 °C. For the TINA lipid experiments, a 0.18 x 10^{-3} M stock solution was prepared for all lipids by dissolving the respective lipid in a 9:1 chloroform/methanol solution. Considering the vial diameter of the 384-well plate to be 3 mm wide in the center, and using the surface area of a circle, molar concentrations for different surface coverages of the lipids were calculated, considering a 30 µL drop volume. Surface areas of interest ranged from 30 $Å^2$/molecule (0.039 x 10^{-3} M) to 100 $Å^2$/molecule (0.0117 x 10^{-3} M), and larger values correspond to lower concentrations and a waiting time of 15 min after addition of samples was maintained to allow for solvent evaporation. Lipid and LPS extract experiments were performed twice with independent samples.
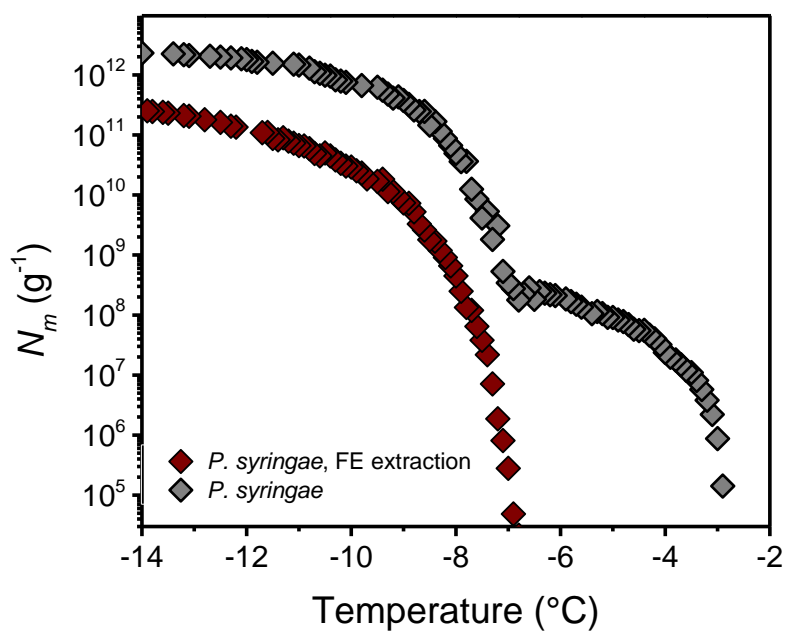
Figure S1 Effect of performing a Folch extraction (FE) on the ice nucleation activity of *P. syringae*. The lipid and proteins fraction were not separated and the organic solvents were evaporated. Shown are the cumulative number of ice nucleators per unit mass of sample (N_m) plotted against temperature.
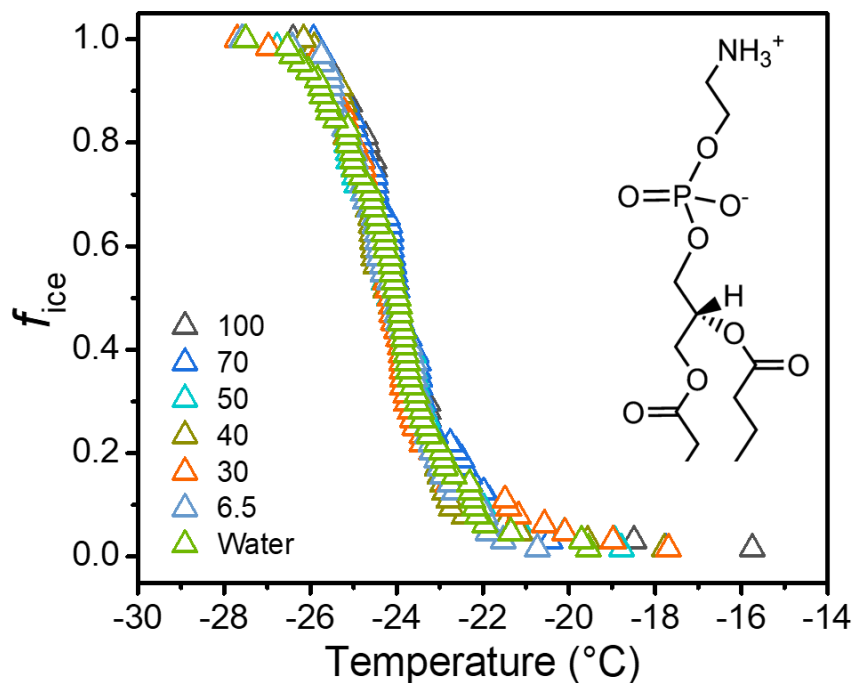
Figure S2 Droplet freezing experiments of the phospholipid DPPG. Shown are the fraction of frozen 1 μL droplets plotted against temperature. DPPG was dissolved in 9:1 chloroform:methanol and measurements were performed with surface coverages ranging from 6.5 to 100 Å^2/molecule on water.
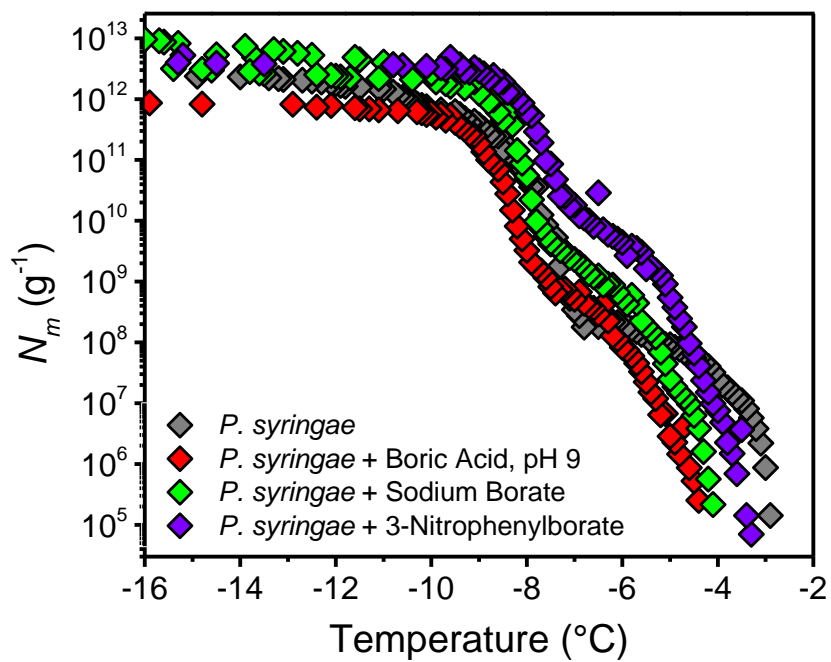
Figure S3 Effect of different borate compounds (0.3 M) on the ice nucleation activity of *P. syringae*. Shown are the cumulative number of ice nucleators per unit mass of sample (N_m) plotted against temperature.

A.7 Eufemio *et al.*, Methods Mol. Bio., 2022

Measurement of Ice Nucleation Activity of biological Samples

R. J. Eufemio[1], R. Schwidetzky[2], and K. Meister[1,2]

[1] University of Alaska Southeast, Juneau, Alaska 99801, United States [2] Max-Planck-Institute for Polymer Research, 55128 Mainz, Germany

Author contributions:

R.S. contributed to creating figures and writing the manuscript.

Title: Measurement of Ice Nucleation Activity of Biological Samples

Authors: R. Eufemio[1]**,** R. Schwidetzky[2], K. Meister[1,2]

Affiliations:

[1]University of Alaska Southeast, 99801 Juneau, AK, United States

[2]Max Planck Institute for Polymer Research, 55128 Mainz, Germany

Author Information

R. Eufemio - University of Alaska Southeast, 99801 Juneau, AK, United States; Email:

rjeufemio@alaska.edu

R. Schwidetzky - Max Planck Institute for Polymer Research, 55128 Mainz, Germany**;** Email:

schwidetzkyr@mpip-mainz.mpg.de

K. Meister **-** University of Alaska Southeast, 99801 Juneau, AK, United States; Max Planck

Institute for Polymer Research, 55128 Mainz, Germany**;** Email: meisterk@mpip-mainz.mpg.de

Measurement of Ice Nucleation Activity of Biological Samples

Abstract

Experimentation with ice nucleating biomolecules is needed to advance the fundamental understanding of biotic heterogeneous ice nucleation. Standard experimental procedures vary with sample type. Here we describe a generalized primary purification and analysis process to measure ice nucleation activity of biological samples using an advanced freezing droplet assay.

1. Introduction

Ice formation is the most prevalent liquid-to-solid phase transition on earth, and is crucial for fields as diverse as cryobiology, geology, and climate science. At ambient conditions, the formation of ice from water is thermodynamically favored at temperatures below 0 ˚C, but this crystallization process is kinetically hindered. Hence, pure water can be supercooled to temperatures as low as -38 °C, below which homogenous ice nucleation occurs. In natural systems, water freezes predominately in a heterogeneous process, facilitated by the presence of ice-nucleating agents of biological and abiotic origins[1]. Natural occurring abiotic ice nucleators (e.g. dust, minerals, clay) typically elevate freezing temperatures to -15 to -30 ˚C, whereas biological ice nucleators are more active and facilitate freezing at temperatures between 0 and -15˚C[2].

Nature provides us with extraordinary examples of how to induce ice formation with high efficiency. Organisms inhabiting cold environments contain biological ice nucleators (INs) that facilitate ice formation at temperatures close to 0 ˚C[3, 4]. The success of biological INs as an

efficient protection against uncontrolled freezing can be witnessed by their wide distribution among different organisms including bacteria, fungi, plants, insects, and lichen[5].

Measuring the activity of the biological INs is key for understanding, and modeling their role in biological and atmospheric cycles. Different instruments have been used for the analysis of INs in immersion freezing experiments, including cloud chambers, continuous flow diffusion chambers and droplet freezing assays[6-10] . Freezing droplet assays are particularly important since they are capable of measuring very small IN concentrations in environmental samples that are active at temperatures above -10°C[7].

The operating principle of freezing droplet assays is the simultaneous cooling of a defined number of aqueous droplets with equal volumes in the pico- to milliliter range. The freezing experiments are usually performed using a stepped temperature profile or a constant cooling rate, which ideally should be similar to those in atmospheric or biological environments where precipitation or extracellular freezing is triggered by the formation of ice crystals. Droplet freezing can be detected using digital cameras based on the reduction of light transmission upon freezing[6, 7], or infrared cameras that detect the latent heat release upon the phase change from liquid water to ice[10-12]. The determination of frozen droplets at a given temperature or after a certain time interval then enables the quantitative assessment of INs, which was established by Vali in 1971[13]. Given the high sensitivity of the freezing process to impurities, it is extremely important to highlight that problems can arise when testing biological samples unless strict control measures are applied[14]. Impurities in materials and solvents pose risks to the integrity of the purification process, so it is critical that for all measurements, especially biological samples, the external conditions must be controlled and documented. The lab workspace and materials must be sterile, and increased efforts

should be made to minimize sources of contamination in solvents, as even minor changes in pH, storing temperature or buffer conditions can drastically alter the experimental results[15-18].

2. Materials

Prepare all samples using pure water from a water purification system such as Millipore Milli-Q® Integral 3 or Barnstead™ GenPure™ xCAD Plus. Autoclave the water at 121°C for 15 minutes and filter through a 0.1 μm-pore-size bottle top filtration unit prior to use[10, 19]. As even lowest concentrations of contaminants can dramatically affect ice nucleation efficiency, impurities represent the highest risk for the experimental determination of the nucleation temperature[14]. Highly active biological ice nucleators tend to stick to surfaces and can contaminate abiotic samples. To minimize this risk of contamination it is necessary to disinfect the bench, fume hood and any materials, such as spatulas, before starting the sample preparation. Consumables (e.g., pipette tips, well plates) should be used directly after opening and ideally have PCR quality. It is further recommended to measure water and control samples when switching to consumables from a new provider. To exclude contaminations in the sample preparation, the ice nucleation activity of water or solvents (buffer, salt solution) must be determined in parallel. To exclude impurities in the solvent, it should be autoclaved as described above. It is further recommended that commercially available buffer solutions should be used. Salts, buffers and other chemicals used for sample preparation must be of the highest available grade and with known formulations.

2.1 Sample Purification

1. Sterile 50 mL centrifuge tubes (autoclaved at 121°C for 15-30 minutes).
2. 0.22 μm sterile membrane syringe filter with appropriately sized syringes or 0.1 μm polyethersulfone membrane bottle top filtration units.

3. Sterile Eppendorf or centrifuge tubes for filtrate collection, storage, and subsequent analysis.

2.2 Freezing Droplet Experiments

1. Sterile Eppendorf tubes (autoclaved at 121°C for 15-30 minutes).

2. Two 384-well multiwell plates of PCR quality.

3. Sterile pipette tips.

4. Liquid handling station (e.g., epMotion ep5073, Eppendorf, Hamburg, Germany).

5. Centrifuge (e.g., MPS 1000 Mini Plate Spinner, Axon Labortechnik GmbH, Germany).

3. Methods

Procedures are typically carried out at room temperature and in a sterile workplace, ideally a laminar flow hood or biosafety cabinet. Use a freezing droplet assay (see 3.2 Freezing Droplet Experiments) to test the background freezing temperature of autoclaved pure water prior to use. Materials (e.g., filters, gloves) may contain particles that act as ice nucleating agents, so perform blank test runs with all materials to quantify and minimize background laboratory contamination[14].

3.1 Sample Purification

1. Collect a known mass of a biological sample in a sterile 50 mL tube.

2. Wash the biological sample (e.g., plant leaf, berries,) with water to remove any impurities located on the sample. Keep the wash water for comparison.

3. If working with highly structured or intact biological samples, such as vegetation fragments, grind the samples in a mortar and pestle or homogenize them in a tissue grinder to break down cell walls[15].

4. Add enough pure water to achieve the desired concentration of the sample, e.g., 40 mg sample in 10 mL water[20]. Keep exact notes about weight and added volume.

5. Centrifuge or vortex the samples. Adapt the procedure to specific biological samples. Examples are:

   - Centrifuge vegetative fragments at 27000 x g for 10 minutes[15]

   - Vortex fungal mycelium three times at 2700 rpm for 1 minute[21]

   - Manually shake suspended pollen grains for 5 minutes, then stir with a stirring bar for approximately 60 minutes[20]

5. If the supernatant is not clear after centrifuging, decant and centrifuge the supernatant again. It should be close to transparent after the second centrifugation.

6. Filter the supernatant into a sterile Eppendorf or centrifuge tube, depending on the volume of filtrate collected. Effective filtration methods include 0.22 μm syringe filters or 0.1 μm bottle top filtration units. We find that the 0.22 μm filters often clog and it is necessary to use more than one per sample.

7. Obtain at least 1.0 mL of filtrate, as this is the minimum volume needed for droplet freezing measurements with robust statistics[10]. The filtrate will contain ice nucleators from the sample. Do not reuse filters for different samples as biomolecules will stick in the filtrate and contaminate subsequent samples.

8. If ice nucleation activity is not tested immediately after purification, store the filtrate at 2-

Measurement of Ice Nucleation Activity of Biological Samples

8°C for a short time or at -18°C for prolonged storage to prevent aging or degradation. Repetitive thawing and freezing should be avoided unless the biological IN remain stable.

3.2 Freezing Droplet Experiments

1. Use a freezing droplet assay that enables robust statistics (e.g., the high-throughput Twin-plate Ice Nucleation Assay (TINA))[10]. Use a liquid handling station to serially dilute the sample. The fully automated experimental procedure will dilute samples, with each dilution consisting of 96 droplets placed in two 384-well plates. Droplet volumes should be consistent and ideally 3 µL. Alternatively, multi-pipettors can be used, but great care must be taken that sample volumes are consistent. For initial measurements it is advantageous to start with the highest available sample concentration. Subsequent sets of experiments can be performed with specific concentrations.

2. Briefly centrifuge the multiwell plates to ensure that droplets are equally distributed in the plates.

3. Cool the 384-well plates at a continuous rate of 1°C/min from 0°C to -30°C. Use infrared cameras or optical light sources to monitor the droplet-freezing and to determine the fraction of frozen droplets. For new droplet freezing assays it is imperative to check whether the temperature gradient is similar at all positions of the multiwall plates[10].

4. Repeat experiments. All experiments should be performed at least three times with independent samples to obtain reliable results.

3.3 Analysis of Experiments

Extract the nucleation temperatures for each droplet. Great care must be taken that the temperature gradient is equal within the cooling block. If the temperature gradient is not similar, then

temperature corrections are needed. Sort the values from the highest temperatures to the lowest temperature.

1. Determine the fraction of frozen droplets. Calculate the fraction of ice (f_{ice}), which is dependent on the number of droplets (f_{ice} = number of frozen droplets/total number). The sorted values represent the number of frozen droplets. Plot the fraction of ice vs the temperature, as shown in Figure 1A.

2. Determine the T_{50} value of your samples. The points at which 50% of the droplets are frozen (*fraction of ice* = 0.5) represents the T_{50} value that is often reported in experimental studies of biological INs.

3. Determine the cumulative ice nucleator number (N_m) of your samples by using the fractions of ice and Vali's equation[13] to calculate the number of active ice nucleators per mass unit of the sample. The calculation assumes that ice nucleation is a time-independent (singular) process, and a typical plot is shown in Figure 1B.

[Figure 1 near here]

Measurement of Ice Nucleation Activity of Biological Samples

References

1   T. Koop, B. Luo, A. Tsias and T. Peter (2000) Nature 406:611-614

2   B. J. Murray, D. O'Sullivan, J. D. Atkinson and M. E. Webb (2012) Chemical Society
       Reviews 41:6519-6554

3   L. R. Maki, E. L. Galyan, M. M. Chang-Chien and D. R. Caldwell (1974) Appl Microbiol
       28:456-459

4   S. Pouleur, C. Richard, J. G. Martin and H. Antoun (1992) Appl Environ Microbiol
       58:2960-2964

5   D. J. Bowles, P. J. Lillford, D. A. Rees, I. A. Shanks and R. Lundheim (2002) Philosophical
       Transactions of the Royal Society of London Series B: Biological Sciences 357:937-943

6   C. Budke and T. Koop (2015) Atmos Meas Tech 8:689-703

7   E. Stopelli, F. Conen, L. Zimmermann, C. Alewell and C. E. Morris (2014) Atmos Meas
       Tech 7:129-134

8   T. F. Whale, B. J. Murray, D. O'Sullivan, T. W. Wilson, N. S. Umo, K. J. Baustian, J. D.
       Atkinson, D. A. Workneh and G. J. Morris (2015) Atmos Meas Tech 8:2437-2447

9   S. Garimella, T. B. Kristensen, K. Ignatius, A. Welti, J. Voigtländer, G. R. Kulkarni, F.
       Sagan, G. L. Kok, J. Dorsey, L. Nichman, D. A. Rothenberg, M. Rösch, A. C. R.
       Kirchgäßner, R. Ladkin, H. Wex, T. W. Wilson, L. A. Ladino, J. P. D. Abbatt, O. Stetzer,
       U. Lohmann, F. Stratmann and D. J. Cziczo (2016) Atmos Meas Tech 9:2781-2795

10   A. T. Kunert, M. Lamneck, F. Helleis, U. Pöschl, M. L. Pöhlker and J. Fröhlich-Nowoisky
       (2018) Atmos Meas Tech 11:6327-6337

11   A. D. Harrison, T. F. Whale, R. Rutledge, S. Lamb, M. D. Tarn, G. C. E. Porter, M. P. Adams, J. B. McQuaid, G. J. Morris and B. J. Murray (2018) Atmos Meas Tech 11:5629-5641

12   D. Zaragotas, N. T. Liolios and E. Anastassopoulos (2016) Cryobiology 72:239-243

13   G. Vali (1971) Journal of Atmospheric Sciences 28:402-409

14   K. R. Barry, T. C. J. Hill, C. Jentzsch, B. F. Moffett, F. Stratmann and P. J. DeMott (2021) Atmospheric Research 250:105419

15   T. L. Kieft and T. Ruscetti (1990) Journal of Bacteriology 172:3519-3523

16   R. Schwidetzky, M. Lukas, A. YazdanYar, A. T. Kunert, U. Pöschl, K. F. Domke, J. Fröhlich-Nowoisky, M. Bonn, T. Koop, Y. Nagata and K. Meister (2021) Chemistry – A European Journal 27:7402-7407

17   M. Lukas, R. Schwidetzky, A. T. Kunert, U. Pöschl, J. Fröhlich-Nowoisky, M. Bonn and K. Meister (2020) Journal of the American Chemical Society 142:6842-6846

18   M. Polen, E. Lawlis and R. C. Sullivan (2016) Journal of Geophysical Research: Atmospheres 121:11,666-611,678

19   R. Schwidetzky, A. T. Kunert, M. Bonn, U. Pöschl, H. Ramløv, A. L. DeVries, J. Fröhlich-Nowoisky and K. Meister (2020) The Journal of Physical Chemistry B 124:4889-4895

20   K. Dreischmeier, C. Budke, L. Wiehemeier, T. Kottke and T. Koop (2017) Scientific Reports 7:41890

21   A. T. Kunert, M. L. Pöhlker, K. Tang, C. S. Krevert, C. Wieder, K. R. Speth, L. E. Hanson, C. E. Morris, D. G. Schmale Iii, U. Pöschl and J. Fröhlich-Nowoisky (2019) Biogeosciences 16:4647-4659

Figure 1. Typical results of freezing experiments of aqueous extracts containing biological ice nucleators (INs). (A) Fraction of frozen droplets for different dilutions of INs from *Fusarium acuminatum*. Symbol colors indicate data from different concentrations and are identical to (B). The dashed line crosses the points at which 50% of the droplets are frozen (*fraction of ice* = 0.5) and represents the T_{50} value that is often reported in experimental studies of biological INs. (B) Cumulative number of INs per unit mass of *F. acuminatum* (N_m) for extracts containing INs from spores and mycelial surfaces.

A.8 Lukas *et al.*, J. Phys. Chem. B., 2022

Toward Unterstanding Bacterial Ice Nucleation

M. Lukas[1], R. Schwidetzky[1], R. J. Eufemio[2], M. Bonn[1], and K. Meister[1,2]

[1] Max-Planck-Institute for Polymer Research, 55128 Mainz, Germany
[2] University of Alaska Southeast, Juneau, Alaska 99801, United States

Author contributions:

R.S. performed the freezing experiments and contributed to analyzing and discussing the results as well as writing the manuscript.

Toward Understanding Bacterial Ice Nucleation

Max Lukas,* Ralph Schwidetzky, Rosemary J. Eufemio, Mischa Bonn, and Konrad Meister*

ACCESS | Metrics & More | Article Recommendations

ABSTRACT: Bacterial ice nucleators (INs) are among the most effective ice nucleators known and are relevant for freezing processes in agriculture, the atmosphere, and the biosphere. Their ability to facilitate ice formation is due to specialized ice-nucleating proteins (INPs) anchored to the outer bacterial cell membrane, enabling the crystallization of water at temperatures up to −2 °C. In this Perspective, we highlight the importance of functional aggregation of INPs for the exceptionally high ice nucleation activity of bacterial ice nucleators. We emphasize that the bacterial cell membrane, as well as environmental conditions, is crucial for a precise functional INP aggregation. Interdisciplinary approaches combining high-through-put droplet freezing assays with advanced physicochemical tools and protein biochemistry are needed to link changes in protein structure or protein−water interactions with changes on the functional level.
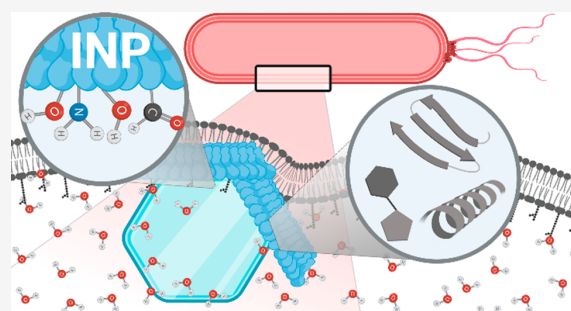
INTRODUCTION

Freezing processes in the atmosphere have a significant influence on the formation of clouds, on precipitation patterns, and on Earth's energy balance.[1,2] Homogeneous ice nucleation at a given temperature requires a certain number of ice-like water molecules. The precise homogeneous nucleation temperature depends on droplet volume, pressure, and the water activity in the presence of potential solutes.[3] Pure water can be supercooled to temperatures as low as −38 °C.[3,4] Above the homogeneous freezing point, ice crystal formation is triggered by particles that serve as heterogeneous ice nucleators (INs). Numerous INs have been identified and their ice nucleation efficiencies are typically characterized using droplet freezing assays.[5−9] In such assays, a large number of droplets containing a well-defined concentration of INs is gradually cooled down and the fraction of frozen droplets as a function of temperature is recorded. The temperature at which half of the droplets are frozen, T_{50}, provides a direct measure for the efficacy of the IN. While mineral dust-based INs (e.g., feldspars, silicates, clay minerals) play a major role in the atmosphere owing to their ubiquity, the ice nucleation efficiency of biological INs derived from bacteria, fungi, lichen, or plants is much higher.[5] Despite its significance and the acceleration of research in this field in recent years, several questions on the molecular-level mechanisms of heterogeneous ice nucleation remain unanswered. This makes it difficult to predict the decisive properties of efficient INs and their role in the environment. Understanding such molecular-level mechanisms could point to novel ways of triggering ice nucleation, desirable not only for artificial snow, for instance, but also for new artificial anti-icing surfaces.[10−12]

Ice-nucleation activity in bacteria was first discovered in *Pseudomonas* in the 1970s.[13,14] Subsequently, several other ice-nucleating bacteria belonging to species in the *Pseudomonadaceae*, *Enterobacteriaceae*, *Xanthomonadaceae*, and *Lysinibacillus* families have been identified.[15−17] The best-characterized bacterial INs are *Pseudomonas syringae*, which enable ice nucleation at temperatures at −2 °C. The ability of bacteria to facilitate ice formation is attributed to specialized proteins anchored to the outer bacterial cell membrane. As a plant pathogen, *P. syringae* causes frost injury to the plant tissue by increasing the nucleation temperature of water, which enables access to nutrients.[9] Moreover, like many other ice-nucleating microbes, *P. syringae* was identified in ice, hail, and snow, indicating that they might contribute to freezing processes in the atmosphere.[5,18] The unique standing of *P. syringae* as a source of exceptional bacterial INs is further emphasized by its commercialization as Snomax. This artificial snowmaking product consists of extracts of sterilized *P. syringae*.

The biomolecules responsible for bacterial ice nucleation are large ice nucleation proteins (INPs) anchored to the outer membranes of the bacterial cells, as schematically shown in Figure 1. The principal function of the INPs is to order water
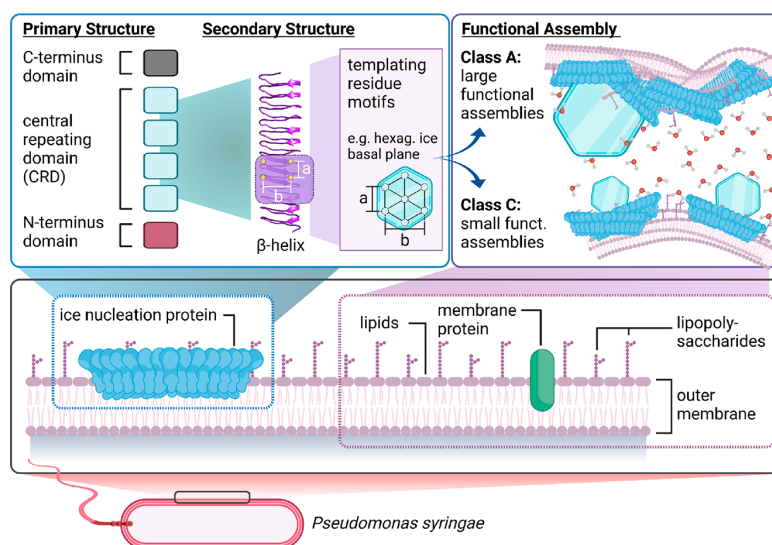
Figure 1. Overview of the proposed structure and working mechanism of bacterial ice nucleation proteins anchored to the outer cell membrane of *P. syringae*. The INP consists of an N-terminal, a C-terminal, and a central repeating domain. Their general function is to order water molecules into an "ice-like" arrangement to nucleate ice formation. This process is facilitated when INPs assemble into larger aggregates.

molecules into an "ice-like" arrangement, thereby facilitating the kinetically hindered phase transition.[19−25]

The amino acid sequence of the INPs of *P. syringae* has been deduced and is widely used to model its structure as shown in Figure 1.[25−28] The INP consists of three domains: (1) a central repeating domain (CRD) comprising ∼81% of the total sequence, (2) an N-terminal domain comprising ∼15% of the sequence, and (3) a C-terminal unique domain (∼4%). The CRD has been proposed to contain the ice nucleation site of the INPs, and molecular simulations have shown that the active site consists of similarly effective hydrophobic TxT and hydrophilic ExSxT amino acid motifs.[29]

The large size and embedment into the membrane still hamper experimental attempts to solve the three-dimensional structure and associated molecular-level details of the INPs. In contrast, the structures of antifreeze proteins (AFPs) containing similar TxT motifs have been solved, oftentimes revealing β-solenoid folds.[19,24,30] A β-helical motif has also been used to model the structure of bacterial INPs,[31] on the basis of the idea that AFPs and INPs share similar folds and ice-binding motifs.[20,29,32]

A central enigma of bacterial ice nucleation arises from the broad distribution of threshold nucleation temperatures ranging from −2 to −12 °C. This is reflected in freezing assays that show not one single T_{50} but a wider range of nucleation temperatures. On the basis of extensive freezing assays of *P. syringae* for different concentrations, three distinct classes of INs have been proposed.[33,34]

Govindarajan and Lindow showed that the largest structures of INs reach the highest threshold temperature, i.e., nucleate ice most efficiently.[35] Southworth et al. revealed a nonlinear relationship between ice nucleation activity and the concentration of INPs in bacterial cells.[36] Together, those findings indicate that the different activation temperatures can be explained by aggregation of INPs, thereby varying the accumulated size of the ice nucleation site. These protein aggregates provide another example of how protein aggregation can have beneficial effects to cellular systems.[37] Simulations have

addressed the role of size and aggregation of the proteins on the freezing temperature and provided quantitative predictions of the ice nucleation temperature vs the number of proteins in the aggregates, as well as to the distance between the monomers in the aggregates.[38] On the basis of freezing assays, the predominant and least efficient fraction of bacterial INs active at ∼−7 °C, *Class C*, has been attributed to small aggregates of INPs (5−10 INPs[38]).[33] The most active *Class A* INs are active at temperatures up to ∼−2 °C and consist of the largest aggregates of the INPs (>30 INPs[38]).[33] Class B INs are rarely observed and responsible for freezing between ∼−5 and ∼−7 °C. Aggregation of the INPs in the cell membrane was described in several studies and it has further been suggested that the membrane plays a major role in enabling the highly active Class A INs.[36,39,40]

■ METHODS

Progress in unraveling the mechanism underlying bacterial ice nucleation requires advanced physicochemical methods and interdisciplinary approaches. Essential for any investigation of INs are droplet freezing assays. High-throughput assays, like the Twin-plate Ice Nucleation Assay (TINA), now enable the simultaneous measurement of complete dilution series (typically 0.1 mg/mL to 1 ng/mL) with robust statistics, enabling the cumulative representation of the complete range of present INs.[41] Observations at the functional level can be accompanied by molecular-scale investigations using spectroscopic tools. Circular dichroism and infrared spectroscopy provide information on the secondary structure, while surface-specific vibrational sum-frequency generation spectroscopy (SFG) is a powerful tool to investigate the molecular-level details of the interface of bacterial INPs and water.[42−46] The biophysical and spectroscopic investigations are further highly dependent on sample quality. Recent progress in ice-affinity purification methods now allows for isolating ice-binding proteins directly from natural sources and with high purity.[44,47−49] In the studies presented here, we utilized inactivated extracts from *P. syringae*, commercially available under the product name Snomax (Snomax Int.).
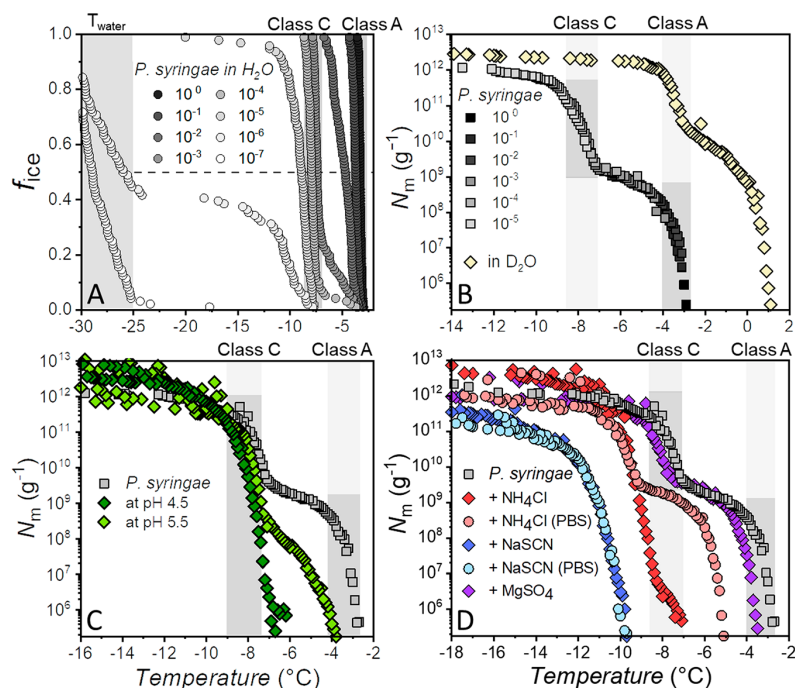
Figure 2. Freezing spectra of aqueous solutions of Snomax, containing bacterial ice nucleators from *P. syringae*. (A) Fraction of frozen droplets (f_{ice}) vs temperature for the dilution series of a *P. syringae* measurement in pure water. (B) Cumulative freezing spectra of *P. syringae* in pure H_2O and D_2O. (C) Freezing spectra of *P. syringae* at pH 6.2 (gray), 5.5 (light green), and 4.5 (dark green), adapted with permission from ref 42. Copyright 2020 American Chemical Society. (D) Freezing spectra of *P. syringae* in pure water and in the presence of 0.5 mol/kg $MgSO_4$ (purple), NaSCN (blue), NH_4Cl (red) in water and of NaSCN (light blue), NH_4Cl (light red) in PBS buffer adapted with permission from ref 46. Copyright 2021 Wiley-VCH. The temperature ranges of Class A and Class C are highlighted in gray and correspond to measurements of *P. syringae* in pure water.
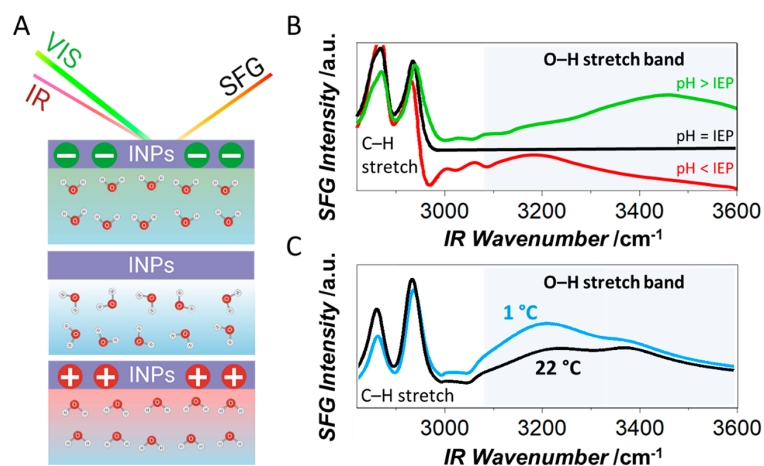

Figure 3. Sum-frequency generation (SFG) spectroscopy of bacterial INPs at the surface of aqueous solutions. (A) The incident IR and VIS beams generate a surface-specific SFG signal from the vibrational resonances. The illustration shows the alignment of interfacial water molecules in the case of a negative net charge as found at the natural pH of ~6.2, in the case of zero net charge at the isoelectric point (IEP) ~ 4.2, and the opposite alignment in the case of a positive net charge at pH values below the IEP. (B) Corresponding SFG spectra. The O−H band intensity is close to zero at the IEP and increases with the charge-induced alignment of the water molecules. The flip of the molecules' orientations causes a frequency shift of the O−H stretch band. (C) Temperature-dependent SFG spectra of the O−H stretch band of interfacial H_2O molecules and the C−H stretch vibrations. The intensity of the O−H stretch band, and therefore the interfacial water alignment, is significantly higher at low temperatures.[42,44]

■ RESULTS AND DISCUSSION

Figure 2 shows freezing spectra of bacterial ice nucleators from *P. syringae* under different environmental conditions. All cumulative freezing spectra are composed of measurements of a 10-fold dilution series. The fraction of frozen droplets (f_{ice})

measurements shown in Figure 2A correspond to the spectra of *P. syringae* INs in pure water (gray curves) in Figure 2B. The cumulative IN concentration (N_m) is calculated using Vali's equation[50] and represents the number of ice nucleators per unit weight that are active above a certain temperature. The two

143

strong increases at ∼−3 and ∼−7.5 °C correspond to the large aggregates (Class A INs) and the smaller aggregates (Class C INs), respectively. The two increases are followed by plateaus, which indicate that fewer INs are active in those temperature ranges.[51]

Figure 2B shows the results of ice nucleation measurements of the bacterial INs in deuterated water (D_2O). The freezing spectrum is shifted ∼+4 °C, which is consistent with the expected shift of +3.82 °C based on the higher melting point of D_2O. Turner et al. previously described a third intermediate Class B of INs, active at around −5 °C, and that examining the effects of substituting D_2O for H_2O allows for differentiation of the different classes on the basis of their isotope-induced shifts in nucleation threshold.[33] As apparent from Figure 2B, the freezing spectra do not show an additional increase assignable to a third class of INs. However, differences in the freezing curves of *P. syringae* in H_2O and D_2O do occur. Measurements in D_2O show a larger number of Class A INs and fewer Class C INs. We explain the observed differences with higher rigidities of INPs in D_2O and fewer structural fluctuations of the INP aggregates due to the stronger intramolecular D-bonds.[52]

Several studies have reported that pH changes of the aqueous solution or the addition of cosolutes affects the Class A INs differently than Class C.[33,34] Figure 2C shows cumulative freezing curves of *P. syringae* as a function of pH.[42] Upon lowering the solution pH, the first rise at ∼−3 °C (Class A) gradually decreases and shifts to lower temperatures while the fraction of INs active at ∼−7.5 °C (Class C) increases. There seems to be a clear interconversion of Class A species into Class C species with decreasing pH. At a pH of ∼4.5, we observe that only Class C INs remain active.

By using interface-specific SFG vibrational spectroscopy as a tool for the determination of the isoelectric point of the bacteria, a possible explanation for this puzzling disappearance of Class A aggregates could be obtained.[42] In SFG spectroscopy, a broadband infrared (IR) beam is used to probe the molecular vibrations in a given frequency region (Figure 3A). The IR beam is combined with a visible beam (VIS) at the sample surface to generate light of the sum-frequency of the two incident fields. This second-order nonlinear process is bulk-forbidden in isotropic media and only ensembles of molecules with a net orientation, e.g., at an interface, generate a detectable signal.

The SFG signal intensity in the O−H stretch region increases with the alignment of the water molecules' dipoles, as, e.g., induced by the net charge of a protein film on the surface (Figure 3A). Consequently, SFG can be used to determine the isoelectric points (IEPs) of proteins by monitoring the O−H stretch signal (Figure 3B).[53−56]

The IEP of the *P. syringae* determined with SFG was found to be ∼4.2, which coincides with the pH at which the Class A INs are completely absent. Apparently, the repulsive forces caused by the net negative charge of the INPs are crucial for the precise alignment of the Class A aggregates, which rely on sub-Ångstrom control over the distances of the single INPs' active sites.[38]

A combination of TINA and SFG experiments further revealed ion-specific effects on *P. syringae* INs that follow the Hofmeister series.[46] Figure 2D shows bacterial freezing spectra in the presence of different salts. NaCl (not shown) was found not to affect the bacterial freezing spectrum except a shift of around −2 °C caused by colligative melting point depression.[57] In contrast, freezing spectra of bacterial solutions containing NH_4Cl, $MgSO_4$, and NaSCN, show ion-specific effects. NH_4Cl

causes the first rise at −3 °C to shift to ∼−7.5 °C, close to the second rise, now found at ∼−9 °C. Interestingly, when freezing spectra of buffered and unbuffered solutions containing NH_4Cl are compared, this effect is solely explainable by salt-induced solution pH changes. In the presence of NaSCN, only a single increase at ∼−11.5 °C remains, indicating a complete loss of Class A and a partial inhibition of Class C INs. The effect is similar for the buffered solution, excluding a pH effect. In the presence of $MgSO_4$, no inhibition is observed. In fact, after correcting for the colligative freezing point depression, the freezing curve is shifted to warmer temperatures, suggesting enhanced ice nucleation efficiency. Comprehensive studies of 16 salts showed that their effects on the INP-mediated freezing temperatures follow the trend of the anions in the Hofmeister series. Weakly hydrated ions, such as thiocyanate, lower the threshold temperatures while more strongly hydrated ions, such as sulfate, have no effect or can apparently facilitate ice nucleation.

SFG experiments revealed that although the ionic strengths and counterions are identical, the salts have different efficiencies in screening the net charge of the bacteria. Weakly hydrated anions decrease the SFG intensity less than strongly hydrated ions. Supported by MD simulations, we explained these results in terms of two effects: Compared to strongly hydrated anions, the weakly hydrated anions preferentially adsorb to the bacterial surfaces, which renders the bacterial surfaces more negative and increases the order of the interfacial water molecules. Additionally, the ions might induce changes in the INP conformation and thereby affect the charge distribution.

The high sensitivity of SFG to the ordering of interfacial water molecules raises the question of whether specific ice-like ordering of water in contact with INPs can be observed close to their biologically relevant working temperature. Pandey et al. reported SFG experiments of *P. syringae* (Snomax) in D_2O at room temperature and 1 °C above the melting point and showed that the SFG signal in the O−D stretch region is increased and red-shifted at low temperature, indicating an increase in the alignment of the water molecules.[43] Shortened INPs with low ice nucleation activity expressed in *E. coli* showed a similar effect, and the observation was attributed to an activation of INPs at lower temperature and the ability to order water, which increases close to the respective freezing temperature.[45] While providing much needed experimental insights into the INP/water interface, these studies and interpretations must be taken with a caveat, given that more recently it has been shown that water ordering at lower temperatures observed with SFG (Figure 3C) are identical for active INPs and heat-denatured INPs that have completely lost their ice nucleation activity.

■ CONCLUSIONS

From our recent studies, we conclude that the outstanding ice nucleation efficiency of bacteria can only be understood in the study of the natural, functional aggregation of the protein. It is evident that a membrane-associated mechanism is responsible for the formation of large Class A aggregates, which are responsible for the exceptionally high freezing temperatures (∼−2 °C) close to water's melting temperature. The process of bacterial ice nucleation at warm temperatures requires an appropriate pH value and intact INP structures.[44] Moreover, the activity of both classes of bacterial INs is strongly influenced by specific interactions with ions. These interactions are highly relevant to correctly predict the ice nucleation efficiency of bacterial INs under natural conditions (e.g., in the atmosphere).

The important role of functional aggregation is further underlined by simulation studies, which have shown that not only Class A but also the smaller Class C INs active at around −7.5 °C are a product of functional aggregation of the proteins and merging of their active sites.[38] Our studies of purified INPs from *P. syringae* have underlined the importance of the membrane for the formation of Class A aggregates,[44] emphasizing its essential role for the ice nucleation activity. We hypothesize that the formation of Class C aggregates might have another molecular mechanism than the membrane-associated mechanism responsible for forming the larger Class A aggregates. Clarification of whether the membrane's role lies merely in providing a matrix or whether it is part of the active ice nucleation site is another critical step for unraveling the molecular origin of bacterial ice nucleation.[58] In addition to unsolved questions regarding the 3D structure of the INP monomer and the interfacial structure of water at the functional site of the INP, information on the precise numbers of INPs in the aggregates, their alignment, and which interactions (e.g., hydrophobic effect, ionic interactions) drive the aggregation is needed (Figure 4).
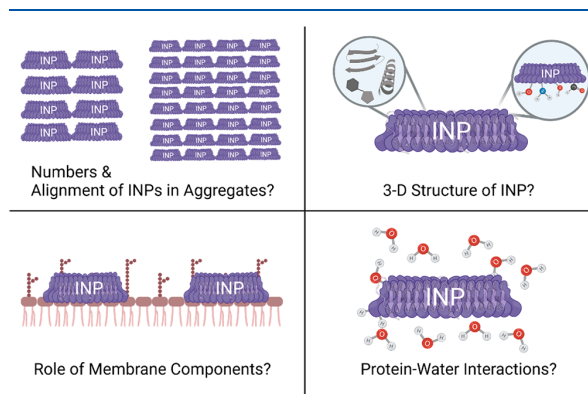

Figure 4. Overview of open questions toward understanding the molecular-level mechanisms of bacterial ice nucleation.

Understanding the molecular-level processes driving bacterial ice nucleation may provide further insights into the role of biological INs in the environment. Answering these questions will likely also enable the community to unravel how nature precisely aligns INPs to be the most efficient ice nucleators known and illuminate how this strategy can be copied for new freezing products and technologies.

■ AUTHOR INFORMATION

Corresponding Authors

Max Lukas − *Max Planck Institute for Polymer Research, 55128 Mainz, Germany;* ● orcid.org/0000-0001-6949-8423; Email: lukas@mpip-mainz.mpg.de

Konrad Meister − *Max Planck Institute for Polymer Research, 55128 Mainz, Germany; University of Alaska Southeast, Juneau, Alaska 99801, United States;* ● orcid.org/0000-0002-6853-6325; Email: meisterk@mpip-mainz.mpg.de

Authors

Ralph Schwidetzky − *Max Planck Institute for Polymer Research, 55128 Mainz, Germany*

Rosemary J. Eufemio − *University of Alaska Southeast, Juneau, Alaska 99801, United States*

Mischa Bonn − *Max Planck Institute for Polymer Research, 55128 Mainz, Germany;* ● orcid.org/0000-0001-6851-8453

Complete contact information is available at:
https://pubs.acs.org/10.1021/acs.jpcb.1c09342

Notes

The authors declare no competing financial interest.

Biographies

Max Lukas obtained his B.S and M.S, in Applied Physics, from the RheinMain University of Applied Sciences, Germany in 2018. He is currently pursuing a Ph.D. degree at the MPI-P, Mainz, Germany, funded by the Max Planck Graduate Center with the Johannes Gutenberg University Mainz. His research interests are focused on the working mechanisms of bacterial ice nucleators and investigating protein−water interactions at the molecular level.

Ralph Schwidetzky obtained his B.S and M.S in Chemistry from the Johannes Gutenberg-University Mainz. He is currently pursuing a Ph.D. degree at the MPI-P, Mainz, Germany. His research interests are focused on the working mechanisms of antifreeze and ice-nucleating proteins.

Rosemary J. Eufemio obtained a B.S in Biology from the University of Alaska Southeast (UAS), Juneau, USA, in 2021. She currently works as a research technician in the Meister laboratory where she focuses on investigating biological ice nucleators from Alaskan ecosystems.

Mischa Bonn is a director at MPI-P, Mainz, Germany. He received his Ph.D. in 1996 from the University of Eindhoven, The Netherlands. After postdoctoral research at the Fritz Haber Institute and Columbia University, he worked at Leiden University. In 2004 he became a group leader at AMOLF, Amsterdam, The Netherlands, and in 2011 he joined the MPI-P. His research interests focus on the structure and dynamics of (water) molecules at diverse interfaces and electron transfer across interfaces.

Konrad Meister received his Ph.D. in physical chemistry from the Ruhr-University Bochum, Germany, in 2013. He did postdoctoral work at AMOLF in The Netherlands, funded by a Marie Curie postdoctoral fellowship. Since 2018 he has been a group leader at the MPI-P, Mainz, Germany, and since 2020 an Assistant Professor at the University of Alaska Southeast, Juneau, USA. His research aims to understand the molecular strategies of cold-adapted organisms and how one can use nature's tricks in applications.

■ ACKNOWLEDGMENTS

■ REFERENCES

(1) Fu, Q.; Liou, K. N. Parameterization of the Radiative Properties of Cirrus Clouds. *J. Atmos. Sci.* **1993**, *50* (13), 2008−2025.

(2) Ramanathan, V.; Cess, R. D.; Harrison, E. F.; Minnis, P.; Barkstrom, B. R.; Ahmad, E.; Hartmann, D. Cloud-Radiative Forcing and Climate: Results from the Earth Radiation Budget Experiment. *Science* **1989**, *243* (4887), 57−63.

(3) Koop, T.; Luo, B.; Tsias, A.; Peter, T. Water Activity as the Determinant for Homogeneous Ice Nucleation in Aqueous Solutions. *Nature* **2000**, *406* (6796), 611−614.

(4) Pruppacher, H. R.; Klett, J. D. *Microphysics of Clouds and Precipitation*, 2nd rev. and expanded ed. with an introduction to cloud chemistry and cloud electricity; Springer, 1997; p 1 Online-Ressource.

(5) Murray, B. J.; O'Sullivan, D.; Atkinson, J. D.; Webb, M. E. Ice Nucleation by Particles Immersed in Supercooled Cloud Droplets. *Chem. Soc. Rev.* **2012**, *41* (19), 6519−6554.

(6) Atkinson, J. D.; Murray, B. J.; Woodhouse, M. T.; Whale, T. F.; Baustian, K. J.; Carslaw, K. S.; Dobbie, S.; O'Sullivan, D.; Malkin, T. L. The Importance of Feldspar for Ice Nucleation by Mineral Dust in Mixed-Phase Clouds. *Nature* **2013**, *498*, 355.

(7) Hasegawa, Y.; Ishihara, Y.; Tokuyama, T. Characteristics of Ice-Nucleation Activity in Fusarium Avenaceum Ifo 7158. *Biosci., Biotechnol., Biochem.* **1994**, *58* (12), 2273−2274.

(8) Davies, P. L. Ice-Binding Proteins: A Remarkable Diversity of Structures for Stopping and Starting Ice Growth. *Trends Biochem. Sci.* **2014**, *39* (11), 548−555.

(9) Lindow, S. E.; Arny, D. C.; Upper, C. D. Bacterial Ice Nucleation: A Factor in Frost Injury to Plants. *Plant Physiol.* **1982**, *70*, 1084.

(10) Warren, G. J. Bacterial Ice Nucleation: Molecular Biology and Applications. *Biotechnol. Genet. Eng. Rev.* **1987**, *5* (1), 107−136.

(11) Margaritis, A.; Bassi, A. S. Principles and Biotechnological Applications of Bacterial Ice Nucleation. *Crit. Rev. Biotechnol.* **1991**, *11* (3), 277−295.

(12) Zwieg, T.; Cucarella, V.; Kauffeld, M. Novel Biomimetically Based Ice-Nucleating Coatings. *Int. J. Mater. Res.* **2007**, *98* (7), 597−602.

(13) Maki, L. R.; Galyan, E. L.; Chang-Chien, M. M.; Caldwell, D. R. Ice Nucleation Induced by Pseudomonas Syringae. *Appl. Microbiol.* **1974**, *28* (3), 456−459.

(14) Arny, D. C.; Lindow, S. E.; Upper, C. D. Frost Sensitivity of Zea Mays Increased by Application of Pseudomonas Syringae. *Nature* **1976**, *262* (5566), 282−284.

(15) Kim, H.; Orser, C.; Lindow, S.; Sands, D. Xanthomonas Campestris Pv. Translucens Strains Active in Ice Nucleation. *Plant Dis.* **1987**, *71* (11), 994−997.

(16) Lindow, S.; Arny, D.; Upper, C. Erwinia Herbicola: A Bacterial Ice Nucleus Active in Increasing Frost Injury to Corn. *Phytopathology* **1978**, *68* (3), 523−527.

(17) Failor, K. C.; Schmale, D. G.; Vinatzer, B. A.; Monteil, C. L. Ice Nucleation Active Bacteria in Precipitation Are Genetically Diverse and Nucleate Ice by Employing Different Mechanisms. *ISME J.* **2017**, *11* (12), 2740−2753.

(18) Morris, C. E.; Conen, F.; Alex Huffman, J.; Phillips, V.; Poschl, U.; Sands, D. C. Bioprecipitation: A Feedback Cycle Linking Earth History, Ecosystem Dynamics and Land Use through Biological Ice Nucleators in the Atmosphere. *Glob. Chang. Biol.* **2014**, *20* (2), 341−351.

(19) Liou, Y. C.; Tocilj, A.; Davies, P. L.; Jia, Z. Mimicry of Ice Structure by Surface Hydroxyls and Water of a Beta-Helix Antifreeze Protein. *Nature* **2000**, *406*, 322−324.

(20) Yang, Z.; Zhou, Y.; Liu, K.; Cheng, Y.; Liu, R.; Chen, G.; Jia, Z. Computational Study on the Function of Water within a B-Helix Antifreeze Protein Dimer and in the Process of Ice-Protein Binding. *Biophys. J.* **2003**, *85* (4), 2599−2605.

(21) Hakim, A.; Thakral, D.; Zhu, D. F.; Nguyen, J. B. Expression, Purification, Crystallization and Preliminary Crystallographic Studies of Rhagium Inquisitor Antifreeze Protein. *Acta Cryst. F* **2012**, *68*, 547−550.

(22) Kumaki, Y.; Kawano, K.; Hikichi, K.; Matsumoto, T.; Matsushima, N. A Circular Loop of the 16-Residue Repeating Unit in Ice Nucleation Protein. *Biochem. Biophys. Res. Commun.* **2008**, *371* (1), 5−9.

(23) Kajava, A. V.; Lindow, S. E. A Model of the Three-Dimensional Structure of Ice Nucleation Proteins. *J. Mol. Biol.* **1993**, *232* (3), 709−717.

(24) Graether, S. P.; Kuiper, M. J.; Gagné, S. M.; Walker, V. K.; Jia, Z.; Sykes, B. D.; Davies, P. L. Beta-Helix Structure and Ice-Binding Properties of a Hyperactive Antifreeze Protein from an Insect. *Nature* **2000**, *406*, 325−328.

(25) Wolber, P. K. Bacterial Ice Nucleation. In *Advances in Microbial Physiology*; Rose, A. H., Ed.; Academic Press, 1993; Vol. 34, pp 203−237.

(26) Orser, C.; Staskawicz, B. J.; Panopoulos, N. J.; Dahlbeck, D.; Lindow, S. E. Cloning and Expression of Bacterial Ice Nucleation Genes in Escherichia Coli. *J. Bacteriol.* **1985**, *164* (1), 359−366.

(27) Green, R. L.; Corotto, L. V.; Warren, G. J. Deletion Mutagenesis of the Ice Nucleation Gene from Pseudomonas Syringae S203. *Mol. Gen. Genet.* **1988**, *215* (1), 165−172.

(28) Green, R. L.; Warren, G. J. Physical and Functional Repetition in a Bacterial Ice Nucleation Gene. *Nature* **1985**, *317* (6038), 645−648.

(29) Hudait, A.; Odendahl, N.; Qiu, Y.; Paesani, F.; Molinero, V. Ice-Nucleating and Antifreeze Proteins Recognize Ice through a Diversity of Anchored Clathrate and Ice-Like Motifs. *J. Am. Chem. Soc.* **2018**, *140* (14), 4905−4912.

(30) Davies, P. L.; Sykes, B. D. Antifreeze Proteins. *Curr. Opin. Struct. Biol.* **1997**, *7* (6), 828−834.

(31) Graether, S. P.; Jia, Z. Modeling Pseudomonas Syringae Ice-Nucleation Protein as a Beta-Helical Protein. *Biophys. J.* **2001**, *80* (3), 1169−1173.

(32) Garnham, C. P.; Campbell, R. L.; Walker, V. K.; Davies, P. L. Novel Dimeric Beta-Helical Model of an Ice Nucleation Protein with Bridged Active Sites. *BMC Struct. Biol.* **2011**, *11*, 36.

(33) Turner, M. A.; Arellano, F.; Kozloff, L. M. Three Separate Classes of Bacterial Ice Nucleation Structures. *J. Bacteriol.* **1990**, *172* (5), 2521−2526.

(34) Yankofsky, S. A.; Levin, Z.; Bertold, T.; Sandlerman, N. Some Basic Characteristics of Bacterial Freezing Nuclei. *J. Appl. Meteorol. Climatol.* **1981**, *20* (9), 1013−1019.

(35) Govindarajan, A. G.; Lindow, S. E. Size of Bacterial Ice-Nucleation Sites Measured *in Situ* by Radiation Inactivation Analysis. *Proc. Natl. Acad. Sci. U.S.A.* **1988**, *85* (5), 1334−1338.

(36) Southworth, M. W.; Wolber, P. K.; Warren, G. J. Nonlinear Relationship between Concentration and Activity of a Bacterial Ice Nucleation Protein. *J. Biol. Chem.* **1988**, *263* (29), 15211−15216.

(37) Gsponer, J.; Babu, M. M. Cellular Strategies for Regulating Functional and Nonfunctional Protein Aggregation. *Cell Reports* **2012**, *2* (5), 1425−1437.

(38) Qiu, Y.; Hudait, A.; Molinero, V. How Size and Aggregation of Ice-Binding Proteins Control Their Ice Nucleation Efficiency. *J. Am. Chem. Soc.* **2019**, *141* (18), 7439−7452.

(39) Kozloff, L. M.; Schofield, M. A.; Lute, M. Ice Nucleating Activity of Pseudomonas Syringae and Erwinia Herbicola. *J. Bacteriol.* **1983**, *153* (1), 222−231.

(40) Kozloff, L. M.; Lute, M.; Westaway, D. Phosphatidylinositol as a Component of the Ice Nucleating Site of Pseudomonas Syringae and Erwinia Herbiola. *Science* **1984**, *226* (4676), 845−846.

(41) Kunert, A. T.; Lamneck, M.; Helleis, F.; Pöschl, U.; Pohlker, M. L.; Fröhlich-Nowoisky, J. Twin-Plate Ice Nucleation Assay (Tina) with Infrared Detection for High-Throughput Droplet Freezing Experiments with Biological Ice Nuclei in Laboratory and Field Samples. *Atmos. Meas. Technol.* **2018**, *11* (11), 6327−6337.

(42) Lukas, M.; Schwidetzky, R.; Kunert, A. T.; Pöschl, U.; Fröhlich-Nowoisky, J.; Bonn, M.; Meister, K. Electrostatic Interactions Control the Functionality of Bacterial Ice Nucleators. *J. Am. Chem. Soc.* **2020**, *142* (15), 6842−6846.

(43) Pandey, R.; Usui, K.; Livingstone, R. A.; Fischer, S. A.; Pfaendtner, J.; Backus, E. H. G.; Nagata, Y.; Fröhlich-Nowoisky, J.; Schmüser, L.; Mauri, S.; et al. Ice-Nucleating Bacteria Control the Order and Dynamics of Interfacial Water. *Sci. Adv.* **2016**, *2* (4), No. e1501630.

(44) Lukas, M.; Schwidetzky, R.; Kunert, A. T.; Backus, E. H. G.; Pöschl, U.; Fröhlich-Nowoisky, J.; Bonn, M.; Meister, K. Interfacial Water Ordering Is Insufficient to Explain Ice-Nucleating Protein Activity. *J. Phys. Chem. Lett.* **2021**, *12*, 218−223.

(45) Roeters, S. J.; Golbek, T. W.; Bregnhøj, M.; Drace, T.; Alamdari, S.; Roseboom, W.; Kramer, G.; Šantl-Temkiv, T.; Finster, K.; Woutersen, S.; et al. The Ice Nucleating Protein Inaz Is Activated by Low Temperature. *bioRxiv* **2020**, DOI: 10.1101/2020.05.15.092684.

146

(46) Schwidetzky, R.; Lukas, M.; YazdanYar, A.; Kunert, A. T.; Pöschl, U.; Domke, K. F.; Fröhlich-Nowoisky, J.; Bonn, M.; Koop, T.; Nagata, Y.; et al. Specific Ion-Protein Interactions Influence Bacterial Ice Nucleation. *Chem.—Eur. J.* **2021**, *27* (26), 7402−7407.

(47) Adar, C.; Sirotinskaya, V.; Bar Dolev, M.; Friehmann, T.; Braslavsky, I. Falling Water Ice Affinity Purification of Ice-Binding Proteins. *Sci. Rep.* **2018**, *8* (1), 11046.

(48) Marshall, C. J.; Basu, K.; Davies, P. L. Ice-Shell Purification of Ice-Binding Proteins. *Cryobiology* **2016**, *72* (3), 258−263.

(49) Tomalty, H. E.; Graham, L. A.; Eves, R.; Gruneberg, A. K.; Davies, P. L. Laboratory-Scale Isolation of Insect Antifreeze Protein for Cryobiology. *Biomolecules* **2019**, *9* (5), 180.

(50) Vali, G. Quantitative Evaluation of Experimental Results an the Heterogeneous Freezing Nucleation of Supercooled Liquids. *Int. J. Atmos. Sci.* **1971**, *28* (3), 402−409.

(51) Budke, C.; Koop, T. Binary: An Optical Freezing Array for Assessing Temperature and Time Dependence of Heterogeneous Ice Nucleation. *Atmos. Meas. Technol.* **2015**, *8* (2), 689−703.

(52) Schwidetzky, R.; Sudera, P.; Backes, A. T.; Pöschl, U.; Bonn, M.; Fröhlich-Nowoisky, J.; Meister, K. Membranes Are Decisive for Maximum Freezing Efficiency of Bacterial Ice Nucleators. *J. Phys. Chem. Lett.* **2021**, *12*, 10783−10787.

(53) Devineau, S.; Inoue, K.-i.; Kusaka, R.; Urashima, S.-H.; Nihonyanagi, S.; Baigl, D.; Tsuneshige, A.; Tahara, T. Change of the Isoelectric Point of Hemoglobin at the Air/Water Interface Probed by the Orientational Flip-Flop of Water Molecules. *Phys. Chem. Chem. Phys.* **2017**, *19* (16), 10292−10300.
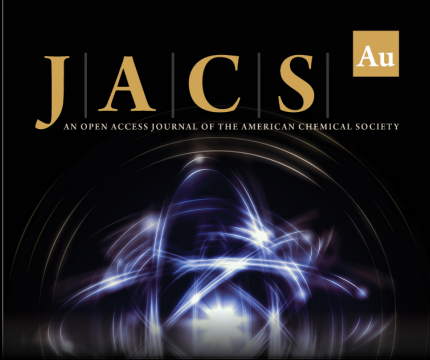
(54) Engelhardt, K.; Peukert, W.; Braunschweig, B. Vibrational Sum-Frequency Generation at Protein Modified Air-Water Interfaces: Effects of Molecular Structure and Surface Charging. *Curr. Opin. Colloid Interface Sci.* **2014**, *19* (3), 207−215.

(55) Strazdaite, S.; Meister, K.; Bakker, H. J. Orientation of Polar Molecules near Charged Protein Interfaces. *Phys. Chem. Chem. Phys.* **2016**, *18* (10), 7414−7418.

(56) Guckeisen, T.; Hosseinpour, S.; Peukert, W. Isoelectric Points of Proteins at the Air/Liquid Interface and in Solution. *Langmuir* **2019**, *35* (14), 5004−5012.

(57) Schwidetzky, R.; Kunert, A. T.; Bonn, M.; Pöschl, U.; Ramløv, H.; DeVries, A. L.; Fröhlich-Nowoisky, J.; Meister, K. Inhibition of Bacterial Ice Nucleators Is Not an Intrinsic Property of Antifreeze Proteins. *J. Phys. Chem. B* **2020**, *124* (24), 4889−4895.

(58) Schwidetzky, R.; Sudera, P.; Backes, A. T.; Pöschl, U.; Bonn, M.; Fröhlich-Nowoisky, J.; Meister, K. Membranes Are Decisive for Maximum Freezing Efficiency of Bacterial Ice Nucleators. *J. Phys. Chem. Lett.* **2021**, *12* (44), 10783−10787.

B In preparation

B.1 Schwidetzky *et al.*, in preparation, 2022

Drastic Enhancement of Bacterial Ice Nucleation Efficiency By Polyols

R. Schwidetzky[1], J. Liu[1], U. Pöschl[2], J. Fröhlich-Nowoisky[2], M. Bonn[1], and K. Meister[1,3]

[1] Max-Planck-Institute for Polymer Research, 55128 Mainz, Germany

[2] Max-Planck-Institute for Chemistry, 55128 Mainz, Germany

[3] University of Alaska Southeast, Juneau, Alaska 99801, United States

Author contributions:

R.S. performed the freezing experiments and contributed to analyzing and discussing the results as well as writing the manuscript.

Drastic Enhancement of Bacterial Ice Nucleation Efficiency By Polyols

Authors: R. Schwidetzky[1], J. Liu[1], U. Pöschl[2], J. Fröhlich-Nowoisky[2], M. Bonn[1], and K. Meister[1,3]

Affiliations:

[1]Max Planck Institute for Polymer Research, 55128 Mainz, Germany

[2]Max Planck Institute for Chemistry, Multiphase Chemistry Department, 55128 Mainz, Germany

[3]University of Alaska Southeast, 99801 Juneau, AK, United States

Abstract:

Numerous materials can act as heterogeneous ice nucleating agents, but not all are equally effective. The best-known ice nucleators are ice-nucleating proteins (INPs) expressed by epiphytic bacteria like *Pseudomonas syringae*. Small INP aggregates can induce ice nucleation around −7.5 ℃, while larger INP aggregates nucleate ice around −2 ℃. The mechanism for large aggregate formation is unknown, and the fraction of large INP aggregates in *P. syringae* is typically less than 1%. Here we report that polyols promote the assembly of INPs into large aggregates, with simple compounds like polyvinyl alcohol increasing the ice nucleation efficiency, i.e., the abundance of large INP aggregates by a factor of 100. We explain this observation with increased stability of INP aggregates owing to membrane-polyol interactions and a viscous adlayer on the membrane surface. Our results indicate that the abundance of large INP aggregates in bacterial ice nucleators can be regulated, enabling their usage in tunable freezing applications for biomedical and technological purposes.

The formation of ice from water is thermodynamically favored at temperatures below 0 ˚C, but this crystallization process is kinetically hindered. As a result, pure water can be supercooled to temperatures as low as −38 °C, below which homogenous ice nucleation occurs[1]. Ice nucleation at higher temperatures requires the presence of heterogeneous ice nucleators (INs). INs are ubiquitous in the environment and can be of abiotic and biological origin[2-3]. Among the best INs are plant-associated bacteria like *Pseudomonas syringae* or *Erwinia herbicola[4]*. As epiphytes, the bacteria are a primary cause of frost damage in plants[5]. The ice-nucleating bacteria have further been identified in atmospheric and precipitation samples, suggesting that they might be involved in cloud glaciation[3, 6]. A long-standing observation in the analysis of bacterial INs has been that the ice-nucleating active bacteria always display a spectrum of nucleation events with threshold temperatures ranging from −2 to −10 °C, and with only one ice nucleator per 1 million cells being active at −2 °C[7]. Based on their activity, the bacterial INs are usually classified in classes A to C, with threshold ice nucleation temperatures of −4.4 °C or warmer (class A), −4.8 to −5.7 °C (class B), and −7.6 °C and colder (class C)[8]. The ability of the bacteria to catalyze ice formation is attributed to specialized ice nucleation proteins (INPs) anchored to their outer cell membrane[9]. Pioneering studies have revealed that the differences in the freezing temperatures are caused by INP assemblies of different sizes and that class A INs consist of the largest INP aggregates[10-11]. These findings are consistent with classical nucleation theory that predicts that larger nucleation sites support higher threshold temperatures for ice nucleation[12]. Recent simulations have addressed the role of size and aggregation of the INPs on the freezing temperature and provided a first quantitative prediction of the ice nucleation temperature *vs.* the number of INPs in the aggregates[13]. The predominant class C INs were attributed to small aggregates of INPs (~5-10 INPs), whereas the most active class A INs consist of larger aggregates of the INPs (>30 INPs)[13]. The class A INs

have further been shown to require an intact bacterial cell membrane[14-15], and several studies have shown that changing environmental conditions (e.g. pH, salts, temperature, cosolutes) mostly affect class A[16-18]. Interestingly, improved ice nucleation efficiency of bacterial INs was recently observed in deuterated water, suggesting that the degree of INP aggregation can be manipulated by INP aggregate stabilization[14].

Polyols have previously been demonstrated to be able to affect the physical properties of lipid layers and to stabilize proteins and protein-lipid interactions to control the degree of assembly and packing for specific applications[19-21]. Targeted INP assembly through polyols would hence provide a unique way of controlling bacterial ice nucleation. Here, we explore common water-soluble polyols like glycerol, sorbitol, ethylene glycol (EG), and polyvinyl alcohol (PVA) as tailoring agents for bacterial ice nucleation. We find that the addition of polyols can drastically enhance IN-activity, enabling their usage in tunable freezing applications.
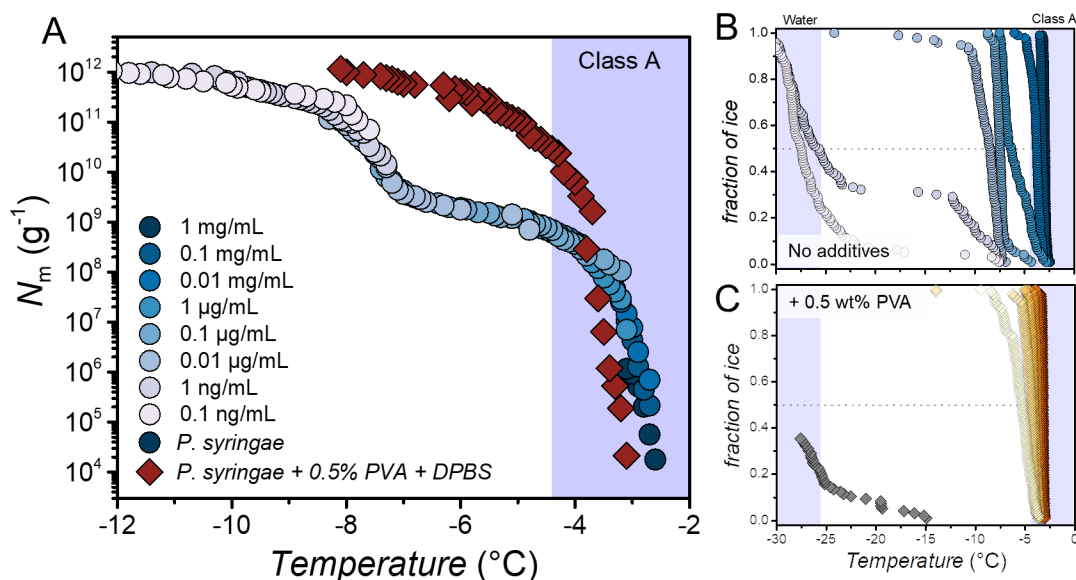
Figure 1: Freezing experiments with aqueous solutions of *P. syringae* in water and in the presence of 0.5 wt% polyvinyl alcohol in DPBS buffer. (A) Cumulative number of ice nucleators per unit mass of sample (N_m) plotted against temperature. (B) Fraction of frozen droplets (f_{ice}) for different *P. syringae* dilutions. Symbol colors indicate data from droplets with different concentrations and are identical to the plots shown in A. (C) Fraction of frozen droplets for different *P. syringae* dilutions in the presence of 0.5 wt% polyvinyl alcohol. Symbol colors represent different concentrations and are identical to concentrations used in (B). The dark grey data points represent a 0.5 wt% polyvinyl alcohol control sample in DPBS buffer. The blue-shaded regions represent the temperature ranges for class A ice nucleators (> -4.4 °C) and when pure water freezes in our system (< -25°C), respectively.

Figure 1A shows the results of freezing experiments of a dilution series of inactivated bacteria cells of *P. syringae* (Snomax®) in water and a 0.1 M Dulbecco's phosphate-buffered saline (DPBS) solution containing 0.5 wt% PVA. The *P. syringae* solutions had a concentration of 1 mg/mL and were serially diluted, resulting in concentrations spanning from 1 mg/mL to 0.1 ng/mL, at constant DPBS and PVA concentration. The cumulative IN number concentration (N_m) was calculated using Vali's formula and represents the number of active INs per unit weight above a certain temperature[22]. The freezing spectra of the bacterial INs in water show two increases in the

cumulative number of INs per unit mass of bacteria, $N_m(T)$, at −2.9 °C and −7.5 °C with plateaus between −4.5 °C and −7 °C and below −9.5 °C. The two increases show that the IN-activity of *P. syringae* is due to two classes of INs with different activation temperatures. The plateaus arise when fewer INs at these temperatures are present. We assign the two classes of INs to class A and C, respectively. Class C INs are small assemblies of INPs, and class A INs originate from larger INP aggregates. Class B INs were not observed in our experiments, consistent with previous works[17, 23-25].

In the presence of 0.5 wt% PVA, the freezing spectrum looks markedly different. The rise at ∼−7.5 °C is absent; instead, we observe a single rise centered at −3.1 °C. Apparently, adding PVA to the solution dramatically promotes the formation of the more efficient class A INs. The overall number of INs remained constant, implying that the presence of PVA in DPBS transformed existing INs into highly efficient class A INs. The small shift in the initial temperature of class A INs from −2.9 °C to −3.1 °C is due to the colligative freezing point depression.

Note that PVA or other polyols do not show ice nucleation activity by themselves (**Figure S1**).

The presence of only class A INs upon adding PVA becomes apparent when comparing the droplet freezing statistics of the different solutions, as shown in Figure 1B. For *P. syringae* in water, the two main IN classes active at ∼−2.9 °C and ∼−7.5 °C are apparent, as well as a third rise at ∼−25 °C. The third rise at ∼−25 °C corresponds to the freezing point of pure water in our system. We observe that the maximal IN-activity caused by class A INs ($T > −4.4$ °C) for aqueous *P. syringae* solutions only occurred at very high concentrations (1 to 0.01 mg/mL). For the PVA-containing samples, we find that maximum IN-activity prevails to concentrations as low as 0.01 µg/mL, drastically improving the efficiency of *P. syringae*. We define the bacterial efficiency as the lowest concentration at which class A ice nucleation activity at temperatures above − 4.4 °C

prevails. By this definition, the presence of PVA increases the bacterial ice nucleation efficiency by at least 100-fold.

Next, we explored whether the PVA enhancement effect is the result of direct polyol-protein interactions, or due to the facilitation of INP assembly through the stabilization of the membrane. To this end, we compare the IN activity of PVA/*P. syringae* mixtures with PVA/purified INP mixtures in DPBS buffer. The first mixture still contains the membrane, whereas lipids and other macromolecules are largely removed from the second mixture. The INPs of *P. syringae* were purified using a combination of Folch extraction (FE) and ice affinity purification (IAP)[14]. FE separates lipid and protein components by partitioning lipids in a biphasic mixture of chloroform and methanol. IAP uses the ability of INPs to bind to ice, and the purification process involves the incorporation of INPs into the growing ice phase while excluding impurities. Figure 2 shows the freezing spectra of *P. syringae*, purified INPs, and purified INPs in the presence of PVA and PVA in DPBS buffer. For the purified INPs, we observe an increase at ~-7.5 °C, and for the purified INPs in the presence of PVA, we find an increase at ~-8.5 °C. We also find that for both purified INP samples, the increase at ~-2.9 °C is missing and that the total number of INPs is reduced. Clearly, the addition of PVA to the purified INPs did not result in an enhancement of activity as observed for the bacteria, highlighting the importance of the membrane for class A formation and maximum ice nucleation activity and suggesting that PVA stabilizes the INP-membrane system[14, 26].
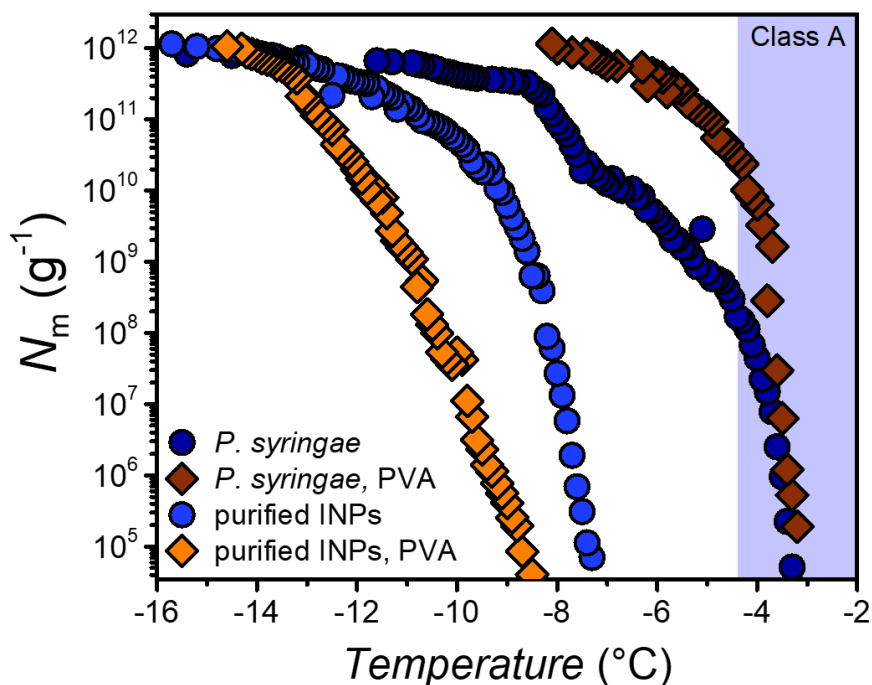
Figure 2: Freezing experiments with aqueous solutions of *P. syringae* (dark blue) and purified INPs (blue) and in the presence of 0.5 wt% PVA (brown, orange), all in DPBS buffer. The cumulative number of ice nucleators per unit mass of sample (N_m) is plotted against temperature. The temperature range for class A ice nucleators is shaded in blue.

Next, we evaluated different polyols to investigate whether the enhancement of bacterial INs is common or specific to PVA. Figure 3 shows T_{50}-values of droplet freezing measurements for buffered solutions of *P. syringae* in the presence of different polyols, at 0.5 to 1 wt% concentration. The T_{50}-value is defined as the temperature at which 50 % of the droplets are frozen, and the corresponding data is reported in the supporting information (**Figure S2**)

We find that for the highest *P. syringae* concentrations, the T_{50}-values of *P. syringae* in buffer and in the presence of polyols are similar, which is expected since *P. syringae* shows the highest IN activity at these concentrations. At lower *P. syringae* concentrations, we observe that all of the investigated polyols increase the T_{50}-values. At the lowest concentrations, the polyols have little

effect, presumably because the concentration of INPs is too low for the polyols to induce aggregation. Our findings of improved efficiency of bacterial ice nucleation in the presence of polyols disagree with previous reports that showed that polyglycerol polymers and PVA inhibit bacterial INactivity[27]. This discrepancy can be explained by the different experimental conditions. All our measurements were performed in DPBS-buffered solutions since changes in the solution pH are known to inhibit bacterial ice nucleation activity[16]. In fact, we find that the addition of PVA alters the solution pH and that bacterial INs in the presence of aqueous PVA solutions show reduced activities (**Figure S3**).
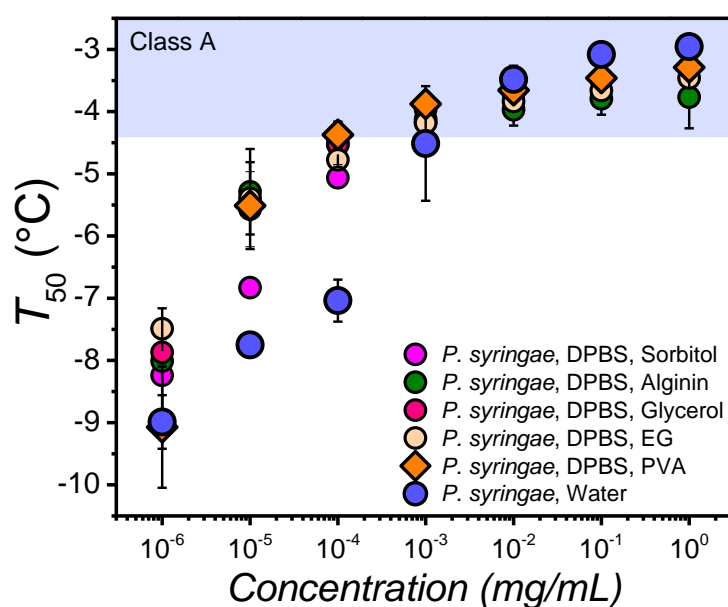

Figure 3: Freezing experiments with aqueous solutions of *P. syringae* in the presence of 1 wt% sorbitol (pink), glycerol (red), ethylene glycol (EG, beige), and in the presence of 0.5 wt% PVA (orange) and alginin (green), all in DPBS buffer. Shown are the T_{50} values as a function of *P. syringae* concentration. T_{50} values are defined as the point at which 50 % of droplets are frozen ($f_{ice} = 0.5$) in our experiments. Error bars represent the standard deviation of 2–5 independent measurements. The temperature range for class A ice nucleators is shaded.

Polyols are known to stabilize liposomes and have been suggested to affect cell membrane properties[28]. Here we show that PVA, EG, glycerol and other polyols affect the formation of INP aggregates within the bacterial membrane, increasing bacterial ice nucleation efficiency at least 100-fold. The addition of polyols to the bacteria further eliminated the known instability and inherent fluctuations in freezing temperatures[18]. We propose that the polyols form a protective adlayer on the membrane surface that reduces structural fluctuations and stabilizes intramolecular INP interactions[26, 28]. The molecular details of the stabilization mechanism remain unknown but could involve changes in the viscoelastic properties of the membrane or perturbations of the lipid organization and local curvatures. This hypothesis would agree with experimental observations that class A INs are not expressed well in fluid membrane lipids[15]. The ability of polyols to control the degree of bacterial INP aggregation is extraordinary. It paves the way to use bacterial INs in tunable freezing applications for biomedical and technological applications at much reduced concentrations.

Associated Content

Experimental setups, experimental methods, Supporting Figures S1-S3

Corresponding Author

meisterk@mpip-mainz.mpg.de

Notes

The authors declare no competing financial interests.

References

1. Koop, T.; Luo, B.; Tsias, A.; Peter, T., Water activity as the determinant for homogeneous ice nucleation in aqueous solutions. *Nature* **2000,** *406* (6796), 611-614.
2. Pummer, B. G.; Budke, C.; Augustin-Bauditz, S.; Niedermeier, D.; Felgitsch, L.; Kampf, C. J.; Huber, R. G.; Liedl, K. R.; Loerting, T.; Moschen, T.; Schauperl, M.; Tollinger, M.; Morris, C. E.; Wex, H.; Grothe, H.; Pöschl, U.; Koop, T.; Fröhlich-Nowoisky, J., Ice nucleation by water-soluble macromolecules. *Atmos. Chem. Phys.* **2015,** *15* (8), 4077-4091.

3.   Murray, B. J.; O'Sullivan, D.; Atkinson, J. D.; Webb, M. E., Ice nucleation by particles immersed in supercooled cloud droplets. *Chemical Society Reviews* **2012,** *41* (19), 6519-6554.

4.   Wolber, P.; Warren, G., Bacterial ice-nucleation proteins. *Trends in Biochemical Sciences* **1989,** *14* (5), 179-182.

5.   Lindow, S. E.; Arny, D. C.; Upper, C. D., Bacterial Ice Nucleation: A Factor in Frost Injury to Plants *Plant Physiology* **1982,** *70* (4), 1084-1089.

6.   Morris, C. E.; Conen, F.; Alex Huffman, J.; Phillips, V.; Pöschl, U.; Sands, D. C., Bioprecipitation: a feedback cycle linking earth history, ecosystem dynamics and land use through biological ice nucleators in the atmosphere. *Glob Chang Biol* **2014,** *20* (2), 341-51.

7.   Ruggles, J. A.; Nemecek-Marshall, M.; Fall, R., Kinetics of appearance and disappearance of classes of bacterial ice nuclei support an aggregation model for ice nucleus assembly. *Journal of bacteriology* **1993,** *175* (22), 7216-7221.

8.   Turner, M. A.; Arellano, F.; Kozloff, L. M., Three separate classes of bacterial ice nucleation structures. *Journal of bacteriology* **1990,** *172* (5), 2521-2526.

9.   Wolber, P. K.; Deininger, C. A.; Southworth, M. W.; Vandekerckhove, J.; van Montagu, M.; Warren, G. J., Identification and purification of a bacterial ice-nucleation protein. *Proc Natl Acad Sci U S A* **1986,** *83* (19), 7256-60.

10.   Govindarajan, A. G.; Lindow, S. E., Size of bacterial ice-nucleation sites measured in situ by radiation inactivation analysis. *Proceedings of the National Academy of Sciences* **1988,** *85* (5), 1334-1338.

11.   Southworth, M. W.; Wolber, P. K.; Warren, G. J., Nonlinear relationship between concentration and activity of a bacterial ice nucleation protein. *J Biol Chem* **1988,** *263* (29), 15211-6.

12.   Fletcher, N. H., Size Effect in Heterogeneous Nucleation. *The Journal of Chemical Physics* **1958,** *29* (3), 572-576.

13.   Qiu, Y.; Hudait, A.; Molinero, V., How Size and Aggregation of Ice-Binding Proteins Control Their Ice Nucleation Efficiency. *Journal of the American Chemical Society* **2019,** *141* (18), 7439-7452.

14.   Schwidetzky, R.; Sudera, P.; Backes, A. T.; Pöschl, U.; Bonn, M.; Fröhlich-Nowoisky, J.; Meister, K., Membranes Are Decisive for Maximum Freezing Efficiency of Bacterial Ice Nucleators. *The Journal of Physical Chemistry Letters* **2021**, 10783-10787.

15.   Govindarajan, A. G.; Lindow, S. E., Phospholipid requirement for expression of ice nuclei in Pseudomonas syringae and in vitro. *J Biol Chem* **1988,** *263* (19), 9333-8.

16.   Lukas, M.; Schwidetzky, R.; Kunert, A. T.; Pöschl, U.; Fröhlich-Nowoisky, J.; Bonn, M.; Meister, K., Electrostatic Interactions Control the Functionality of Bacterial Ice Nucleators. *Journal of the American Chemical Society* **2020,** *142* (15), 6842-6846.

17.   Schwidetzky, R.; Lukas, M.; YazdanYar, A.; Kunert, A. T.; Pöschl, U.; Domke, K. F.; Fröhlich-Nowoisky, J.; Bonn, M.; Koop, T.; Nagata, Y.; Meister, K., Specific Ion–Protein Interactions Influence Bacterial Ice Nucleation. *Chemistry – A European Journal* **2021,** *27* (26), 7402-7407.

18.   Polen, M.; Lawlis, E.; Sullivan, R. C., The unstable ice nucleation properties of Snomax® bacterial particles. *Journal of Geophysical Research: Atmospheres* **2016,** *121* (19), 11,666-11,678.

19.   Mishra, R.; Seckler, R.; Bhat, R., Efficient Refolding of Aggregation-prone Citrate Synthase by Polyol Osmolytes: HOW WELL ARE PROTEIN FOLDING AND STABILITY ASPECTS COUPLED? *. *Journal of Biological Chemistry* **2005,** *280* (16), 15553-15560.

20.   Budziak, I.; Arczewska, M.; Sachadyn-Król, M.; Matwijczuk, A.; Waśko, A.; Gagoś, M.; Terpiłowski, K.; Kamiński, D. M., Effect of polyols on the DMPC lipid monolayers and bilayers. *Biochimica et Biophysica Acta (BBA) - Biomembranes* **2018,** *1860* (11), 2166-2174.

21.   Hincha, D. K.; Hagemann, M., Stabilization of model membranes during drying by compatible solutes involved in the stress tolerance of plants and microorganisms. *Biochem J* **2004,** *383* (Pt 2), 277-283.

22.	Vali, G., Quantitative Evaluation of Experimental Results an the Heterogeneous Freezing Nucleation of Supercooled Liquids. *Journal of Atmospheric Sciences* **1971,** *28* (3), 402-409.

23.	Budke, C.; Koop, T., BINARY: an optical freezing array for assessing temperature and time dependence of heterogeneous ice nucleation. *Atmos. Meas. Tech.* **2015,** *8* (2), 689-703.

24.	Schwidetzky, R.; Kunert, A. T.; Bonn, M.; Pöschl, U.; Ramløv, H.; DeVries, A. L.; Fröhlich-Nowoisky, J.; Meister, K., Inhibition of Bacterial Ice Nucleators Is Not an Intrinsic Property of Antifreeze Proteins. *The Journal of Physical Chemistry B* **2020,** *124* (24), 4889-4895.

25.	Kunert, A. T.; Lamneck, M.; Helleis, F.; Pöschl, U.; Pöhlker, M. L.; Fröhlich-Nowoisky, J., Twin-plate Ice Nucleation Assay (TINA) with infrared detection for high-throughput droplet freezing experiments with biological ice nuclei in laboratory and field samples. *Atmos. Meas. Tech.* **2018,** *11* (11), 6327-6337.

26.	Mu, X.; Zhong, Z., Preparation and properties of poly(vinyl alcohol)-stabilized liposomes. *Int J Pharm* **2006,** *318* (1-2), 55-61.

27.	Wowk, B.; Fahy, G. M., Inhibition of bacterial ice nucleation by polyglycerol polymers. *Cryobiology* **2002,** *44* (1), 14-23.

28.	Pocivavsek, L.; Gavrilov, K.; Cao, K. D.; Chi, E. Y.; Li, D.; Lin, B.; Meron, M.; Majewski, J.; Lee, K. Y. C., Glycerol-induced membrane stiffening: the role of viscous fluid adlayers. *Biophysical journal* **2011,** *101* (1), 118-127.

Supporting Information:

Drastic Enhancement of Bacterial Ice Nucleation Efficiency By Polyols

Authors: R. Schwidetzky[1], J. Liu[1], U. Pöschl[2], J. Fröhlich-Nowoisky[2], M. Bonn[1], and K. Meister[1,3]

Affiliations:

[1]Max Planck Institute for Polymer Research, 55128 Mainz, Germany

[2]Max Planck Institute for Chemistry, Multiphase Chemistry Department, 55128 Mainz, Germany

[3]University of Alaska Southeast, 99801 Juneau, AK, United States

Materials & Methods:

Materials. Pure water was obtained from Millipore Milli-Q® Integral 3 water purification system (Merck Chemicals GmbH, Darmstadt, Germany), autoclaved at 121 °C for 15 min, and filtered through a 0.1 µm bottle top filtration unit (VWR International GmbH, Darmstadt, Germany). Polyols were obtained from Alfa Aesar (PVA, (98-99% hydrolysed, low MW), Alginic acid sodium salt (low viscosity)). Snomax® was purchased from SMI Snow Makers AG (Thun, Switzerland) and consists of a preparation of inactivated bacteria cells of *P. syringae*.

TINA Experiments. Ice nucleation experiments were performed using the high-throughput Twin-plate Ice Nucleation Assay (TINA), which has been described in detail elsewhere[1]. In a typical experiment, a sample with a concentration of 1 mg/mL IN in a water/buffer-polyol mixture was prepared. This sample was serially diluted 10-fold by a liquid handling station (epMotion ep5073, Eppendorf, Hamburg, Germany). 96 droplets (3 µL) per dilution were placed on two 384-well plates and tested with a continuous cooling-rate of 1 °C/min from 0 °C to −30 °C with a temperature uncertainty of ±0.2 °C. The droplet-freezing was determined by two infrared cameras (Seek Therman Compact XR, Seek Thermal Inc., Santa Barbara, CA, USA). The obtained fraction of frozen droplets was used to calculate the cumulative number of ice nucleators using the Vali formula[2]. Experiments were performed multiple times with independent samples. Background freezing of pure water occurred at ∼−25 ±2 °C.
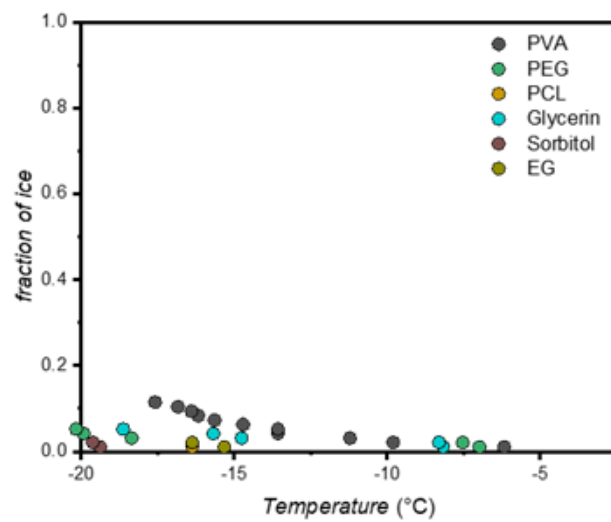
Figure S1: Freezing experiments with aqueous polyol solutions in DPBS buffer. Shown is the fraction of ice for different 1 wt% polyol solutions in DPBS buffer.
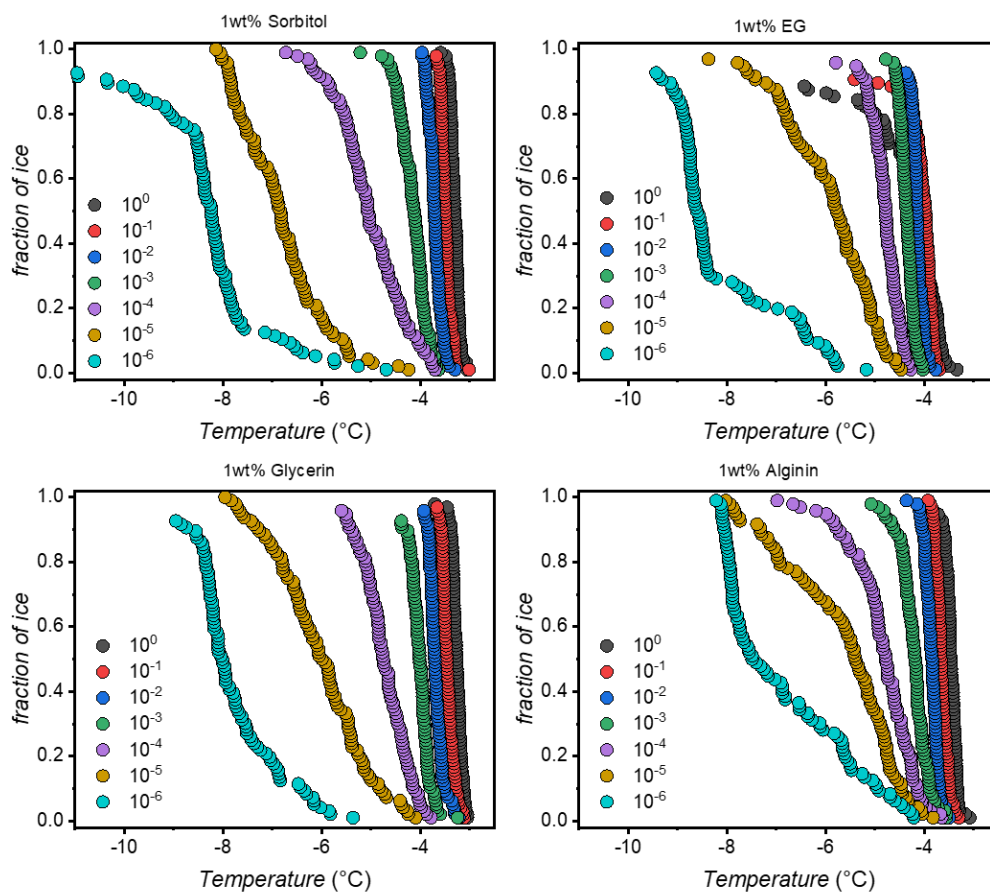
Figure S2: Freezing experiments with aqueous polyol solutions in DPBS buffer. Shown are the fraction of ice for different 1 wt% polyol solutions in DPBS buffer. Symbol colors represent different concentrations.
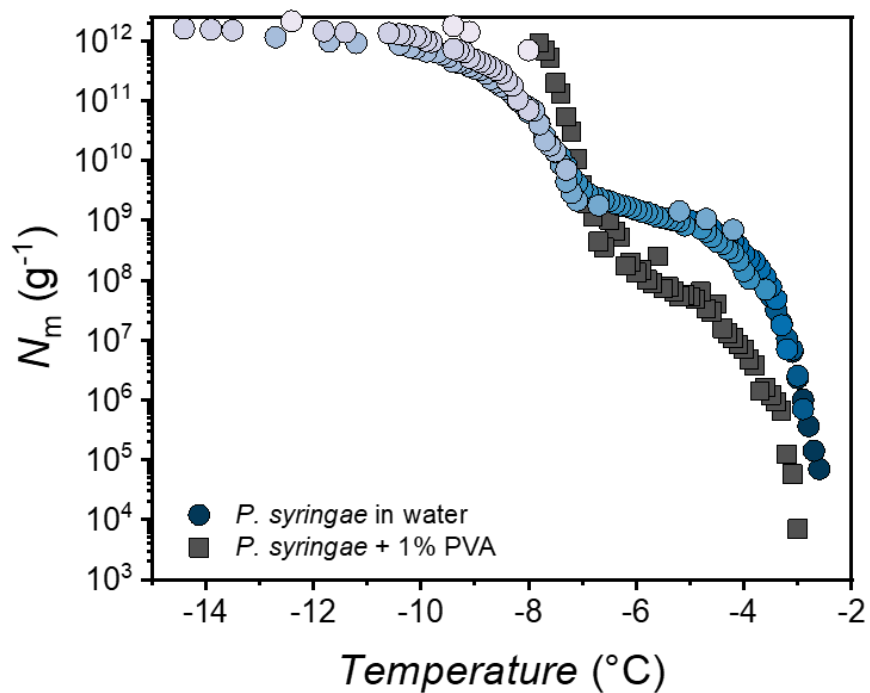
Figure S3: Freezing experiments with aqueous solutions of *P. syringae* in water and the presence of 1 wt% PVA. Shown is the cumulative number of ice nucleators per unit mass of sample (N_m) plotted against temperature.

References:

1.   Kunert, A. T.; Lamneck, M.; Helleis, F.; Pöschl, U.; Pöhlker, M. L.; Fröhlich-Nowoisky, J., Twin-plate Ice Nucleation Assay (TINA) with infrared detection for high-throughput droplet freezing experiments with biological ice nuclei in laboratory and field samples. *Atmos. Meas. Tech.* **2018,** *11* (11), 6327-6337.
2.   Vali, G., Quantitative Evaluation of Experimental Results an the Heterogeneous Freezing Nucleation of Supercooled Liquids. *Journal of Atmospheric Sciences* **1971,** *28* (3), 402-409.

B.2 Schwidetzky *et al.*, in preparation, 2022

Protein Aggregates Enable Fungal Ice Nucleation

R. Schwidetzky[1], Y. Sun[1], A. T. Backes[2], A. L. DeVries[3], M. Bonn[1], J. Fröhlich-Nowoisky[2], and K. Meister[1,4]

[1] Max-Planck-Institute for Polymer Research, 55128 Mainz, Germany

[2] Max-Planck-Institute for Chemistry, 55128 Mainz, Germany

[3] University of Illinois at Urbana– Champaign, Urbana, Illinois 61801, United States

[4] University of Alaska Southeast, Juneau, Alaska 99801, United States

Author contributions:

R.S. performed the freezing experiments and contributed to analyzing and discussing the results as well as writing the manuscript.

1   **Title: Protein Aggregates Enable Fungal Ice Nucleation**

2

3   **Authors:** R. Schwidetzky[1], Y. Sun[1], N. Bothen[2], A. T. Backes[2], U. Pöschl[2], A. L. DeVries[3],

4   M. Bonn[1], J. Fröhlich-Nowoisky[2], and K. Meister[1,4]

5   **Affiliations:**

6   [1]Max Planck Institute for Polymer Research, 55128 Mainz, Germany

7   [2]Max Planck Institute for Chemistry, 55128 Mainz, Germany

8   [3]University of Illinois at Urbana-Champaign, 61801 Urbana, IL, United States

9   [4]University of Alaska Southeast, 99801 Juneau, AK, United States

10

11

12   **Classification:**

13   Ice-Nucleating Proteins, Heterogeneous Ice Nucleation, Ice-Binding Proteins, Protein

14   Assembly,

15   **Abstract:**

16   Large numbers of biological aerosol particles are emitted into the atmosphere and can act as

17   potential nuclei for ice formation and cloud glaciation. While biological ice nucleation has been

18   known for decades, many details underlying the molecular composition and working

19   mechanism of such ice nucleators (INs) have remained elusive. Here, we report that INs derived

20   from fungi consist of small protein subunits that assemble into larger ice-nucleating protein

21   complexes. The protein subunits exhibit ice shaping activity typical of ice-binding proteins

22   (IBPs), supporing a possible link between ice growth promotion and inhibition. We propose

23   that making biological INs by utilizing smaller protein building blocks is a common strategy

24   among organisms and that copying nature's assembly strategy may enable tuneable freezing

25   technologies.

26

Introduction:

Ice formation is the most prevalent liquid-to-solid phase transition on earth and is crucial for fields as diverse as cryobiology, geology, and climate science. Under ambient conditions, ice formation is thermodynamically favored at temperatures below 0 ˚C, but the crystallization process is kinetically hindered. As a result, pure water can be supercooled to temperatures as low as -38 °C, below which homogenous ice nucleation occurs[1]. In natural systems, the freezing of water is usually a heterogeneous process facilitated by ice nucleators (INs) of biological and abiotic origins. Ice-nucleation active fungi produce some of the most effective and widespread biological INs, enabling the crystallization of water at temperatures close to 0 °C[2-3]. These fungi can cause frost damage to plants and are found in ice, hail, and snow, suggesting that they may influence regional and global precipitation patterns[4-7]. Fungal ice nucleation was first discovered in the genus *Fusarium* and later also in multiple other genera (e.g., *Isaria, Mortierella, Sarocladium, Puccinia*) [8-10]. The cosmopolitan genus *Fusarium* comprises saprophytes and pathogens of plants and animals, and it is the most studied ice-nucleation-active fungus[2-3]. Although widely distributed in soil and on plants, it has also been detected in atmospheric and cloud water samples, making it an important biological and atmospherical model system[9, 11]. The biomolecules responsible for ice nucleation in fungi remain unknown, but the available information for *Fusarium* suggests that they are large, cell-free, and at least partially proteinaceous[3, 12]. Besides ice-nucleating proteins (INPs), cold-adapted organisms also developed a number of biomolecular cryoprotectants, collectively known as ice-binding proteins (IBPs). IBPs are responsible for survival mechanisms like freezing point depression (thermal hysteresis), ice recrystallization inhibition (IRI) and ice-adhesion, and have been identified in several kingdoms of life. Here, we investigate the composition, structure, and ice-nucleation activity of INs from *Fusarium acuminatum,* showing that assemblies of small proteins can act as INPs.
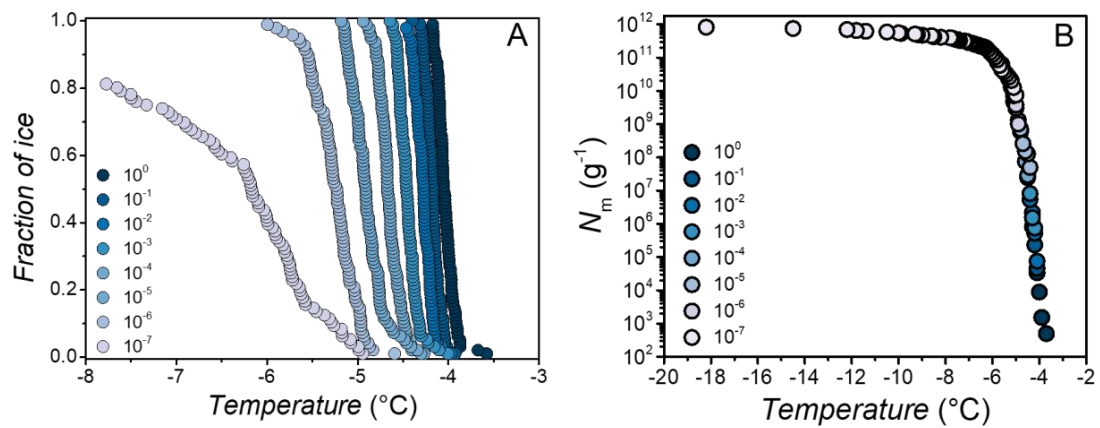
3

170

57

Fig. 1. Freezing experiments of aqueous extracts containing fungal INs from *F. acuminatum*. (A) Fraction of frozen droplets for different dilutions of INs from *F. acuminatum*. Symbol colors indicate data from different concentrations and are identical to (B). Cumulative number of INs per unit mass of *F. acuminatum* (N_m) for extracts containing INs from spores and mycelial surfaces.

Results:

To investigate the freezing power of INs from spores and mycelial surfaces of *F. acuminatum,* aqueous *Fusarium* extracts were serially diluted tenfold, resulting in a concentration range spanning from ~5.6 mg/mL to ~5.6 ng/mL. For each concentration, the freezing of 96 3 µL - sized droplets was followed with a cooling rate of 1 ˚C/min. These measurements provide the fraction of frozen droplets as a function of temperature, for different concentrations as shown in Figure 1A. The results can be combined into a single freezing curve of *F. acuminatum,* as shown in Figure 1B [13-15]. The cumulative IN number concentration (*Nm*) was calculated using Vali's formula and represents the total number of INs that are active above a certain temperature. The strong increase in the cumulative number of INs per unit mass, $N_m(T)$ at ~−3.8 °C reveals the presence of one type of highly efficient IN.

We investigated the size of the *Fusarium* INs by filtration experiments. Figure 2 shows freezing curves of *F. acuminatum* after passing the purified solution through 50 kDa and 30 kDa filters. Filtrations decreased the cumulative number of IN per gram of mycelium and shifted the initial freezing temperature towards lower temperatures. Interestingly, a significant ice nucleation activity remained ($N_m(T) \sim −5$ °C) even after filtration through a 30 kDa filter. By comparing the N_m plots and the fraction of ice of the filtered and unfiltered solutions (Figure 2B), we find that after passing the *Fusarium* extract through a 50 kDa molecular weight cut-off filter, the ice nucleation number is similar to the 10^{-5} dilution of the initial sample. The finding that ice nucleation persists in the filtrates implies that the aqueous extraxt of Fusarium consists of smaller molecules which aggregate to larger ice-nucleating complexes in solution. Filtration likely breaks some of the complexes apart, allowing some subunits to pass through the filter. These subunits must reassemble to larger complexes as shown by the warm ice nucleation temperature. This hypothesis is supported by dynamic light scattering experiments that show similar hydrodynamic radii of ~200 nm for the different dilutions of the *Fusarium* extract as well as the filtered samples (Figure 1D).

172
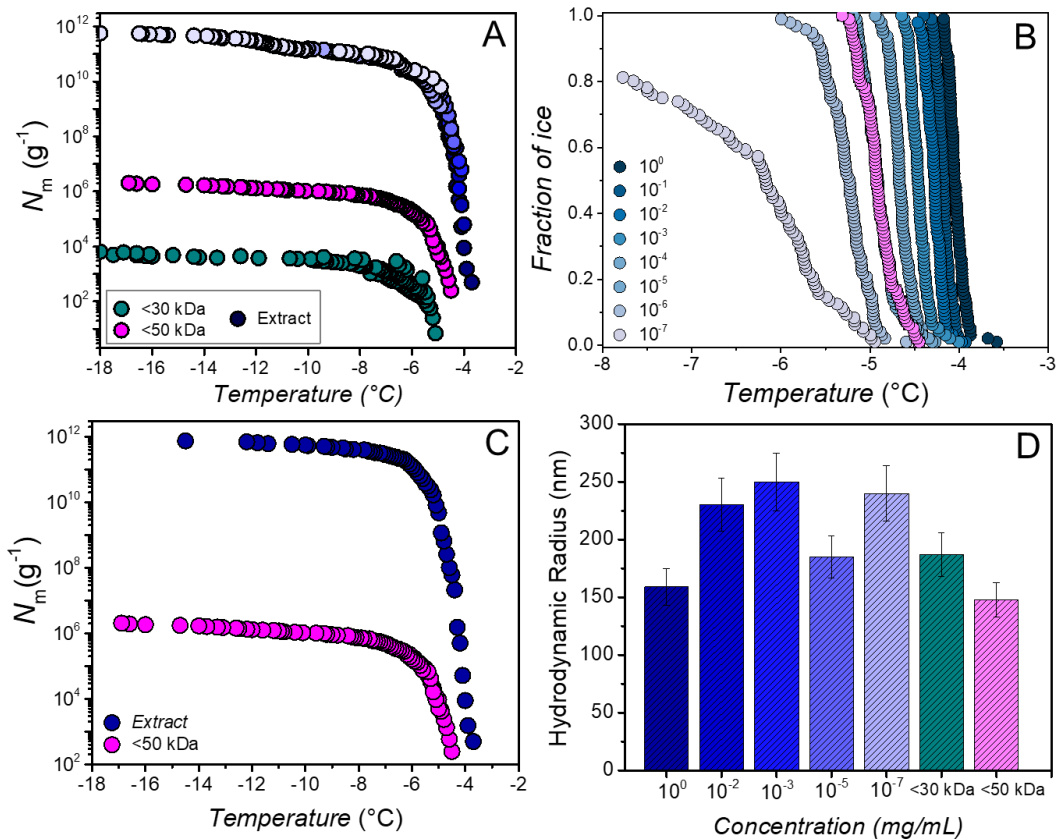
**Fig. 2.** Size determination of fungal ice nucleators (INs) from *F. acuminatum* upon filtration (A) Cumulative number of INs per unit mass of *F. acuminatum* (N_m) for extracts containing INs from spores and mycelial surfaces and samples that were passed through 50 kDa (mangenta) and 30 kDa (green) filters. (B) Fraction of frozen droplets for different dilutions of INs from *F. acuminatum* and the highest concentration of the samples that was passed through a 50 kDA filter. (C) Cumulative number of INs per unit mass of *F. acuminatum* (N_m) before and after filtration through a 50 kDa filter. (D) Hydrodynamic radii for different dilutions of fungal INs and of samples passed through 50 kDa (mangenta) and 30 kDa (green) filters. Radii were determined using dynamic light scattering and error bars represent the standard error of the measurements.

Next, we purified the IN of the aqueous *F. acuminatum* extracts using ice-affinity purification [16-17]. The purification process involves the incorporation of the ice-binding INs into a slowly growing ice phase and the exclusion of non-ice-binding macromolecules and impurities. Thus, we isolated all the ice-binding macromolecules present in *F. acuminatum*, and the success of the process was assessed by determining the activity of the purified IN as shown in Figure 3A. The freezing curve of the ice-purified INs looks very similar to the curve of the aqueous

6

Fusarium extract, with only a slight decrease in the number of IN. The presence of ice-binding macromolecules was further evaluated by investigating ice-shaping activities of the ice-purified Fusarium INs. Using Nanoliter Cryoscopy we observed that when a ~15 μm ice disc was slowly cooled, faceting occurred, and the disc transforms into a hexagon, as shown in Figure 3B. The presence of hexagonally shaped ice crystals confirms the ice-binding properties of the purified macromolecules in the F. acuminatum samples.
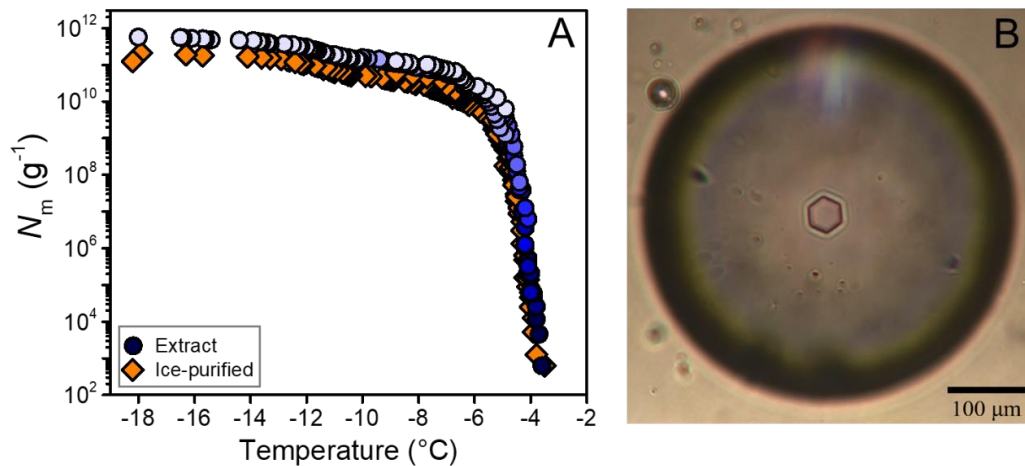

Fig. 3. Freezing experiments of aqueous extracts containing fungal ice nucleators from F. acuminatum. (A) Shown are the cumulative number of ice nucleators per unit mass of F. acuminatum (N_m) for extracts containing ice nucleators from spores and mycelial surfaces and for ice-purified ice nucleators (orange). (B) Cryomicroscopic image of a hexagonal ice crystal grown in a Fusarium ice nucleator solutions.

Next, we determined the exact size of the Fusarium IN units using matrix-assisted laser desorption/ionization-time-of-flight (MALDI-TOF) spectroscopy. Figure 4A shows MALDI spectra of the large (>30 kDa) and small fractions (<30 kDa) of filtered, ice-purified solutions of F. acuminatum. The MALDI spectra of the fractions are similar, dominated by a signal at ~5.3 kDa. Such mass corresponds to molecular diameters well below ~6 nm, the minimal size of the nucleation site required to initiate ice formation at temperatures as high as -5 °C, according to classical nucleation theory[18-19]. Hence, the large Fusarium IN must consist of biomolecules that assemble to larger complexes in solution. We used circular dichroism (CD) spectroscopy to explore the molecular structure of the Fusarium IN. Figure 2B shows the CD spectra of the large (>30 kDa) and small fractions (<30 kDa) of ice-purified solutions of F.

7

134   *acuminatum*. The CD spectrum of the large fraction looks unusual, with a maximum molar

135   ellipticity at ~235 nm and a minimum at ~205 nm. Spectral analysis and fold recognition using

136   BeStSel software reveals a 34% antiparallel β-sheet and 18% helical content[20]. The spectral

137   shape further shows similarities with CD spectra of self-assembled hydrophobins derived from

138   *Grifola frondosa*[21]. The CD spectrum of the small fraction (<30 kDa) is much noisier due to

139   limited sample availability. Scaling of the spectrum, however, shows clear similarity to the

140   larger fraction. Our findings that the fungal INs are proteins is consistent with previoues

141   findings that showed that high temperatures eliminate the fungal ice nucleation activity{Kunert,

142   2019 #67}. We performed an amino acid analysis to unambiguously confirm the proteinaceous

143   nature of the *Fusarium* IN. The amino acid content showed unusually high contents of threonine

144   (10%), serine (8%) as well as aspartic (15%) and glutamic acids (19%) (acid or amide form)

145   (Figure S1). It is worth mentioning that high *β*-sheet contents and high serine, threonine, and

146   glutamine contents were also found in INPs derived from bacteria[17, 19, 22]. We conclude that the

147   large *Fusarium* INs consist of small ~5.3 kDa protein subunits that self-assemble to form large

148   INP-complexes active at ~-3.5 °C. This conclusion is consistent line with the dynamic light

149   scattering measurements that show similar sizes of solution aggregates of the filtered and

150   unfiltered fractions of *Fusarium* INs (Figure 2D).
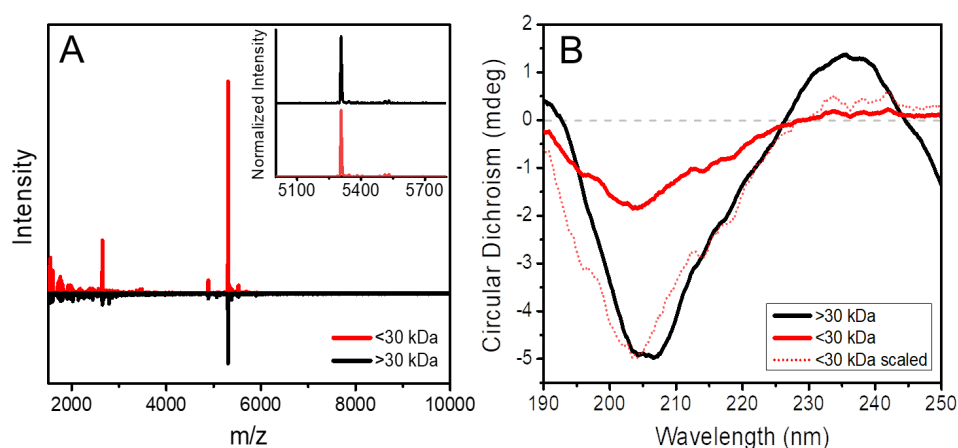
151

152   **Fig. 4.** Characterization of aqueous solutions containing large (>30 kDa) and small fractions
153   (<30 kDa) of filtered, ice-purified fungal ice nucleators from *F. acuminatum*. (A) MALDI
154   spectra show a dominant signal at ~5300, highlighted in the inset. (B) CD spectra reveal
155   similarities between large and small fractions, with minima at ~205 nm and maxima at ~235
156   nm.

157

Discussion:

Biological ice nucleation and the potential impact of biogenic particles on cloud glaciation and the formation of precipitation is poorly understood and constitutes a large gap in our understanding of the interactions and coevolution of life and climate. Here, we provide conclusive evidence that INs derived from *Fusarium* consist of proteins that can self-assemble into larger clusters. We propose that the ability to serve as building blocks of larger protein clusters that can act as biological ice nucleators is a general function of IBPs. Such cluster formation may occur via self-assembly of a single species or in combination with other biomolecular building blocks (lipids, carbohydrates, proteins). The ability of *Fusarium* to finetune their ice growth promotion is remarkable and may present direct ecological advantages. Organisms are likely energetically better off producing many smaller multifunctional proteins than a few large, more error-prone ones.

Methods:

Fungal culture and sample preparation. 75 plates of the ice nucleation-active fungal strain *Fusarium acuminatum* were grown on full-strength potato dextrose agar plates (VWR International GmbH, Darmstadt, Germany). Growth occurred at room temperature for one week and then at 6 °C for about four weeks. Pure water was obtained from Millipore Milli-Q® Integral 3 water purification system (Merck Chemicals GmbH, Darmstadt, Germany), autoclaved at 121 °C for 15 min, and filtered through a 0.1 µm bottle top filtration unit (VWR International GmbH, Darmstadt, Germany). For the droplet freezing experiments, aqueous extracts of fungal mycelium were prepared as described previously[3] with the following modifications. The fungal mycelium of five agar plates was collected in a sterile 50 mL tube, and the weight of the mycelium was determined gravimetrically. Aliquots of 50 mL of pure water were added to the mycelium. The samples were vortexed three times at 2700 rpm for 1 min. The aqueous extracts for all experiments were filtered through a bottle top filtration unit (VWR International GmbH), and the resulting aqueous extracts contained ice nucleators from spores and mycelial surfaces. For the filtration experiments, the 0.1 µm filtrate was filtered through either 30.000 or 50.000 dalton MWCO PES ultra centrifugation units (Thermo Fisher Scientific, Braunschweig, Germany), and the ice nucleator concentration was determined by TINA measurements.

176

187   *Ice Affinity Purification.* Rotary ice-shell purification was used to purify the ice-nucleating
188   biomolecules of the crude fungal extract. Details of the purification method have been described
189   elsewhere[16-17]. In short, in a 500 mL flask, ~20–30 mL water were used to form an ice-shell
190   using a dry ice-ethanol bath for 30–60 s. The flask was then rotated in a temperature-controlled
191   ethylene glycol bath, and the temperature of the bath was set to −2 °C. 100 mL precooled fungal
192   extract was added, and the flask rotated continuously in the bath until 30% of the solution was
193   frozen. The ice was melted and freeze-dried to obtain a mixture of the ice-binding proteins
194   present from *F. acuminatum*. The success of the purification was checked by determining the
195   ice nucleation activity of the purified *Fusarium* samples using TINA measurements. The ice-
196   purified solution was used for filtration experiments and to obtain MALDI, ATIR, and CD
197   spectra.

198

199 *TINA Experiments.* Ice nucleation experiments were performed using the high-throughput

200 Twin-plate Ice Nucleation Assay (TINA), which has been described in detail elsewhere[13]. In a

201 typical experiment, the investigated IN sample was serially diluted 10-fold by a liquid handling

202 station (epMotion ep5073, Eppendorf, Hamburg, Germany). 96 droplets (3 µL) per dilution

203 were placed on two 384-well plates and tested with a continuous cooling-rate of 1 °C/min from

204 0 °C to −20 °C with a temperature uncertainty of ±0.2 °C. The droplet-freezing was determined

205 by two infrared cameras (Seek Therman Compact XR, Seek Thermal Inc., Santa Barbara, CA,

206 USA). The obtained fraction of frozen droplets was used to calculate the cumulative number of

207 ice nucleators using the Vali formula[15]. All experiments were performed multiple times (Figure

208 1, 3-5 samples) with independent samples. Background freezing of pure (autoclaved MilliQ)

209 water in our system occurred at ∼−25 °C.

210 *CD spectroscopy.* CD spectra were recorded at a 1 nm interval from 260 to 180 nm using a

211 Jasco J-1500 spectrometer. CD measurements were performed in a rectangular cell with the

212 optical path of 0.1 cm. Equilibration time for every sample before each set of measurements

213 was 15 min. All spectra were background subtracted and processed using the Spectra Manager

214 Analysis program from JASCO.

215 *DLS.* Dynamic light scattering measurements were performed on an ALV spectrometer

216 consisting of a goniometer and an ALV-5004 multiple-tau full-digital correlator (320 channels),

217 which allows measurements over an angular range from 30° to 150°. A He-Ne Laser

218 (wavelength of 632.8 nm) was used as the light source. Measurements were performed at 20 °C

219 at 9 angles ranging from 30° to 150°. The hydrodynamic radii (Rh) of ~1 mg/ml filtered *F.*

220 *acuminatum* solutions were determined using dynamic light scattering (DLS). The Rh of the

221 smaller and larger fractions of *F. acuminatum* was found to be similar.

222 *IR spectroscopy.* For the ATR-IR experiments, ATR-IR spectra were recorded with a

223 Bruker Platinum ATR Tensor II spectrometer in the range of 4000–400 cm^{-1}. The

224 spectrometer was purged with N_2 and spectra were recorded at room temperature.

11

MALDI-TOF. MALDI measurements were carried out on a rapifleXTM MALDI-TOF/TOF mass spectrometer from Bruker Daltonik GmbH. The instrument is equipped with a scanning smartbeam 3D 10 kHz Nd:YAG laser at a wavelength of 355nm and a 10 bit 5 GHz digitizer. The acceleration voltage was set to 20 kV and the mass spectra were recorded in positive ion mode. Calibration was done with the Bruker peptide mix and the Bruker protein calibration standard I and II in a mass range up to 70 kDa. Samples were measured with random walk ionization across the sample spot. Typically 8000 shots were averaged per spectrum.

Nanoliter Cryoscopy. Thermal hysteresis activity was determined at a *Fusarium* concentration of ~10 mg/mL in water using a Clifton Nanoliter Osmometer, as described elsewhere[23]. The hysteresis measurements were performed with a cooling rate of 0.075 °C/min and without annealing. Measurements were performed 2-4 times on independent samples.

Ice Recrystallization Inhibition Measurements. IRI activity was determined using the splat cooling method[23]. The ice-purified and filtered *Fusarium* samples were dissolved in pure water or in PBS buffer (Dulbecco's Phosphate-Buffered Saline, 1×, without calcium and magnesium chloride), with a final protein concentration of ~1 mg/mL.

Amino Acid Analysis. Amino acid analysis was performed by the Molecular Structure Facility at UC Davies as described elsewhere and the used samples were ice-purified and filtered[24].

Supporting Information

Fig. S1. Amino acid content of the ice-purified *Fusarium* sample.

Corresponding Author

meisterk@mpip-mainz.mpg.de

Notes

The authors declare no competing financial interests.

12

References

1.   Koop, T.; Luo, B.; Tsias, A.; Peter, T., Water activity as the determinant for homogeneous ice nucleation in aqueous solutions. *Nature* **2000,** *406* (6796), 611-614.

2.   Pouleur, S.; Richard, C.; Martin, J. G.; Antoun, H., Ice Nucleation Activity in Fusarium acuminatum and Fusarium avenaceum. *Appl Environ Microbiol* **1992,** *58* (9), 2960-4.

3.   Kunert, A. T.; Pöhlker, M. L.; Tang, K.; Krevert, C. S.; Wieder, C.; Speth, K. R.; Hanson, L. E.; Morris, C. E.; Schmale Iii, D. G.; Pöschl, U.; Fröhlich-Nowoisky, J., Macromolecular fungal ice nuclei in Fusarium: effects of physical and chemical processing. *Biogeosciences* **2019,** *16* (23), 4647-4659.

4.   Després, V.; Huffman, J. A.; Burrows, S. M.; Hoose, C.; Safatov, A.; Buryak, G.; Fröhlich-Nowoisky, J.; Elbert, W.; Andreae, M.; Pöschl, U.; Jaenicke, R., Primary biological aerosol particles in the atmosphere: a review. *Tellus B: Chemical and Physical Meteorology* **2012,** *64* (1), 15598.

5.   Du, R.; Du, P.; Lu, Z.; Ren, W.; Liang, Z.; Qin, S.; Li, Z.; Wang, Y.; Fu, P., Evidence for a missing source of efficient ice nuclei. *Scientific Reports* **2017,** *7* (1), 39673.

6.   Beall, C. M.; Michaud, J. M.; Fish, M. A.; Dinasquet, J.; Cornwell, G. C.; Stokes, M. D.; Burkart, M. D.; Hill, T. C.; DeMott, P. J.; Prather, K. A., Cultivable halotolerant ice-nucleating bacteria and fungi in coastal precipitation. *Atmos. Chem. Phys.* **2021,** *21* (11), 9031-9045.

7.   Smith, M. N., Pathological Factors Affecting Survival of Winter Barley Following Controlled Freeze Tests. *Phytopathology* **1978,** *68*, 773.

8.   Fröhlich-Nowoisky, J.; Hill, T. C. J.; Pummer, B. G.; Yordanova, P.; Franc, G. D.; Pöschl, U., Ice nucleation activity in the widespread soil fungus <i>Mortierella alpina</i>. *Biogeosciences* **2015,** *12* (4), 1057-1071.

9.   Huffman, J. A.; Prenni, A. J.; DeMott, P. J.; Pöhlker, C.; Mason, R. H.; Robinson, N. H.; Fröhlich-Nowoisky, J.; Tobo, Y.; Després, V. R.; Garcia, E.; Gochis, D. J.; Harris, E.; Müller-Germann, I.; Ruzene, C.; Schmer, B.; Sinha, B.; Day, D. A.; Andreae, M. O.; Jimenez, J. L.; Gallagher, M.; Kreidenweis, S. M.; Bertram, A. K.; Pöschl, U., High concentrations of biological aerosol particles and ice nuclei during and after rain. *Atmos. Chem. Phys.* **2013,** *13* (13), 6151-6164.

10.   Morris, C. E.; Sands, D. C.; Glaux, C.; Samsatly, J.; Asaad, S.; Moukahel, A. R.; Gonçalves, F. L. T.; Bigg, E. K., Urediospores of rust fungi are ice nucleation active at > −10 °C and harbor ice nucleation active bacteria. *Atmos. Chem. Phys.* **2013,** *13* (8), 4223-4233.

11.   O'Sullivan, D.; Murray, B. J.; Ross, J. F.; Whale, T. F.; Price, H. C.; Atkinson, J. D.; Umo, N. S.; Webb, M. E., The relevance of nanoscale biological fragments for ice nucleation in clouds. *Scientific Reports* **2015,** *5* (1), 8082.

12.   Hasegawa, Y.; Ishihara, Y.; Tokuyama, T., Characteristics of ice-nucleation activity in Fusarium avenaceum IFO 7158. *Biosci Biotechnol Biochem* **1994,** *58* (12), 2273-4.

13.   Kunert, A. T.; Lamneck, M.; Helleis, F.; Pöschl, U.; Pöhlker, M. L.; Fröhlich-Nowoisky, J., Twin-plate Ice Nucleation Assay (TINA) with infrared detection for high-throughput droplet freezing experiments with biological ice nuclei in laboratory and field samples. *Atmos. Meas. Tech.* **2018,** *11* (11), 6327-6337.

14.   Schwidetzky, R.; Kunert, A. T.; Bonn, M.; Pöschl, U.; Ramløv, H.; DeVries, A. L.; Fröhlich-Nowoisky, J.; Meister, K., Inhibition of Bacterial Ice Nucleators Is Not an Intrinsic Property of Antifreeze Proteins. *The Journal of Physical Chemistry B* **2020,** *124* (24), 4889-4895.

15.   Vali, G., Quantitative Evaluation of Experimental Results an the Heterogeneous Freezing Nucleation of Supercooled Liquids. *Journal of Atmospheric Sciences* **1971,** *28* (3), 402-409.

16.   Tomalty, H. E.; Graham, L. A.; Eves, R.; Gruneberg, A. K.; Davies, P. L., Laboratory-Scale Isolation of Insect Antifreeze Protein for Cryobiology. *Biomolecules* **2019,** *9* (5), 180.

17.   Lukas, M.; Schwidetzky, R.; Kunert, A. T.; Backus, E. H. G.; Pöschl, U.; Fröhlich-Nowoisky, J.; Bonn, M.; Meister, K., Interfacial Water Ordering Is Insufficient to Explain Ice-Nucleating Protein Activity. *The Journal of Physical Chemistry Letters* **2021,** *12* (1), 218-223.

18.   Eickhoff, L.; Dreischmeier, K.; Zipori, A.; Sirotinskaya, V.; Adar, C.; Reicher, N.; Braslavsky, I.; Rudich, Y.; Koop, T., Contrasting Behavior of Antifreeze Proteins: Ice Growth Inhibitors and Ice Nucleation Promoters. *The Journal of Physical Chemistry Letters* **2019,** *10* (5), 966-972.

180

307 19.   Qiu, Y.; Hudait, A.; Molinero, V., How Size and Aggregation of Ice-Binding Proteins Control Their
308 Ice Nucleation Efficiency. *Journal of the American Chemical Society* **2019,** *141* (18), 7439-7452.
309 20.   Micsonai, A.; Wien, F.; Kernya, L.; Lee, Y.-H.; Goto, Y.; Réfrégiers, M.; Kardos, J., Accurate
310 secondary structure prediction and fold recognition for circular dichroism spectroscopy. *Proceedings*
311 *of the National Academy of Sciences* **2015,** *112* (24), E3095-E3103.
312 21.   Wang, X.; Song, D.; Wang, B.; Yang, J.; Ge, L.; Zhao, L.; Xu, H.; Qiao, M., A mutant of
313 hydrophobin HGFI tuning the self-assembly behaviour and biosurfactant activity. *Applied Microbiology*
314 *and Biotechnology* **2017,** *101* (23), 8419-8430.
315 22.   Garnham, C. P.; Campbell, R. L.; Walker, V. K.; Davies, P. L., Novel dimeric β-helical model of an
316 ice nucleation protein with bridged active sites. *BMC Struct Biol* **2011,** *11*, 36.
317 23.   Sun, Y.; Giubertoni, G.; Bakker, H. J.; Liu, J.; Wagner, M.; Ng, D. Y. W.; Devries, A. L.; Meister,
318 K., Disaccharide Residues are Required for Native Antifreeze Glycoprotein Activity. *Biomacromolecules*
319 **2021,** *22* (6), 2595-2603.
320 24.   Cooper, C., Packer, N., and Williams, K, *Amino Acid Analysis Protocols*. Humana Press: 2000;
321 Vol. 159.

322